MODELLING THE DYNAMICS OF CUTTING DURING TURNING

Saoudi TAIBI

Doctor of Philosophy

THE UNIVERSITY OF ASTON IN BIRMINGHAM

March 1994

THE UNIVERSITY OF ASTON IN BIRMINGHAM

MODELLING THE DYNAMICS OF CUTTING DURING TURNING

TAIBI Saoudi, Doctor of Philosophy
March 1994

SYNOPSIS

This thesis presents an approach to cutting dynamics during turning based upon the mechanism of deformation of work material around the tool nose known as "ploughing". Starting from the shearing process in the cutting zone and accounting for "ploughing", new mathematical models relating turning force components to cutting conditions, tool geometry and tool vibration are developed. These models are developed separately for steady state and for oscillatory turning with new and worn tools.

Experimental results are used to determine mathematical functions expressing the parameters introduced by the steady state model in the case of a new tool. The form of these functions are of general validity though their coefficients are dependent on work and tool materials. Good agreement is achieved between experimental and predicted forces. The model is extended on one hand to include different work material by introducing a hardness factor. The model provides good predictions when predicted forces are compared to present and published experimental results. On the other hand, the extension of the ploughing model to turning with a worn edge showed the ability of the model in predicting machining forces during steady state turning with the worn flank of the tool.

In the development of the dynamic models, the dynamic turning force equations define the cutting process as being a system for which vibration of the tool tip in the feed direction is the input and measured forces are the output. The model takes into account the shear plane oscillation and the cutting configuration variation in response to tool motion. Theoretical expressions of the turning forces are obtained for new and worn cutting edges. The dynamic analysis revealed the interaction between the cutting mechanism and the machine tool structure. The effect of the machine tool and tool post is accounted for by using experimental data of the transfer function of the tool post system. Steady state coefficients are corrected to include the changes in the cutting configuration with tool vibration and are used in the dynamic model. A series of oscillatory cutting tests at various conditions and various tool flank wear levels are carried out and experimental results are compared with model–predicted forces. Good agreement between predictions and experiments were achieved over a wide range of cutting conditions.

This research bridges the gap between the analysis of vibration and turning forces in turning. It offers an explicit expression of the dynamic turning force generated during machining and highlights the relationships between tool wear, tool vibration and turning force. Spectral analysis of tool acceleration and turning force components led to define an "Inertance Power Ratio" as a flank wear monitoring factor. A formulation of an on–line flank wear monitoring methodology is presented and shows how the results of the present model can be applied to practical in–process tool wear monitoring in turning operations.

Key words: Flank wear, metal cutting mechanics, monitoring, tool vibration, turning.

DEDICATION

To the memory of my father, Ali Ben Haj Lahbib, may his soul rest in peace.

I would like to express my deep appreciation to my mother, brother, sister, sister in law for their understanding and encouragements throughout this work.

To Ayoub and Zouhair.

ACKNOWLEDGEMENTS

The work presented in this dissertation was carried out in the department of mechanical and Electrical Engineering at The University of Aston in Birmingham. This work is a part of the cultural relationship between The University of Aston and Ecole Mohammadia d'Igénieurs, Morocco supported by the British Council.

The author wishes to express his thanks to Dr. Penny, J.E.T. and Dr. Maiden J.D. from The University of Aston and Pr. Bennouna M. from Ecole Mohammadia d'Ingénieurs for their valuable guidance, advice and continued enthusiastic support throughout the duration of the programme.

My gratitude extends to Dr. Garvey S., Dr. Friswell and Dr. Upton for their advice given and interest shown in the research conducted.

Thanks are also due to the British Council for its financial support.

TABLE OF CONTENTS

LIST OF FIGURES

LIST OF TABLES

NOMENCLATURE

A_s	Shear plane area.
C_p	Ploughing forces ratio.
C_s	Rake forces ratio.
C_{si}	Instantaneous rake forces ratio.
F_s	Shear force.
F_x	Turning force component in the feed direction.
F_{xi}	Instantaneous turning force component in the feed direction.
F_{xs}	Rake force component in the feed direction.
F_z	Turning force component in the mean cutting direction.
F_{zi}	Instantaneous turning force component in the mean cutting direction.
F_{zs}	Rake force component in the mean cutting direction.
H_d	FRF of dynamometer and tool post system.
k	Mean shear stress.
k_i	Instantaneous mean shear stress.
N	Rotation speed of the workpiece.
P_x	Component of the ploughing force in the feed direction.
P_{xi}	Instantaneous component of the ploughing force in the feed direction.
p_s	Ploughing factor.
P_z	Component of the ploughing force in the mean cutting direction.
P_{zi}	Instantaneous component of the ploughing force in the mean cutting direction.
r	chip thickness ratio.
R	Radius of the tool nose.
S	Mean dynamic chip thickness.
S_c	Deformed chip thickness.

S_i Instantaneous chip thickness.

S_0 Undeformed chip thickness.

t Time (in seconds).

T_{int} Temperature of the chip–tool contact.

T_1 Incremental coefficient of the variation of the shear angle with the chip thickness oscillation.

T_2 Incremental coefficient of the variation of the shear angle with the rake angle.

T_3 Incremental coefficient of the variation of the shear angle with the slope of the cut surface.

u(t,z) Wave function describing the displacement at time t of a point of coordinate z on the cutting edge.

u_1 Incremental coefficient of the variation of the rake forces ratio with the chip thickness oscillation.

u_2 Incremental coefficient of the variation of the rake forces ratio with the rake angle.

V Mean cutting speed.

Wf Average width of the flank wear land in the central part of the active cutting edge.

V_i Instantaneous cutting speed.

w Depth of cut.

X Amplitude of the tool displacement.

x(t) Instantaneous tool displacement.

$\dot{x}$ Velocity of tool vibration.

$x_0(t)$ Instantaneous variation of the workpiece surface.

$\dot{x}_0(t)$ rate of change of x_0.

α Rake angle of the tool.

α_i Instantaneous rake angle.

b Equivalent mean friction angle along the rake of the tool.

γ Flank angle of the cutting edge.

γ_i Instantaneous flank angle.

δ Slope of the machined surface.

δ_0 Slope of the work surface.

ϕ Shear angle.

ϕ_i Instantaneous shear angle.

ψ Slope of the surface relative to the instantaneous cutting speed.

ζ Depth of the tool penetration.

ζ_α incremental coefficient of variation of the depth of the tool penetration with rake angle.

$\xi(z)$ Function measuring the depth of the tool penetration as function of z.

μ Equivalent mean friction coefficient on the tool chip interface.

μ_f Equivalent mean friction coefficient along the flank face of the tool tip.

ε Geometrical lead of the free end of the shear plane relative to the cutting edge.

ω Angular velocity of tool displacement.

τ Equivalent mean friction angle along the flank face of the tool.

τ_α incremental variation of the flank friction angle coefficient with the rake angle.

κ Overlap factor.

Chapter 1

INTRODUCTION

The aim of the present work is to develop a model of the turning process for tool wear monitoring purposes. As will be discussed in Chapter 2, the most widely used methods for wear monitoring in turning are based on the analysis of machining forces or vibrations. Experimental results conducted in the first stages of this work showed, in agreement with published results, that neither the forces nor the vibration information can be used alone for tool wear monitoring in turning. However, useful information about the state of the cutting edge can be made when both vibration and machining forces are analysed simultaneously. Moreover, while under practical conditions it is much easier to measure tool vibrations it is not convenient to design a machine tool for mass production with a built–in force dynamometer. As a consequence the present work aims to develop a model that can predict turning forces from tool vibration measurements and use the predicted forces and measured vibration to monitor tool wear.

In this chapter a general background to machining and the scope of the thesis are presented. This presents a brief discussion of the main difficulties encountered in the developments of metal machining. It also highlights the need for tool wear monitoring systems that are not based on pattern recognitions of signals but on theoretical models so that they can be used for a wide range of cutting conditions (details are reported in Chapter 2).

1.1. BACKGROUND

The cutting process involves a tool that when properly driven converts mechanical energy into plastic deformation in the material against which it presses. In turn, this plastic deformation results in failure by shear, and in chips. Some energy is wasted in friction, some in chatter or vibration. Temperature, wear, elastic deformations and fracture are problems associated with cutting tools. The situation at the tool edge is demanding and complex.

There is a world-wide demand for the development and application of optimization technology in metal cutting manufacturing. The factors responsible for the requirement are both economic and technical.

The economic factors stem from the large amount of money spent on such manufacturing. The cost of metal machining operations represents a significant percentage of the value of the gross national product (GNP) of the industrially developed countries of the world. For example, in the USA, approximately 5% of the GNP is spent annually on the machining of metal. Thus, the economic necessity for optimization of the machining process is very great.

The technical factors are found in the important changes which are taking place in manufacturing technology. Among these changes are the following:

1. Greater product variety resulting in decreasing lot sizes. This trend results in the need for greater versatility and thus the use of variable–program–type automation in machining.
2. Closer tolerances resulting in a need for greater use of automatic control in machining.

3. An increasing variety of work materials with generally higher strength levels. This trend results in a need for manufacturing to acquire increased ability to adapt to changing work material properties and to machine high strength materials economically.

In the light of all economic and technical factors, and because of the need for finer finishes, closer tolerances, faster production, better economy, harder materials; there exists a strong need for developing further understanding of the aspects of the machining process which have the greatest influence on machining costs, namely tool wear and surface quality. In particular, there is a need to develop means to replace present–day empirical, qualitative methods of estimating these with the ability to predict them quantitatively from the structure and properties of the tool, work material and related considerations. Certainly there is a need for mathematical models to design an adaptive control system and there is a need as well for another mathematical model of the machining process to enable the monitoring system to be self–optimising.

In the turning process the choice of "optimal" cutting conditions for maximum productivity and minimum cost has always posed problems. It usually calls for a very careful compromise between the selection of higher cutting conditions, to reduce time and obtain low cost for the components, and the inherent increase in tool wear and its consequence on the quality of the products and consequent scrap rate which can result when tool failures occur.

This problem has been exacerbated by the developments in the automation of metal cutting machine tools. Monitoring of cutting conditions has become a subject of great interest. Different methods have been developed for monitoring the cutting process to predict tool life, prevent tool breakage and to select better sets of cutting conditions that

avoid chatter. Research and development areas for adaptive control of machine tools and indirect methods of production control are a subject of concern.

The productivity of a machine tool is limited by its power or by vibration or chatter. In the turning process, the tool is clamped at one end and free at the other end at the cutting edge, so that it forms the weakest part in the machining operation. Any disturbing force during machining can easily excite the operating turning system resulting in either poor machining, accelerated tool wear or unstable cutting process which may lead to premature tool failure.

In a general sense, tool holder vibration or chatter during machining is classified into the following three main categories: forced, self–excited without regeneration, and self–excited with regeneration. Briefly, forced chatter is caused by an excitation force which has its origin outside the cutting zone, such as from a vibrating base, or from rotary unbalance in the workpiece being machined or in gears or shafts of the machine tool under operation. The main characteristic of forced vibration is that the predominant frequency components of the forced vibration of the cutting tool are usually equal to the frequency components of the excitation forces. The theory of forced vibration is well developed, so forced vibration is relatively easy to deal with. For example, when identifying the driving force causing the chatter, the forced vibration can be eliminated by accurate balancing, mounting on vibration isolators, etc...

Self–excited vibration can be explained using the falling characteristic of the cutting forces with the cutting speed as follows as first introduced by Arnold (1941). There are two cases for a velocity difference of tool and workpiece. The actual speed V varies between the limits V_1 and V_2 when the tool vibrates as shown in Fig. 1.1. The cutting speed V_1 exists at the instant when the tool is in midposition on its way down because

the relative velocity is at a minimum. A relative velocity maximum exists when the tool is again in midposition on the way up. Since the V_1 speed is associated with the higher cutting force F_1, an additional force $(F - F_1)$ is exerted on the tool on its way down and another such additional force $(F - F_2)$ on its way up. In every case, an additional force exists in the direction of motion. This is the criterion for self–excited vibration. Therefore, the appearance of the drop in cutting force with the increase in cutting speed prevents vibration–free machining. Under circumstances where damping is small, external energy is fed into the elastic system at an increasing rate, dynamic instability of the machining operation will eventually occur.

One of the main concerns of this thesis is relating self–excited chatter to machining forces in a turning process. The main characteristics of self–excited chatter are that the excitation force acting on the tool originates mainly from the cutting zone and interacts with the cutting conditions together with the tool state and the tool motion. In other words, the excitation force affecting the motion of the cutting tool is governed by the motion it self.

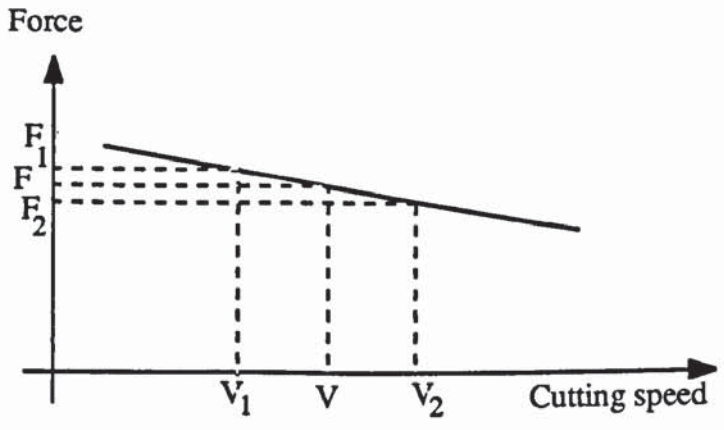

Fig. 1.1 Machining force versus cutting speed.

Depending on cutting conditions and tool wear level, both types of self–excited chatter are possible. The concept of regeneration comes from the fact that the vibrating tool leaves an undulated surface behind, which is cut by the tool in the following revolution (Fig. 5.3). This generates a new undulation one revolution later, and so forth. In most turning processes, self–excited chatter is the primary type of vibration encountered. Under certain cutting conditions for a given tool structure, the magnitude of tool vibration may increase as the machining process progresses particularly because of changes in the tool geometry, a phenomenon called the occurrence of system instability. Therefore, self–excited chatter is a basic performance limitation in the productivity of the turning process.

Published works have showed that self–excited chatter instability occurs as cutting speed and/or depth of cut are increased. Other factors can also be introduced such as the increase in flank wear which directly affects the geometry of the cutting edge and leads to an increase in turning forces and amplitudes of tool vibration. Therefore, the maximum metal removal rate and thus the machining productivity that can be achieved without instability occurring is directly dependent upon the dynamic stability of the turning system. Furthermore, with the rapid development of computer–aided manufacturing systems (CNC machines), specifying cutting data such as cutting speed, depth of cut and feed is usually done during the programming stage referring to new cutting edges. However, the tool wear is increasing as the cutting progresses and the rate of its increase is affected by the cutting conditions, the cutting configuration and work material. Henceforth, if a model for machining control is needed to be developed, this model should account for tool wear as well as for the effect of tool vibration.

As to the former, adhesive and abrasive wear are the most commonly encountered mechanisms. When dealing with metal cutting, the elevated temperatures and high

stresses imposed on the tool bring other processes into play, the most important are the adhesive wear, abrasive wear, fracture wear, wear by oxidation, diffusion wear and superficial plastic deformation.

This general description of wear mechanisms concentrates on the events that occur at commercially relevant speeds. Hence, while adhesive wear is strongly associated with built–up edge formation, the latter rarely occurs at the speeds attainable with carbide turning tools. This is not to say that adhesive wear does not occur at higher rates of metal removal. As the cutting speed increases, the size of the built–up edge (B.U.E) decreases and even vanishes at relatively high speeds, the chip cleans the tool rake face and cutting edge region so the contact surface is free from organic contaminants and oxides henceforth an increasing opportunity for adhesive wear, particularly in view of the intimate contact between chip and cutting tool. Abrasive wear involves the removal of tool material by the scoring action of hard phase inclusions in the chip.

The inherent brittleness of the carbide tools renders them susceptible to severe damage by cracking if sudden loads or thermal gradients are applied to their edge. While such difficulties can be encountered in the milling process and in any interrupted cuts, this may also be the case in the turning process as the tool encounters the workpiece. In fact, unpredictable tool breakage cannot be tolerated and this type of tool failure is to be avoided by the choice of the cutting conditions such as lower feed rates. Catastrophic failure is not therefore considered as a major influence in the steady state wear problems and moreover, in tool wear monitoring systems, tool fracture can be detected by a sudden increase followed by a sudden decrease in the cutting forces if the tool edge looses contact with the work material. Furthermore, at higher cutting speeds, the oxygen cannot penetrate to the rear of the chip–tool contact area and transfer continues to form only on the sides. In orthogonal turning tools, such transfer has been observed

to form at the extremity of the depth of cut and immediately behind the nose radius and after a long cutting time, deep notches can be observed in both these regions.

Mechanisms such as adhesion and abrasion are perceived as being enhanced by elevated temperature, but not as critically dependent on temperature rise as diffusion or plastic deformation. Diffusion involves transport of material into the moving chip and in the case of carbide tools it is predominantly controlled by the solubility of the carbide phase into the chip material. It has been proposed that this is the major cause of crater wear at high speeds.

The chip, deformed at a very high strain rate, can exert a sufficient shear stress onto the surface layers of the tool to deform the latter at a low strain rate which can wear the tool along the rake. In many respects such a mechanism, relying on intimate contact and tangential shear of the tool material, can be regarded as a gross form of adhesive wear. The most serious form of wear involves thermal weakening of the cutting edge region and deformation under the applied normal load. Once this deformation occurs the worn edge causes an additional heat source as it rubs on the machined workpiece, further weakening the material and leading to plastic collapse.

These wear mechanisms take place simultaneously during machining and lead to the deterioration of all the surfaces that can be in contact with the workpiece material. These are the rake face and the flank face of the cutting tool. The way of wear of these surfaces are mostly dependent upon the tool material, cutting conditions and the work material. The types of failure encountered with carbide cutting tools can be classified as follows:

1. Flank wear
2. Crater wear
3. Combination of crater and flank wear
4. Spalling or crumbling of the cutting edge
5. Fracturing or major chipping of the cutting edge.

Fracturing and chipping of the cutting tools can be minimised if not avoided by a good choice of the cutting conditions for a given workpiece material and also by a limitation of the maximum wear of the cutting edge. While spalling and crumbling can be avoided by choice of tool material and cutting conditions.

The remaining factors, flank wear, crater wear or some combination of the two are important modes of tool failure encountered in carbide tools (Fig. 1.2). Analyses of cutting tool wear have traditionally emphasized upon flank wear more than crater wear, and the reason is the more direct influence that flank wear has on the quality of the product. The on–set of the crater wear results in changes in the mechanics of the cutting process and reduces the tool rigidity. Flank wear, on the other hand, results in changes in the mechanics of cutting process, tendency for chatter and changes in the dimensions of the product. Henceforth because it is the deciding factor in most cases, the present study will be confined to the study of effect of flank wear on the machining process.

Flank wear occurs along the clearance face of the cutting tool (Fig. 1.2) and the height of the wear land is usually used as a limiting criterion. Optimization of tool life is depending upon the required product quality, nonetheless the ISO limits the flank wear Wf to 300μm in case of uniform wear land or to Wf_{max} = 600μm in case of irregular

Fig. 1.2 Data defining the wear on turning cutting tool (Boothroyd, 1981).

wear or chipping. The need for better quality of machined parts with minimum cost increases the need for unmanned machining and the need for better understanding of the inter–action between all the machining factors mentioned above upon the mechanics of machining. This therefore is leading to increasing demand for models of cutting process for sake of analysis of machining mechanics and for machine control.

Over the years many mathematical models have been proposed to describe the turning machining system. Several system analysis techniques have dealt with cutting under steady state conditions and/or dynamic conditions for new as well as for worn cutting edges. As the review of Chapter 2 will show the following features stand out prominently from the research work that have been carried out in this field:

1. The cutting process can be represented by a thin shear plane solution in dynamic as well as in steady state conditions.
2. The turning tool is represented at the cutting point by a simple one–degree of freedom mass–spring–damper system vibrating in a direction normal to the mean cutting direction.
3. The dynamic cutting force is related mainly to the motion of the lumped mass–spring–damper system in the direction normal to the machined surface.
4. Flank wear has more effect on cutting process and on machined surface quality for normal cutting conditions than crater wear.

The discrepancies arising between the theoretical approaches and the practice are very important so that mathematical modelling and system analysis in the previous theoretical approach have a number of drawbacks as will be discussed in Chapter 2, the most serious being:

1. When developing a new cutting force equation, the effect of the tool size is mostly ignored and as a result the prediction of the turning force is not sufficiently defined.
2. Most of the developed models lack flexibility in application because there application is confined generally to a narrow band of cutting conditions and to some laboratory conditions that are rarely met in work floor conditions. Moreover, these models are

usually limited to a particular work material and do not provide a simple way of extending the model to cover other work materials and other conditions.

3. The system models in the previous approach are time–invariant since system parameters in the models are stationary with respect to time during turning operations. The dynamic coefficients are mostly predicted from steady state conditions but are not corrected with respect to the dynamic configuration of the cutting process. Therefore, to fully describe the dynamic cutting process it is necessary to introduce the instantaneous cutting conditions in the system analysis.

4. The effect of tool vibration in the feed direction upon dynamic forces and amplitude of their oscillations has not yet been well investigated. Tool vibration in the feed direction is directly affected by the state of the cutting edge and leads to chatter vibration that in turn results in poor quality of the machined surfaces.

In summary (see Chapter 2), the system models and the analysis developed in the previous theoretical approach do not fully characterise the underlying physical mechanism in the turning machining operation and, under certain circumstances, may even produce misleading conclusions.

1.2. SCOPE OF THE THESIS

The purpose of this thesis is to develop a state variable system model to aid in steady state and dynamic analysis of the turning machining system when new and worn tools are used. Specifically, there are four main objectives of this thesis:

1. Development of new a system model which will describe the turning process under steady state and dynamic turning in more details than the current models. This model should be able to represent the regenerative machining in a way that facilitates system

analysis with a minimum set of system parameters and should include the effect of the ploughing process.

2. The development of a turning force model for which the dynamic coefficients are determined from steady state data but corrected for dynamic configuration. The turning force model building approach is based on the fundamental aspects of the cutting process and should be verified through the comparison of measured, published and predicted data for the steady state and through experimental and predicted data for the dynamic turning process.

3. A model for turning with different tool wear levels will be developed and will be used to incorporate the effect of flank wear during machining. The predicted results will thereafter be compared to experimental results from tests covering a wide range of the cutting conditions under steady state as well as under dynamic conditions.

4. Flexibility of the developed model so that, upon replacing time–invariant parameters by time–varying parameters, the present model can be used to monitor tool wear and to study the dynamic characteristics of turning process.

In the light of these objectives, this thesis presents a systematic study of the turning process. The main phases of this work deal with modelling, simulation and experimental verification.

1.3. OUTLINE OF THE THESIS PRESENTATION

There are nine chapters to this thesis. Although each chapter has been written to be self–contained, each chapter builds on the results of preceding chapters. The content of each chapter are summarised below.

Chapter 2 gives an overview of the relevant literature. There is fairly extensive literature pertaining to the turning process because this problem has attracted the attention of many investigators. An attempt has been made to present a comprehensive picture in order to put this thesis in proper perspective.

Chapter 3 describes the steady state model for the turning process. This model takes into account the effect of chip flow on the rake of the tool as well as the effect of the rubbing contact between the cut surface and the flank of the tool when turning under conditions of continuous chip. The former is due to chip formation associated with the shearing effect and the latter is due to the indentation effect arising around the tool nose. This model is based upon the assumption that the elementary force at an arbitrary point of the tool edge in contact with machined surface is proportional to the depth of tool penetration resulting from material deformation around tool nose. Theoretical expressions of tangential and feed forces are developed. Furthermore, a series of cutting tests covering a large range of cutting conditions are run to determine the model coefficients. Thereafter, the model is used to predict the turning forces under steady state conditions for different sets of cutting conditions, different cutting configurations and different work materials. The predicted results are compared to measured and previously published data.

The steady state model is extended in Chapter 4 to the case of machining with tools at different flank wear levels. This model is used to predict the force for different conditions for a flank wear of up to 280μm and predicted results are compared with experimental forces.

Chapter 5 deals with the modelling of the dynamic cutting process. Two considerations have been incorporated into the dynamic modelling. The first one refers to the

replacement of the regenerative effect by an equivalent instantaneous chip thickness and by the consideration of the instantaneous cutting conditions. The former recovers the use of steady state data into the dynamic process. The latter comes from considering dynamic oscillations of the ploughing forces around the cutting edge as the tool is vibrating in the feed direction. Because of considering tool vibration in feed direction, dynamic turning process is fully described when machining with a new cutting edge.

Chapter 6 gives a full description of the cutting rig, machine tool and work material used in the experimental work. It also highlights the effect of the tool–post and tool-holder upon the dynamics of the cutting process.

A dynamic experimental investigation is carried out in Chapter 7. The acceleration of the tool vibration as measured at the tool tip is fed into the dynamic model developed in chapter 5 to yield the dynamic components of the turning force. These are compared to the measured force components in a dynamic turning operation.

The dynamic model is extended in chapter 8 to account for the effect of flank wear. This chapter also provides a study into the possibilities of defining a flank wear monitoring parameter. Whereas the steady state wear model (chapter 4) is predicting the average state of the cutting process with large prediction errors, the dynamic model is found to be more useful for on–line monitoring of flank wear. It also permits one to examine the nature and the source of the dynamic force frequency spectrum and determines the extent of the correlation between the characteristic peak frequency and tool wear.

Chapter 9 summarises the thesis and provides recommendations on continuing research in this field.

Chapter 2

LITERATURE REVIEW

2.1. INTRODUCTION

This chapter presents a background survey pertaining to the turning machining process. As the aim of this study is to present a formulation of dynamic turning with new and worn cutting edge for in–process tool wear monitoring, the review is divided into four sections, developments in the cutting process, tool wear and tool condition monitoring, metal cutting theories for steady state and dynamic turning followed by a brief discussion of the adaptive control principles. A section on adaptive control is introduced to present general modelling basis of metal cutting and machine tool used in building adaptive controllers. At the end a summary commenting on the previous approach with a view to justifying the approach proposed in this thesis is included.

2.2. DEVELOPMENTS IN MACHINING PROCESS

Any machining system basically consists of two subsystems, i.e. the cutting process and the machine tool structure. Over the years, many efforts have been made to develop models for machining processes that can predict and thus explain the experimental findings during metal removing. These studies are concerned mostly with the study of the metal machining process to investigate the effect of the machining conditions, the tool geometry and machine structure upon the tool life, the quality of the machined surfaces and the accuracy in machining. The links between these two

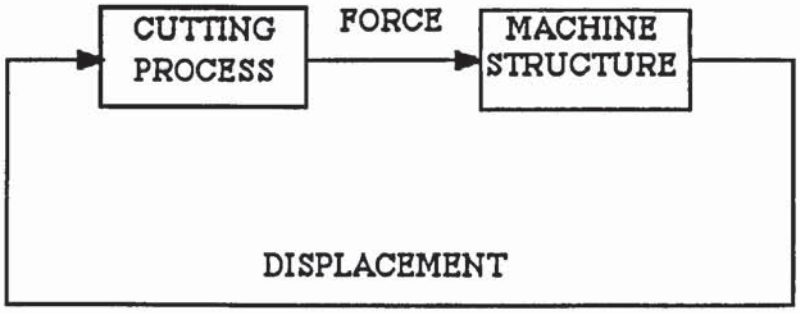

Fig. 2.1. Structure and cutting process dynamic loop

subsystems mentioned above are the forces and the displacement of the tool motion as indicated in Fig. 2.1. The dynamic nature of the machining systems arises from the fact that these links form a closed–loop between these two subsystems.

To meet the demands for diversified products and market competition, modern machining technology is developing towards flexible manufacturing systems (FMS), that is, automatic production systems with good flexibility and high efficiency. To a large degree, the performance of FMS depends on the operations of various supervising devices at all aspects of production. Being one of the essential steps to ensure high quality of the workpieces, tool conditions assurance in automatic machining processes is considered as a key to FMS. But so far, it is still a problem not solved satisfactorily in workshop conditions (Tlusty, 1983).

Even though the first attempt to model the machining process was made by Merchant in 1942, the focus of research during the last decade is upon the establishment of a predictive theory or analytical system (Usui *et al.*, 1984; Stephenson *et al.*, 1988) which enables prediction of aspects of the cutting performances such as chip formation, cutting forces, cutting temperature, tool wear and surface finish, rather than

the development of theories of a descriptive nature which only explain the mechanism of the metal cutting phenomena. In other words, metal cutting theories need to be developed in order to be utilised for practical machine–shop problems such as the determination of optimum conditions for a given operation. In order to obtain the optimum cutting conditions (Jang *et al.*, 1992), machining troubles such as chatter vibration (Minis *et al.*, 1990; Kasahara, 1992) and cutting edge failure (Moriwaki, 1984) must also be predicted analytically, and the conditions should be optimised while avoiding the machining troubles and minimising the evaluation function of machining economics under some practical constraints (Evans, 1987; Jelty, 1984).

This need for the prediction and the monitoring of the tool state under different conditions led to the development of different methods for metal modelling during steady state or dynamic machining with new or worn cutting edges. The following section gives a brief presentation and discussion of different methods used for tool wear prediction or monitoring. These methods are generally based upon pattern recognition of the measured signals and/or a theoretical backgrounds. Discussion of the limitation of these methods highlights the importance of modelling of metal machining to answer practical problems.

2.3. TOOL WEAR AND TOOL CONDITION MONITORING

It is well known, in actual tool wear, that several different wear mechanisms, as reported in Chapter 1, such as adhesion, abrasion, oxidation, diffusion, fatigue, fracture and superficial plastic flow can operate simultaneously in a given situation. Determining the dominant mechanism is always a problem. No matter what the tool wear mechanism is, parameters such as force, vibration or temperature etc... that can

be related directly or indirectly to tool wear should be predicted or monitored as controlling factors to determine the wear rate and machine performance.

A cutting tool is said to have failed when it no longer performs its function and the failure criterion is dependent on the surface quality required. In the present study tool failure refers to the time when the tool no longer fulfils the requirements according to surface finish and limited loads applied on the machine. Furthermore, tool life or useful tool life is defined as being the time during which the tool failure has not yet occurred. The useful tool life depends on the optimisation criterion and is therefore determined by tool failure. While the state and the geometry of the cutting edge are important factors which influence the tool life (Rubenstein, 1976), it is known that the tool wear is one of the most important factors limiting the useful tool life by weakening the cutting edge, leading to chatter conditions and affecting the quality of the surface finish; and henceforth different direct and indirect methods were developed over the last decades to monitor tool wear (Tipton, 1982; Tlusty *et al.*, 1983).

Direct tool wear methods are based upon a measurements of the actual wear on the cutting edge by using a stylus, a microscope or profile projector or by measuring the radioactivity levels when using coated tools with radioactive isotopes (Jetly *et al.*, 1987). While direct methods are more accurate than indirect methods, they are not of practical use because the machining has to be interrupted for wear measurements. In contrast, indirect methods are more suitable for numerically controlled machines because it can be possible to monitor the tool wear while the machining is still in progress.

Indirect methods use different signals such as the acoustic emission, the cutting forces, cut surface roughness, input power or current, temperature of the tool or the chip and vibration measures to indirectly determine the wear affecting the cutting edge.

Acoustic emission (AE) signals (Moriwaki, 1980; Yee *et al.*, 1986) of the cutting process showed a large amplitude when the tool failure takes place. Uehara (1984) and Inasaki *et al.* (1987) observed, however, that the influence of the work material on the power of the AE signals is very pronounced whereas the influence of the tool wear on the pattern of the power spectra is not conspicuous. Although the AE methods show a dependency upon the cutting conditions and the tool wear, the signals are very sensitive to the work material and moreover, the use of such signals presents difficulties due to the need for development of appropriate filtering techniques and algorithms to separate signals from the background noise generated in the metal working process.

Furthermore, Weller *et al.* (1969) reported upon the development of a sensor based on the analysis of the sound generated from a worn cutting tool. Concentrating on two band–widths of 0–4kHz and 4–8kHz, they found the energy contained in the former did not change appreciably with the progression of the tool flank wear, though that contained in the latter was observed to increase substantially. However, the ratio between the energy of profiles (energy contained in 4–8kHz / energy contained in 0–4kHz) was observed to increase with the tool wear. While analysis of the cutting sound (Yamazaki *et al.*,1974) showed that the frequency of the peak amplitude, which appeared in the vicinity of the resonant frequency of the cutting system (10–11kHz), decreased monotonously with an increase of the flank wear.

The major disadvantage of the sound based sensors is that they are very sensitive to the environment of the cutting process as well as to the sound due to the neighbouring machines.

Matsuchima *et al.* (1982) monitored the spindle motor current and used it to detect tool breakage. They found that the tool breakage caused unusual variation of the cutting torque, which they calculated using the spindle motor current and the spindle speed. It was found that tool breakage is characterised by a small decrease of the signal due to idle cutting revolutions before a sudden increase in the current. These findings were in agreement with those of Tlusty & Andrews (1983) who sensed the current, voltage and rotational speed of the spindle drive. These measures were used to calculate the cutting power and torque and by subtracting from the total torque the initial torque corresponding to the idling regime. the net torque is obtained and was reported to provide indications of tool wear and breakage.

The basic limitations of the power / torque techniques are that firstly, torque (power) increments due to tool wear are likely to be small and so difficult to detect, secondly the increment (Altintas, 1992) may not be easily separable from those due to other events, e.g. encountering hard spots in the workpiece material.

As the tool wears the contact area between the tool and the workpiece increases which tends to increase the cutting forces of the machining process. It has been stated by Ridley (1982) that for each 0.1mm width of wear land, the tangential force increases typically by 10%, the feed force by 25% and the passive force by 30%. Taraman *et al.* (1974) and Wolf *et al.* (1981) used the increase of the cutting force with the increase of the contact between the tool and the workpiece to monitor the tool wear. This relationship is not as simple as first appears, as, while the cutting forces are sensitive to

tool wear they are also sensitive to changes and variations in the cutting conditions, tool geometry, tool and workpiece material. To overcome the influence of some unneeded parameters, some workers (Mackinnon *et al.*, 1986; Goforth *et al.*, 1983) tried to use the ratio between the components of the machining force instead of their amplitudes. This technique presents same difficulties in tool wear prediction as the cutting conditions and changes in the tool geometry lead to different tendencies in variations of the machining forces ratio.

Similar to the effect of the tool wear upon the machining force components, the amplitude of vibration is also related to the state of the cutting tool. Martin *et al.* (1974) and Bhaoyal (1988) correlated the vertical vibration of a cutting tool and tool flank wear in the turning operation. Martin's experimental method involved the recording of the vibration signal received from an accelerometer mounted on the upper surface of the tool, whilst cutting two types of work material at various cutting speeds, feed rates and wear levels. They found that the majority of the power is centred around 2.5kHz, which corresponds to the fundamental frequency of the tool–holder. The increase of the power around this frequency was shown to increase linearly with the tool flank wear.

Beside their dependency upon the cutting conditions, the cutting forces change with the tool wear with a time delay relatively important compared to the time of tool failure. However, the vibration signals are more sensitive to any changes in the machining process and can detect tool failure within a reasonable time nonetheless their sensitivity is also affected by the machine structure and the non-homogeneity of the cut material. These two limit cases in sensitivity between the turning forces and the vibration led to consider the effect of tool geometry and cutting conditions not only on one of these signals but on both signals in the time domain (Yellowley *et al.*, 1987) as well as in the

frequency domain (Tomita *et al.*, 1988). The time domain analysis does not provide useful information since in the analysis the effects of the machine and tool structure is not singled out as is the case for the frequency domain analysis (Barker *et al.*, 1993; Lee *et al.*, 1989).

Rao (1986) used the spectral analysis of both the cutting force and the amplitude of the tool vibration in order to have better and more useful information about tool wear. His analysis led to the definition of a 'wear index' which was a ratio between the force amplitude and the amplitude of the tool vibration at the tool–holder natural frequency. The experimental data showed a linear relationship between the defined wear index and the average flank wear of the cutting tool and that this ratio is largely independent of the cutting process variables.

Examining these conclusions, it can be summed up that monitoring the amplitude of the dynamic stiffness at the first frequency of the tool–tool holder system leads to more accurate presentation of the state of the cutting edge. However, when different cutting tool geometry is used, experimental results (Taibi *et al.*, 1990) show that the natural frequency of the system can be influenced by the tool wear. Therefore, monitoring the tool wear by measuring of either the inertance (Taibi *et al.*) or the dynamic stiffness (Rao) amplitude at the natural frequency of the tool–tool holder will lead to incorrect decisions.

From the brief discussion above it is seen that, with the development of automation in manufacturing, in–process monitoring of tool failure has become more important than ever before and that, up to now, a number of methods have been developed to cover this need. It has been found that a number of factors are correlated with the condition of the tool, such as forces, temperature (Venuvinod *et al.*, 1990; Kannatez–Asibu,

1985), vibration and acoustic emission etc... All these methods are based upon the experimental changes in the patterns with tool wear and therefore, it is impossible to set the threshold for detecting tool failure due to the changes in cutting conditions including tool geometry and machining parameters, i.e. cutting conditions, tool and workpiece materials. It is necessary to develop a wear criteria which relates the level of variation of a specified parameter to the acceptable tool wear and which will be able to change the level of the defined parameter according to changes in either cutting conditions or tool geometry. This updating criteria can only be possible when the changes in the monitored parameter are based upon theoretical modelling of the cutting process.

As an alternative approach, during the last two decades, attempts have been also made to apply control theory especially in the study of turning, milling and drilling machining operations (Freidman, 1963; Koren, 1979; Weston *et al.*, 1989). The basic assumptions which open the door of metal cutting research to control theory are associated with how to define the tool motion during machining. In stead of using the cutting parameters of depth of cut and feed, another two equivalent cutting parameters of width of cut and chip thickness are introduced.

Based on the control approach, Nachtigal & Cook (1970) first demonstrated the applicability of an active control scheme to a turning operation. The designed controller consisted of two hydraulic chambers and a servovalve. Based on the detected force and torque signals, the controller actuated the tool tip to compensate the tool displacement from its dynamic equilibrium position. Difficulties, however, were met during the experimental work. Since then, whenever control theory is applied, the following two assumptions are made:

– The tool motion occurs only in the direction of the uncut chip thickness.

– The dynamic characteristics of the tool motion at every point along the width of cut is identical.

Because of these two assumptions, the cutting process can be described by the loop gains in the system model development (Fig. 2.1). The regenerative mechanism in the machining process, in almost all previous work as introduced by Tobias (1965), is treated as a positive time–delay feedback path. The delay time is equal to the rotational speed of the spindle for the turning process. Usually to describe a machining system in terms of control theory (Fig. 2.1. and Fig. 2.8), there is a need for developing dynamic equations for the dynamic cutting conditions as input, dynamic cutting force and dynamic effect of the machine structure. Applying therefore control theory in the metal cutting process relies on the accuracy of the theoretical prediction of the cutting process it self in relation to the cutting conditions and the machine in use. This forms the main reasons for limiting the development of machining control. Thus; a need is arising for more accurate and complete theoretical modelling of the machining process. This can be achieved by considering the mean values of the measured parameters (forces, temperature...) in steady state conditions or by considering the dynamic variations of these parameters during dynamic machining.

2.4. METAL REMOVING THEORIES

Since 1942, different models have been developed to analyse the cutting process in response to the input of independent parameters such as depth of cut, feed and cutting speed. These models aim to predict the cutting forces and/or the quality of the turned surfaces under different conditions. The former informations are used in machine tool design while the latter is directly related to the productivity of the machine and the

process it self. The metal cutting models can be grouped into steady state or dynamic models. The steady state models are concerned with the cutting process at low frequency, theoretically at 0Hz whereas the dynamic model introduce the effect of the oscillations in the dynamic conditions upon the controlled parameters. The following sections provide a general discussion of the models developed for both steady state and dynamic turning and highlights the range of their validity together with their limitation.

2.4.1. Steady state metal machining

The first analysis providing the shear angle solution was developed by Ernst & Merchant (1941). In their analysis the tool was assumed to be perfectly sharp and the chip was assumed to act as a rigid body which is held in equilibrium by the action of a resultant force transmitted across the shear plane and the chip–tool interface (Fig. 2.2). Ernst *at al.* (1941, 1945) supported the thin shear zone model whereby the geometry of the cutting process was specified in terms of one independent angle, namely rake angle α and two dependent angles, namely shear angle ϕ and friction angle along the rake of the cutting tool (Fig. 2.3). While the scale factor of this model was expressed in terms of two independent parameters, namely undeformed chip thickness S_0 and width of cut w, and one dependent parameter, namely the mean shear stress k along the shear plane. Based on the assumption of minimum energy, the shear angle was expressed as:

$$\phi = \frac{\pi}{4} - \frac{1}{2}(\beta - \alpha) \qquad (2.1)$$

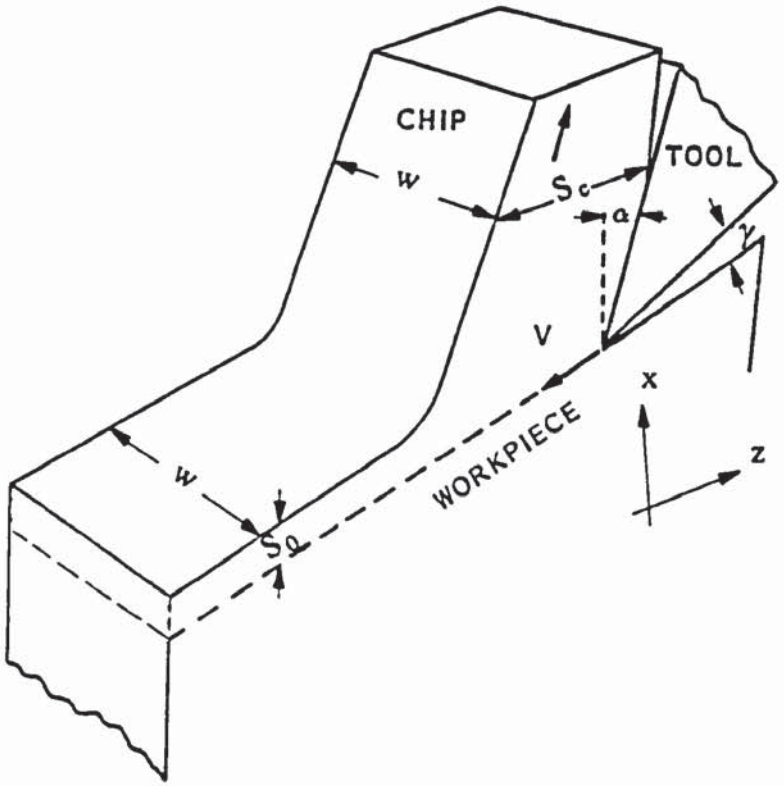

Fig. 2.2 Orthogonal model for cutting process

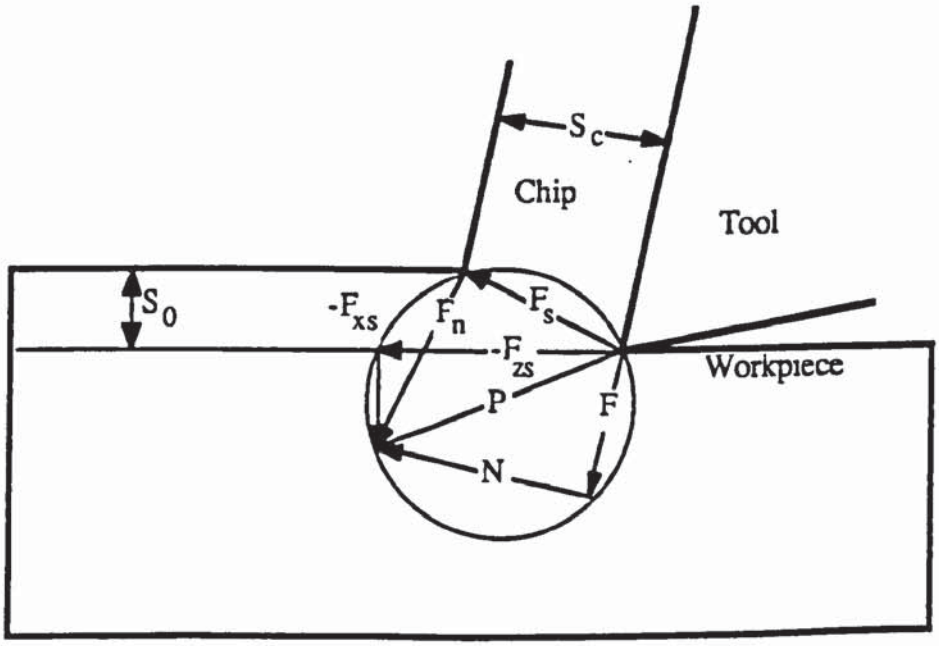

Fig. 2.3 Configuration of steady state machining process

In contrast to the assumption of the thin shear angle of this model, Okushima *et al.* (1961) suggested a cutting model considering a thick deformation zone. These considerations were further investigated by Bitans *et al.* (1965) and it was showed that under different machining conditions the deformation approximates to one or other of these shear models. After examining motion picture film and photo–micrographic evidence (Bitans *et al.*, 1965), it was concluded that, especially when the metal is in an annealed state, the thick model is more appropriate at low cutting speed, whereas at high cutting speed region the situation approaches the thin–zone model.

Lee & Shaffer (1951), adopting the same hypothesis and considering a portion of the chip as an ideal plastic solid (Fig. 2.4.a), have used the slip line field theory to develop an other shear relationship:

$$\phi = \frac{\pi}{4} - (\beta - \alpha) \qquad (2.2)$$

(2.1) and (2.2) are both based upon the assumption of a plane of maximum shear stress, the mean shear flow stress of the cut material is assumed constant (absence of the strain hardening, strain rate and temperature effect) and the stress along the tool face is uniformly distributed.

In a second analysis, Lee & Shaffer (1951) introduced the effect of a small built–up edge (B.U.E) as represented by a circular arc as shown in Fig. 2.4.b. Their slip line field consisted of two parts, a rigid region ABC and a region of varying stress ADB where the lines of maximum shear stress consisted of radial lines and circular area. Again, by applying Mohr's circle analysis for both regions a relation for the shear angle introducing the effect of the B.U.E was derived as:

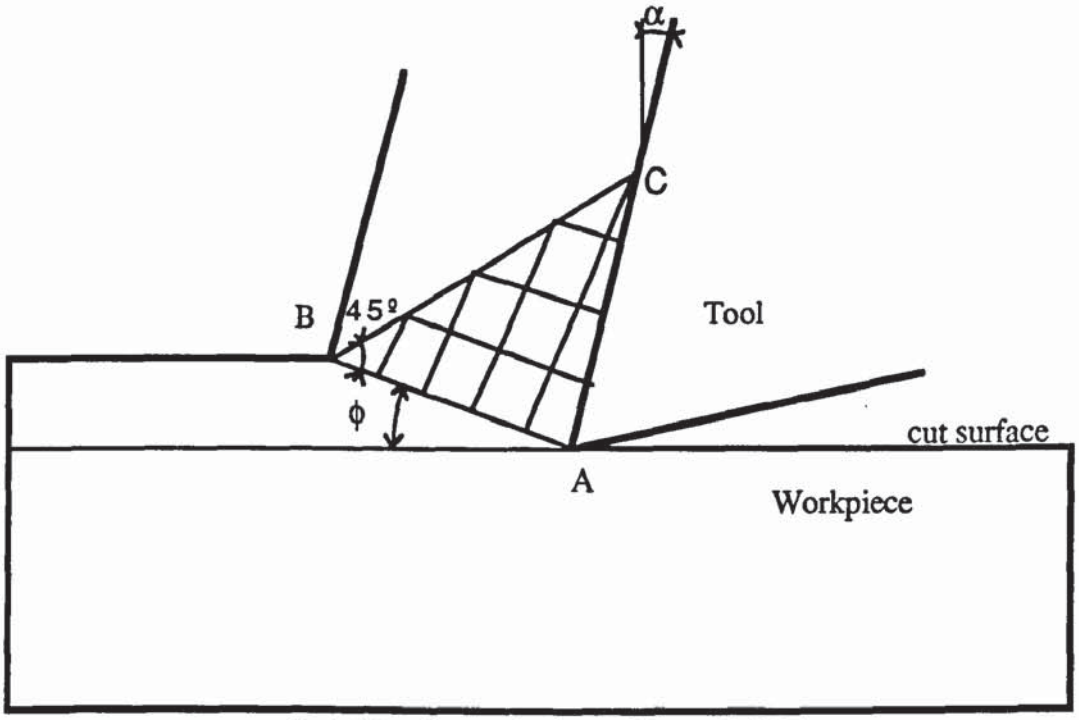

(a) Slip–line solution without B.U.E.

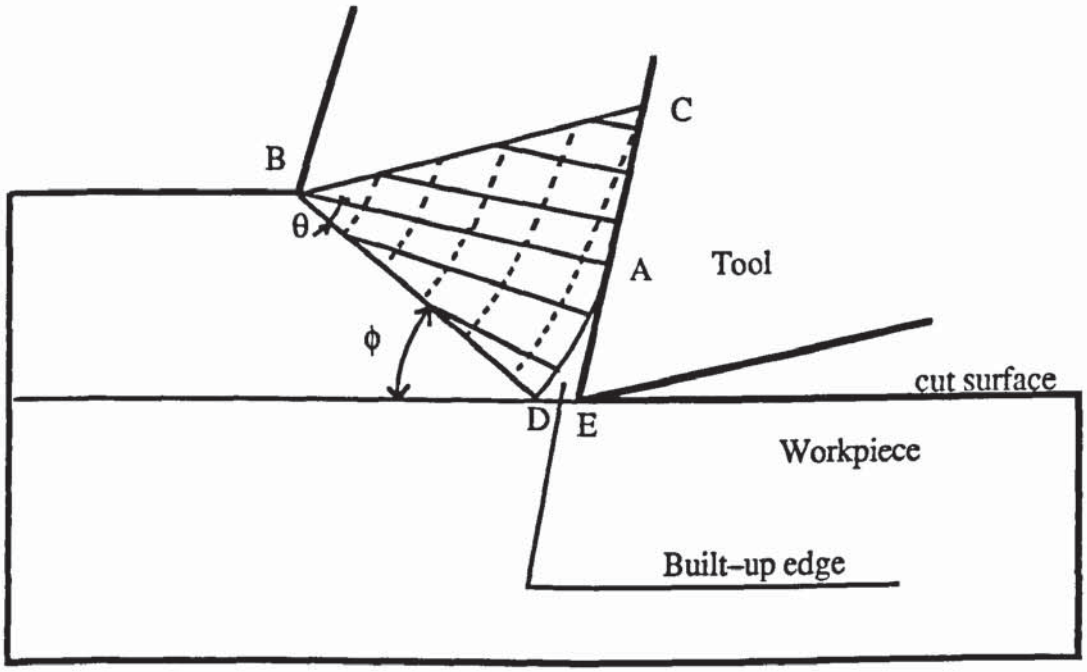

(b) Slip–line solution with B.U.E.

Fig. 2.4 Ideal plastic solution for stress field at the tool point
(After Lee and Shaffer)

$$\phi = \frac{\pi}{4} + \theta - (\beta - \alpha) \qquad (2.3)$$

θ is the angle defining the size of the B.U.E.

Although (2.1) to (2.3) show the dependence of the shear angle ϕ on the mean friction angle β, they do not have the ability to predict the cutting state because the tool face 'friction' does not follow the simple Coulomb's law, and cannot be predicted from the usual friction experiments (Bailey, 1975; Finnie, 1956).

(2.3) has the advantage of introducing the effect of the B.U.E as an increasing factor of the rake angle. However, Slip line analysis (Lee & Shaffer, 1951) for rigid, perfectly plastic material has the same difficulties of predicting and describing the cutting process (Shi *et al.*, 1991), since the slip line solutions cannot be constructed unless the frictional stress distribution along the tool face is specified in advance.

To analyse the chip formation process as the tool nears the end of the workpiece in planing operations, Klamecki (1985) adopted the minimum energy model for chip formation and assumed the work material shear strength to vary linearly with the amount of deformation imposed by the cutting conditions. The length of the shear plane was also supposed to depend upon the depth of cut and the distance from the cutting edge to the end of the workpiece. Despite the good agreement between the predicted and the measured results, this analysis did not include the effect of the friction upon the shear angle since the cutting tests were concerned with very low cutting speeds (maximum of 30 m/min). In these conditions of low speeds, sufficient time exists for the generation of surface contaminant oxide films on the underside of the chip which prevent adhesion at the chip–tool interface and allows conditions of

sliding friction to exist as was introduced earlier by Zorev (1966). The friction on the tool face can be separated into sticking friction where the frictional stress is constant and sliding friction where the coefficient of friction is constant (Wallace, 1964) which explains the findings of Klamecki (1985).

In parallel to previous theories (Merchant, 1945), Oxley (1984) tried to turn the cutting theory from descriptive to predictive form by including the mutual dependency between the phenomena in the shear plane and along the tool face. He calculated the frictional stress τ_s on the tool face for an arbitrary value of the shear angle through the analysis in the shear zone, in which the theory of velocity–modified temperature is considered, the material flow stress properties and the iteration of temperature calculation are combined. For the same value of the shear angle, the frictional stress τ' due to the contact between the chip and the tool rake was independently obtained and the value of the shear angle that respects the condition of $\tau_s = \tau'$ was regarded as the solution, and the cutting forces, stress and temperature are thereafter determined.

Similar analysis of the temperature in the secondary deformation zone was carried out by Boothroyd (1963). In this analysis it was assumed that the heat source introduced by the friction resistance in the secondary shear zone is plane heat source of uniform strength. This is to say that heat is only flowing into the workpiece by conduction. Prediction of the developed model showed good agreement with experimental results. However, as the cutting speed or feed are increased, the heat is generated over a wide zone (Rapier, 1954) which affects the heat transfer into the workpiece.

It was reported that the theory of Oxley can be convenient for practical use even though some empirical equations and considerations are involved which makes it very limited such as that this analysis does not include the equivalent friction parallel to the rake of

the tool. The above results are based on the assumption of constant friction parallel to the rake of the tool. Bailey (1975) concluded that the apparent linear relationships between ϕ and $(\beta - \alpha)$ observed in previous experimental works are a consequence of the method of presentation of the results and cannot be used to describe the effect of the friction angle on the shear angle.

In contrast to previous studies, Bailey (1975) suggested that the friction depends on the tool rake angle and upon the cutting conditions. It has been generally observed (Zorev, 1966; Eggleston, 1959) that an increase in the tool rake angle at constant cutting speed produces a decrease in the mean coefficient of friction and in the resulting cutting forces. Zorev (1966) observed that the mean friction angle depends also on the depth of cut because of the presence of the forces on the tool nose. Nonetheless when the tool forces are corrected for the presence of the tool nose forces the mean friction angle becomes independent of the depth of cut. However, at small depths of cut, a B.U.E tends to develop on the rake of the tool which changes the effective rake and henceforth affects the calculated values of the friction angle.

Dimensional analysis was applied by Hsu (1967) to include the effect of the cutting conditions upon the shear and the friction angles. This technique provided good results when it was used to analyse the experimental results of shaping aluminium alloy with high speed steel tools with restricted contact length. Based on the thin shear plane solution, Nigm *et al.* (1977) successfully used this technique to formulate relationships relating the cutting forces ratio and chip thickness ratio to the cutting conditions and rake angle of the tool. Analysis of the experimental forces results led to determine an explicit relationship for the existence of the B.U.E. and therefore providing the range of applicability of the model.

This analysis has the advantage of expressing the cutting parameters in terms of the controllable parameters such as rake angle α, uncut chip thickness S_0 and cutting speed V. Nevertheless, the effect of the size of the tool was not included and no attempts were made to introduce the effect of the forces around the tool nose despite the fact that a component of the cutting force that is not contributing to the chip removal (Nigm *et al.*, 1977) was felt to exist in the experimental results.

The effect of the tool nose was introduced by Masuko (1953) as an indentation and by Albrecht (1960) as a ploughing effect around the cutting tool nose (Fig. 2.5). This concept was suggested by the fact that when measured forces are plotted versus the undeformed chip thickness their intercepts at $S_0 = 0$ are not nil. The analysis of Albrecht showed that the friction coefficient remains independent of the rake angle when the ploughing components are subtracted from the experimental force components. Although this analysis is promising, no further details were reported about the effect of the different cutting conditions and the clearance angle of the tool. Beside, some major assumptions made by Albrecht and by Masuko such as:

– The friction coefficient along the rake is independent of the undeformed chip thickness.
– The ploughing component bisects the included angle.

are questionable and can be shown to be incorrect from experimental investigation (Bailey, 1975; Rubenstein, 1985). Moreover, their analysis supposed the total ploughing force is only applied on the tool nose instead of acting on the whole contact area between the tool and the workpiece. More details were presented by Rubenstein (1985) and Liu *et al.* (1976a) about the deformation mechanism of the workpiece

Fig. 2.5 Flow of workpiece material around tool nose (Enahoro & Oxley, 1966).

material in contact with the cutting edge as will be discussed throughout the modelling in Chapter 3.

The ploughing mechanism was confirmed by metallurgical analysis of the cut surface carried out by Liu *et al.* (1976). Their study revealed a size effect of the depth of cut on the conditions of the sublayer in machined surface, namely the apparent strain energy density per unit volume of metal removal increases as the depth of cut increases. Lau *et al.* (1972) showed that the depth and the degree of the surface hardening increase, on one hand, with the increase in the uncut chip thickness or the flank wear level and, on the other hand, with a decrease in the rake angle, clearance angle and cutting speed.

When the cutting edge is not affected by flank wear, the ploughing components are comparatively smaller than the forces due to shearing process. This explains the reasons why the ploughing mechanism is not considered in steady state models. However, as the flank wear increases the effect of the secondary face of the tool is increased accordingly. This is usually interpretated as a rubbing effect along the contact between the workpiece and the flank of the tool rather than being interpretated as the ploughing mechanism. However, as experimental results (Ridly, 1982) show the feed force is more sensitive to flank wear than the cutting force it is therefore understandable that there is a deformation of the material in the feed direction. This deformation results in an additional feed force by resistance of the work material to deformations and in a tangential or vertical force introduced by friction (Lau & Rubenstein, 1972). The ploughing mechanism has received more attention in dynamic modelling of the cutting process as the forces along the flank of the tool are affecting the stability of the cutting process as discussed in what follows.

2.4.2. Dynamic metal machining

At an early stage of research into the problem of steady state and dynamic machining, the cutting mechanics received most attention (Merchant, 1945; Arnold, 1946). Chip formation, built–up edge, tool geometry with and without wear effect were thought to be the main factors causing the oscillatory nature of the cutting force (Tobias, 1956). A major contribution was made in the 1940's by Arnold (1946) who proposed that the drop in the cutting force with increase in the cutting speed is the cause for self–excited vibration.

On the other hand, it was also recognised that the most powerful sources of self–excitation during machining are not associated with the cutting mechanics. These are

rather associated with the structural dynamics of the machine tool and the feedback between subsequent cuts, namely, mode coupling and regeneration (Tobias, 1956; Merritt, 1956). In the meantime, the two aspects were combined, when dealing with chatter analysis. A machining operation is assumed to have two subsystems, i.e., the cutting process and the machine tool structure, and a feedback mechanism which forms the link between the cutting process and the machine tool structure (Fig. 2.1).

While Arnold (1951) and Hahn *et al.* (1953) introduced physical interpretation of the chatter based upon descriptive hypothesis, Tobias *et al.* (1956) formulated the response of the dynamic cutting process in chatter using an incremental force model. Their analysis was limited to the determination of the variation of the dynamic cutting force when small variations of the one of the cutting conditions takes place namely chip thickness S_0, penetration rate of the cutting tool representing the depth of deformation of work material around tool nose. The variation of the rotational speed of the spindle was neglected. The incremental coefficient corresponding to the variation of the turning force to the tool penetration rate was found to be positive from regenerative chatter tests which indicated that the dynamic cutting force is leading the chip thickness variation. This led to the conclusion that the cutting process is by its nature stable. This conclusion is in contradiction with the results of Doi *et al.* (1956) showing that the cutting force lags rather than leads the chip thickness variation.

These results are based upon linear analysis of the cutting process and do not include the dependency between different parameters. A model based on dimensional analysis was developed by Nigm *et al.* (1972a, 1972b, 1977a, 1977b) and the predicted results were compared to the findings of previous workers as well as to experimental results. Extensive experimental investigations were conducted over a wide range of cutting conditions using a mild steel work material. The shear angle oscillations were analysed

by using a high speed camera for both wave generation and wave removing processes. The former mode was obtained by forcing the tool to vibrate in the feed direction during one workpiece revolution.

It was shown that the shear angle responds to the variation of the cutting conditions and that its oscillations together with the dynamic forces are not in phase with the chip thickness undulation. The experimental results (Nigm *et al.*, 1977a) supported the theoretical analysis conducted by Das & Tobias (1967) introducing a new configuration for the dynamic cutting process. The dynamic coefficients of the model were derived from steady state cutting tests (Nigm *et al.*, 1972a, 1972b, 1977b) that led to the determination of the threshold of the cutting stability when the tool is assumed to have one degree of freedom in the feed direction.

According to the above discussions, some important facts regarding the causes of chatter vibration are highlighted, for example, the falling characteristic of the cutting force with respect to the cutting speed and the shear angle oscillations in response to small variations in cutting conditions. Moreover, these studies, based upon the Merchant cutting configuration, consider the contact between the tool and the work material is only along the rake of the tool. Recent studies (Marui *et al.*, 1983a, 1983b) have shown in more details the effect of the tool–work contact along the flank and the relief faces of the tool during metal machining.

The influence of the configuration of the cutting edge as well as that of the cutting conditions on the primary chatter vibration were investigated by Marui *et al.* (1983a, 1983b). Theoretical and experimental results were examined to clarify the energy supplying the mechanism in the primary chatter vibration by including the effect of the tool–work interference along the tool relief face. The workpiece was cut so as to have a

continuous variation of the cutting width which increases by about 1.5 mm/m of the cutting distance (Fig. 2.6). Straight tools with a varying relief angle and bending tools (Fig. 2.6) with a varying cutting height were used to analyse the effect of the natural frequency of the tool and the effect of the tool–work interference on the occurrence of chatter vibration in the turning process.

The interference cutting force of the shank of the tool was defined as the extrapolated cutting force to zero cutting depth. It was observed, on the one hand, that the amplitude of chatter vibration increases and tends to a stable value which is higher, the higher the cutting speed. On the other hand, the smaller the relief angle the larger the rate of increase of the chatter vibration amplitude with the cutting width. The latter observation suggested that the stability limit is a function of the interference force which introduces a negative damping which may be large enough to overcome the positive damping of the cutting system.

Kaneto *et al.* (1984) used a model based on the interference force to explain the phase lag between the horizontal and the vertical displacement as well as that between the tool displacement and the cutting forces (Fig. 2.7.a and Fig. 2.7.b). Throughout the experimental tests the workpiece was described as a two degree of freedom system:

– In the vertical direction (z) and in the horizontal direction (x), experimental results on the motion of a workpiece showed that the vertical displacement when plotted versus the horizontal displacement draws a counter-clockwise loop, whose average slope was positive (Fig. 2.7.a). The vertical motion is therefore slightly lagging behind the horizontal motion.

Fig. 2.6. Cutting configuration (Marui *et al.*, 1983).

Fig. 2.7.a Behaviour of the workpiece motion during self–excited vibration (Kaneto, 1984).

Fig. 2.7.b Behaviour of the horizontal displacement versus feed force (Kaneto, 1984).

– The horizontal component of the cutting force draws a clockwise loop with a negative slope when plotted versus the horizontal displacement (Fig. 2.7.b). The above results suggested that the cutting force is larger when the workpiece moves away from the tool than that exerted when the motion happens in the opposite direction and therefore this self–excitation mechanism, in complete accordance with the descriptive explanation of Arnold (1946), causes the vibration to be maintained.

To explain these experimental results an analytical model was developed (Kaneto *et al.*, 1984) whereby the vibratory motion of the workpiece was represented by two dashpots one in each direction. Solution of the resulting equations of motion by assuming the cutting forces in the horizontal and vertical direction to be proportional to the cutting area revealed that the adopted model correlated well with the cutting force displacement behaviour observed experimentally. Furthermore, the vertical displacement versus the horizontal one showed a positive slope as observed experimentally. However, the looping behaviour was not predicted by the model. It is worth mentioning here, that the introduction of a resistive horizontal force (corresponding to a ploughing force) which was taken as inversely proportional to the cutting speed and proportional to the relative velocity between the tool and the work allowed the experimentally observed counter-clockwise looping behaviour to be predicted when the vertical displacement was plotted versus the horizontal displacement. The introduction of this resistive force as modelled by Kaneto was used also by Kasahara *et al.* (1992) to explain the phase between the inner and the outer modulation of the cut surface and the cut chip respectively during chatter conditions.

More recently, Wu & Liu (1985a, 1985b) developed a dynamic model for an orthogonal turning operation from a pseudo–static geometric configuration of the cutting process using the steady state Merchant (1945) approach. They assumed that

the mean coefficient of friction at the tool rake–chip contact area varies exponentially with the cutting speed and that the length of the shear plane is constant. They further assumed the effect of the tool nose and flank interference with the workpiece to be represented by a force proportional to the tool vibrational velocity and inversely proportional to the cutting speed as assumed by Kaneto (1984). This model suggested that the rubbing action of the chip on the tool rake face may cause a negative damping force to excite the primary chatter vibrations and that the interference of the workpiece material near the tool nose region introduces a positive damping to limit the amplitude of chatter.

These results of Wu *et al.* (1985a, 1985b) seem to be in contradiction with the work of Marui *et al.* (1983b) who considered the primary chatter vibrational energy to be supplied by the frictional force acting on the tool nose and flank–workpiece contact area, and that the tool rake–chip rubbing action provides a stabilising effect.

Furthermore, Liu *et al.* (1985) have shown experimentally that the stability of an orthogonal process may be significantly enhanced by controlling the tool rake and the flank angles during the cutting process. On the other hand, increasing the flank angle was found to decrease the stability range. These results seem to be at variance of the finding of Cook (1959) and Marui *et al.* (1983) stating respectively that flank rubbing action can excite vibration for a single degree of freedom system while for two degrees of freedom systems the rubbing action stabilises the motion.

In a recent work, Rahman (1986, 1988) carried out a comparison between different methods for the detection of chatter vibration. He concluded that the best method for machine tool chatter detection is the horizontal deflection method rather than the methods using changes in the noise level and those which use cutting force

components. According to Rahman, The cutting force components method detect chatter onset after chatter marks have occurred in the cutting operation, while the horizontal deflection method detect the chatter onset before the chatter marks begin to be seen. Moreover, Rahman noticed that while the depth of cut increases the phase difference, between the horizontal deflection and the radial component of the cutting force, increases. This was given then as a main reason leading to chatter vibrations. This method can, however, be only applied to workpieces with small diameters where the workpiece deflection can be very sensitive to chatter occurrence and therefore it only deals with low cutting speed range. Moreover, the above results did not include the discussion of the effect of different cutting conditions and was confined to only one set of controllable cutting parameters.

An attempt was made by Hinduja *et al.* (1985) and Arsecularatne *et al.* (1992) to develop a direct search procedure for optimum cutting conditions. This procedure is based upon the so called w–S_0 (depth–feed) diagram. The w–S_0 plane is approximated to a quadrilateral, divided into a 20 x 20 grid and split into two regions of feasible and non–feasible regions. The separation line between the above–mentioned regions was determined by a set of constraints based upon limitations in the machine power and allowable cutting conditions. Constraints based on the machine instability was also introduced by Arsecularatne *et al.*. The applicability of the results of Hinduja was limited because in the force prediction an empirical force equation was used. This force formulation using equivalent chip thickness provides a good estimation of the cutting forces but is not suitable for the feed and radial force. Moreover, the dynamic instability used by Arsecularatne *et al.* is based upon the radial deflection of the workpiece as suggested by Rahman (1988). Despite of the fact that this method considered the effect of changes in workpiece geometry and henceforth changes in its flexibility, this model of chatter vibration is questionable since it is based on a two–

nodes beam model. Moreover, this criteria cannot be held valid, particularly in the case of turning workpieces with large diameter to length ratios. The modelling of the instability constraints was limited to the workpiece flexibility regardless of the effect of machine structure, tool post and tool geometry.

It is seen therefore that the development in cutting theory and in the prediction of chatter vibration is largely based, on one hand, upon the Merchant approach by adopting the thin shear angle solution and, on the other hand, upon the dynamic configuration developed by Das & Tobias (1967). This model will be discussed in more detail in Chapter 5. The shear angle oscillations due to dynamic cutting are shown to be of great importance in predicting dynamic machining forces.

The effect of the tool nose was analysed by Wu (1989) when the resultant force in the feed direction and resulting from the material deformation under the cutting edge was assumed to be proportional to the deformed volume of the work material. The vertical nose force was determined from the feed force by assuming a constant friction angle along the contact area. Theoretical predictions were compared to previously published data and showed good prediction of the dynamic force variation in both the feed and cutting direction. However, in this model, the friction coefficient along the flank was assumed constant and its values were determined from published data. Moreover, the derivation of the vertical force from the feed force was then made by neglecting the roundness of the cutting edge and by considering the tool flank parallel to the mean cutting direction.

Cutting theory to date has been concerned with analyses of the chip flow on the tool rake face using a perfectly sharp tool. Some efforts have been put forward to introduce the effect of the radius of the cutting edge. None of the existing theories have provided

an analytical formulation of the forces acting on the tool nose and the secondary edge of the cutting tool. Moreover, analytical formulation of these forces have to be developed to account for the flank wear effect.

During machining, the cutting tool is subjected to vibration due to variations in the dynamic cutting force induced by variations in the workpiece hardness and by the regenerative effect of the vibrational relative motion between the tool and the workpiece. In general, machining chatter is due to the interaction between the dynamics of the machine tool and the metal cutting process. The machine tool affects the machining process through its effect upon the cutting conditions, and in a general sense throughout its effect on the cutting configuration. In the above discussions, results of previous workers highlighted the effect of the forces along the secondary face of the tool but a lack of analytical formulation of these components led to controversial conclusions (Wu *et al.*, 1985b; Marui *et al.*, 1983b, Liu *et al.*, 1985). A model with detailed analytical formulation of the ploughing forces for new and worn tool is needed to describe dynamic turning. The dynamic modelling approach can be well understood by looking at the adaptive control modelling procedure. The adaptive control models show how the effect of different elements such as the cutting process and machine structure can be accounted for in a dynamic modelling. Therefore, the aim of the following section is not to provide a complete presentation of the type of adaptive control models but to show the general approach adopted in this field.

2.5. ASPECTS OF ADAPTIVE CONTROL

While much effort is made to develop theories for steady state as well as for the dynamic cutting process, mathematical modelling for adaptive control is carried out generally without paying attention to the cutting mechanism and models are constructed

based upon simple coefficients or constants introduced in the assumed forces or vibration expressions.

In the beginning of the adaptive control stage modelling of the cutting process (Friedman, 1963), the force controller was generally based on the assumption that the force is proportional to the instantaneous chip load (Koren, 1979) and therefore, the average resultant cutting force proportional to the normal chip load is expressed as:

$$F = \lambda (w S_0) \qquad (2.4)$$

Where λ is a proportionality coefficient.

Common sense dictates that the proportionality coefficient λ is a function of the workpiece material, tool geometry including wear effect, and cutting conditions. In order to obtain an estimation of the proportionality coefficient λ, a mathematical form to describe such a functional relation is necessary. A vast number of experimental tests were carried out throughout the past three decades to develop cutting force models from the estimation of λ.

Based upon the discussions through the modelling of the dynamic cutting process, one can see that, the general block diagram of machining should include the effect of the cutting process, the effect of the machine structure and effect of the regenerative mechanism treated usually as a positive time-delay feedback path (Fig. 2.8). The delay time is equal to the rotational speed of the spindle in the case of turning.

Several models based on the simple relationship (2.4) were developed for machining control and tool wear monitoring (Kegg, 1978; Matias *et al.*, 1980; Shield *et al.*, 1987;

Yee *et al.*, 1983). Some of these models proposed different forms of the basic monitoring equation by considering that the cutting force is not only a function of the chip thickness but also of the penetration rate and the cutting speed as first introduced by Tobias (1967). The incremental parameters were related to the cutting conditions and the tool geometry by including the wear effect on the rake and/or the flank of the cutting tool.

By employing a dynamometer or the thermal characteristics, the turning forces in terms of its three spatial components (feed, cutting and radial forces) are measured under given cutting conditions and specified tool geometries. Afterwards, a mathematical relationship is proposed to fit the experimental force data. However, the turning force relationships developed in such way are empirical in nature. In fact, it is relatively easy to find such empirical cutting force relationships in various cutting handbooks (Machinability data center, 1980). Upon examining these empirical relationships carefully, one finds wide ranges for constant terms in them, indicating the uncertainty

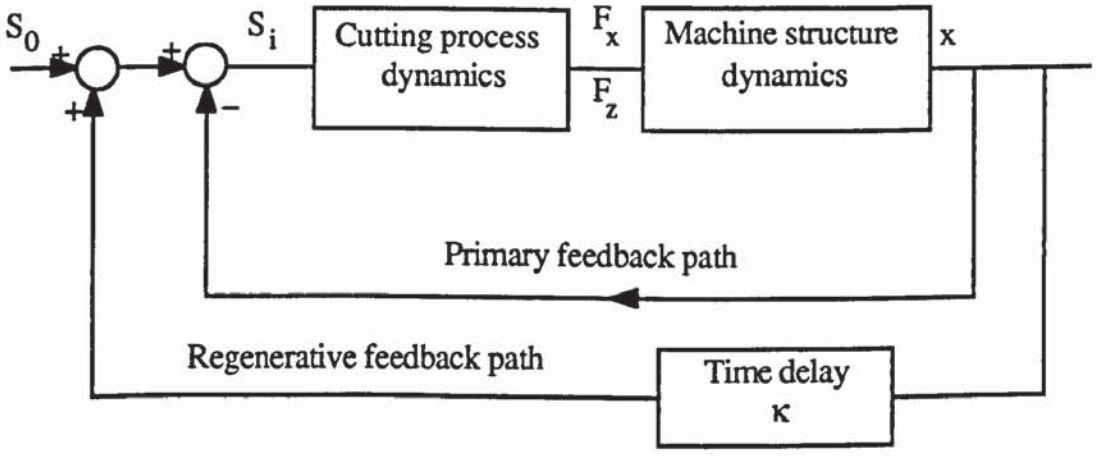

Fig. 2.8 General diagram block of machining for adaptive control systems

of the data in question. The reason for such uncertainties is because experimental data necessary to explain the cutting process in a mechanistic sense were not gathered in previous relationships developments. Therefore, empirical cutting force relationships are very incomplete and unreliable from the present point of view. It is impossible to fairly make cutting force or tool wear predictions because of the wide ranges for the constant terms in these models.

The major limitations in the application of the adaptive control model are related to the modelling of the cutting process. Therefore, if the adaptive control approach of machining process and mathematical modelling of turning based upon the dynamics of machining are met an important contribution to the turning control will be achieved. The present work aims to develop an analytical model of the turning process for the purpose of tool wear monitoring. This aim resulted from the need presented by turning development and the short comings of the published work as summarised below.

2.6. SUMMARY

In view of the previous literature survey, researchers have been actively working for decades on the solution of tool wear monitoring, self–excited vibration and, steady state and dynamic modelling of the turning process. The major short comings of many of these efforts are as follows:

– Efforts have been put forwards to introduce the effect of the radius of the cutting edge but, nonetheless, none of the existing theories have provided an analytical formulation of the forces acting on the tool nose and along the flank face of the tool. Moreover, detailed analytical analysis of the ploughing forces have yet to be developed for tools under different wear levels.

– Numerous researches were concerned with determining the cause of vibration in the machine tools. The presence of relative vibration between the tool and the workpiece reduces the tool life and leads to poor surface finish. Although considerable knowledge of the conditions likely to cause chatter has been attained, the relevant mechanism is not yet well understood. From the above discussions, it seems that, together with the cutting conditions, both the rake and the flank rubbing forces and tool geometry have a significant influence on the occurrence of chatter, nevertheless, none of the published methods have presented a detailed analytical analysis of the interference forces which led to controversial conclusions (Wu, 1985b; Marui, 1983b, Liu, 1985).

– Methods to obtain system parameter estimation are experimentally based, and no supporting analytical models have been well investigated. The results of experimental studies are difficult to extrapolate to different machining conditions.

In the light of the above discussion, it can be seen that there is a strong need for developing an analytical model for the turning process which can be used for tool wear monitoring. This represents the major aim of this thesis. This model will introduce the effect of the shearing process as well as the ploughing process together with the effect of the cutting tool geometry such as tool wear and the effect of chatter vibration. The coefficient for this model are determined from steady state data and will predict the steady state force and the dynamic force for different cutting conditions and cutting configurations when machining with new and worn cutting tools.

Chapter 3

TURNING PROCESS UNDER STEADY STATE CUTTING CONDITIONS

3.1. INTRODUCTION

The goal of metal machining research is to predict the quality of the machined surface and improve the accuracy of workpiece dimensions with minimum costs. To achieve this goal, more precise prediction is needed for both cutting edge conditions and relative oscillating behaviour of the tool to the machined surface. Previous investigations (Klamecki, 1985) showed that the metal removing mechanism is a dynamic process for which the governing parameters are strongly related to those of steady state cutting conditions. Owing to the difficulties encountered to determine dynamic coefficients from direct cutting tests (Tobias, 1965), dynamic turning is usually described by a different sets of coefficients called steady state coefficients and determined from a non-vibratory tests by considering the steady state components of turning force (Nigm *et al.*, 1977b; Klamecki, 1985). This steady state values are commonly taken as measured force components at 0Hz.

In this Chapter, a model for the turning process during steady state machining is developed. This steady state model considers the tool as a rigid body moving into the work material and takes into consideration the effect of both secondary shear zone, along the rake face of the tool, and material deformation around the tool edge and along flank face of the tool. The model is developed under the assumption of a thin shear

plane and is valid only when cutting under conditions where the chip is continuous and there is no built–up edge. Present experimental results conducted on tube and over a large range of cutting conditions is used to determine an explicit expressions of the dependent parameters, namely mean shear stress, mean equivalent–frictional angle along the rake, mean frictional angle along the flank, rake forces ratio, chip thickness ratio and depth of tool penetration, in terms of independent parameters, namely tool geometry, feed rate and cutting speed.

The developed model is thereafter used, on the one hand, to predict the cutting forces in turning for different sets of cutting conditions, different tool geometries, cutting configurations and work materials, and predicted forces are compared with both experimental results and published data for positive rake angle tools. On the other hand, beside its ability to predict the turning force components for positive rake angles, the present model also shows good agreement between theoretical and experimental turning forces when cutting with negative rake angle tools. The material of this Chapter is considered as a step towards the investigation of the dynamic turning process.

3.2. BACKGROUND TO MODEL DEVELOPMENT

Several researches with close examination of the structure of chip and workpiece (Shaw, 1984; Stevenson, 1992) showed that due to the complicated deformation process and its varieties, some simplifications must be made for an analytical approach of the mechanism of chip formation. It is now accepted that the chip formation process is a plastic shearing process and that the deformation is extremely localised. Basically, the chip formation process can be most easily explained by considering the two–dimensional simple case of "orthogonal cutting" in which a single cutting edge is held perpendicular to the relative motion between tool and workpiece (Fig. 2.2.). In

practice, actual cutting operations often involve a cutting edge which is inclined at some angle other than 90º to give "oblique cutting process", but the nature of chip formation is nevertheless similar in both cases.

A simplified model for the cutting process, as presented firstly by Merchant (1945) and supported by recent metal investigations (Boothroyd, 1983; Bayoumi, 1991), is represented in Fig. 2.3. This model considers the workpiece moving with a velocity V relative to the cutting tool which removes an undeformed chip thickness S_0 and producing a chip of thickness S_c by the shearing process along the shear plane. Consequentially, the metal moves as a rigid material until it reaches the shear surface where it is deformed by the shearing process and 'slides' thereafter along the tool face without additional deformation. Therefore, the actual chip formation process is simplified to a shearing process along the shear plane and to sliding friction phenomenon along the rake of the tool. Since this model was adopted by Merchant in 1942, enormous researches on metal cutting theory over the last 50 years have not much changed the basis of the machining modelling but have rather supported Merchant's model however simple its theoretical considerations . These studies showed that the main deformation in machining is caused by shear and accordingly the distribution of the dynamic shear stress within the workpiece material along the deformation zone is an essential component for better understanding and/or control of the machining process. However, this thin shear plane solution model is subject to serious shortcomings of which the most important are as follows:

– The cutting edge is assumed to be sharp.

– The shear deformation in the primary zone deformation is confined to occur within a narrow band that can be represented by a plane called the shear plane.

– The contact between the tool rake and the chip is represented by a friction defined as a mean value of the tool–chip friction coefficient which is represented by the ratio between the forces along and normal to the tool rake face.

3.2.1. Sharpness of cutting tools

An analysis of the tool edge conducted by Albrecht (1960) and by Boothroyd (1981) showed that tool sharpness varies from 0.005 to 0.03mm for high speed steel tools. When a sharp edge is considered, an infinite stress will develop along this edge and will lead to an elastic and plastic deformations to give a radius at the tip of the tool. In addition to the primary and the secondary deformation zones introduced by shearing process and the contact between chip and rake of the tool. A third deformation zone is introduced as a result of roundness of the cutting edge (Fig. 3.1.). The material deformation within the tertiary deformation zone will create additional forces, known as ploughing forces (Albrecht, 1960) or indentation (Masuko, 1953) forces, at the vicinity of the edge and along the contact between the cut surface and the flank of the tool. The deformation process around the tool tip is accordingly named, throughout this thesis, the ploughing process.

Several researchers have considered the effect of the tool size, or the radius of the cutting edge, but none of the published work has provided an analytical expression of the ploughing components of the turning force under steady state conditions and henceforth the mechanism of the flow of material around the edge is not fully understood. In this chapter an analytical expression of the steady state ploughing turning force components is developed based upon physical considerations and the

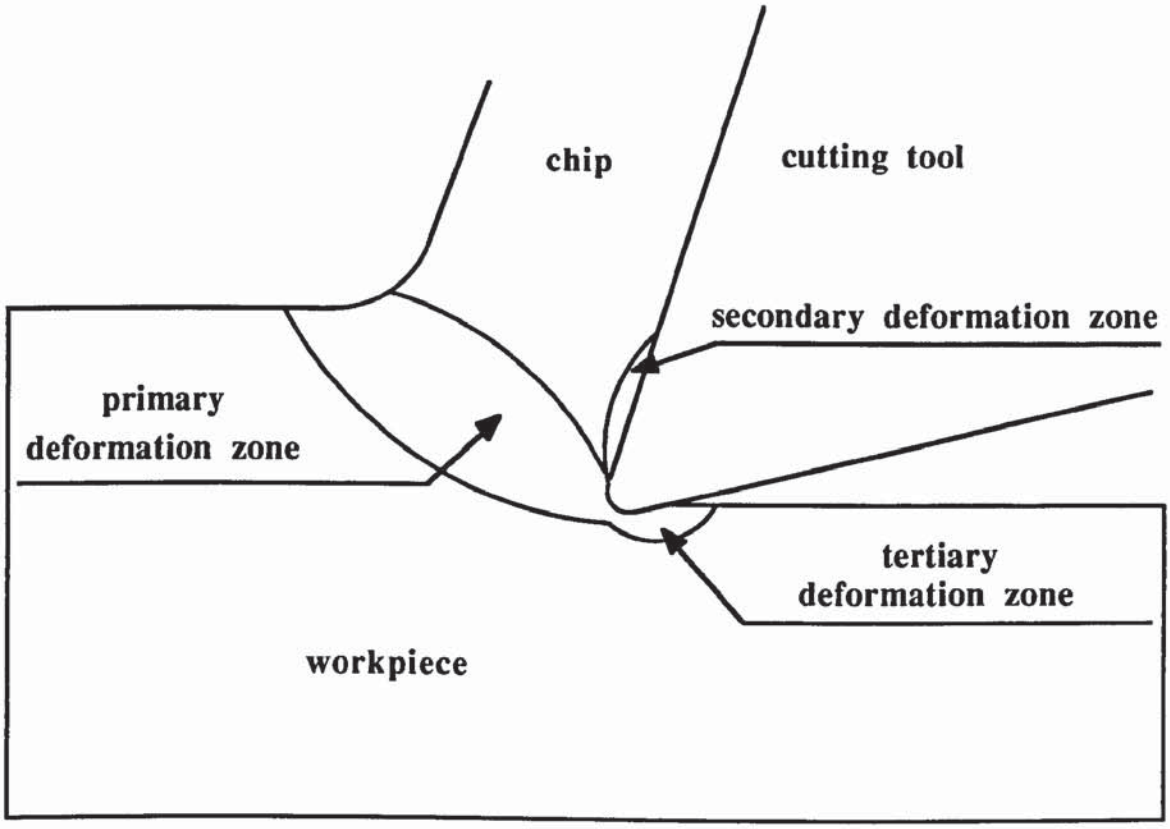

Fig. 3.1 Deformation zones in metal cutting.

corresponding coefficients will be determined through experimental orthogonal turning data.

3.2.2. Primary and secondary deformation zones

The principal mechanism in chip formation is recognised to be a shearing process taking place along a shear zone as shown in Fig. 2.3. Several researches have attempted to give a precise description of the deformation process within this zone and showed that the deformation and the resistance to deformations parallel to the rake are severe and difficult to relate to conditions in common material tests, from which common conceptions about material behaviour are drawn. Different models place different degrees of emphasis on aspects of material behaviour such as strain hardening, strain rate, temperature effect, in relation to the effect of the tool geometry, built–up edge and cutting conditions. These require quite different sets of input parameters to describe the material behaviour.

Many of the drawbacks of the geometric stress, strain and strain rate measures are addressed by using tensor strain or strain rate measures calculated from assumed or velocity distributions. This ensures that the deformation is uniquely characterised and compatibility conditions are satisfied at all points, at least in the plastic zone. Thereafter, the stress measures can be calculated from the strain or the strain rate (Stephensen *et al.*, 1988a, 1988b). This approach is more suited to upper bound analysis of steady, unconfined plastic flow problems (Malvern, 1969) but is unfortunately model dependent. The shape of the deformation zone and material velocity or displacement distributions must be calculated from idealized assumptions of conditions and of machining configurations. The constitutive equations must also be assumed, which is a drawback when material behaviour is being investigated.

Analysis of the effect of the work hardening received by the work material during machining indicated that the strain rate and temperature effects are much more significant than strain hardening at high strain rates (Clifton, 1983; Johnson *et al.*, 1983a, 1983b). Therefore, it seems more reasonable, as the temperature effects are included fully in the shear zone, to use a model of a thin primary shear zone that considers the effect of strains and strain rate rather than the effect of the work material hardening and where the dependency between the model parameters and the machining inputs may account for temperature effect.

From the above discussions it can be seen that modelling of metal machining can be carried out by considering a simple cutting configuration, such as Merchant's machining configuration, where the model parameters are estimated in more general forms from turning test data. These parameters will indirectly include the effect of all the dependent cutting parameters and will provide a more solid basis for extrapolating results to larger machining conditions.

3.3. STEADY STATE MODEL FOR TURNING PROCESS

It is shown from the above discussions that the forces acting on the tool during turning result from the shearing and the ploughing process. The forces due to the shearing process are applied upon the upper surface of the tool (rake face) and are named throughout this thesis rake forces. While the forces due to the ploughing process are applied around the tool nose and along the clearance face and are named ploughing forces.

3.3.1. Modelling turning force along the rake of the tool

The primary and the secondary deformation zones are respectively characterised by the shear stress k and the chip–tool contact in the thin shear plane model (Fig. 2.3. and Fig. 3.1.). The resistance to shear deformation is usually described by a mean constant friction coefficient characterising the the tool–chip contact, in the case of a continuous chip, and defined as:

$$\mu = \frac{F}{N} \qquad (3.1)$$

Where F and N are the tangential and normal force to the rake of the tool.

This parameter has been widely used in the past (Shaw,1984; Boothroyd, 1981; Bailey, 1975). However, since it does not account for tool nose and wear effects, the sliding and sticking nature of the contact (Zorev, 1963), and the built–up edge effects, many recent researchers preferred to use the friction stress in the sticking zone (Dewhurst, 1978) or more complicated two– or three–parameter descriptions (Iwata *et al.*, 1984). These approaches provide more realistic descriptions of contact conditions, but do not appear to be useful for material characterisation over a wide range of inputs, since the relevant stress distributions can only be measured using cumbersome techniques (Barrow *et al.*, 1982). In this thesis, the ease with which μ can be calculated from simple force measurements outweighs the advantages of a more complicated approach.

The simplest and most widely used stress for the cutting process is the average geometric measure derived from the shear plane zone models (Fig. 2.3.). In these models the shear stress k of the work is the projected force parallel to the shear plane divided by the area of this plane:

$$k = \frac{F_s}{A_s} \qquad (3.2)$$

The shear deformation is assumed in this model to occur along a single plane or a narrow zone centred on a plane, and the deformation variables depend primarily upon the shear angle ϕ:

$$\phi = \Phi(V, S_0, \alpha) \qquad (3.3)$$

V, S_0 and α are respectively the cutting speed, the undeformed chip thickness and the tool rake angle. The functional relationship Φ is determined from geometrical considerations as:

$$\Phi(V, S_0, \alpha) = \tan^{-1}\left[\frac{r\cos(\alpha)}{1 - r\sin(\alpha)}\right] \qquad (3.4)$$

$$r = \frac{S_0}{S_c} \qquad (3.5)$$

r is the chip thickness ratio defined as a ratio between the thickness of undeformed to deformed chip thickness (3.5). Usually the shearing process is accompanied by a plastic deformation increase in the thickness S_c of the cut chip in the direction of feed and absolutely no deformation is observed in width of chip or depth of cut for the case of turning (Eggleston *et al.*, 1959).

Using the minimum energy criteria, the rake force components on tool rake face can be therefore expressed as:

$$F_{xs} = \frac{w\, C_s\, S_0\, k}{\sin(\phi)\,(\cos(\phi) - C_s \sin(\phi))} \qquad (3.6)$$

$$F_{zs} = \frac{w\, S_0\, k}{\sin(\phi)\,(\cos(\phi) - C_s \sin(\phi))} \qquad (3.7)$$

w is the depth of cut, the shear angle ϕ is determined from (3.3) and k is the mean shear stress along the shear plane. In real conditions, the real shear stress along the shear plane is at least the required stress to provoke the shearing within the work material but under the assumption of the minimum energy, the true shear stress is supposed to be confined to only the stress needed to take off the chip from the work material. However, when the shear stress is determined from experimental data and not only from material characteristics, the discrepancies that can occur between these two quantities, of real and shear stress predicted by the model, are minimised.

$$C_s = \frac{F_{xs}}{F_{zs}} \qquad (3.8)$$

The rake forces ratio C_S, as defined in, (3.8) is usually used to determine the mean friction coefficient characterising the tool–chip contact μ as:

$$\mu = M(V, S_0, \alpha) \qquad (3.9)$$

Where M is a mean friction function defined as:

$$M(V, S_0, \alpha) = \frac{C_s + \tan(\alpha)}{1 - C_s \tan(\alpha)} \qquad (3.10)$$

When the rake forces ratio and the ploughing forces ratio are experimentally expressed as functions of the independent cutting parameters, the assumption of considering a

mean coefficient of friction parallel to the rake and to the flank of the tool becomes more realistic and near the reality since these coefficients are not Coulomb friction coefficients but are parameters which depend on the cutting conditions and which are introduced to describe respectively the resistance to the shearing on the rake and to the work material deformation along the flank of the tool.

The above parameters as given by (3.9) and (3.10), in the context of a thin shear plane model and a continuous chip, characterises the material deformation during the machining process. Furthermore, the parameters introduced in the rake forces equations are average, scalar, measures which do not uniquely characterise the deformation and which are difficult to relate to the measures used in other processes in which material behaviour is well understood. However, they are relatively model dependent and are easily determined from routine measurements; moreover since many investigators have used these measures there is considerable data in the literature on their variations and inter–dependencies. However, since in the present study the effect of the tool nose is introduced into considerations, more precise determination of these parameters is made possible.

3.3.2. Ploughing mechanism in machining

The principal purpose of the modelling carried out in this work is to develop explicit expressions of forces as a result of ploughing process. This ploughing process is due to the finite sharpness of the cutting edge which in turn introduces additional deformation of work material at the tool tip.

In common models the tool is usually supposed to be sharp by ignoring the small rounding of the cutting edge (Fig. 2.3). Due to that simplification, the whole chip–tool

pressure has a constant direction, provided the coefficient of friction does not vary along the tool rake, and can be summed up in one resultant force of the same direction. This has been the usual assumption for the development of the metal cutting process. To take account of the finite sharpness, it is necessary to add to the foregoing concept a rounding on the extreme cutting edge as shown in Fig. 3.2. Just as on the tool rake, pressure will occur along the rounded portion (Fig. 3.1), but the direction of this pressure is different from that on the tool rake and varies from point to point. Also, the coefficient of friction on the rounded surface and the flank of the tool is expected to have a different value from that on the tool rake, especially if the built–up edge covers this portion of the tool as is usually the case at low cutting speeds. Because of this rounding on the extreme cutting edge it will be more enlightening if the entire system of chip–tool pressures, including those on the rounded edge are not summed up into one resultant force.

In order to describe the term "ploughing" or "indentation" in the cutting process it is necessary to define what is happening to the work material in front of the cutting edge, shown in Fig. 2.5 and Fig. 3.2. Referring to Fig. 3.2, as the tool progresses into the workpiece, the material in front of the rounded edge should moves one way or another (Rubenstein *et al.*, 1985). If this material were to be pressed into the workpiece the tool would be constantly moved up or deformed and would progress along some inclined line by the virtue of the fact that more material would be beneath the tool. Because the experience shows that the tool does not move out of the cut, but keeps a constant amount of removed material in each workpiece revolution, it is then concluded that there will be a certain point A on the rounded edge called here the separation point. The material above this point A will be removed in the form of the chip while the material below will be deformed by the edge and will be increasingly pressed as it flows from A to B and will elastically recover between B and C where the deformed material is

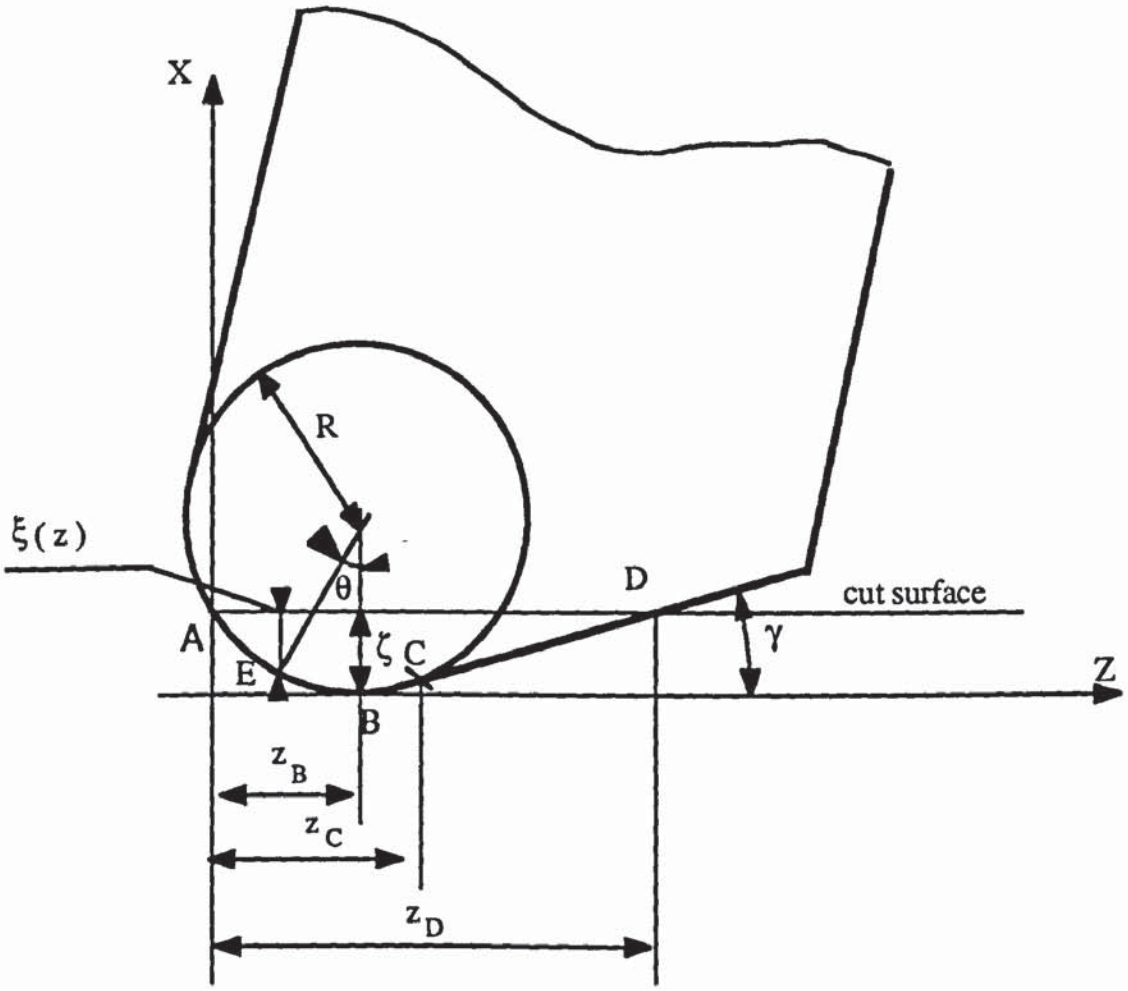

Fig. 3.2 Tool penetration in steady state turning.

pressed against the flank of the tool edge with a decreasing deformation pressure from B to C. This whole action is termed ploughing. Regarding the increase and the decrease of the pressure in the fresh cut surface respectively within AB and BC, A–B can be called the loading cycle and B–C the unloading cycle. After it loses contact with the tool flank face, a small portion of the material is pressed plastically into the work surface and therefore accommodating more material into the work surface will cause compression stresses known as residual stresses in machined surfaces (Rubenstein *et al.*, 1985; Liu *et al.*, 1976). The deformation of material around the tool edge and along the flank will introduce new forces to the cutting process referred to as ploughing forces.

3.3.3. Modelling the turning force along the rounded cutting edge and the flank face of the tool.

At the vicinity of the cutting edge, the material is, as discussed above, compressed in the direction of the feed (x direction, Fig. 3.2) and that the depth of deformation ξ is varying from the starting point A of deformation according to the tool edge geometry as shown in Fig. 3.2. After the deformation stress is released, the remaining plastic deformation in the upper–surface of the workpiece was shown by Rubenstein *et al.* (1985) and Liu *et al.* (1976) to be of small order compared to the elastic deformation and therefore the cut surface of workpiece is assumed to be at the same level as the starting point A of the deformation. The depth of tool penetration can be expressed along the contact between workpiece surface and tool as:

$$\xi(z) = \zeta + \sqrt{R^2 - (z - z_B)^2} - R \qquad \text{for } 0 \le z \le z_c \quad (3.11)$$

$$\xi(z) = \zeta - R(1 - \cos(\gamma)) - (z - z_C)\tan(\gamma) \quad \text{for } z_C \le z \le z_D \quad (3.12)$$

ζ is the depth of tool penetration at the lowest point B of the tool. At the starting point of deformation A and at the point D where the workpiece loses contact with the tool the depth of deformation is as: $\xi(0) = \xi(z_D) = 0$, and therefore:

$$z_B = \sqrt{\zeta(2R - \zeta)} \qquad (3.13)$$

$$z_D = z_C + \frac{\zeta - R(1 - \cos(\gamma))}{\tan(\gamma)} \qquad (3.14)$$

Where z_C is determined from geometrical considerations as:

$$z_C = z_B + R \sin(\gamma) \qquad (3.15)$$

R is the radius of tool nose.

The resulting elementary force in the direction of feed can be considered as being proportional to the depth $\xi(z)$ of the deformation for elastic deformations. The deformation resistance in the cutting direction is described by a constant friction angle along the nose and flank of the cutting tool. Under these assumptions, elementary ploughing components dP_x and dP_z of the turning force, at an arbitrary point E (Fig. 3.2), in feed and in cutting directions can be expressed respectively as:

$$dP_x = p_s w \xi(z) dz \qquad (3.16)$$

$$dP_z = p_s w \xi(z) \tan(\tau + \theta) dz \qquad \text{for } 0 \leq z \leq z_C \qquad (3.17)$$

Where:

– p_s: ploughing factor which is characterising the proportionality between the deformed volume of the material and the resulting force.

– w: depth of cut

– τ: equivalent mean frictional angle along the flank and the rounded edge of the tool.

– γ: flank angle of the tool.

– θ: defines the angular position of the point E on the rounded cutting edge.

Integration of (3.16), (3.17) and (3.18) from A to D along the secondary edge of the tool yields the ploughing forces as follows:

$$P_x = w\,p_s\left\{ R\,(z_D - z_C)\cos(\gamma) - (R - \zeta)\,z_D - \frac{1}{2}\tan(\gamma)\,(z_D - z_C)^2 \right\}$$

$$+\frac{1}{2}w\,p_s\left\{ z_B\sqrt{R^2 - z_B^2} + (z_C - z_B)\sqrt{R^2 - (z_C - z_B)^2} \right\}$$

$$+\frac{1}{2}w\,p_s\;R^2\left\{ \arcsin\left[\frac{z_B}{R}\right] + \arcsin\left[\frac{z_C - z_B}{R}\right] \right\} \qquad (3.19)$$

and

$$P_z = w\,p_s(\zeta - R)\frac{R\,(1+\tan^2(\tau))}{\tan^2(\tau)}\left\{ \log\left[\frac{R - z_B\tan(\tau)}{R - (z_C - z_B)\tan(\tau)}\right] + \frac{2\,z_B - z_C}{\tan(\tau)} \right\}$$

$$- w\,p_s\frac{R^2}{\tan(\tau)}\left[\frac{3}{2} - \frac{\tan^2(\tau) - 1}{\tan^2(\tau)}\right]\left(\arcsin\left[\frac{z_C - z_B}{R}\right] - \arcsin\left[\frac{z_B}{R}\right]\right)$$

$$- w p_s \frac{R^2}{\tan(\tau)} \left[\frac{3}{2} - \frac{\tan^2(\tau) - 1}{\tan^2(\tau)} \right] \left(\arcsin\left[\frac{z_C - z_B}{R} \right] - \arcsin\left[\frac{z_B}{R} \right] \right)$$

$$+ w p_s \frac{R^2(\tan^4(\tau) - 1)}{\tan^3(\tau)\sqrt{\tan^2(\tau) - 1}} \log \left[\frac{1 - \frac{z_B}{R}\tan(\tau)}{1 - \tan(\tau) + \sqrt{\tan^2(\tau) - 1}\sqrt{1 - \left(\frac{z_B}{R}\right)^2}} \right]$$

$$- w p_s \frac{R^2(\tan^4(\tau) - 1)}{\tan^3(\tau)\sqrt{\tan^2(\tau) - 1}} \log \left[\frac{1 - \frac{z_C - z_B}{R}\tan(\tau)}{1 - \tan(\tau) + \sqrt{\tan^2(\tau) - 1}\sqrt{1 - \left(\frac{z_C - z_B}{R}\right)^2}} \right]$$

$$+ w p_s \left\{ \left[\zeta - R(1 - \cos(\gamma)) \right](z_D - z_C) - \frac{1}{2}\tan(\gamma)(z_D - z_C)^2 \right\} \tan(\tau - \gamma)$$

(3.20)

When the radius of the tool is of very small order (Appendix A1), (3.19) and (3.20) can be reduced to:

$$P_x = \frac{1}{2} \frac{p_s w \zeta^2}{\tan(\gamma)} \qquad (3.21)$$

$$P_z = \frac{1}{2} \frac{p_s w \zeta^2}{\tan(\gamma)} \tan(\tau - \gamma) \qquad (3.22)$$

Similarly to the rake forces ratio, a ploughing forces ratio can be defined as:

$$C_p = \frac{P_z}{P_x} = \tan(\tau - \gamma) \qquad (3.23)$$

Whereas the rake forces ratio C_s characterises the resistance to shearing across the rake of the tool in terms of a mean friction angle β ($\beta = \tan^{-1}(\mu)$), the ploughing forces ratio C_p characterises the resistance to deformation, in the direction of mean cutting speed, around the nose and across the flank of the tool in terms of a mean friction angle τ. In the expression of turning force components, the ratio Cp is replaced by its expression of (3.23) because an expression is preferred to be determined for the friction coefficient along the flank of the tool than the coefficient Cp.

An increase in the clearance angle γ results in a decrease in the ploughing forces components P_x, P_z and in the ploughing forces ratio C_p. While an increase in the rake angle decreases the values of C_s and of the rake forces. The ploughing force is more sensitive to the clearance angle variations in the feed direction than in the mean cutting direction. Similarly, the rake force is more sensitive to changes in the rake angle in the mean cutting direction than in the feed direction.

3.3.4. Steady state turning force components

The measured force components (F_x and F_z) are the resultant of both the force components occurring upon the rake (F_{xs} and F_{zs}) as well as along the flank of the tool and around the tool nose (P_x and P_z). These are as follows ((3.6), (3.7), (3.21) and (3.22)):

$$F_x = \frac{w\, C_s\, S_0\, k}{\sin(\phi)\,(\cos(\phi) - C_s \sin(\phi))} + \frac{1}{2}\,\frac{p_s\, w\, \zeta^2}{\tan(\gamma)} \qquad (3.23)$$

$$F_z = \frac{w\, S_0\, k}{\sin(\phi)\,(\cos(\phi) - C_s \sin(\phi))} + \frac{1}{2}\,\frac{p_s\, w\, \zeta^2}{\tan(\gamma)}\tan(\tau - \gamma) \qquad (3.24)$$

It is therefore shown that when considering the geometry of the orthogonal cutting process, as illustrated in Fig. 3.2, the turning force components can be fully described in terms of the shear angle ϕ, the mean shear stress k, the rake forces ratio C_s, the depth of tool penetration ζ and the ploughing forces ratio C_p as dependent parameters. Usually the shear angle ϕ is experimentally determined by the chip thickness ratio r using (3.3) and (3.4).

The dependent parameters in (3.23) and (3.24) are strongly influenced by the cutting parameters, namely, rake angle α, chip thickness S_0, cutting speed V and flank angle γ. While the effect of both the rake angle and the flank angle on the process of chip formation can, as a geometrical constraint, be envisaged on a pure geometrical basis, the role of S_0 and V is indirectly performed through their effect on the strain rate and temperature rise in the primary, secondary and tertiary deformation zones.

In a complex process such as the chip formation, it is more convenient to determine these dependent parameters as a function directly of the input parameters such as the cutting speed and the feed rather than determining the effect of the independent parameters upon the temperature rise and the strain rate and relate the latter to the dependent cutting parameters in (3.23) and (3.24). The effect of the temperature will be accounted for by introducing the effect of the independent parameters S_0 and V upon the mean shear stress k and mean friction angle β and τ.

In this model, other properties are excluded on the basis that the tool and the work materials enter the chip formation process in so many ways that the possibility of substituting other materials, as can often be done in heat transfer and fluid mechanics

problems, seems to be too remote. That is to say that the correlation of the machining results of lead, for example, with those of steel seems, at least for the time being, not feasible. Therefore, considering more properties of the tool and work materials will complicate the solution, possibly, without gaining much more generality. This investigation is confined to the case of orthogonal dry cutting of an unpreheated workpiece with new edge and hence properties of the cutting fluid, initial workpiece temperature are all excluded. However, as will be shown further on, the material properties can be introduced as a proportionality coefficient in the mean shear stress k and in the ploughing factor p_s.

3.4. EXPERIMENTAL TESTS

3.4.1. Cutting configuration

As mentioned earlier, the form of the function relating the geometry of the chip formation process to the independent cutting parameters is to be determined from steady state cutting data. A series of cutting tests, the specification of which is summarised in Table 3.1., have been carried out on a CNC TORSHALLA lathe (Fig. 3.3).The cutting edge is set normal to both the feed and the cutting direction. Moreover, the cutting configuration is in orthogonal conditions as a tube is used as a workpiece with a wall of 4mm so that the depth of the cut is greater than 10 times the undeformed chip thickness (Shaw, 1984).

In these tests, the tangential and normal components of the resultant turning force are measured using a three components piezo-electric dynamometer (Fig. 3.3). The outputs of the dynamometer are filtered in a low pass filter of 10Hz, amplified thereafter through a Kistler charge amplifier and stored on a disk of a Macintosh

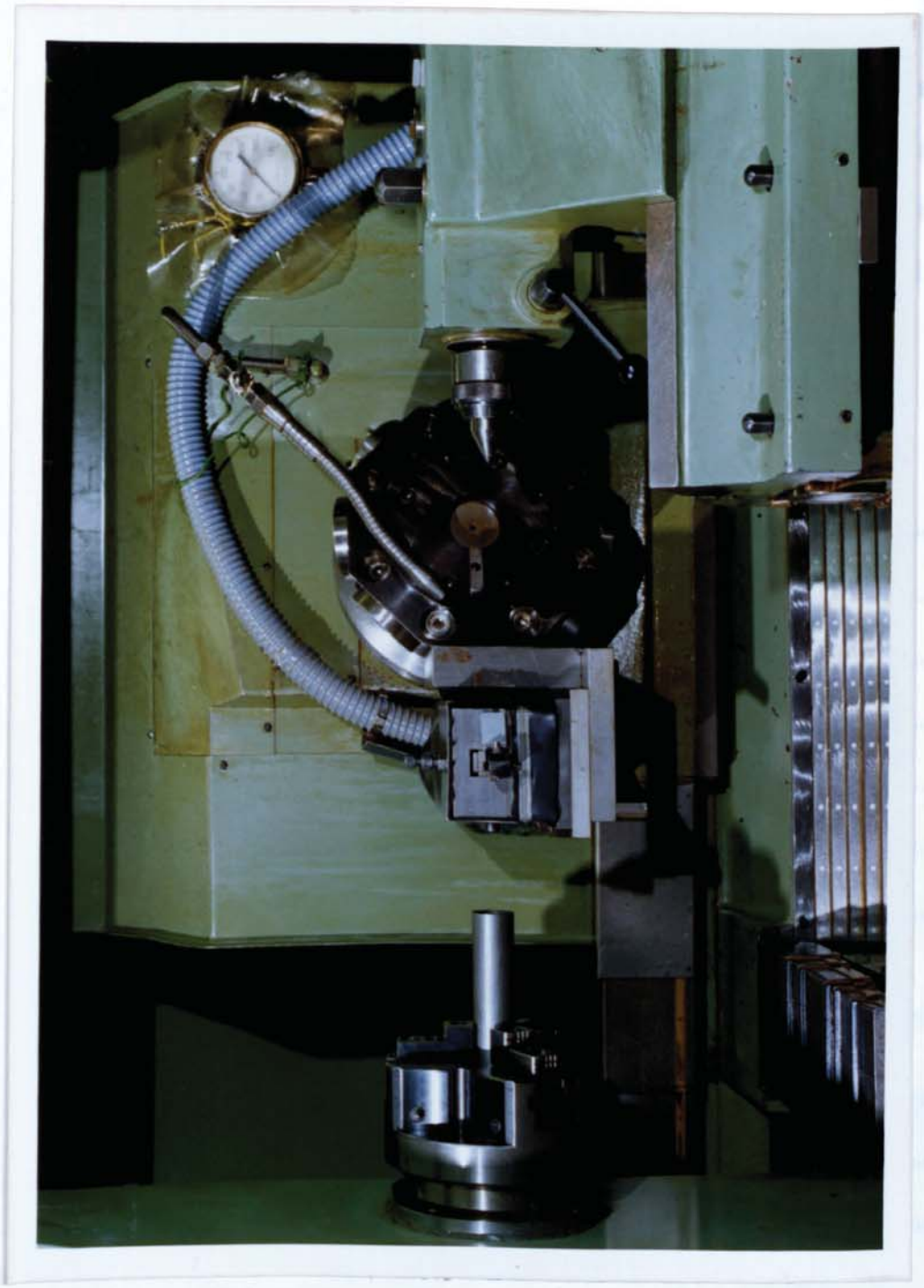

Fig. 3.3 Experimental set–up.

computer. The stored signals are later analysed to yield the average steady state turning force components.

The average deformed chip thickness S_c is determined by determining the average of five measures of the collected chips using a micrometer. The cutting tests are run for aa short a time as possible consistent with the steady state conditions (at least five revolutions of the workpiece) and a new tip is used for each run to avoid the wear effect. The rake angle has been varied in these tests by rotating the tool holder to give different rake angles with an error less than 0.01 deg.

3.4.2. Cutting conditions

work material	Tube CDS2, B.S. 980
out side diameter (mm)	38.10
Cutting configuration	Orthogonal dry bar turning
Uncut chip thickness (mm)	0.10, 0.20, 0.25
Cutting speed (m/s)	0.43, 0.92, 1.57, 2.31, 3.40, 5.20, 7.27, 8.33
Depth of cut (mm)	4.00
Cutting tool	Standard steel cutting Grade tungsten carbide tools: TPUN 160304 edge radius less than 0.004 mm
Flank angle (deg)	5
Rake angle (deg)	0, 6, 10, 15

Table 3.1 Experimental cutting conditions.

3.4.3. Experimental results

A sample of the experimental forces as well as the chip thickness ratios for different cutting conditions and different rake angles are plotted in Fig. 3.4 to Fig. 3.6 as a function of the cutting speed for the conditions investigated. It can be seen that the measured forces are decreasing with the cutting speed for all the speed range under investigation. After each cutting test, the tool tip was examined and has shown that there is no built–up edge (B.U.E.) for the material used even for the lowest cutting speed investigated. Therefore, the falling characteristic of the cutting forces with the cutting speed cannot be attributed to the increase in the effective rake angle resulting from the decrease of the size of B.U.E. as was suggested by Zorev (1966) but can rather be attributed to the effect of the temperature within the work material which tends to soften the workpiece material through the primary shearing zone.

Moreover, Fig. 3.6, represents the variation of the experimental forces with the uncut chip thickness. It is shown that the turning force components are proportional to the uncut chip thickness and that when extrapolated to zero–feed, they exhibit an intercept which is also depends upon the cutting conditions and representing the ploughing components.

3.5. EXPERIMENTAL DETERMINATION OF THE MODEL DEPENDENT PARAMETERS

In this section an experimental determination of the model dependent parameters, namely the average shear stress, the rake forces ratio, the tool penetration and the mean

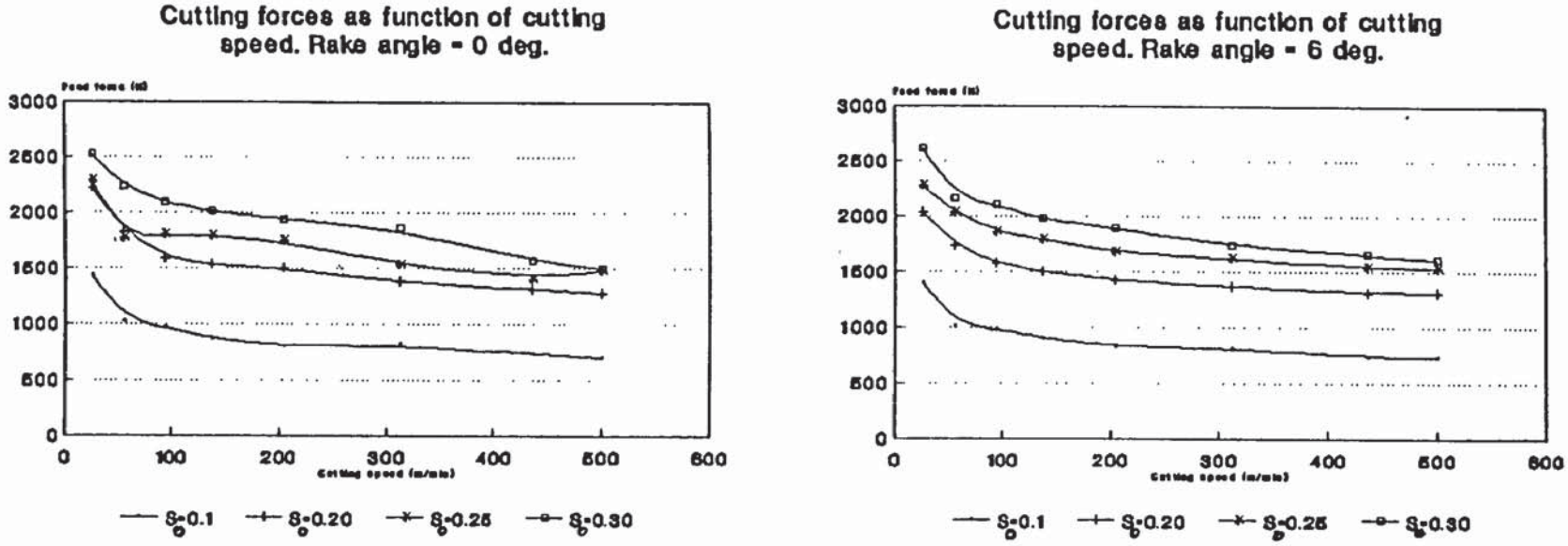

Fig. 3.4 Experimental cutting force versus cutting speed.

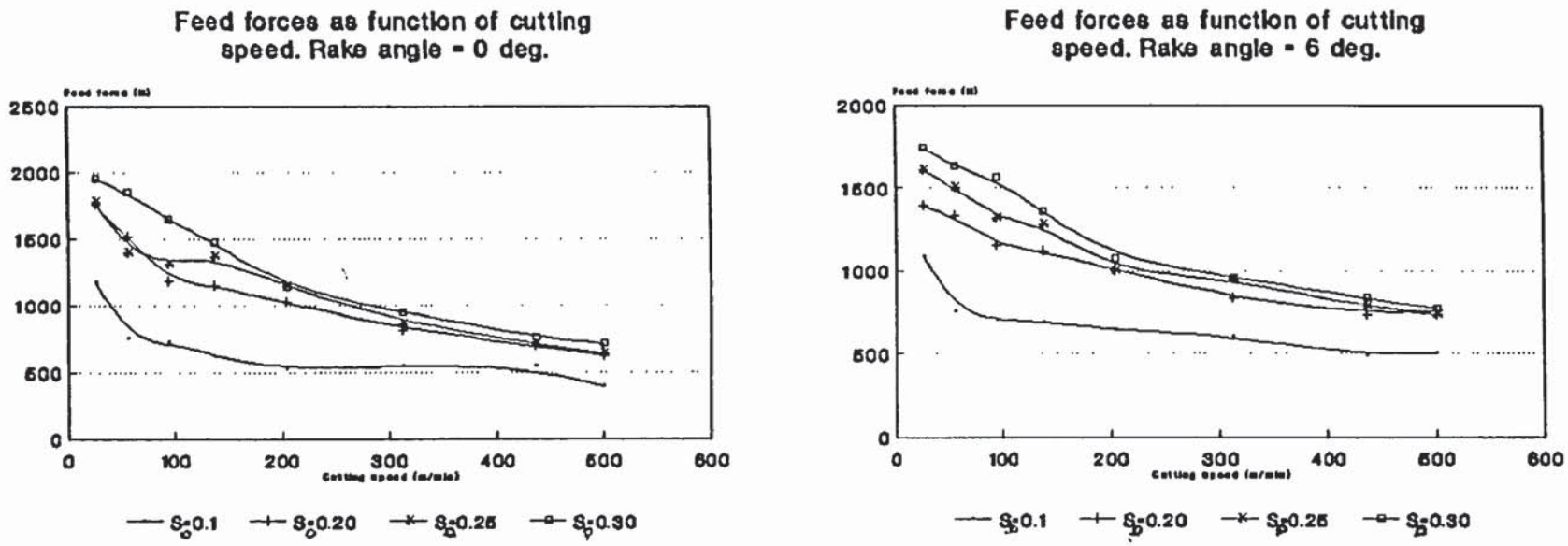

Fig. 3.5 Experimental feed force versus cutting speed.

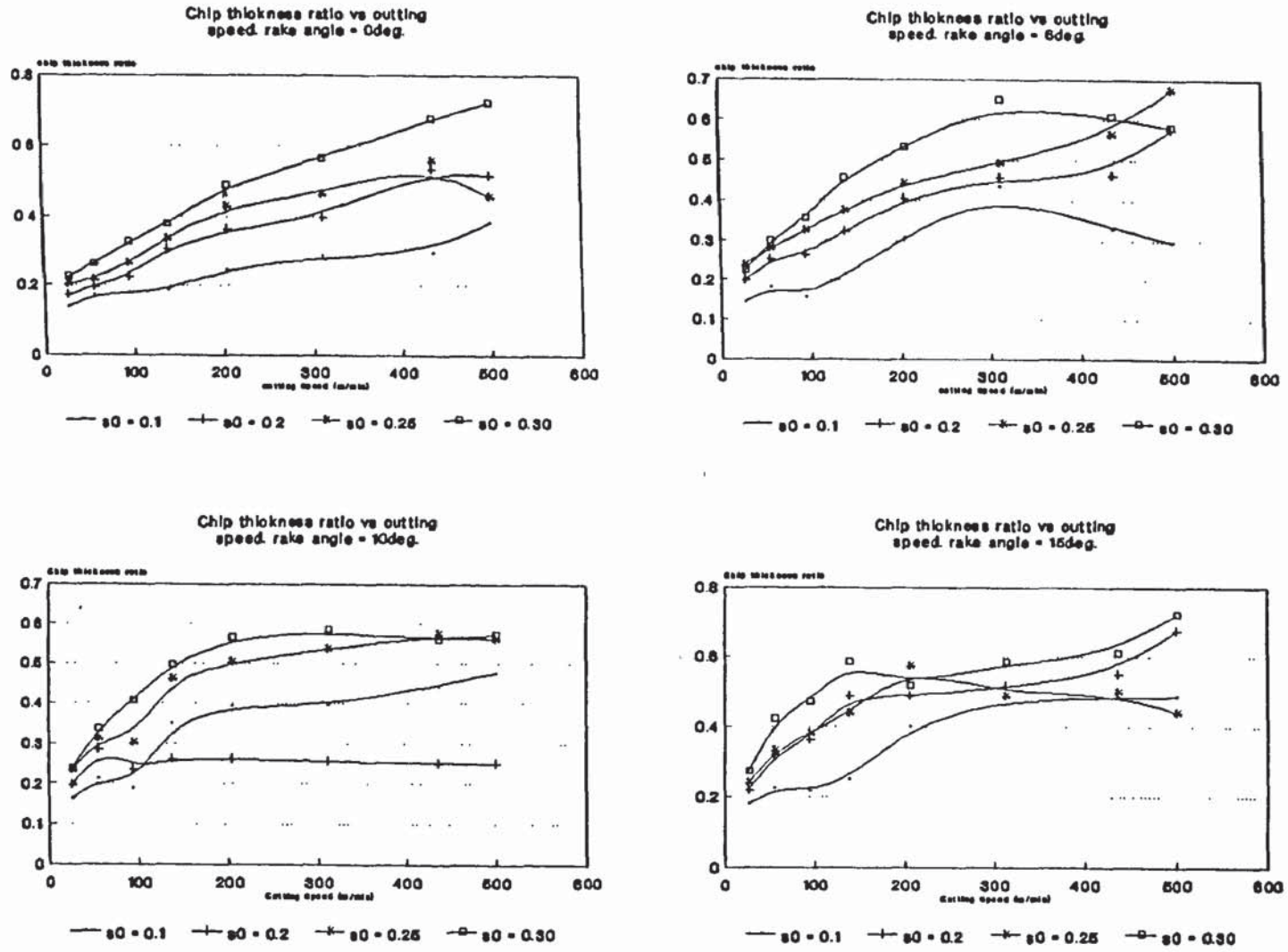

Fig. 3.6 Chip thickness ratio versus cutting speed.

frictional angle along the flank of the tool, as a function of the independent parameters, namely feed, speed and tool geometry, is carried out.

3.5.1. Rake force and ploughing force components

The expressions of the turning force components ((3.23) and (3.24)) showed that the ploughing part of these forces correspond to the intercept of the the turning force at a nil feed. Experimental results (Fig. 3.7) show that the feed and the cutting forces are linear functions of the undeformed chip thickness with a correlation factor larger that 0.98. It is worth mentioning that in the presence of the built–up edge, the rake force decreases with the size of the B.U.E. while the ploughing component is not affected since generally the secondary cutting edge of the tool does not change with the size of the B.U.E.. Therefore, the intercept of the ploughing force to nile feed provides the ploughing components regardless of the presence or not of the built–up edge.

A respective subtraction of the ploughing parts of the measured forces yields the rake force component resulting from the shearing process and hence the two parts, ploughing and rake forces, are computed to determine the different coefficients for the steady state model. In the following, the above mentioned experimental results are analysed in order to determine functional relationships of the dependent parameters by using different fitting methods based upon the least squares method (William, 1986).

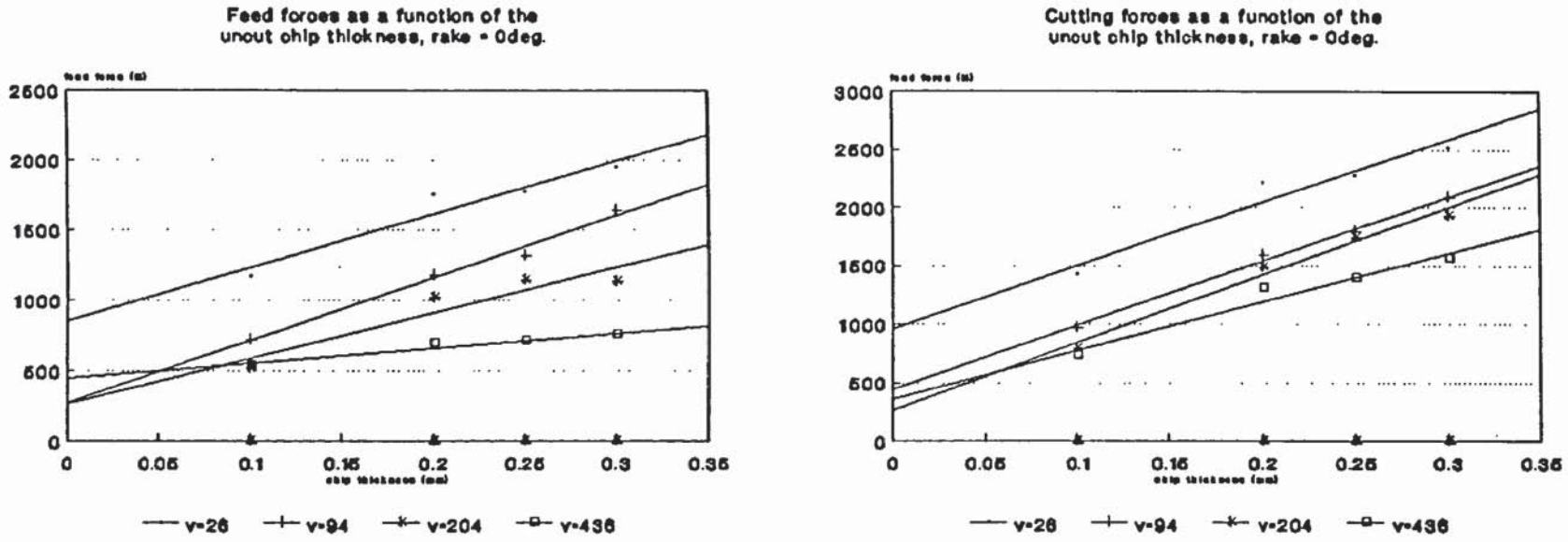

Fig. 3.7 Experimental turning force components versus uncut chip thickness.

3.5.2. Chip thickness ratio and rake forces ratio

The obtained chip thickness ratio r and rake forces ratio C_s, (3.5) and (3.8), are shown in Fig. 3.6 and from Fig. 3.8 to Fig. 3. 12 as a function of the rake angle, the cutting speed and the undeformed chip thickness. It was found that for constant cutting speed and feed, the relationship C_s–sin(α) and r–sin(α) are linear as illustrated in Fig. 3.8 and Fig. 3.9. This is the case of the investigated conditions for the used workpiece material where no built–up edge is exhibited. The two sets of straight lines of Fig. 3.8 to Fig. 3.10 respectively can thus be represented by the following equations:

$$C_s = C_{s0} + C_{s1} \sin(\alpha) \qquad (3.25)$$

$$r = r_0 + r_1 \sin(\alpha) \qquad (3.26)$$

Where C_{s0} and r_0 are the intercepts of the C_s and r respectively, while C_{s1} and r_1 are the slopes of the C_s–sin(α) and r–sin(α) linear relationships respectively. For various feeds, the intercepts C_{s0} and r_0 and the slopes C_{s0} and r_0 are found to be linearly proportional to the feed. Moreover, analysis of the effect of the cutting speed (Fig. 3.6, Fig. 3.10) showed that the intercept C_{s0} and the slope C_{s1} of the rake forces ratio are quadratic function of the cutting speed whereas the slope r_0 of the chip thickness ratio is a linear function of cutting speed while the slope is a cubic function of cutting speed.

The numerical fitting of the experimental data led to express the intercepts and the slopes of the rake forces ratio and the chip thickness ratio respectively in the following forms:

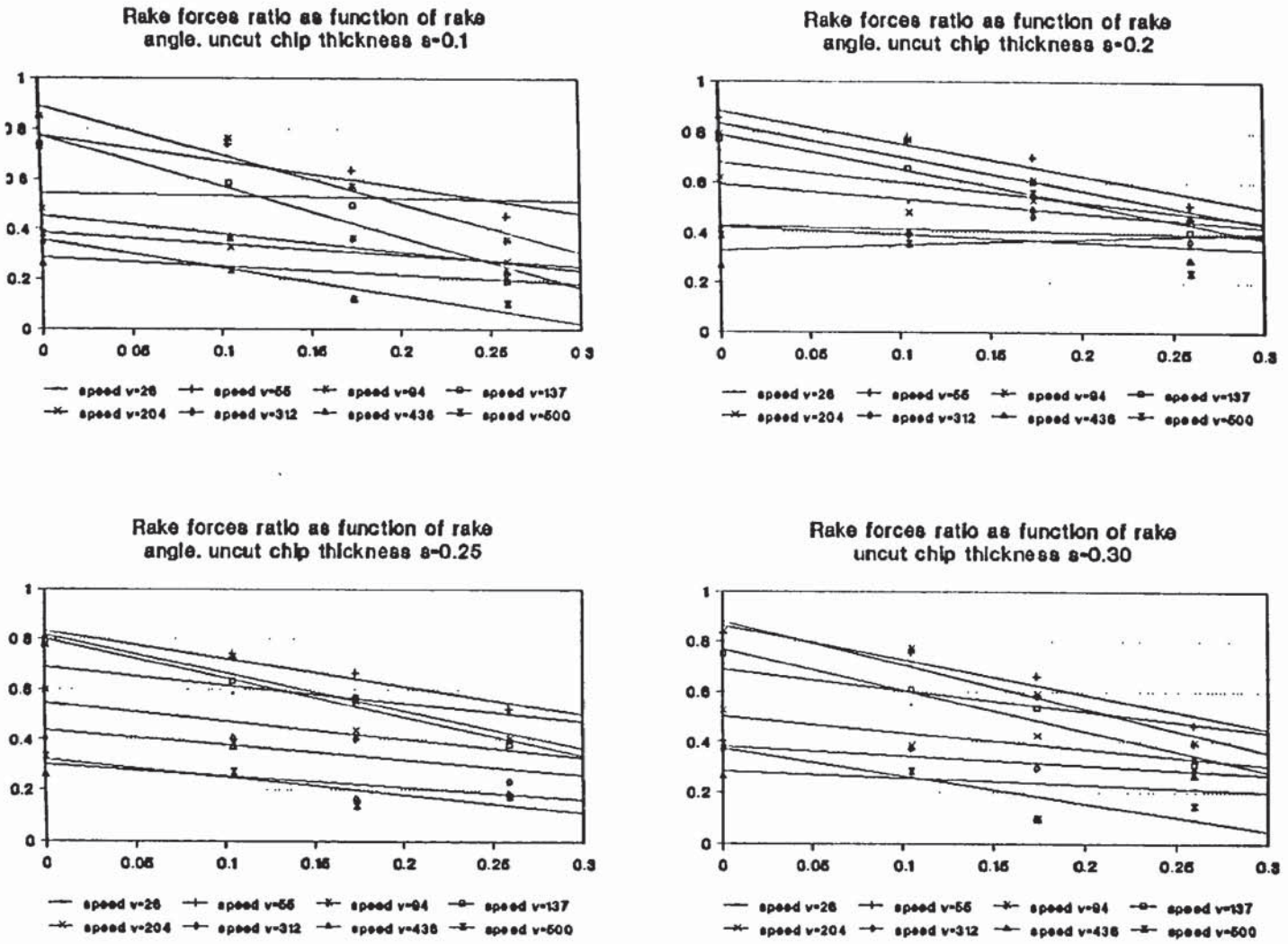

Fig. 3.8 Rake forces ratio versus rake angle of the cutting tool.

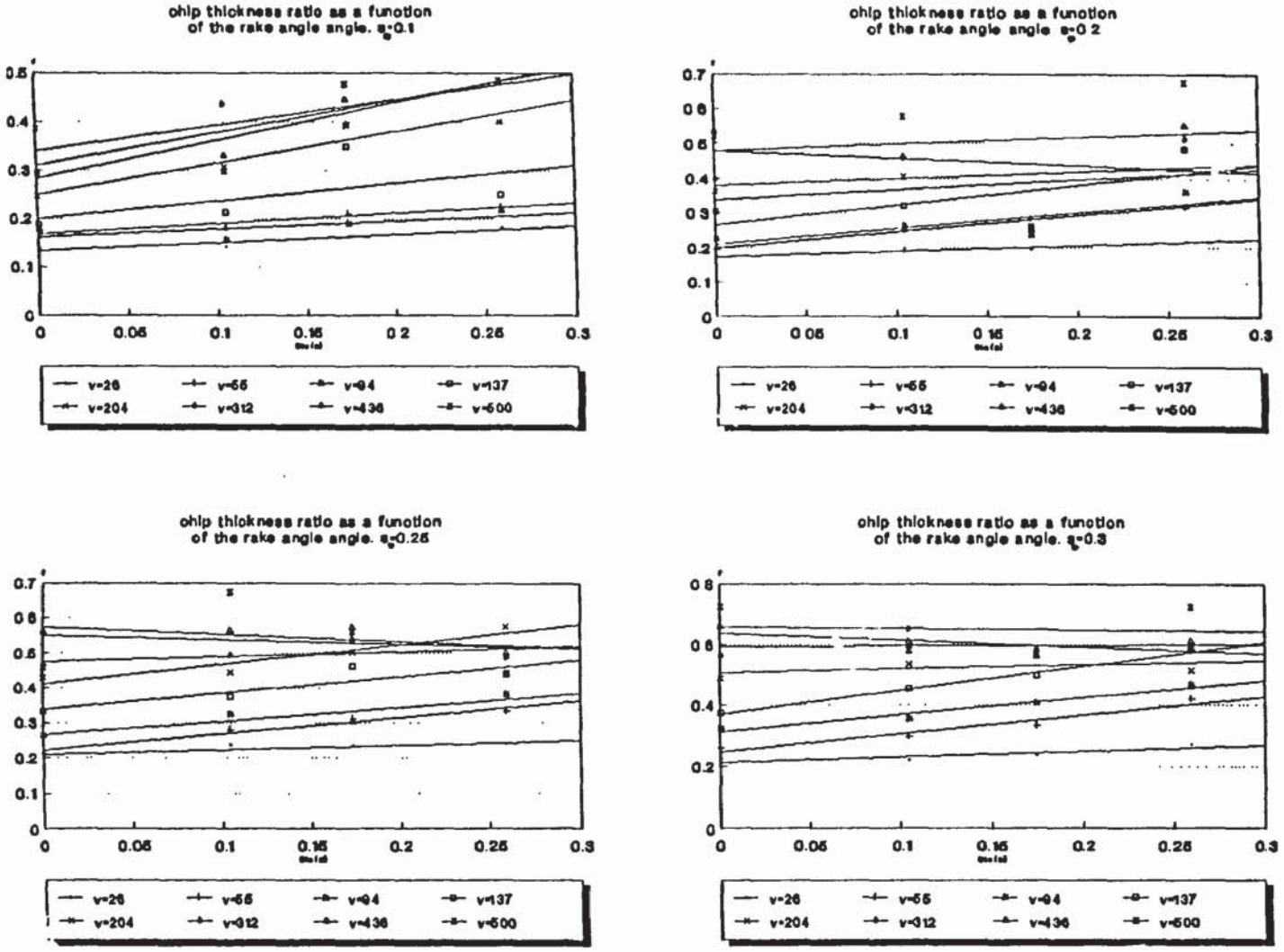

Fig. 3.9 Chip thickness ratio versus rake angle of the cutting tool.

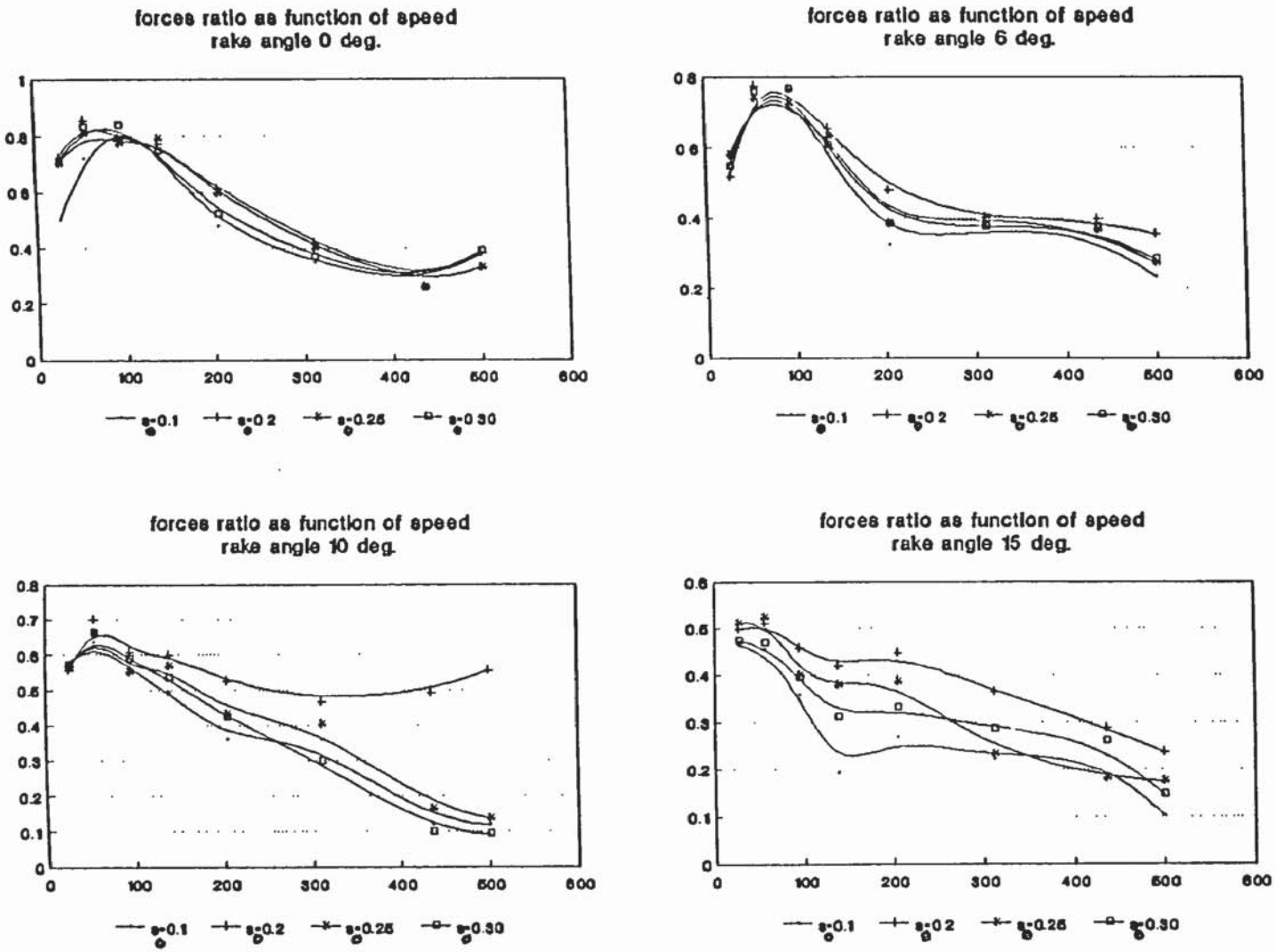

Fig. 3.10 Rake forces ratio versus cutting speed.

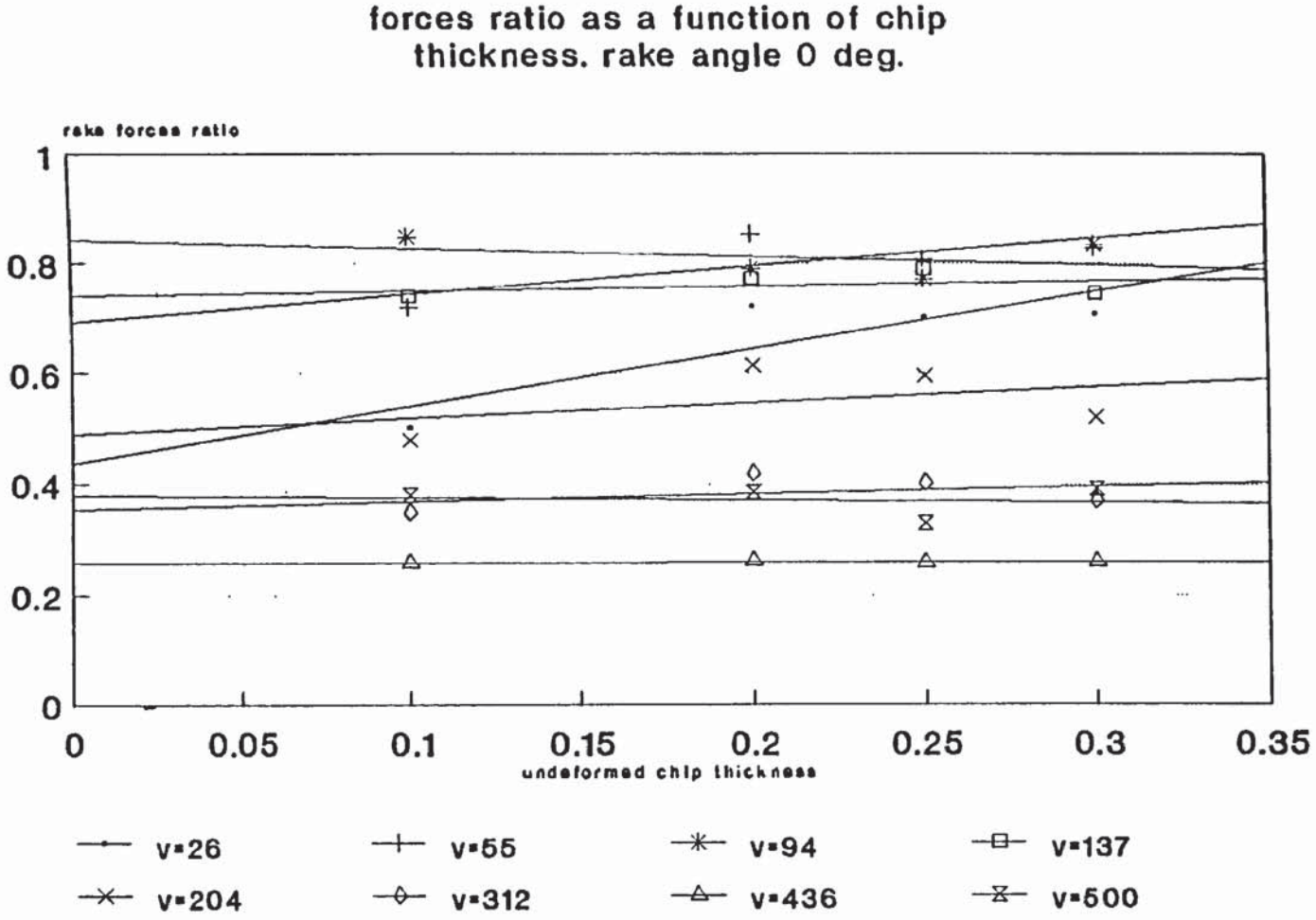

Fig. 3.11 Rake forces versus uncut chip thickness.

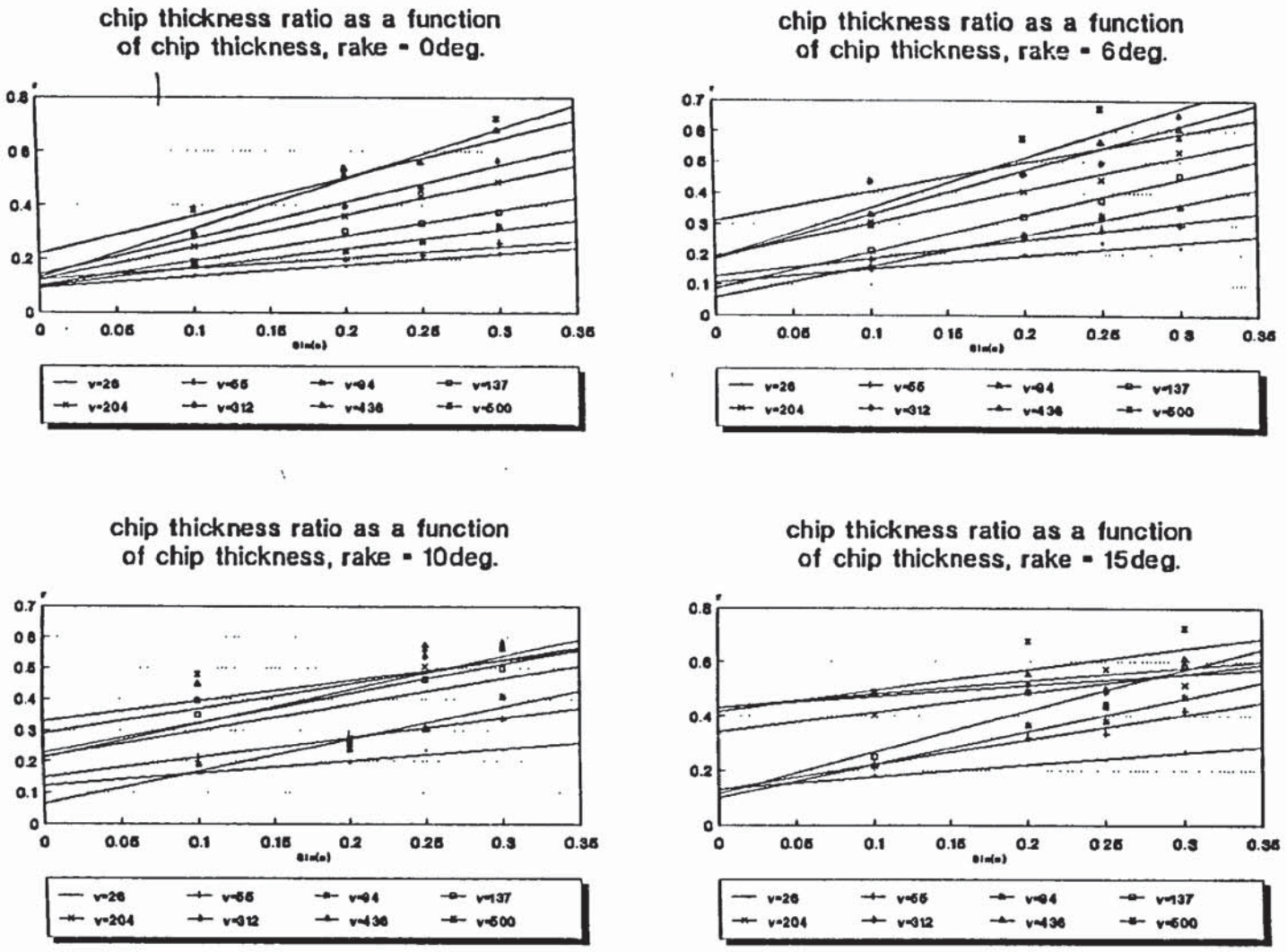

Fig. 3.12 Chip thickness ratio versus uncut chip thickness.

$$C_{s0} = [\,1\ S_0]\begin{bmatrix} 0.74 & -0.07 & -0.01 \\ 547.50 & -343.30 & 48.30 \end{bmatrix}\begin{bmatrix} 1 \\ 0.6\ V \\ (0.6\ V)^2 \end{bmatrix} \qquad (3.27)$$

$$C_{s1} = [\,1\ S_0]\begin{bmatrix} -0.99 & 0.10 & -0.03 \\ -866.20 & -365.30 & 334.70 \end{bmatrix}\begin{bmatrix} 1 \\ 0.6\ V \\ (0.6\ V)^2 \end{bmatrix} \qquad (3.28)$$

$$r_0 = [\,1\ S_0]\begin{bmatrix} 0.09 & 0.01 \\ 449.00 & 279.40 \end{bmatrix}\begin{bmatrix} 1 \\ 0.6\ V \end{bmatrix} \qquad (3.29)$$

$$r_1 = [\,1\ S_0]\begin{bmatrix} 0.19 & -0.35 & 0.39 & -0.06 \\ -540.90 & 4759.70 & -3256.50 & 438.80 \end{bmatrix}\begin{bmatrix} 1 \\ 0.6\ V \\ (0.6\ V)^2 \\ (0.6\ V)^3 \end{bmatrix} \qquad (3.30)$$

where S_0 is in m/rev and V in m/s.

The above expressions (3.27) through (3.30) provide the effect of the steady state cutting conditions upon the chip thickness ratio and the rake forces ratio and henceforth provide the variation of the mean friction angle on the rake of the tool and the shear angle ((3.3), (3.4), (3.9) and (3.10)).

3.5.3. Mean shear stress

In order to investigate the effect of the cutting conditions upon the machining mean shear stress, the shear plane area A_s as well as the shearing force F_s along that plane

are determined for all the cutting conditions investigated. These are estimated according to the geometry of Fig. 3.2 from the following equations:

$$A_s = \frac{w\, S_0}{\sin(\phi)} \qquad (3.31)$$

$$F_s = F_{zs}\cos(\phi) - F_{xs}\sin(\phi) \qquad (3.32)$$

Where F_{zs} and F_{xs} are the rake forces in the direction of the cutting speed and the feed as measured by the dynamometer and ϕ is the shear angle as determined by (3.3) and (3.4) together with the experimentally obtained chip–thickness ratio r.

Experimental results show that the mean shear stress is dependent on the cutting conditions and linear regression analysis showed that the k–sin(α) and k–S_0 are linear with a correlation coefficient higher than 0.996 while the relationship k–V is a quadratic function. These observations together with the experimental data led to express the mean shear stress as:

$$k = \begin{bmatrix} 1 & 1000\,S_0 & 0.6\,V & (0.6\,V)^2 \end{bmatrix} \begin{bmatrix} 66.02 & 353.41 \\ 585.31 & -477.14 \\ 117.48 & -227.29 \\ -17.22 & 35.57 \end{bmatrix} \begin{bmatrix} 1 \\ \sin(\alpha) \end{bmatrix} \qquad (3.33)$$

Where S_0 and V are expressed in m/rev and m/s respectively.

The experimental investigation shows that the mean shear stress along the shear plane depends strongly upon the cutting conditions. As far as k is concerned, the following can be drawn:

– The mean shear stress is increasing with the cutting speed up to 7.27m/s and it starts decreasing afterwards.
– The mean shear stress increases with the undeformed chip thickness and with the rake angle.

Under the same temperature along the shear zone, the limit shear stress of the material is expected to be constant. However, as evident from the experimental results, the calculated shear stress is varying with the cutting inputs because of the effect of the temperature along the shear zones affecting the strain and strain rate within this zone. Also, the criteria of minimum energy does not hold good and the real shear stress along the shear plane is not necessarily the minimum shear needed for shearing deformations. Considering the experimental data to determine experimental relationships for the shear stress with the cutting conditions introduces indirectly the effect of the temperature and can predict the real stress within the shear plane more accurately.

3.5.4. Depth of the tool penetration and mean friction coefficient along the rake of the tool

The experimental results (Fig. 3.13) show that the tool penetration decreases with the cutting speed up to 2.28m/s and increases thereafter. The larger the rake angle, the smaller the depth of the tool penetration which is attributed to the decrease in the deformation stress with the rake angle. The mean friction coefficient μ along the rake of the tool is increasing with the rake angle and decreases with the cutting speed.

Previous analysis of the work material suggested that the tool penetration resulting from the indentation effect around the cutting edge is depending upon the cutting conditions but no explicit relationship was provided (Haslam *et al.*, 1970; Lin *et al.*,

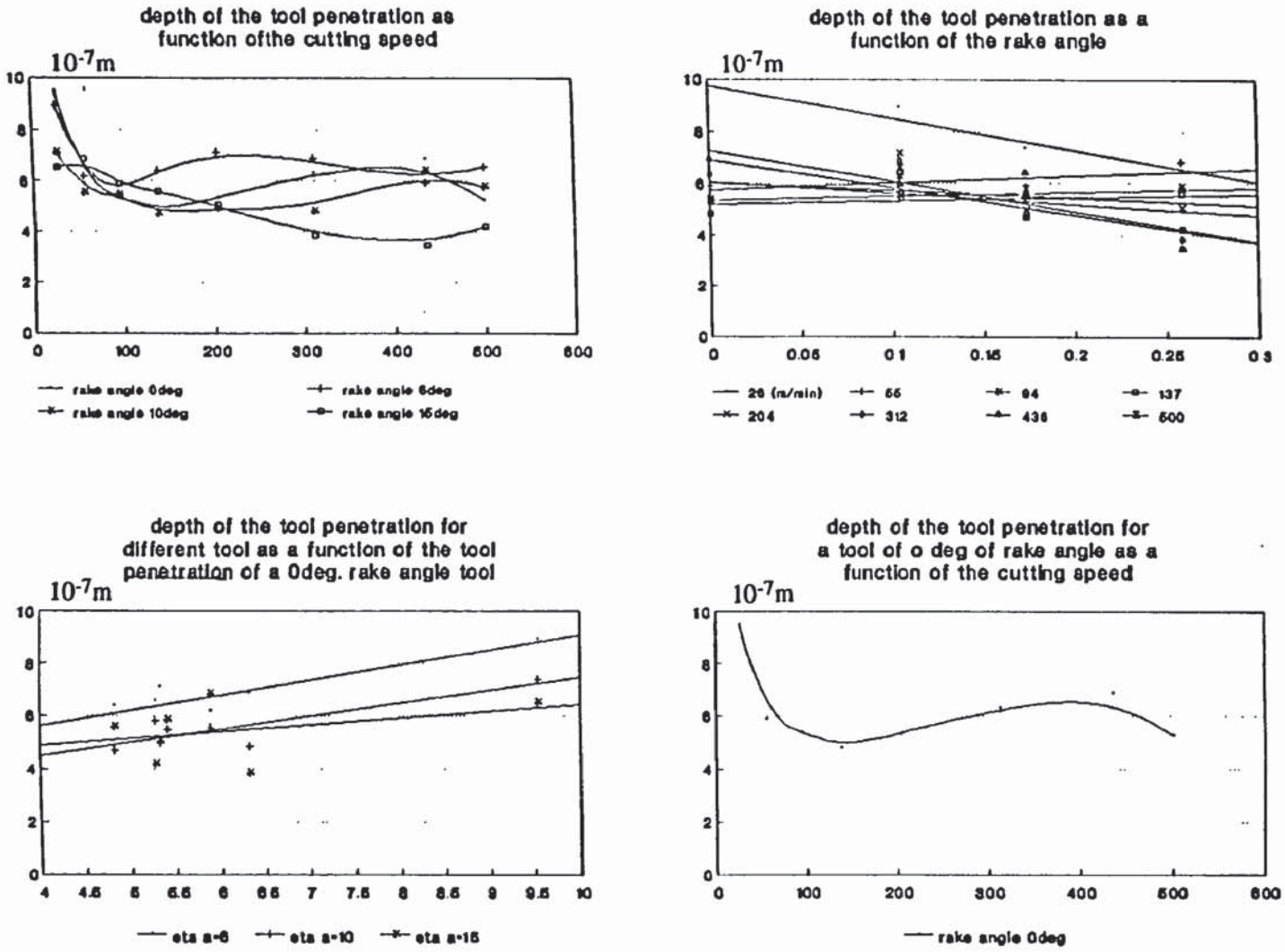

Fig. 3.13 Depth of the tool penetration.

1982). This dependency is attributed to the effect of the thermal expansion of the work material at the vicinity of the cutting tip. As the cutting speed is increased, the temperature generated at the tip is increased leading to higher thermal expansion and therefore the deformation or the tool penetration is higher for the same stress of contact between the tool nose and the work material. Moreover, a larger speed decreases the time of applied deformation and hence under the same deformation rate, the tool penetration is decreased. The effect of these two opposite tendencies determines the size of the tool penetration ζ as shown by the experimental results of Fig. 3.13.

The effect of the cutting conditions and tool geometry, namely feed, cutting speed and rake angle, is manifested on the depth of the tool penetration and the mean friction angle through their effect upon the strain rate and the temperature rise in the tertiary deformation zone. These depend on the thermal diffusivities of both the workpiece and tool materials together with the characteristic time delay of the workpiece material. the latter is the minimum time required for plastic and elastic deformation to be completed under a certain applied stress. The characteristic time delay, therefore, describes the speed effect on the deformation received by the cut surface material.

Using the experimental results, it is found that the tool penetration as well as the mean friction coefficient along the flank are linear functions with the tool rake angle and thus can be represented by:

$$\zeta = \zeta_0 + \zeta_1 \sin(\alpha) \qquad (3.34)$$

$$\mu_f = \mu_{f0} + \mu_{f1} \sin(\alpha) \qquad (3.35)$$

Where ζ_0 and μ_{f0} are the intercepts of ζ and μ_f respectively and, ζ_1 and μ_{f1} are the slopes of the ζ–sin(α) and μ_f–sin(α). For the feeds and speeds investigated, the intercepts ζ_0 and μ_{f0} are found to be linearly proportional to the slopes ζ_1 and μ_{f1}. These linear relationships are given by:

$$\zeta_1 = a - b\ \zeta_0 \qquad (3.36)$$

$$\mu_{f1} = c - d\ \mu_{f0} \qquad (3.37)$$

Substitution of the values of ζ_1 and μ_{f1} as given by (3.36) and (3.37) into (3.34) and (3.35) renders the following relationships for ζ and μ_f:

$$\zeta = a\ \sin(\alpha) + (\ 1 - b\ \sin(\alpha)\ )\ \zeta_0 \qquad (3.38)$$

$$\mu_f = c\ \sin(\alpha) + (\ 1 - d\ \sin(\alpha)\ )\ \mu_{f0} \qquad (3.39)$$

Where a, b, c and d are constant coefficients, the value of which, for the conditions investigated, are given in Table 3.2.

a	b	c	d
$3.72\ 10^{-6}$	3.55	6.01	4.44

Table 3.2 Coefficients for tool penetration and equivalent mean friction on the flank.

ζ_0 and μ_{f0} are the depth of the tool penetration and the mean friction angle along the tool flank for a tool with nil rake angle, these are:

$$\zeta_0 = \frac{1}{10^6}\begin{bmatrix} 1.36 & -0.31 & 0.05 \end{bmatrix}\begin{bmatrix} 1 \\ 0.6\,V \\ (0.6\,V)^2 \end{bmatrix} \qquad (3.40)$$

$$\mu_{f0} = 1.99 - 0.27\ V + 0.06\ (0.6\,V)^2 \qquad (3.41)$$

The mean friction coefficient μ_{f0} as defined here to represent the resistance to the deformation under the tool nose as a decreasing function with the cutting speed for low speeds and reaches its minimum at a cutting speed of 5.86 m/s above which the resistance to deformation is increasing. As discussed above, these trends are attributed to the effects of the temperature and the time delay.

3.5.5. Verification of the model

A model for the steady state turning process has been developed based upon the characteristics of the metal deformation and geometrical considerations. The aim of the following section is to use the same cutting conditions as those used for determining the model coefficients and compare between the predicted and the experimentally measured turning forces so that the quality of the fitting for the different parameters will be highlighted.

The measured as well as the model predicted turning force components are shown in Fig. 3.14 to Fig. 3.20. It is shown that the force is decreasing with the cutting speed for the range of speeds investigated and no built-up edge was exhibited during the experiments. Generally, the error in force prediction is less than 10% and is within the

repeatability of the forces values. This differences is slightly higher for low cutting speeds and feeds when higher rake angles are used.

For tools with nil or with 6 degrees as rake angle (Fig. 3.14 to Fig. 3.17), the error is always less than 8% for low range of speeds. However, when the rake angle is increased up to 10 or 15 degrees, this error may be as large as 60% for some points. This is the case for speed higher than 3.40 m/s for 10 degrees rake angle tool and for 0.20 or 0.30 mm/rev as a feed.

Except for these particular points, the model provides a satisfactory prediction of the components of the turning forces with a precision laying within the range of repeatability of its measured values.

The model is shown to be capable of predicting turning forces in the case of tube turning. The next stage is to use the model, with some corrections, to predict the turning forces under different circumstances. These are as follows:

– Bar turning with positive rake angle tools for the same cutting conditions as those used to build the model and the results are compared to experimental data.

– Bar turning with different workpiece material, different cutting conditions and different tool geometries as those used to build the model. The predicted forces are compared to published data (Wu, 1985).

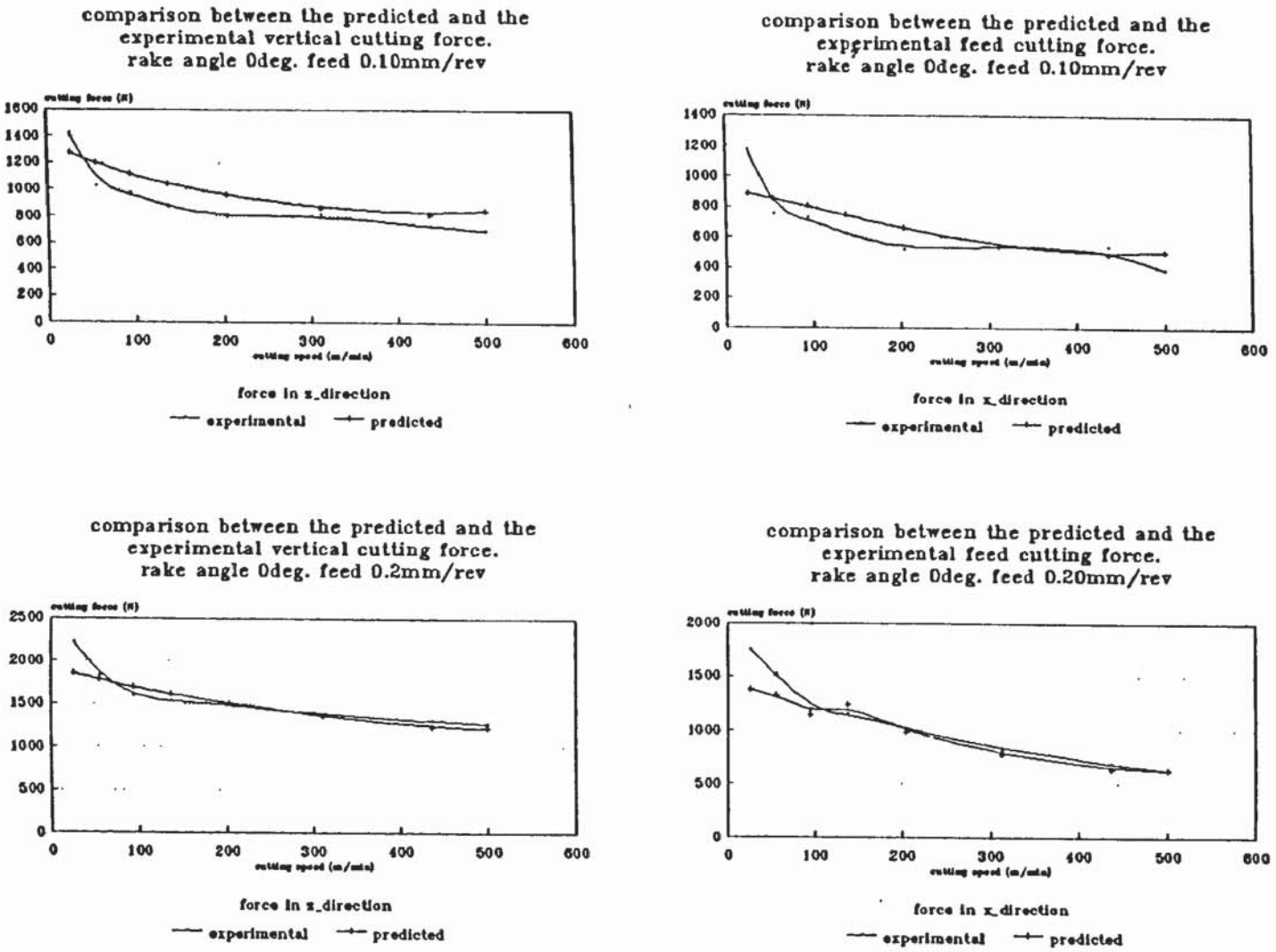

Fig. 3.14 Predicted and experimental forces, rake angle = 0 deg.

$S_0 = 0.10,\ 0.20$ mm/rev.

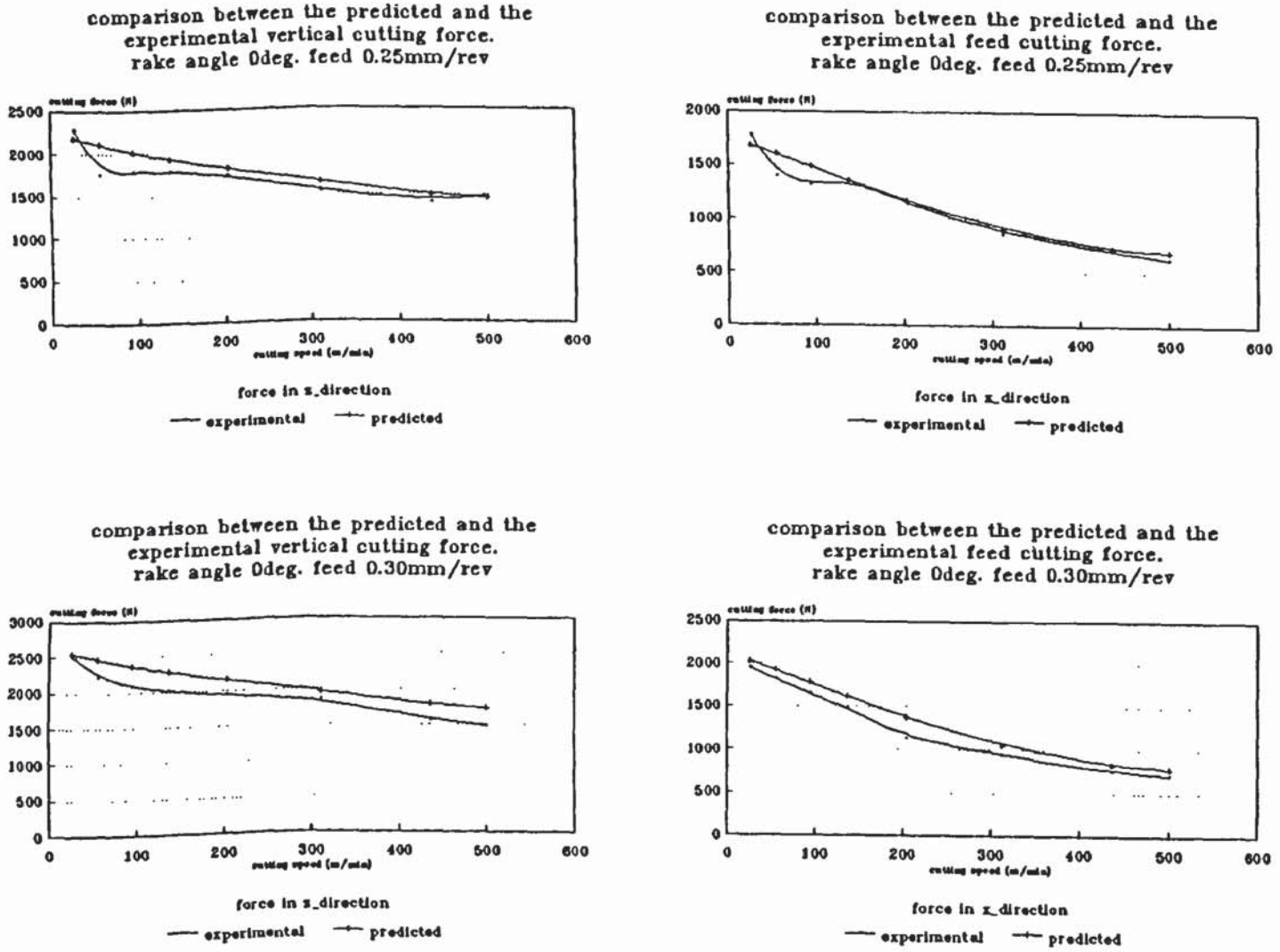

Fig. 3.15 Predicted and experimental forces, rake angle = 0 deg.

$S_0 = 0.25,\ 0.30$ mm/rev.

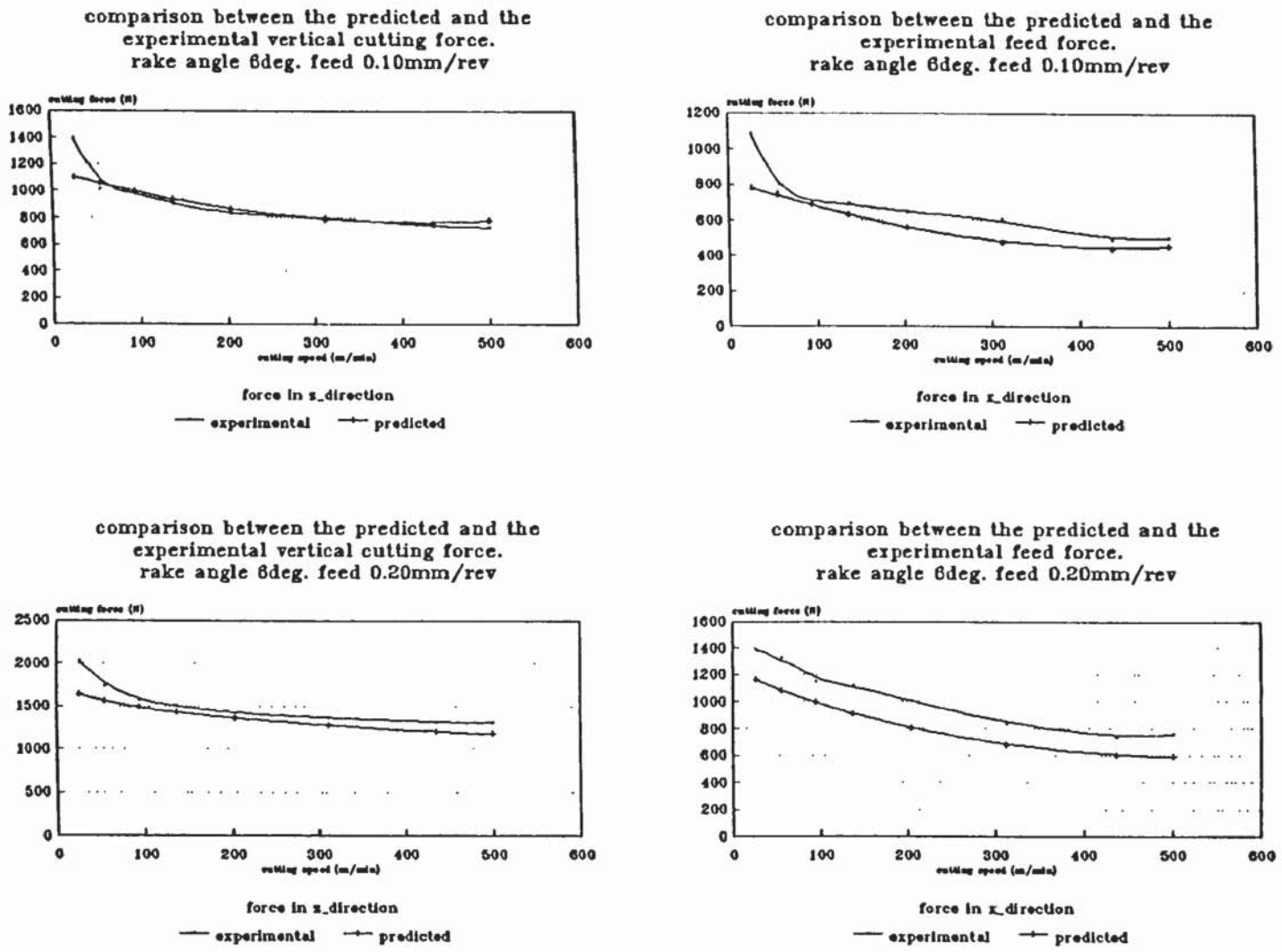

Fig. 3.16 Predicted and experimental forces, rake angle = 6 deg.

$S_0 = 0.10,\ 0.20$ mm/rev.

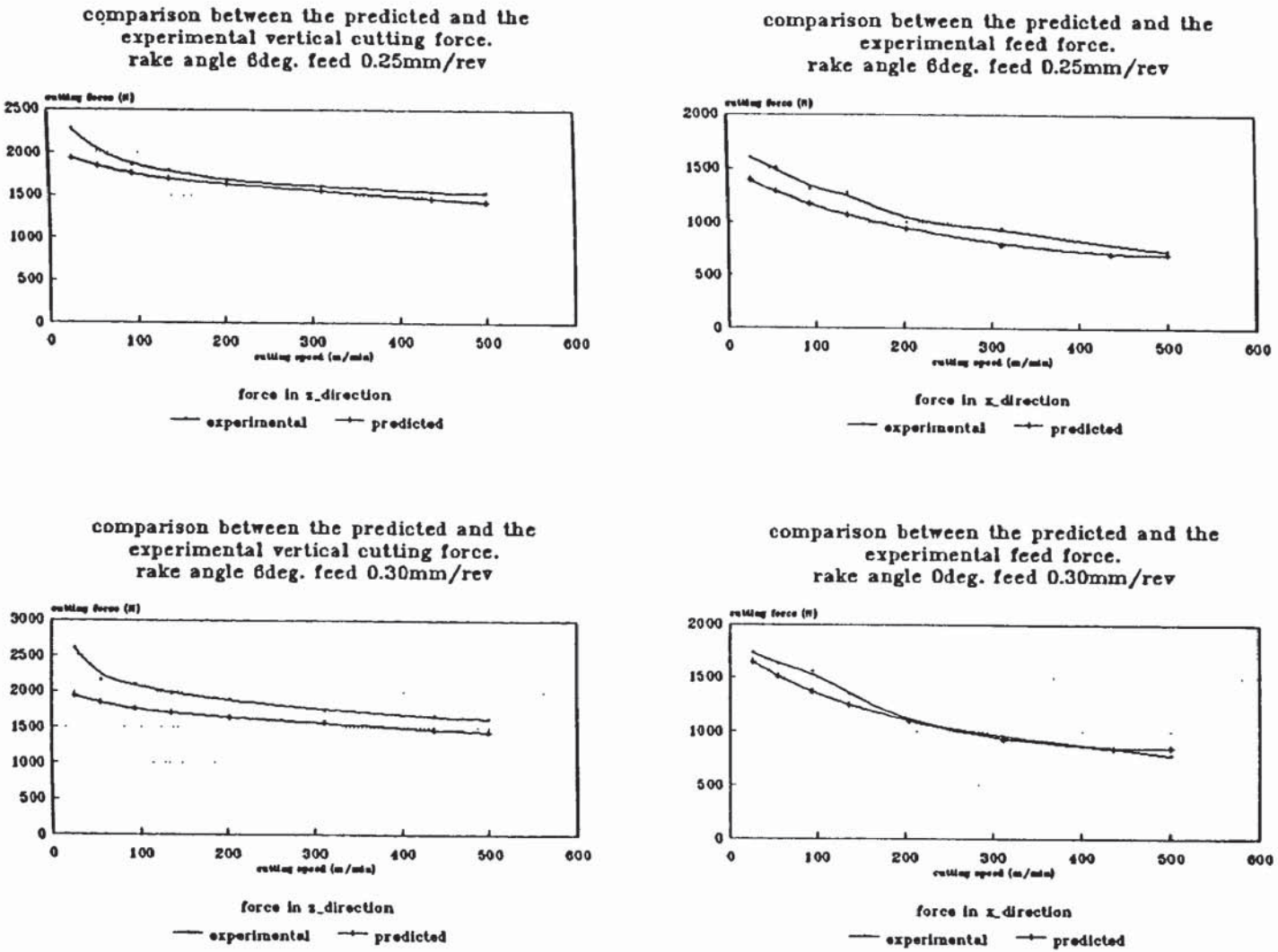

Fig. 3.17 Predicted and experimental forces, rake angle = 6 deg.

$S_0 = 0.25,\ 0.30$ mm/rev.

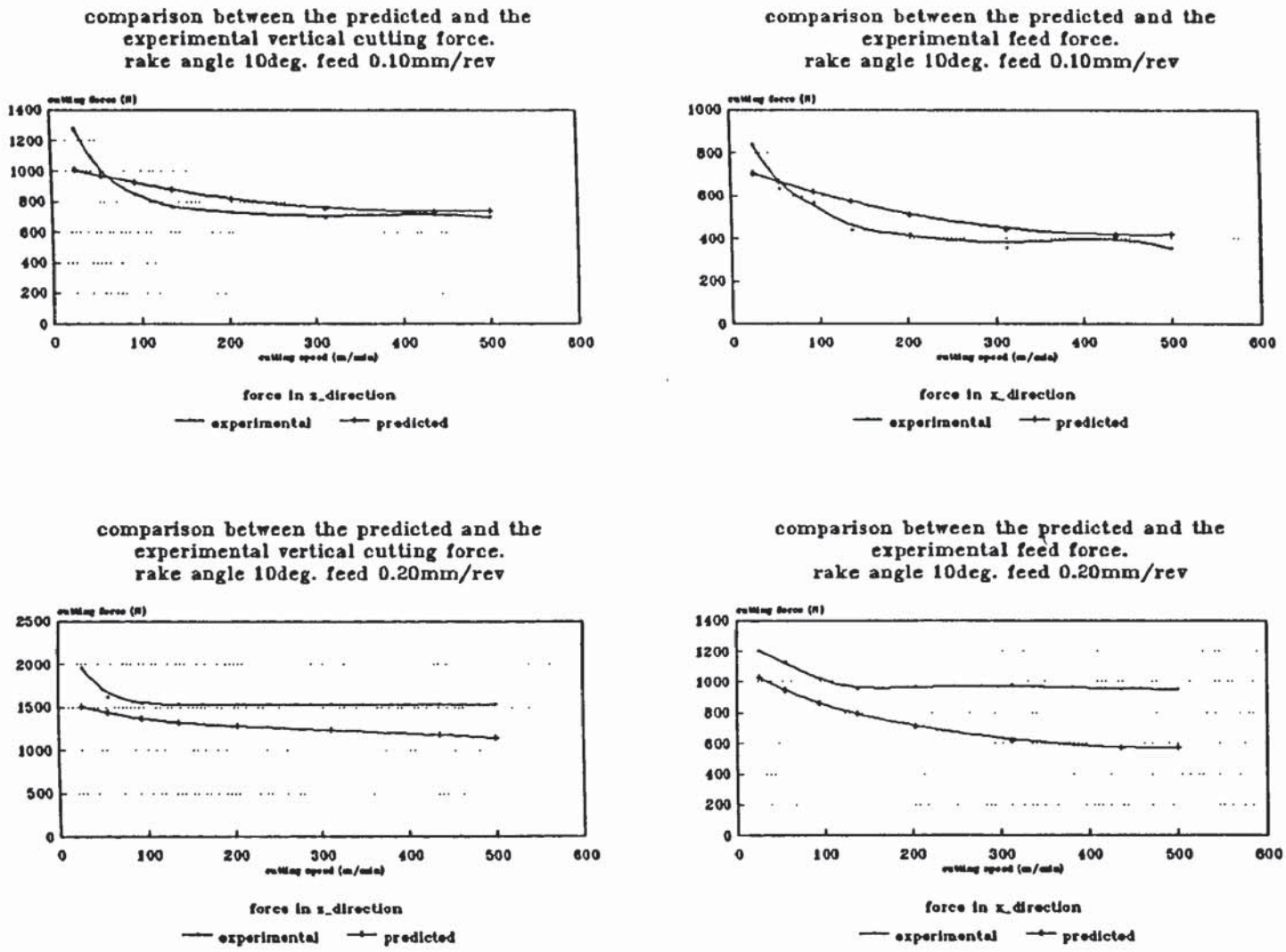

Fig. 3.18 Predicted and experimental forces, rake angle = 10 deg.

$S_0 = 0.10,\ 0.20$ mm/rev.

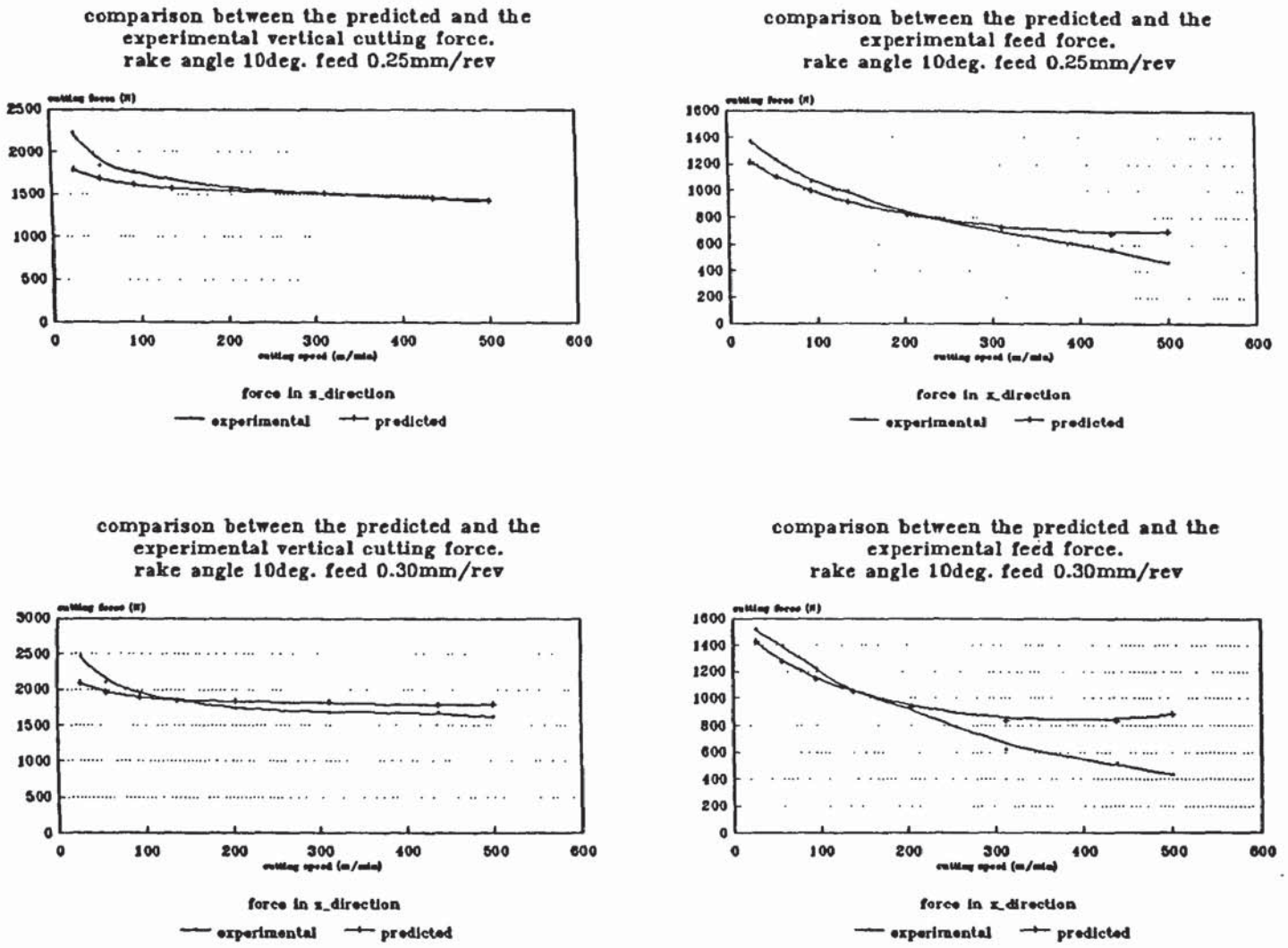

Fig. 3.19 Predicted and experimental forces, rake angle = 10 deg.

$S_0 = 0.25,\ 0.30$ mm/rev.

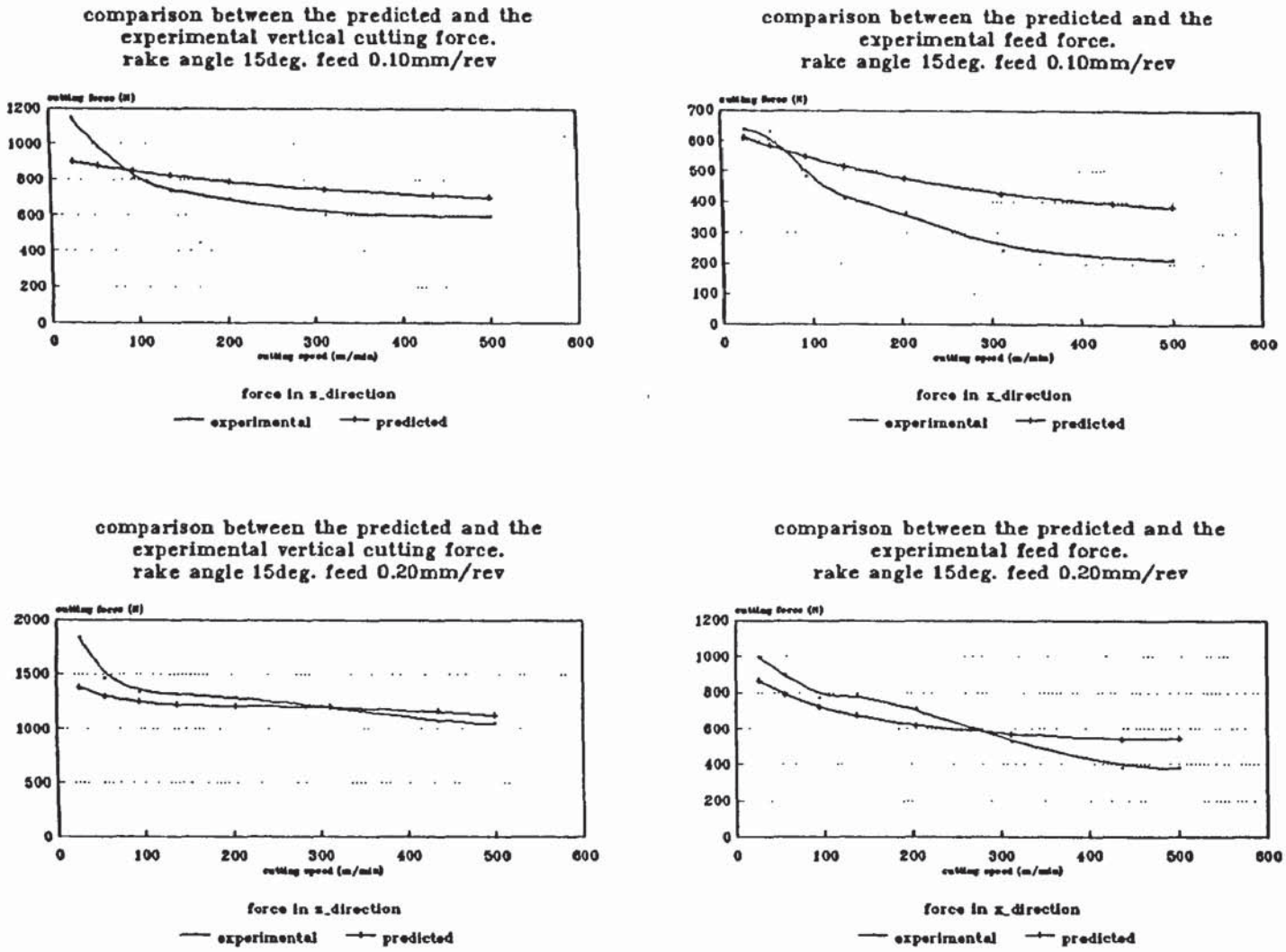

Fig. 3.20 Predicted and experimental forces, rake angle = 15 deg.

$S_0 = 0.10,\ 0.20$ mm/rev.

– The model is also used to predict the turning force components for the case of negative rake angle when machining same material as used in model building and the model predictions are compared to experimental measurements.

3.6. MODEL APPLICATION TO BAR TURNING WITH POSITIVE RAKE ANGLE TOOLS

In this section a verification of the ability of force predicting of the model is carried out through tests with same tool geometry machining different work material to that used to determine the coefficients of the model on the one hand. On the other hand this verification is also made through comparison of the predicted and the published results of Wu (1985) where a different tool geometry, work material and cutting conditions were used.

3.6.1. Bar turning with similar tool geometry

Turning tests were carried out on the Torshalla lathe for machining a S.A.E. 1045 under the cutting conditions summarized in Table 3.3. for which the experimental and the model calculated force components are shown in Fig. 3.21.

In contrast to the CDS2 used to determine the model coefficients, the forces are increasing for low speeds and reach a maximum value after which they decrease by the increase of the cutting speed (Fig. 3.21). The increasing characteristic of the cutting forces at low speeds can be attributed to the built–up edge which is typical of the workpiece material used. The examination of the tool edge, after cutting showed that a B.U.E. was present (Fig. 3.21) for all the cutting speeds falling to the left of the

work material	S.A.E. 1045 steel
out side diameter (mm)	38.10
Cutting configuration	Orthogonal dry bar turning
Uncut chip thickness (mm)	0.20, 0.25
Cutting speed (m/s)	0.43, 0.92, 1.57, 2.31, 3.40, 5.20, 7.27, 8.33
Depth of cut (mm)	1.50
Cutting tool	Standard steel cutting Grade tungsten carbide tools: TPUN 160304 edge radius less than 0.004 mm
Flank angle (deg)	5
Rake angle (deg)	6

Table 3.3 Experimental cutting conditions for bar turning.

speed corresponding the the maximum of the turning force components, and vice versa, i.e. no B.U.E. could be detected for the cutting speeds falling to the right of the speed at which the force components are maximum (Nigm *et al.*, 1972a). In the presence of the B.U.E., the effective rake angle appreciably increases over its nominal value set by the tool geometry. The difference between the effective and nominal rake angles increases with the increase in the B.U.E. size as shown by Zorev (1966) and decreases with the cutting speed as shown by Heginbotham *et al.* (1961). The increasing characteristic of the forces curves can thus be attributed to the decrease in the effective rake angle, resulting from the decrease of the B.U.E. size by the increase of the cutting speed (Ohgo, 1978). Moreover, the cutting conditions where the force components are maximum correspond to the eventual vanishing of the B.U.E. and the

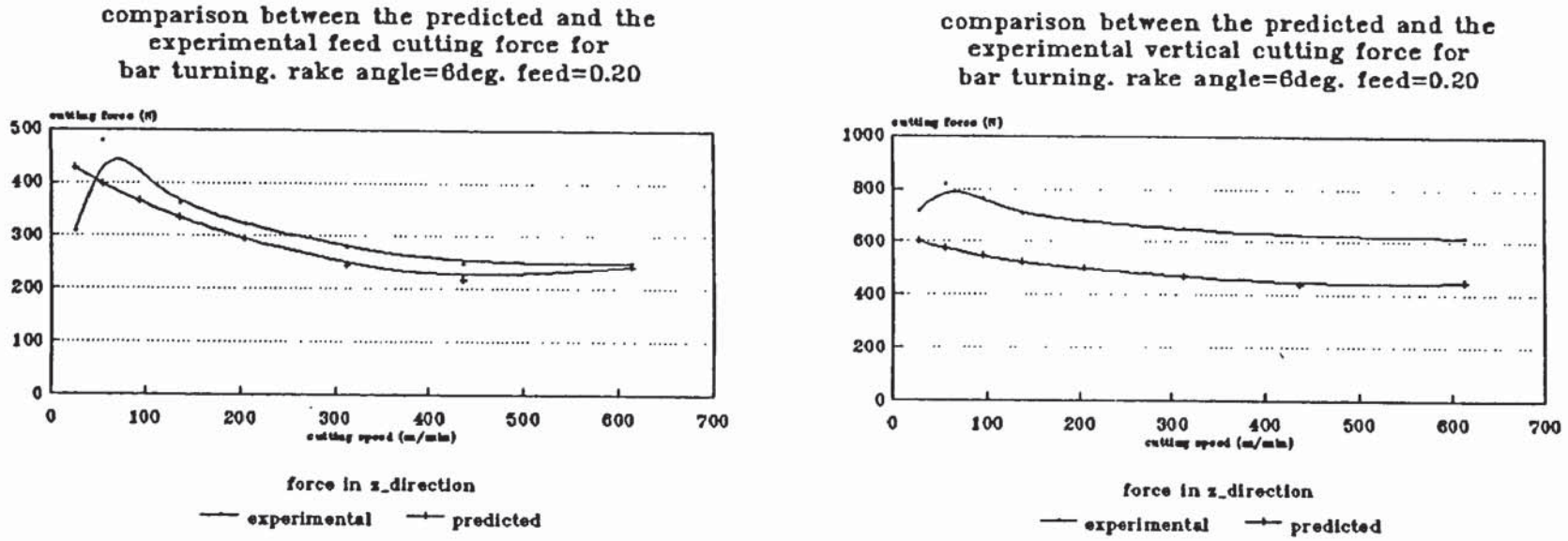

Fig. 3.21 Predicted and experimental force for bar–turning,

non modified model.

appearance of a thin built–up edge layer on the chip tool interface as stated by Zorev that at high cutting speeds a built–up edge still exists in the form of a thin film.

A first comparison between the measured and the predicted forces for bar turning showed that the model under–estimates the feed and cutting force with a an almost constant factor (Fig. 3.21). This difference may be attributed to the difference in the workpiece materials. As shown by (3.23) and (3.24), the turning force components are proportional to the material characteristics, these are the mean shear stress k and the ploughing factor p_s. Therefore, as the material used to build the model is softer than the bar material, the model is expected to underestimate the forces introduced by the machining process and the differences are attributed to the difference in the hardness of the two materials.

The hardness affects the turning forces system through its complex effect upon the chip thickness ratio r, the shear angle and the shear stress. It was shown (Wu *et al.*, 1990) that for ceramic tools, and for speeds of the order of 1.52m/s and feeds of 0.15 to 0.89 mm/rev, the chip thickness ratio as well as the shear angle increase with the hardness of the work material. However, under similar cutting range, the turning force components were observed to decrease with the hardness as the hardness increases up to about 44 Rc, where the turning force components reach their minimum, and above which a sharp increase in the values of these components is observed.

This is to say that the effect of the hardness upon the turning forces is not straight forwards understood and needs to be studied in more detail in a further work. As far as this work is concerned, the analysis is confined to determine a proportionality factor H called the "hardness factor" to correct the model predicted forces based on the results of

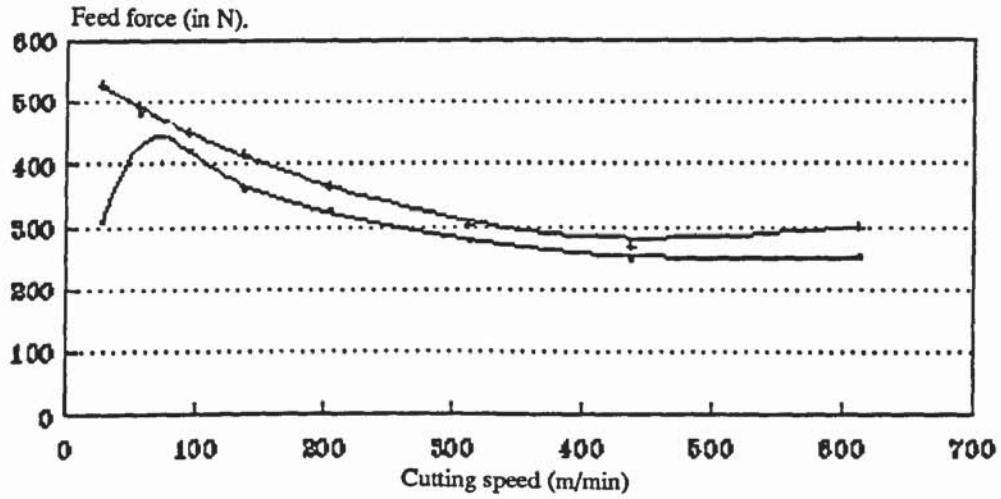

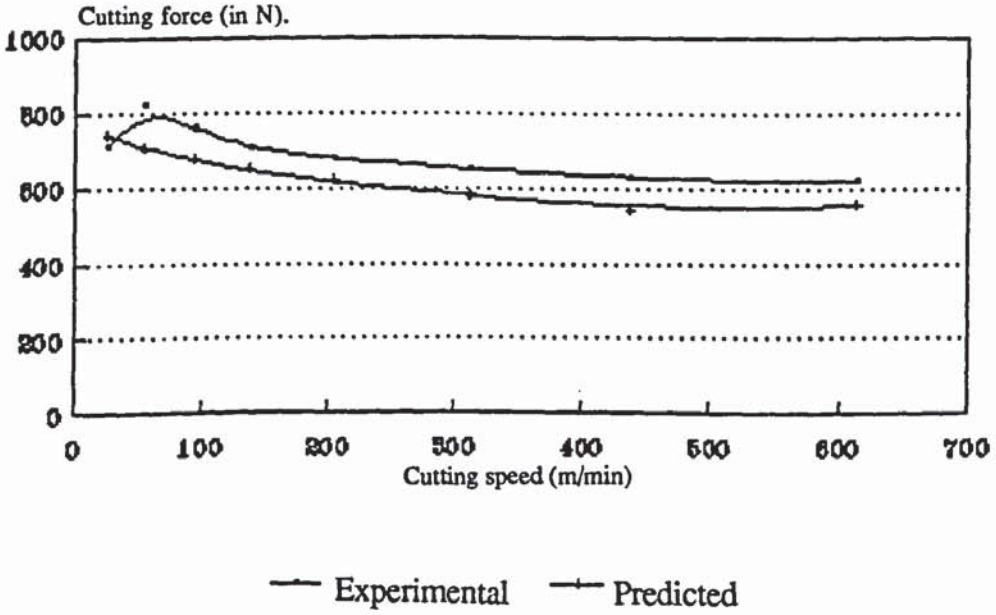

Fig. 3.22 Predicted and experimental turning force components for bar turning $\alpha = 6$ deg. $S_0 = 0.20$ mm/rev.

the predicted and the measured forces. For the sake of simulating the real work shop condition when a prediction of machining forces is to be made, it was decided to determine this hardness factor for an arbitrary set of cutting conditions that is: 3.4 m/s as speed and 0.20 mm/rev as feed. The determined factor using (3.42) is as given by (3.43).

$$H = \left[\frac{\left(F_x^2 + F_z^2\right)_{measured}}{\left(F_x^2 + F_z^2\right)_{predicted}} \right]^{\frac{1}{2}} \qquad (3.42)$$

$$H = 1.24 \qquad (3.43)$$

Using the hardness factor H of (3.43), the predicted forces are found to represent the experimental turning forces (Fig. 3.22)by an error less than 7.6% for the range of cutting conditions where no built–up edge exists. However, at low speed and because of the existence of the B.U.E., the error in the force prediction is much higher as the model was built on the assumption that no built–up edge is present with the range of its validity.

The complex phenomenon of the built–up edge is a result of several factors characterising the chip formation process. Zorev (1966) and Nakajima *et al.* (1968) stated that the B.U.E. exists whenever there is a stressed state on the chip–tool interface at which the plasticity condition is not satisfied. In metal cutting this condition is governed by the normal and tangential stress on the chip tool interface as well as the flow stress of the chip adjacent to the tool rake face. Moreover, Shaw (1984) attributed the B.U.E. to both the pressure welding between the chip and tool rake face and the strain hardening tendency of the metal, and showed that there will be no tendency for

B.U.E. formation when the temperature of the metal is equal to or higher than the recrystalisation temperature of the work metal. The built–up edge can therefore be considered as a phenomenon which is to a great deal capable of characterising the state on the chip–tool interface and in the primary shear zone. Consequentially, a unique model cannot hold the effect of the cutting conditions on the turning force components as well as predicting the size and the effect of the built–up edge upon the chip formation process. Furthermore, because no B.U.E. exists at high machining conditions which are of most concern to the present investigation, the model is valid within the range of the investigated conditions where the B.U.E. does not exist.

3.6.2. Bar turning with different tool geometry

Wu *et al.* (1985) carried out an experimental set of tests for turning a low carbon steel ASE 1020 with carbide tools as summarised in Table 3.4.

work material	S.A.E. 1020 steel
Cutting configuration	Orthogonal dry bar turning
Uncut chip thickness (mm)	0.13, 0.152, 0.178, 0.211
Cutting speed (m/s)	3, 4, 5, 6
Depth of cut (mm)	1.61
Cutting tool	ANSI TPN 431 carbide
Flank angle (deg)	7
Rake angle (deg)	4

Table 3.4 Experimental cutting conditions for bar turning (Wu *et al.*, 1985).

Similarly to previous investigation (3.6.1), the model under–estimates the bar turning force (Fig. 3.23) as the material on which the model was based is softer than the material used by Wu *et al.*. However, the proportionality coefficient or the hardness factor was determined using (3.42) at an arbitrary set of cutting conditions , these are cutting speed of 3m/s and feed of 0.13 mm/rev. The hardness factor is found to be:

$$H = 1.73 \qquad (3.44)$$

The predicted forces for the above conditions (Table 3.4) are corrected by the hardness factor and the obtained results (Fig. 3.24 to Fig. 3.27) show that the error in predicting the turning force components is always less than 10% except for the cutting force at 4m/s as speed and 0.211mm/rev as feed where the error reaches 13.4%.

It is seen therefore that the model provides a satisfactory prediction of the turning forces components for a harder material which is cut under a different set of machining conditions by a cutting tool of a different geometry as those used in the experimental data for the determination of the model coefficients.

Measured (Wu) and predicted (model)
feed force in turning: $\alpha = 4$ deg. $\gamma = 7$ deg., $S_0 = 0.130$mm/rev.
model non corrected.

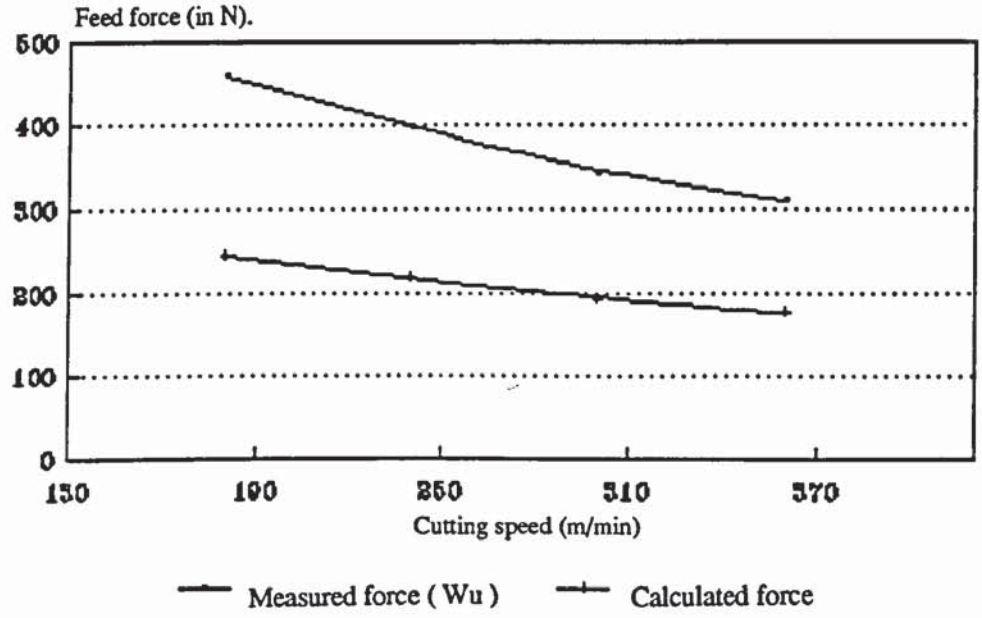

Measured (Wu) and predicted (model)
cutting force in turning: $\alpha = 4$ deg. $\gamma = 7$ deg., $S_0 = 0.130$mm/rev.
model non corrected.

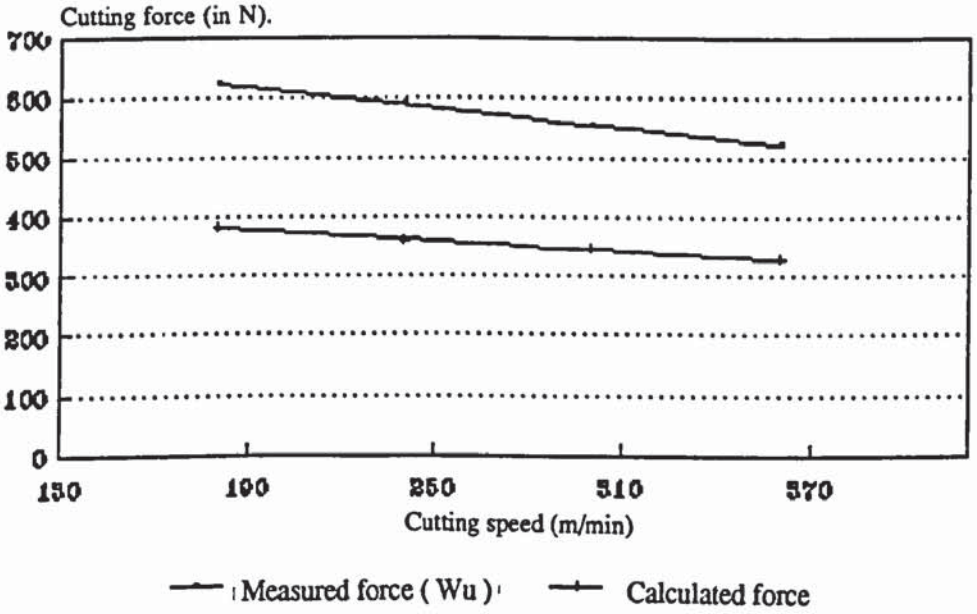

Fig. 3.23 Predicted and experimental turning force components (Wu, 1985)

bar turning, non–modified model.

Measured (Wu) and predicted (model)
feed force in turning: $\alpha = 4$ deg. $\gamma = 7$ deg., $S_0 = 0.130$mm/rev.

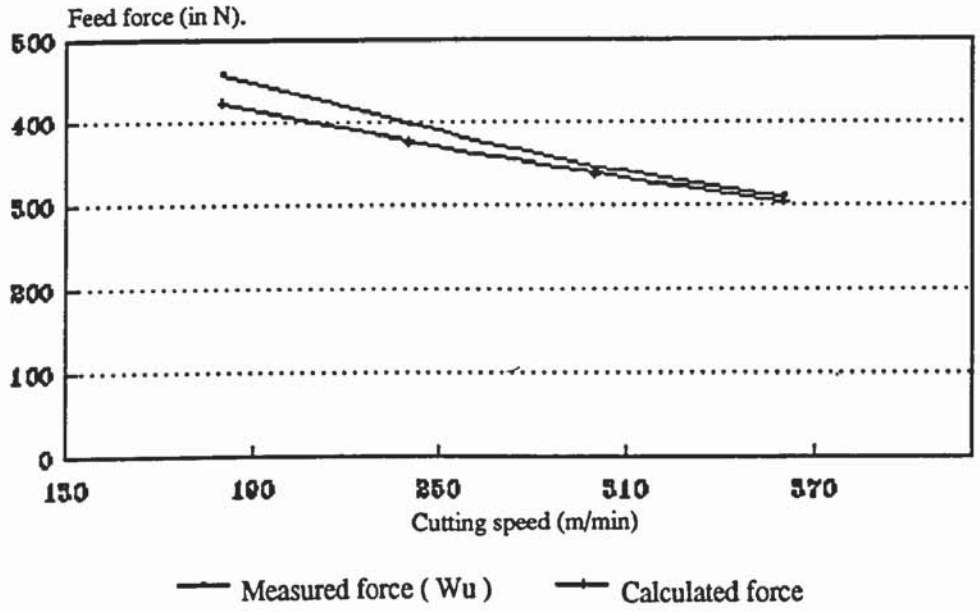

Measured (Wu) and predicted (model)
cutting force in turning: $\alpha = 4$ deg. $\gamma = 7$ deg., $S_0 = 0.130$mm/rev.

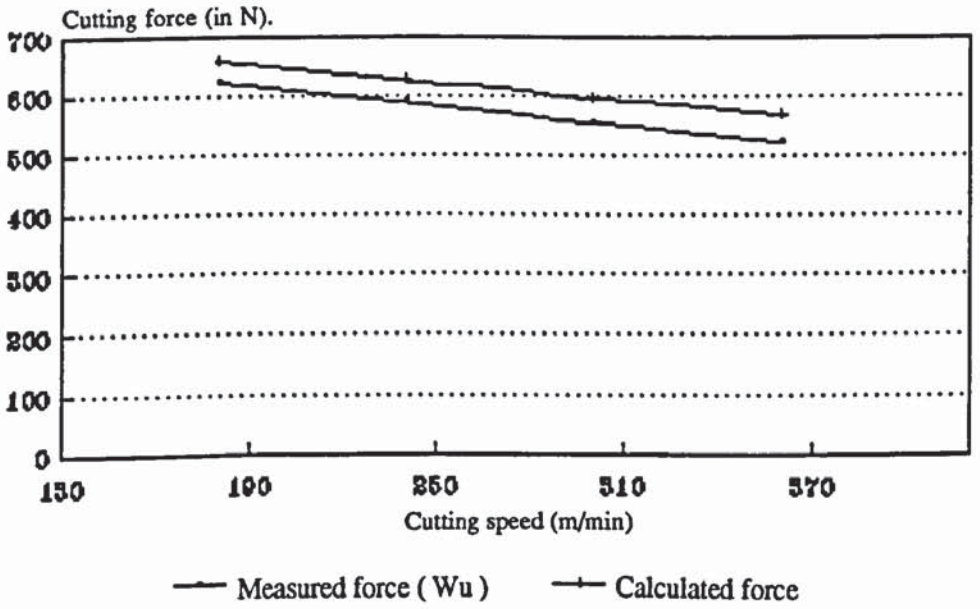

Fig. 3.24 Predicted and experimental turning force components (Wu, 1985)

$S_0 = 0.130$ mm/rev.

Measured (Wu) and predicted (model)
feed force in turning: $\alpha = 4$ deg. $\gamma = 7$ deg., $S_0 = 0.162$mm/rev.

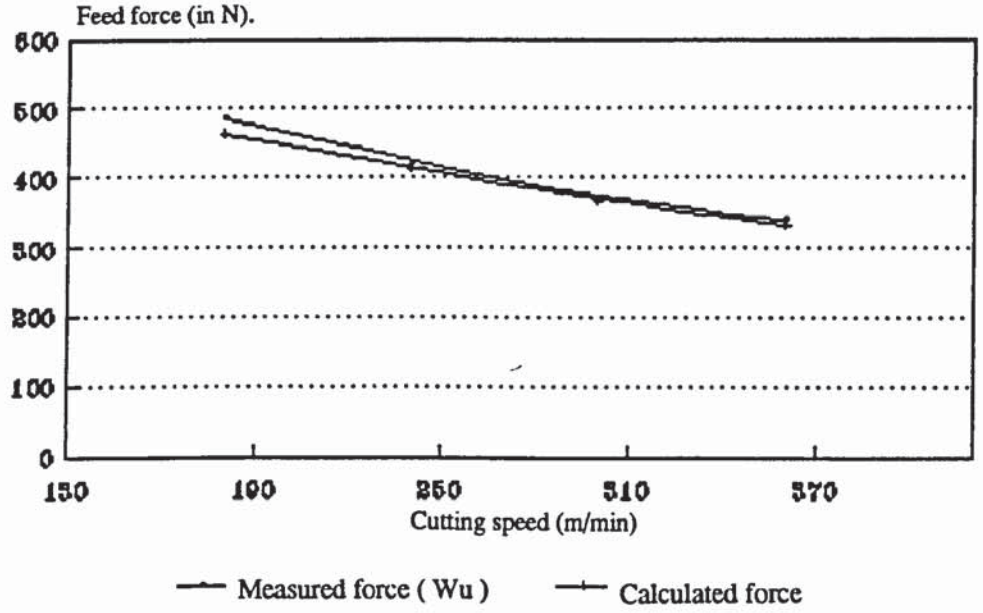

Measured (Wu) and predicted (model)
cutting force in turning: $\alpha = 4$ deg. $\gamma = 7$ deg., $S_0 = 0.162$mm/rev.

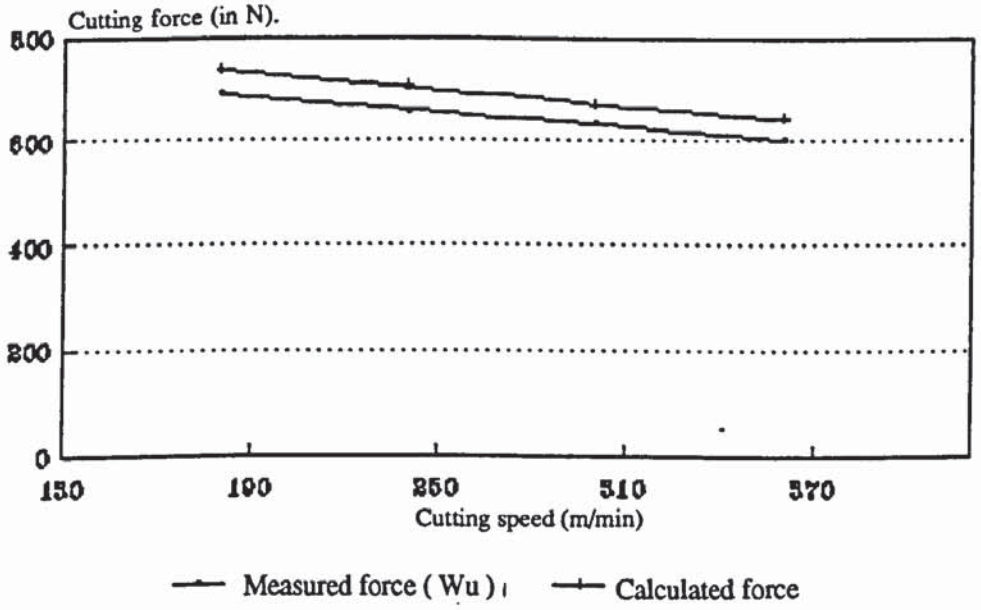

Fig. 3.25 Predicted and experimental turning force components (Wu, 1985)

$S_0 = 0.152$ mm/rev.

Measured (Wu) and predicted (model)
feed force in turning: $\alpha = 4$ deg. $\gamma = 7$ deg., $S_0 = 0.178$mm/rev.

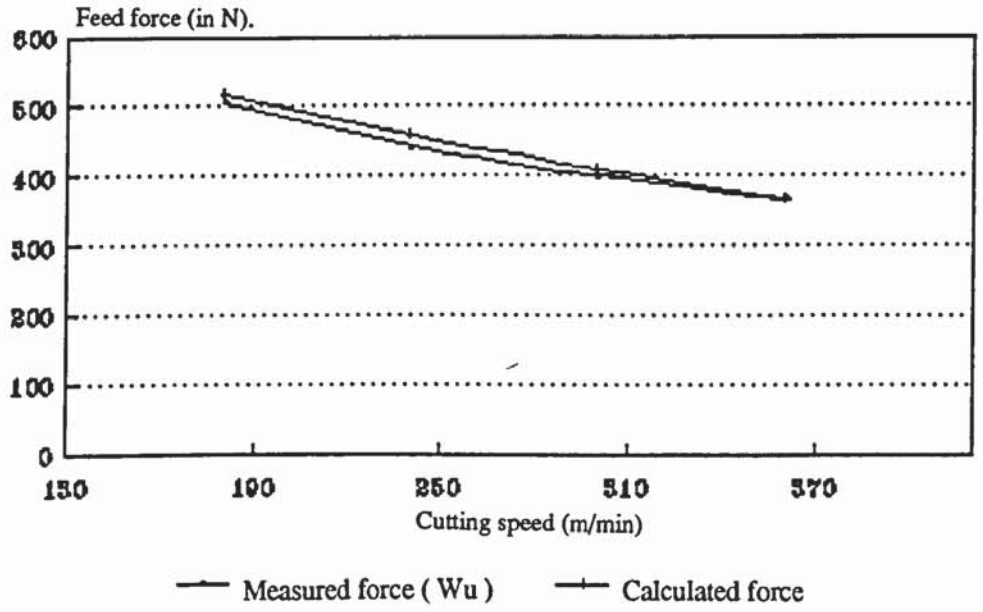

Measured (Wu) and predicted (model)
cutting force in turning: $\alpha = 4$ deg. $\gamma = 7$ deg., $S_0 = 0.178$mm/rev

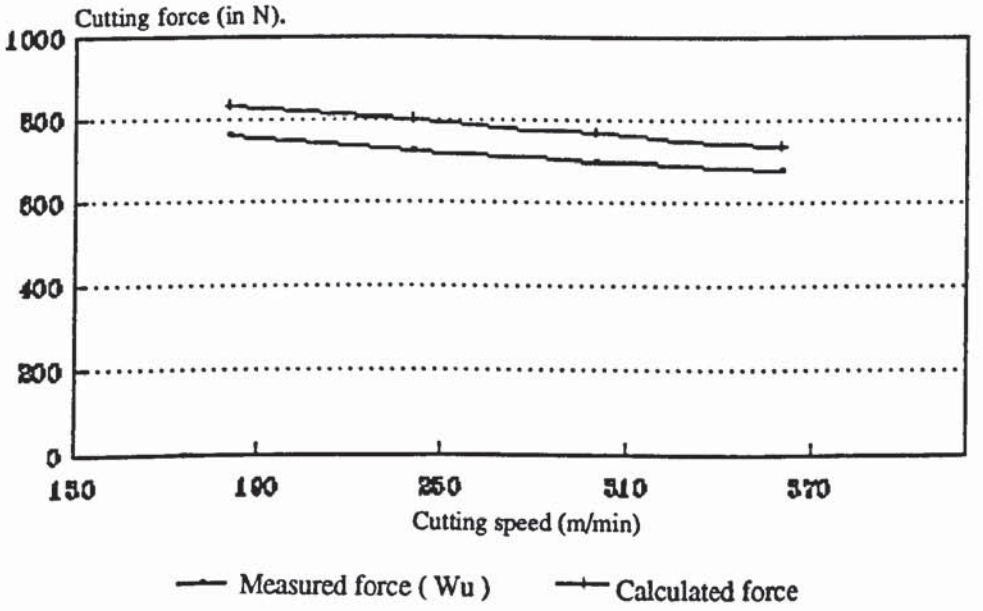

Fig. 3.26 Predicted and experimental turning force components (Wu, 1985)

$S_0 = 0.178$ mm/rev.

Measured (Wu) and predicted (model)
feed force in turning: $\alpha = 4$ deg. $\gamma = 7$ deg., $S_0 = 0.211$mm/rev.

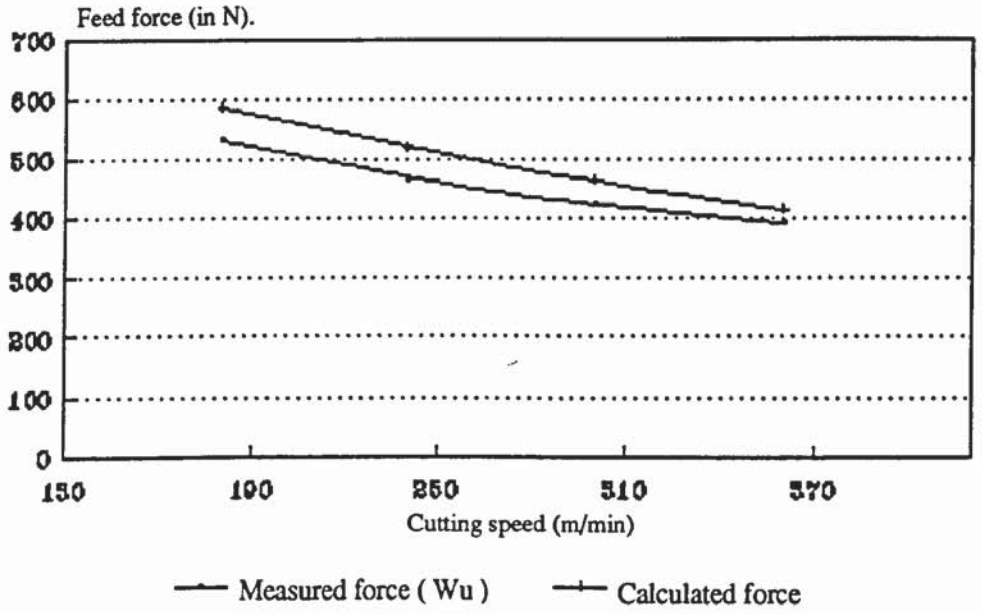

Measured (Wu) and predicted (model)
cutting force in turning: $\alpha = 4$ deg. $\gamma = 7$ deg., $S_0 = 0.211$mm/rev.

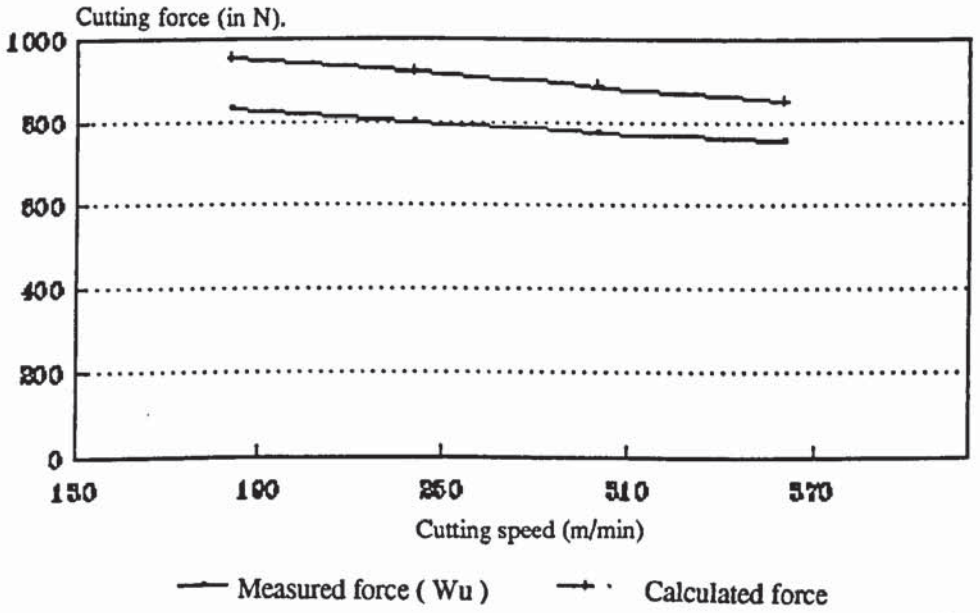

Fig. 3.27 Predicted and experimental turning force components (Wu, 1985)

$S_0 = 0.211$ mm/rev.

3.7. MODEL APPLICATION TO NEGATIVE RAKE ANGLE TOOLS

This section discusses briefly the prediction of the turning force components when a tool of negative rake angle is used.

The experiments were conducted on the Torshalla lathe (Fig. 3.3) and the tool holder was turned around to have negative rake angles as shown in Table 3.5. It is worth mentioning that for these tests, similar cutting conditions, namely feed and cutting speed, are adopted as those used to build the model but with two values of negative rake angle –5 and –10 degrees.

work material	Tube CDS2, B.S. 980
out side diameter (mm)	38.10
Cutting configuration	Orthogonal dry bar turning
Uncut chip thickness (mm)	0.10, 0.20, 0.25
Cutting speed (m/s)	0.43, 0.92, 1.57, 2.31, 3.40, 5.20, 7.27, 8.33
Depth of cut (mm)	4.00
Cutting tool	Standard steel cutting Grade tungsten carbide tools: TPUN 160304 edge radius less than 0.004 mm
Flank angle (deg)	5
Rake angle (deg)	– 5, – 10

Table 3.5 Experimental cutting conditions for turning with negative rake angle tool.

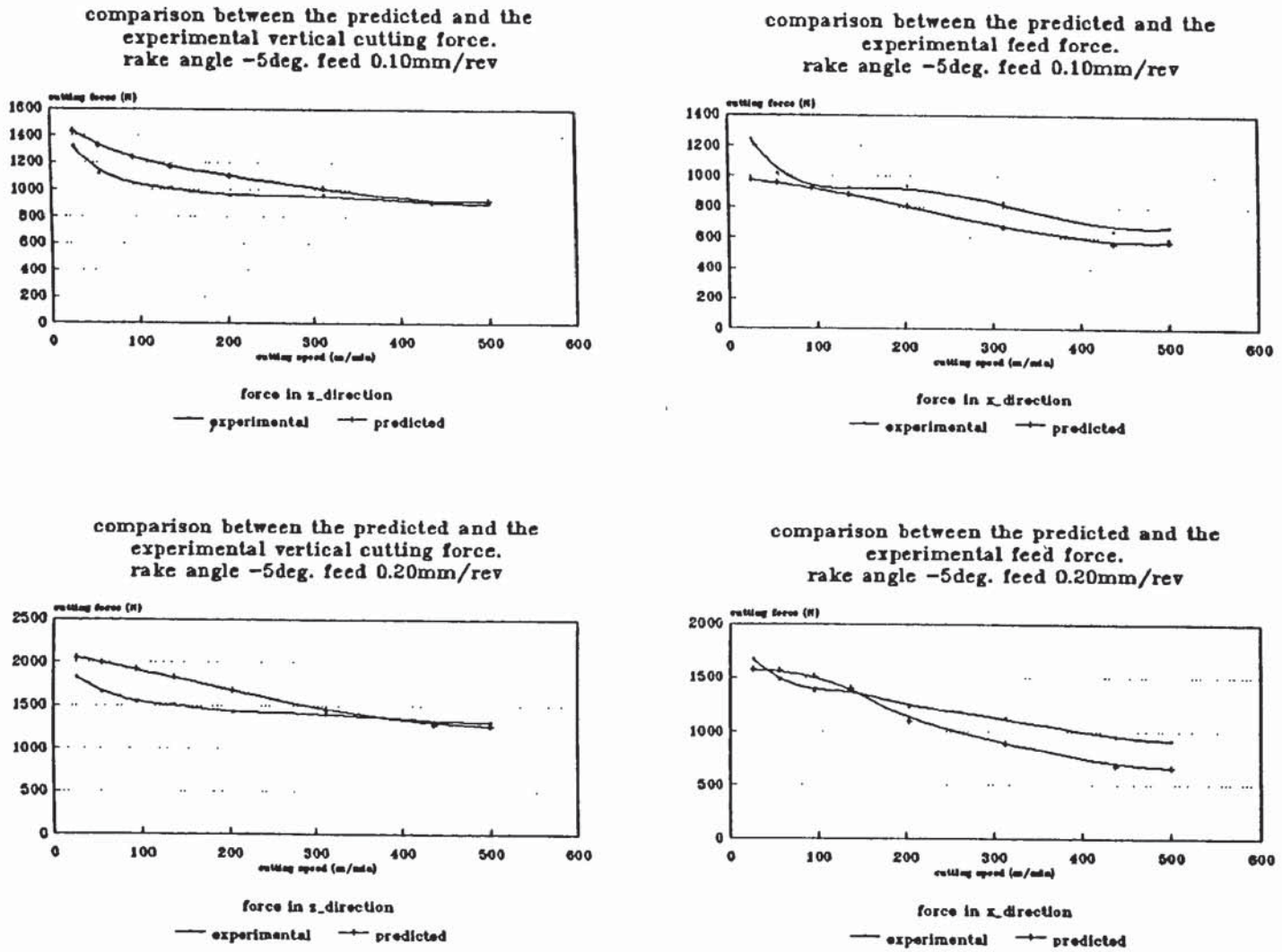

Fig. 3.28 Predicted and experimental turning force components

rake angle = –5 deg., S_0 = 0.10, 0.20 mm/rev.

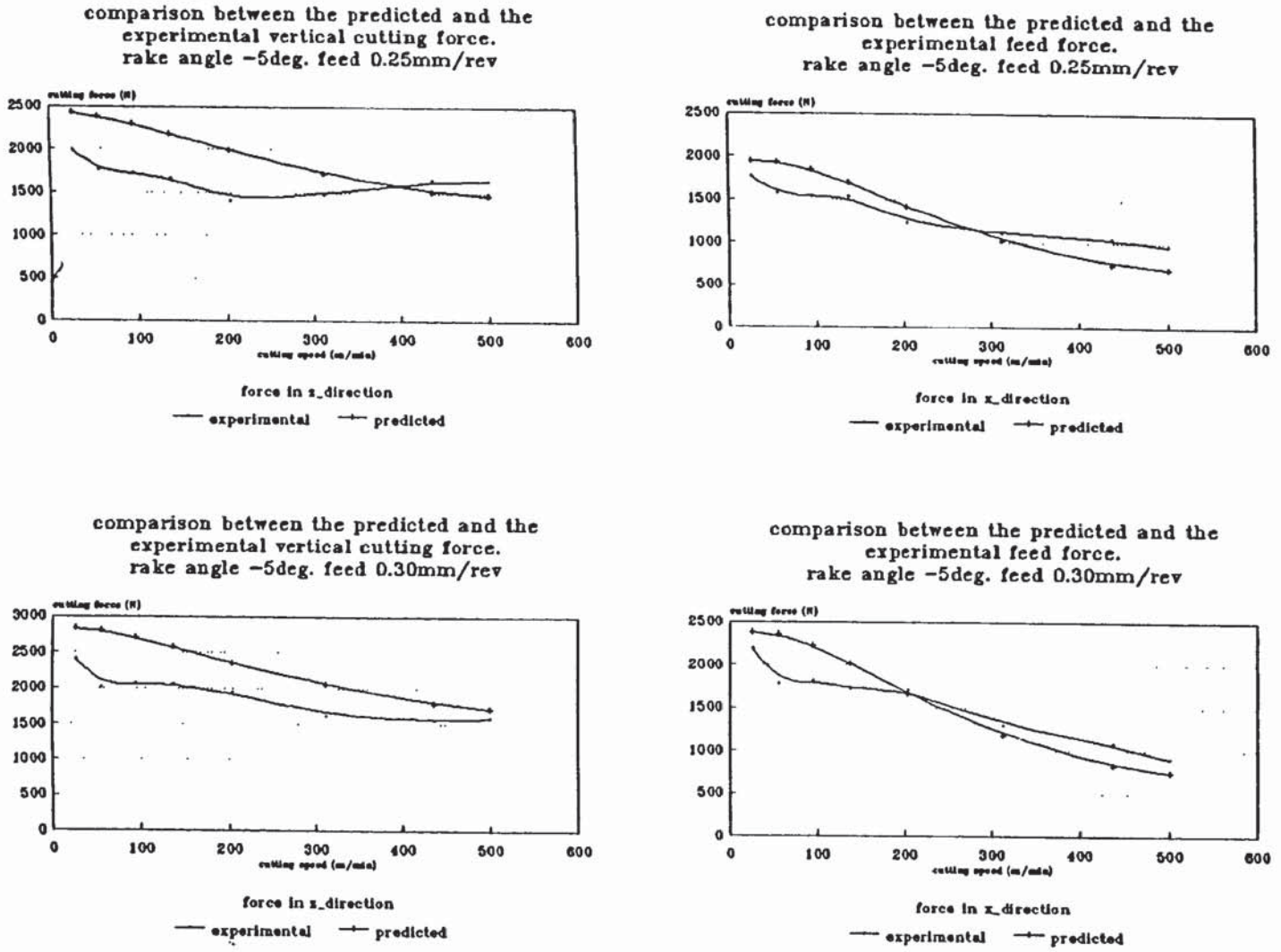

Fig. 3.29 Predicted and experimental turning force components

rake angle = –5 deg., S_0 = 0.25, 0.30 mm/rev.

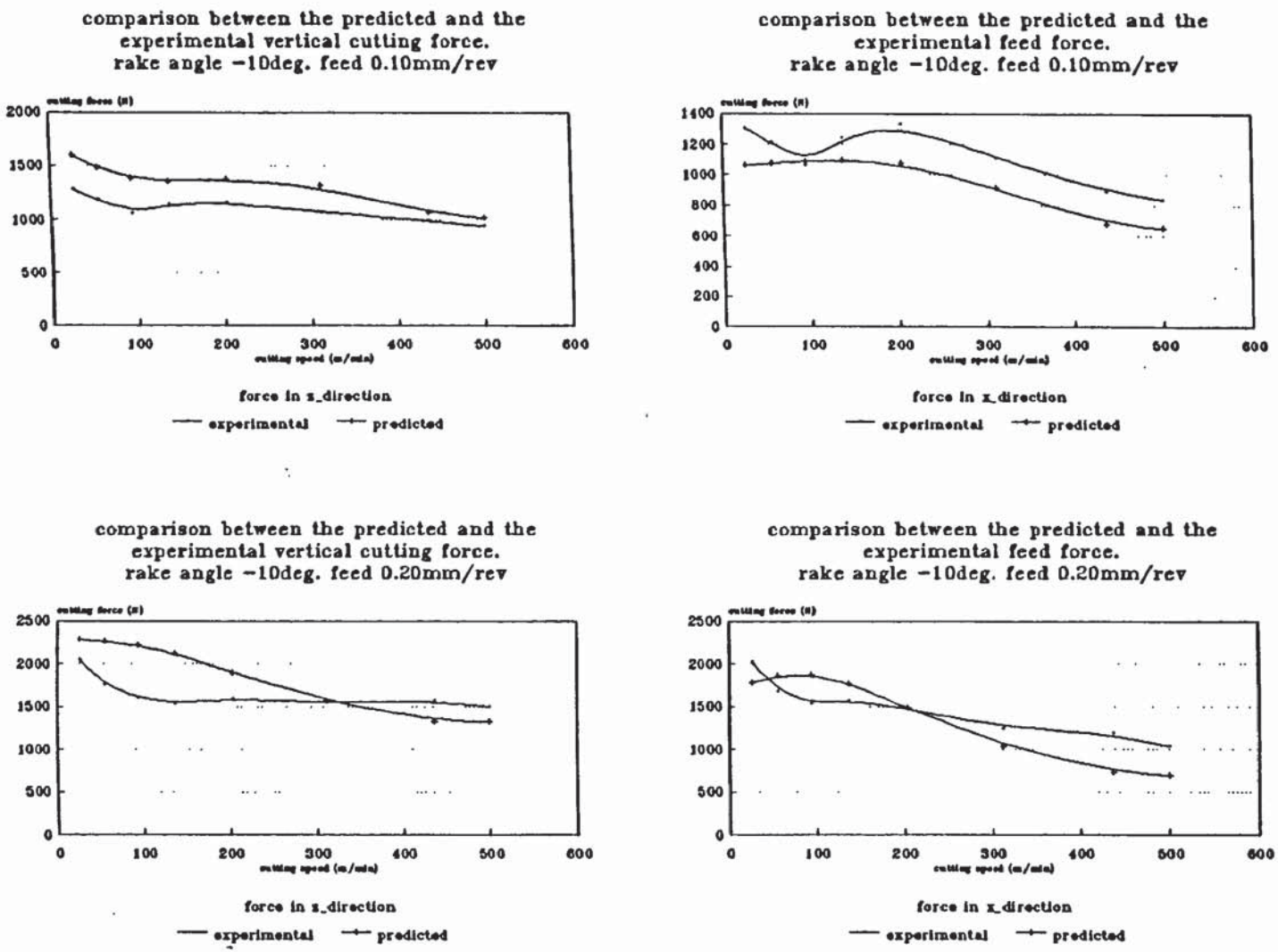

Fig. 3.30 Predicted and experimental turning force components

rake angle = –10 deg., S_0 = 0.10, 0.20 mm/rev.

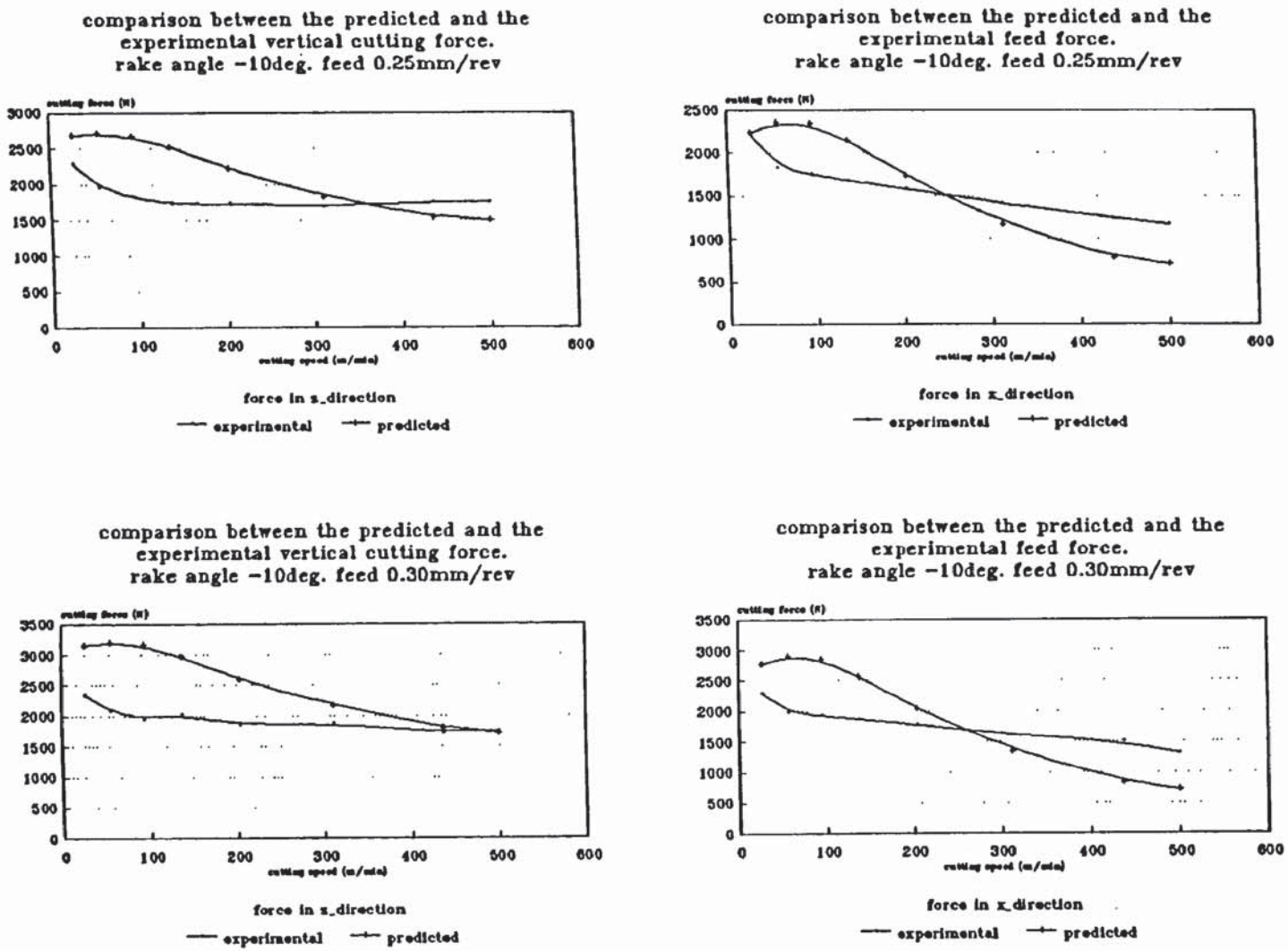

Fig. 3.31 Predicted and experimental turning force components

rake angle = −10 deg., S_0 = 0.25, 0.30 mm/rev.

Fig. 3.28 to Fig. 3.31 show the plots of the measured and the predicted turning force components for the cutting conditions in Table 3.5.

The model provides a satisfactory prediction of the forces for low feeds and also for higher speeds than 5 m/s this error remains smaller than 15% when the feed increases from 0.10 to 0.30 mm/rev. However, for lower speeds, the error in predicting the cutting forces is generally increased by the feed. Nevertheless, for low speeds, some differences between the predicted and the measured forces are observed and can even be as large as 50%. This is still in support of the model since the negative rake angle tools are usually used for high machining conditions

3.8. CONCLUSION

This investigation has shown the possibility of machining forces during turning by considering both the contact between the tool and the chip along the rake and the deformation around the tool nose and along the flank of the tool. The former action is attributed to the shearing process and the latter to the ploughing mechanism.

The theoretical analysis has led to establish a new theoretical relationships for the turning force components where new parameters controlling the cutting force are introduced to include the effect of the tool size. Experimental data was obtained from turning tube in orthogonal conditions and used to yield an analytical expression of the rake force ratio, the uncut chip thickness ratio, the mean shear stress, the depth of the tool penetration and the mean friction coefficient on the flank of the tool.

Moreover, the model was used to predict the turning force over a wide range of the cutting conditions when machining different work materials using different tool geometries and the following conclusions are drawn:

– Good prediction of the forces is obtained for bar turning of different materials when a hardness factor is introduced.
– The model also provides a good prediction of the turning force when negative rake angle tools are used to cut a tubular workpiece and best prediction is obtained for high speeds and low feeds.

A direct consequence of the findings of this investigations is that the steady state coefficients for a particular work and tool geometry can be established over a wide range of the cutting conditions from a relatively small number of the machining tests. The expressions of the model steady state coefficients will be used in Chapter 4 to predict the forces for a worn tool and suitably adjusted in Chapter 7 to predict the machining forces in dynamic turning.

Chapter 4

EXTENSION OF STEADY STATE MODEL TO INCLUDE FLANK WEAR OF THE TOOL

4.1. INTRODUCTION

A model for steady state turning with new tool was developed in Chapter 3 and its coefficients were determined through a set of cutting tests. As the cutting process progresses, the tool edge is subject to range of failure possibilities and its life is limited. In the following chapter, the model developed in Chapter 3 for steady state turning with new cutting edge is extended to include the effect of flank wear. Analyses of tool wear, throughout the last three decades, have more emphasized on the flank wear than on the crater wear because of its direct effect on the quality of the machining process. Flank wear results in an increased tendency for chatter vibrations and in poor dimensions and quality of machined surfaces (Chapter 1). The developed model in the following chapter is confined to modelling the turning process with tool flank wear and predictions of the model are compared to experimental measurements to justify the approaches of the actual modelling. It is also aimed in this chapter to show which component of the turning force is more suitable for flank wear monitoring.

4.2. MODEL OF STEADY STATE TURNING WITH WORN CUTTING EDGE

The flow of the work material around the cutting edge of a new tool was investigated and discussed in Chapter 3. As shown in Fig. 3.4(a) and because of the ploughing

mechanism, the material is compressed as it traverses the region AB and then recovers elastically as it clears the lowest point B of the tool edge, and then traverses the region BD.

Similar to the material flow under unworn tool, the material below a tool with flank wear Wf can be represented as shown in Fig. 4.1. Here again, the material is compressed in feed direction as it traverses AB but, in contrast to material flow around new tool (3.3.3), it is not possible for the workpiece material to begin elastic recovery as it clears B because of the presence of the wear land Wf = BC (Rubenstein *et al.*, 1985). The material will maintain constant depth of deformation as it flows from B to C and this is because the flank surface is assumed to be parallel to the cutting speed. This assumption is adopted by almost all the authors dealing with flank wear modelling. However, experimental simulation of flank wear together with observation using Scanning Electron Microscope (S. E. M.) showed that tool wears to form a negative flank angle and more details are reported in section 4.3.2. Applying the same assumptions as presented in 3.3.3., it can be seen that the worn tool configuration of Fig. 4.1 is similar to the configuration of new tool between A and B and between C and D of Fig. 3.4. The only difference is the introduction of new intermediate surface BC that schematically refers to flank wear. The depth of tool penetration between A and B and between C and D is given by 3.11 and 3.12 respectively whilst along the worn area BC tool penetration is expressed as:

$$\xi(z) = \zeta \qquad \text{for } z_B \leq z \leq z_C \qquad (4.1)$$

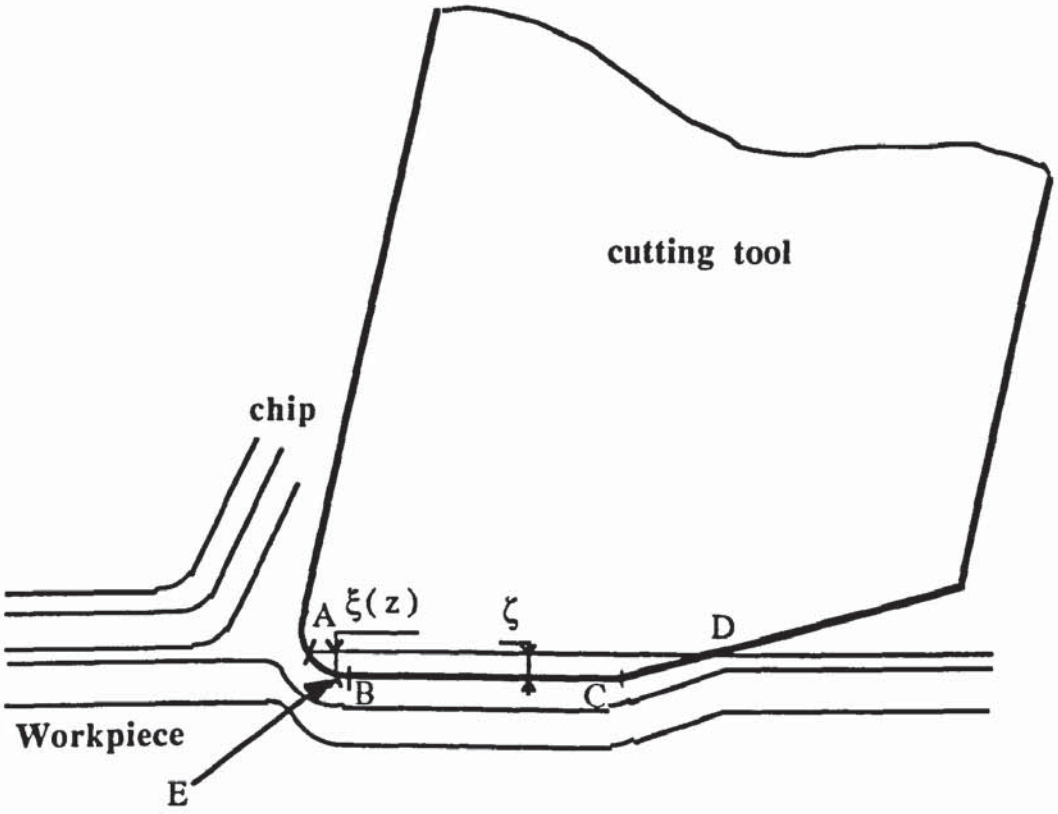

Fig. 4.1 Flow of work material around worn cutting edge.

ζ is the depth of the material deformation at the lowest point of the cutting edge. At the starting point A of deformation and at the last point of contact the material is not deformed and $\xi(0) = \xi(z_D) = 0$, therefore z_B is as given by (3.13) and:

$$z_C = z_B + Wf \qquad (4.2)$$

$$z_D = z_C + \frac{\zeta}{\tan(\gamma)} \qquad (4.3)$$

Considering that the elementary force in direction of feed at an arbitrary point E is proportional to the depth of deformation for elastic deformations and characterising the contact tool–workpiece by an equivalent mean friction angle τ, the elementary ploughing force components along the flank of the tool can be expressed as:

$$dP_x = p_s w \xi(z)\, dz \qquad (4.4)$$

$$dP_z = p_s w \xi(z) \tan(\tau + \theta)\, dz \qquad \text{for } 0 \le z \le z_B \qquad (4.5)$$

$$dP_z = p_s w \xi(z) \tan(\tau)\, dz \qquad \text{for } z_B \le z \le z_C \qquad (4.6)$$

$$dP_z = p_s w \xi(z) \tan(\tau - \gamma)\, dz \qquad \text{for } z_C \le z \le z_D \qquad (4.7)$$

Integration of (4.4) to (4.7) from A to D along the secondary edge of the cutting tool lead to express the ploughing components of the turning force in the case of worn edge in the following form:

$$P_x = (P_x)_{Wf=0} + w\ p_s\ Wf \qquad (4.8)$$

$$P_z = (P_z)_{Wf=0} + w\ p_s\ Wf\ \tan(\tau) \qquad (4.9)$$

Where $(P_x)_{Wf=0}$ and $(P_z)_{Wf=0}$ refer to the ploughing components in x and z directions for new cutting edge and are given by (3.19) and (3.20).

As the effect of the crater wear is not introduced in this study, recalling from 3.3.4. of Chapter 3 together with (4.8) and (4.9), in case of cutting with worn flank the turning force components can be expressed as:

$$F_x = \frac{w\,C_s\,S_0\,k}{\sin(\phi)\,(\cos(\phi) - C_s\sin(\phi))} + w\,p_s\,\zeta\left\{Wf + \frac{1}{2}\frac{\zeta}{\tan(\gamma)}\right\} \qquad (4.10)$$

$$F_z = \frac{w\,S_0\,k}{\sin(\phi)\,(\cos(\phi) - C_s\sin(\phi))}$$

$$+ w\,p_s\,\zeta\left\{Wf\tan(\tau) + \frac{1}{2}\frac{\zeta}{\tan(\gamma)}\tan(\tau - \gamma)\right\} \qquad (4.11)$$

(4.10) and (4.11) show that turning force components are increasing linearly with flank wear Wf, and that the force introduced by the worn surface increases more rapidly in feed direction than in cutting direction and this force is proportional to depth of tool penetration, depth of cut and to the specific ploughing factor. Moreover, the ratio of the vertical to the horizontal components of the ploughing force introduced by flank wear is equal to the equivalent friction coefficient along the worn area.

The present ploughing model expresses the turning force acting upon worn tool in terms of dependent and independent parameters. As the cutting configuration shown in Fig. 4.1 remains similar to the original configuration of Chapter 3, the dependent parameters can be determined from results of steady state turning tests with new tool. These were obtained through the analysis conducted in the previous chapter and their expressions will be used to predict the turning force components for different wear levels and cutting conditions.

4.3. EXPERIMENTAL INVESTIGATION

4.3.1. Cutting conditions

The cutting tests are carried out on TORSHALLA CNC–lathe using the same experimental set–up as 3.6.1. The cutting conditions used are summarised in Table 4.1. Flank wear is considered as the average of the flank wear before and after each cutting test. Work material of the same specifications as 3.6.1. is used when cutting a bar workpiece under orthogonal machining configuration. Turning force components in feed and cutting directions are sensed by a piezoelectric dynamometer, amplified through a Kistler amplifier and recorded onto Macintosh hard disk using Maclab hardware. The steady state forces are obtained by cutting off all frequencies higher than 10Hz.

4.3.2. Tool wear simulation

Tool wear is a very complex process as discussed in Chapter 1 and tool failure is generally caused by a combination of crater wear, flank wear, thermal shock, etc; so that true wear can only be achieved under operational conditions. As carbide tips are

Work material	S.A.E. 1045 steel
Out side diameter (mm)	76.20
Cutting configuration	Orthogonal dry bar turning
Flank wear (μm)	0, 35, 121, 160, 230, 280
EFFECT OF FEED	
Feed (mm/rev)	0.15, 0.20, 0.25, 0.30
Cutting speed (m/s)	3.40
EFFECT OF SPEED	
Cutting speed (m/s)	2.28, 3.40, 5.20, 7.27
Feed (mm/rev)	0.20
Depth of cut (mm)	1.50
Cutting tool	Standard steel cutting Grade tungsten carbide tools: TPUN 160304 edge radius less than 0.004 mm
Flank angle (deg.)	5
Rake angle (deg.)	6

Table 4.1 Experimental conditions for steady state bar turning with worn tool.

used, the extended tool wear testing is very consuming in both workpieces and time, it is necessary to devise a method which would either simulate or accelerate the tool wear.

The importance of flank wear as indication of overall cutting is known. In an attempt to establish what degrees of flank wear would correspond with blunt or worn tool

condition, tests were carried out at various cutting speeds and feeds and when a noticeable deterioration in the cutting performances occurred, the tool is removed and examined under a tool room microscope. These examinations showed that apart from localised heat discolouration and some evidence of small criterion on the rake of the tool, the most notable wear region appears to occur in the region of the tool flank (Fig. 4.2). The clearance face of the tool is worn away and a flat established along the cutting edge and around the tool nose. Repeated tests with new edges established that a flank wear higher than 250μm usually leads to a chipping and tool breakage because of higher wear resistance, as the case for carbide, is accompanied by greater brittleness of tool material.

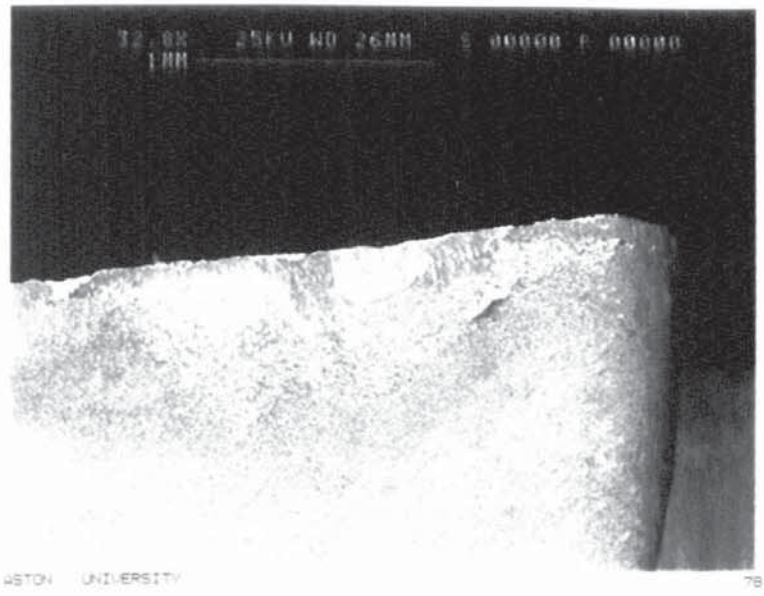

Fig. 4.2 S. E. M. photograph of the cutting edge.

It was therefore decided to simulate worn tools by grinding an artificial wear land onto the cutting edge. Initial tests found these cut either almost as well as new tools or too fragile so they chip away by the first contact with the workpiece. The former is because a new tool edge is grounded whereas the latter is attributed to the existence of some grooves along the cutting edge due to the grinding process. Experimental investigation showed, however, that worn tools can be produced by grinding an artificial wear land with a slightly negative clearance. Many previous works assume the worn flank as parallel to the mean cutting speed because the contact between the tool and the workpiece is along a surface parallel to the cutting speed which indirectly considers wear rate constant along the active edge of the tool. Studies of the rate of tool flank wear have shown however that, on one hand, the flank wear rate is depending on the temperature and the position along the workpiece–tool contact and that, on the other hand, the temperature is maximum at the tool tip and decreases along the flank edge as the distance from the cutting edge increases (Boothroyd, 1981). This therefore shows that the overall wear will lead to the formation of negative flank angle rather than nil angle. Nonetheless, the experimental observations (Fig. 4.2) proved that this negative angle is of small value ($\approx$ –0.5 to –0.8deg.) and therefore modelling the worn flank as parallel to the mean direction of the cutting speed will not much affect the accuracy of the prediction of machining force components.

For tool wear simulation, it was not feasible to obtain with grinding process values of flank wear lower than 150µm because of the small value of the flank angle. It was decided therefore to naturally wear the tools for lower values of flank wear and for higher wear levels, to proceed first by initiating the wear by grinding a small amount of flank wear and finish it by machining to the desired amount of wear.

4.3.3. Experimental results

The obtained experimental turning force components are presented in Fig. 4.3 to Fig. 4.6 for the cutting conditions under investigation. It can be seen as first remark that both feed and cutting forces are increasing with flank wear as is expected. This increase can be approximated with linear variation with good correlation factor. However, as can be seen from Fig. 4.3 and Fig. 4.4, the increase is happening with two different slopes. The feed force is increasing with flank wear but with small variation rate for lower width of flank wear than 120μm whilst when the amount of wear exceeds this value the feed force is observed to become more sensitive to flank wear and increases with much higher rate. In contrast, cutting force is found to have a constant slope of variation with flank wear.

Furthermore, it is found that the sensitivity of increase of turning force components depends upon the amount of wear and the cutting speed. At low cutting speed the feed force increases by 40% while at higher speed as 7.27m/s it increases by 94% as the wear increases up to 280μm. Whereas, for the same increase of flank wear, the cutting force increases by 14.5% when cutting at 2.28m/s and by 7.31% at cutting speed of 7.27m/s. The sensitivity of the feed force to flank wear is increasing while that of the cutting force is decreasing with cutting speed. No consistent trend can be found between the sensitivity of flank wear increase and feed rate. In other words, the variation of the turning force components with flank wear does not appear to be a simple linear function of the feed. Similar results were obtained by Shi *et al.* (1990) where feed force was found to increase more rapidly with flank wear than the cutting force.

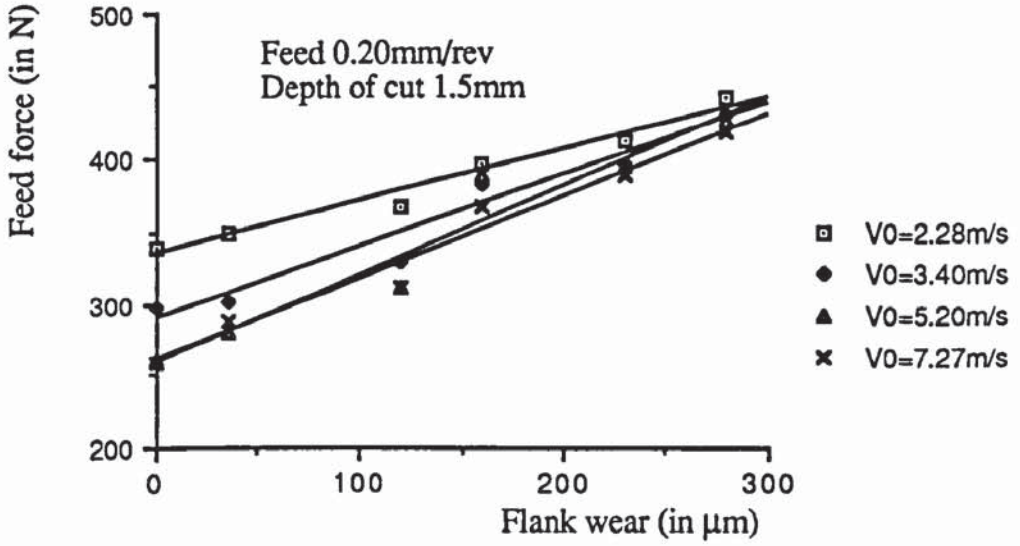

Fig. 4.3 Variation of the feed force with flank wear for different cutting speeds.

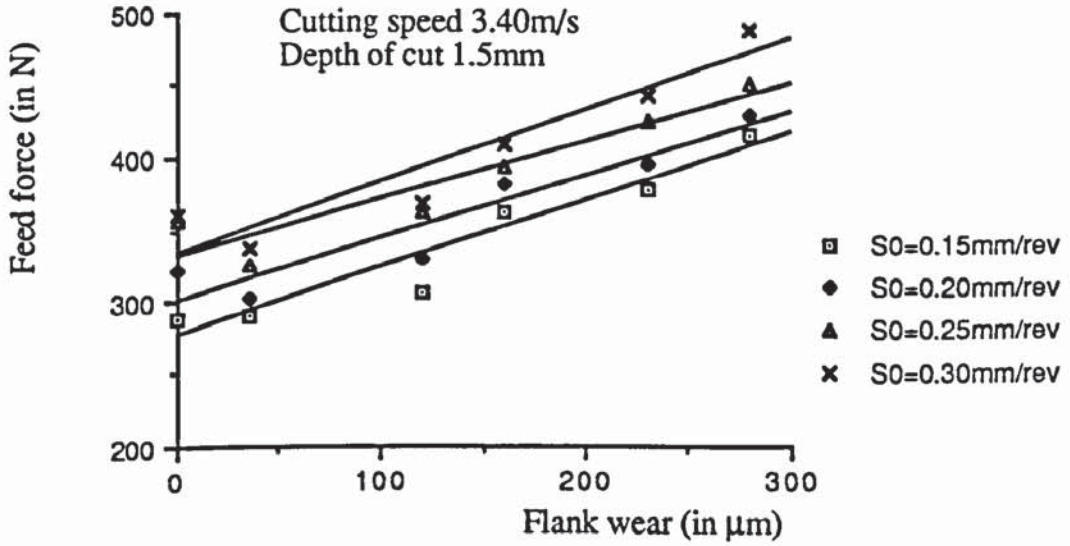

Fig. 4.4 Variation of the feed force with flank wear for different feeds.

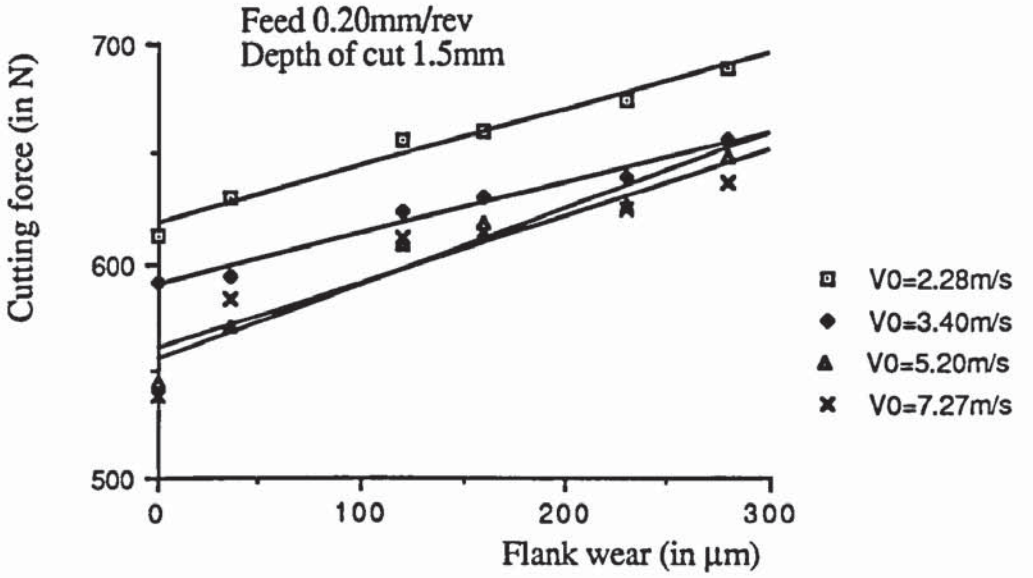

Fig. 4.5 Variation of the cutting force with flank wear for different cutting speeds.

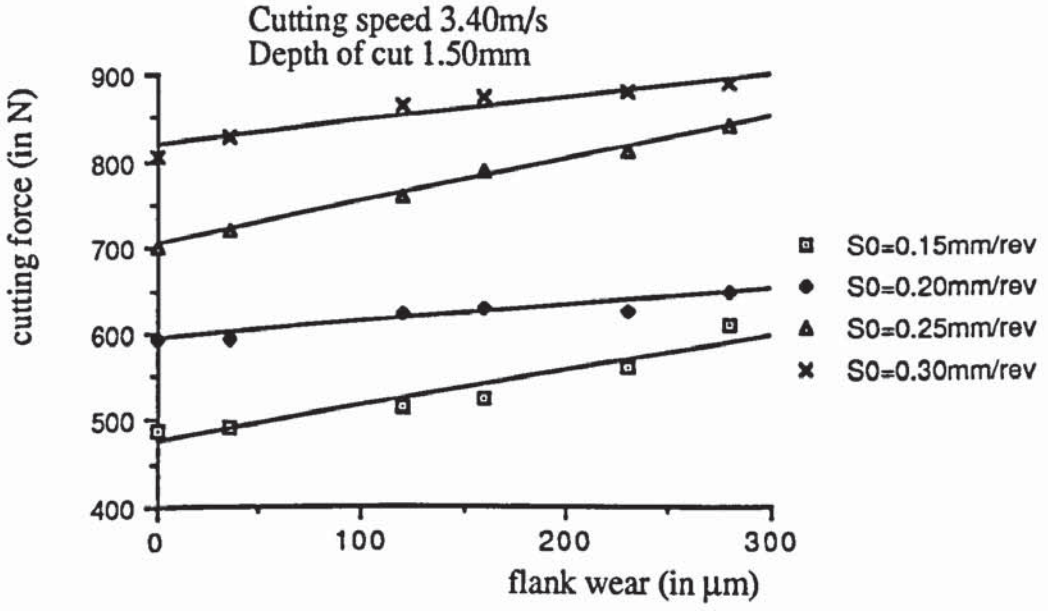

Fig. 4.6 Variation of the cutting force with flank wear for different feeds.

As the flank wear increases, the volume of the deformed material increases as a result of increase of BC of Fig. 4.1. This lead to an increase in feed force as the resistance of the material to deformation is in the direction of feed. The corresponding increase in the cutting force is the product of the increase in feed force times the equivalent friction coefficient along the flank of the tool. Henceforth the increase in cutting force is less than in feed force. Furthermore, an increase in flank wear increases the temperature of contact along the flank of the tool and then results in a decrease in the equivalent friction coefficient. This explains the reason why the feed force becomes more increasing with flank wear for advanced wear levels while the cutting force becomes less sensitive to it.

It is shown therefore that feed force is more suitable for flank wear monitoring at high speed and flank wear levels while at low speeds and low values of flank wear cutting force is more convenient for wear monitoring.

4.4. COMPARISON BETWEEN MEASURED AND PREDICTED TURNING FORCE USING WORN TOOLS

In the following section, the developed ploughing model is used to predict the turning force components for different flank wear levels. In this study, the coefficients introduced by the modelling in (4.10) and (4.11) are determined from data of turning with new tool data under steady state conditions as presented in Chapter 3. A programme is hence developed to determine the feed and cutting forces using results of Chapter 3 for the conditions summarised in Table 4.1.

In Fig. 4.7 to Fig. 4.12, the measured and predicted forces are presented versus flank wear for the investigated cutting conditions. It is generally seen that the model provides

better prediction of feed force than cutting force for flank wear up to 300μm. For 0μm of flank wear corresponding to new tool the model is shown as in Chapter 3 to yield good predictions of the turning force components with a maximum error of 14.5%.

The prediction error is defined here as follows:

$$100\,\frac{\text{Predicted force} - \text{Measured force}}{\text{Predicted force}} \qquad (4.12)$$

This expression is adopted for the reason that in practical conditions the force is predicted theoretically and then when the error is known it is easier to use (4.12) to determine the measured or real value of the corresponding force component.

Furthermore, the predicted and experimental feed forces show good agreement with maximum error of 16%. The prediction error is increasing with cutting speed and with flank wear. Analysing (4.10) it can be seen that the component of the feed force introduced by the worn part of the tool flank is proportional to the depth of the tool penetration and to the specific ploughing factor p_s. The former factor is determined from steady state data when new tool is used (Chapter 3) whereas the latter is extrapolated by Wu (1989) from previously published work (Liu & Barash, 1976). Liu & Barash (1976) showed that the depth of the sublayer deformed by chip–removal process decreases with flank wear and therefore the tool penetration is decreasing with wear. On the other hand, as shown by several researches, the contact temperature is increasing with flank wear. This conclusion was debated from different point of views. Some experimental results showed that as the flank wear increases, the temperature first decreases until a certain value of wear, then increases with subsequent tool wear (Zakaria, 1975). While most of the published work show that the temperature of

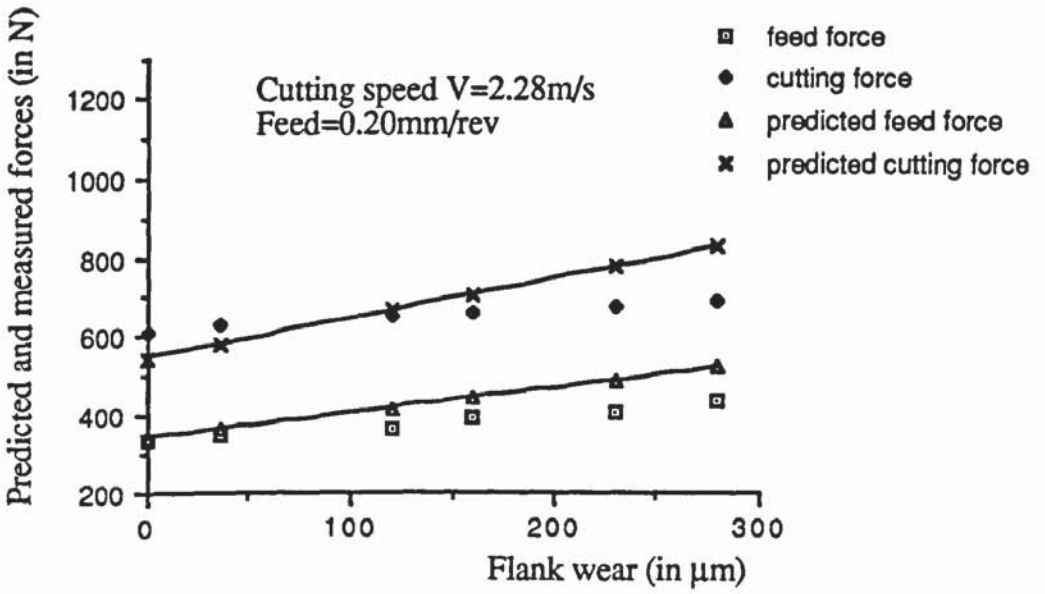

Fig. 4.7 Predicted and experimental forces, S_0=0.20mm/rev, V=2.2833m/s.

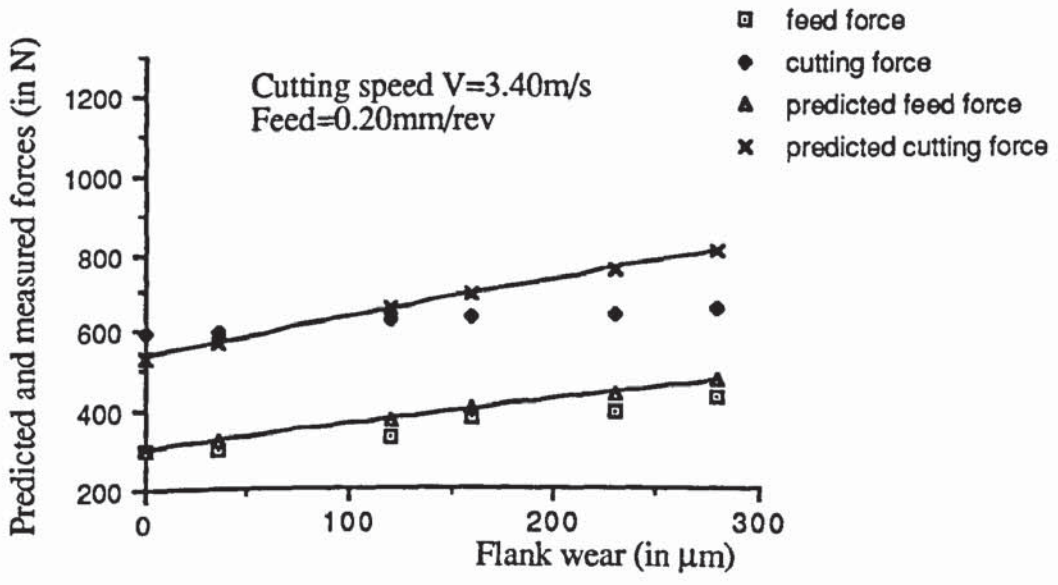

Fig. 4.8 Predicted and experimental forces, S_0=0.20mm/rev, V=3.40m/s.

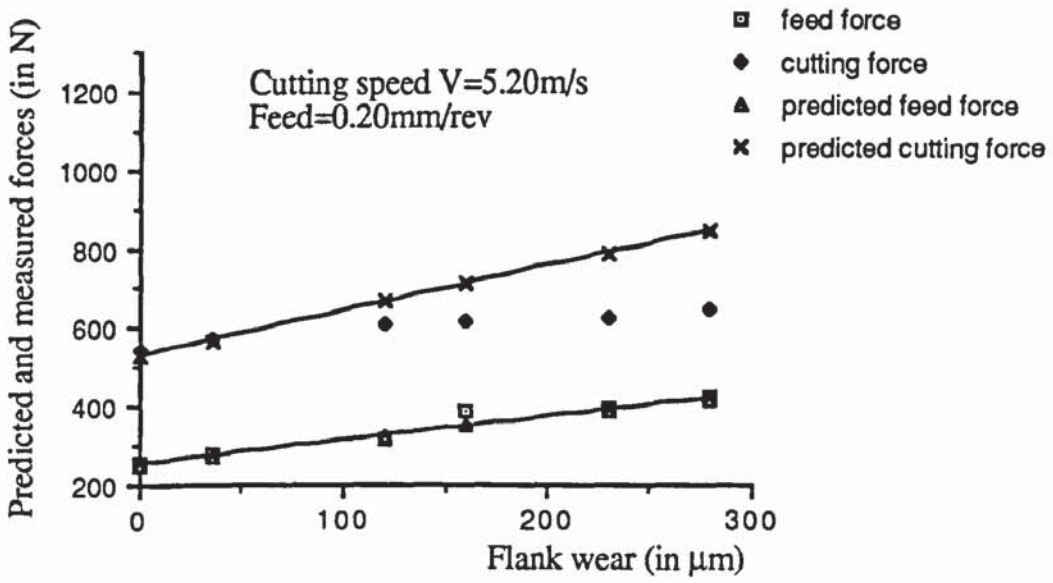

Fig. 4.9 Predicted and experimental forces, S_0=0.20mm/rev, V=5.20m/s.

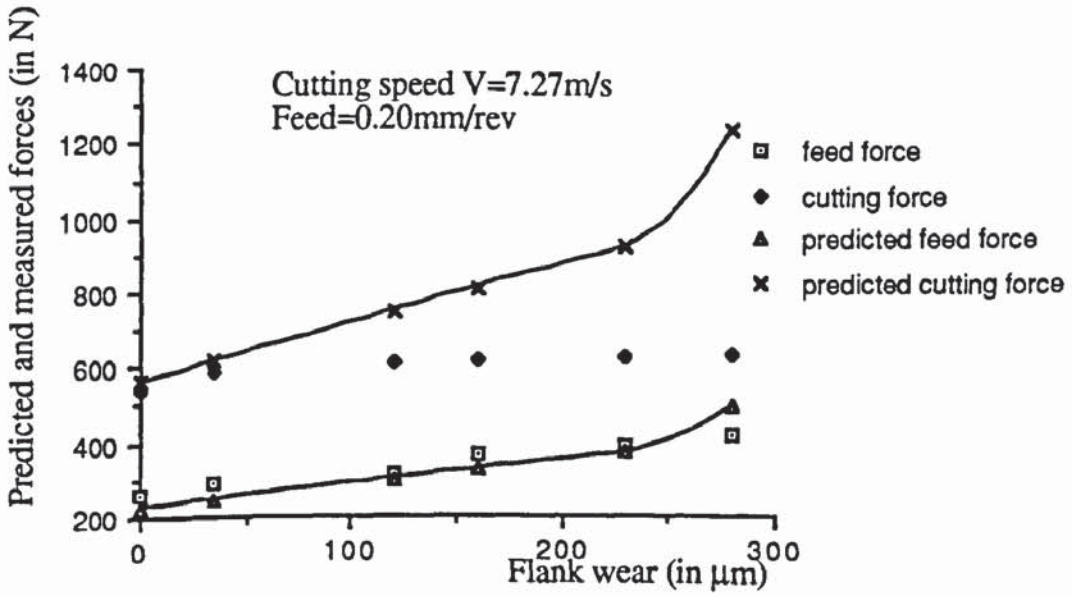

Fig. 4.10 Predicted and experimental forces, S_0=0.20mm/rev, V=7.27m/s.

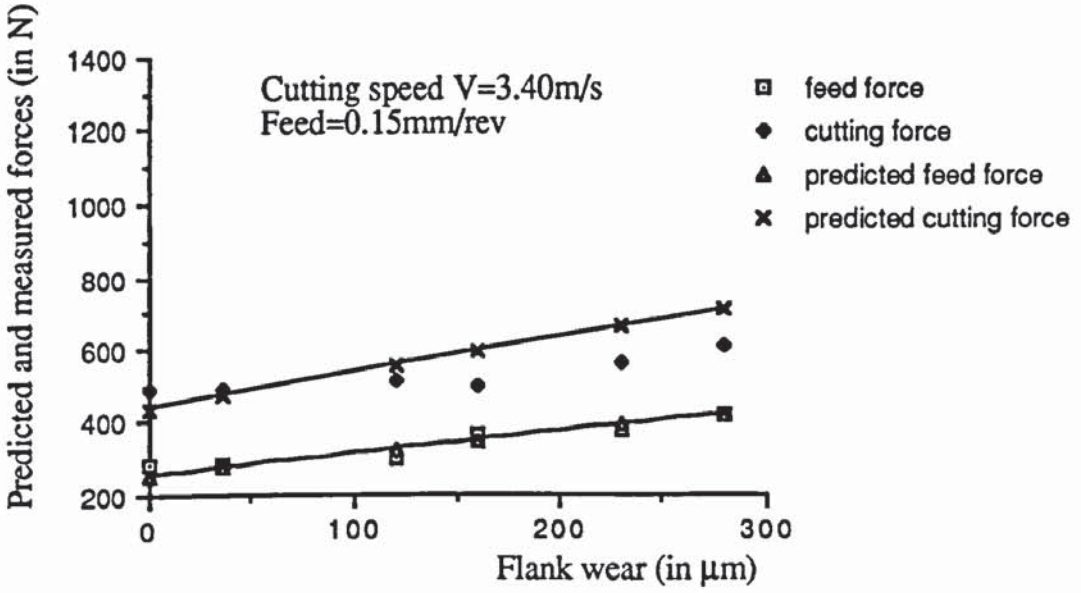

Fig. 4.11 Predicted and experimental forces, S_0=0.15mm/rev, V=3.40m/s.

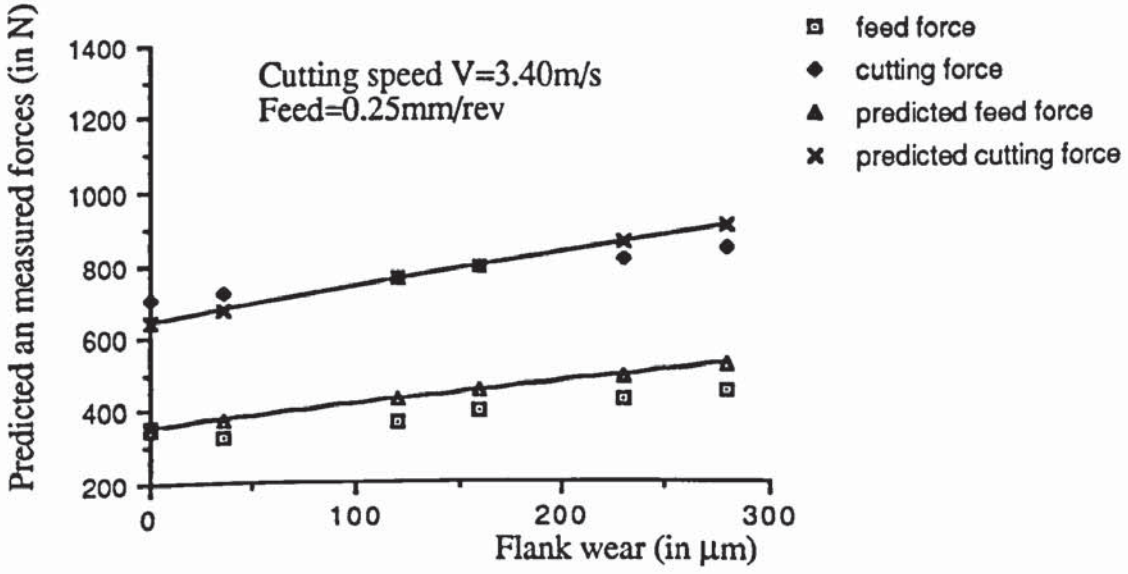

Fig. 4.12 Predicted and experimental forces, S_0=0.25mm/rev, V=3.40m/s.

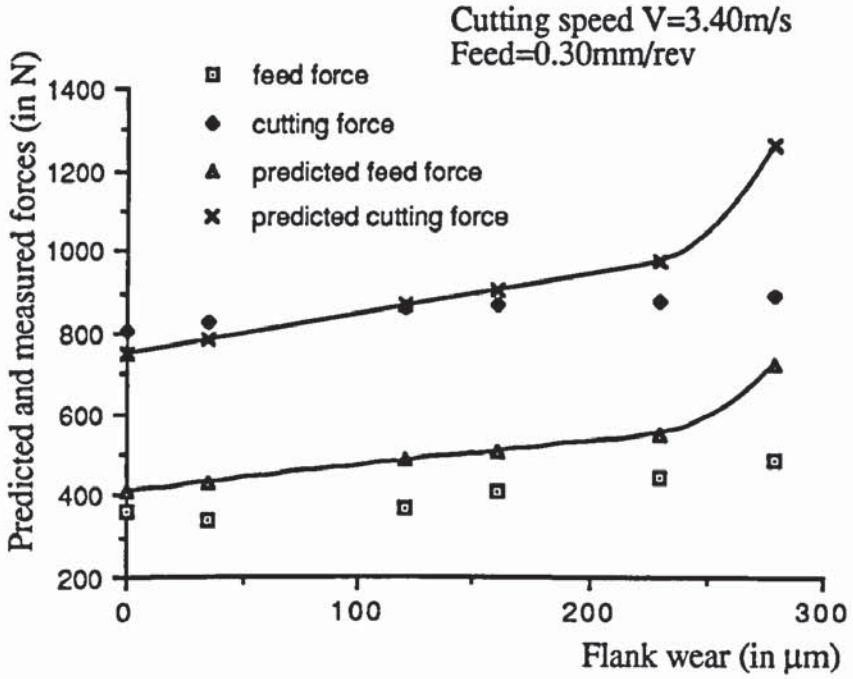

Fig. 4.13 Predicted and experimental forces, S_0=0.30mm/rev, V=3.40m/s.

contact is usually increasing with flank wear. An increase in the temperature of the work material along its contact with the cutting edge will soften the work material which will result in a decrease in the specific ploughing factor. The decrease of specific ploughing factor and tool penetration with flank wear lead to a decrease in the slope of the component of the feed force introduced by the worn flank. This explains the discrepancies observed between the predicted and measured feed force for higher values of flank wear.

Regarding to the prediction of the cutting force, Fig. 4.7 to Fig. 4.13 show that predictions of the model are made with an error less than 19% for most cases except for higher value of wear and cutting speed where the error in prediction reaches 44%.

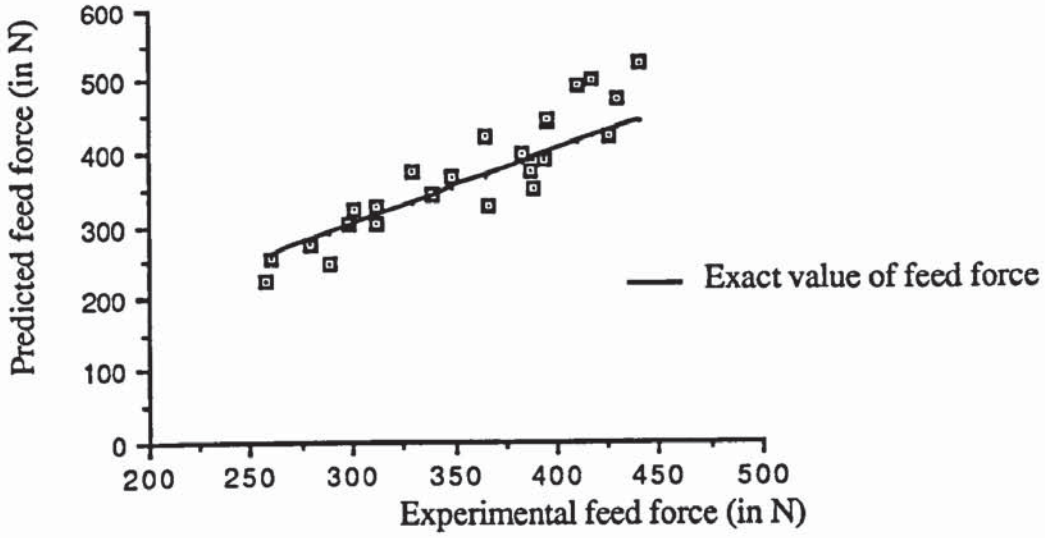

Fig. 4.14 Predicted versus experimental feed force.

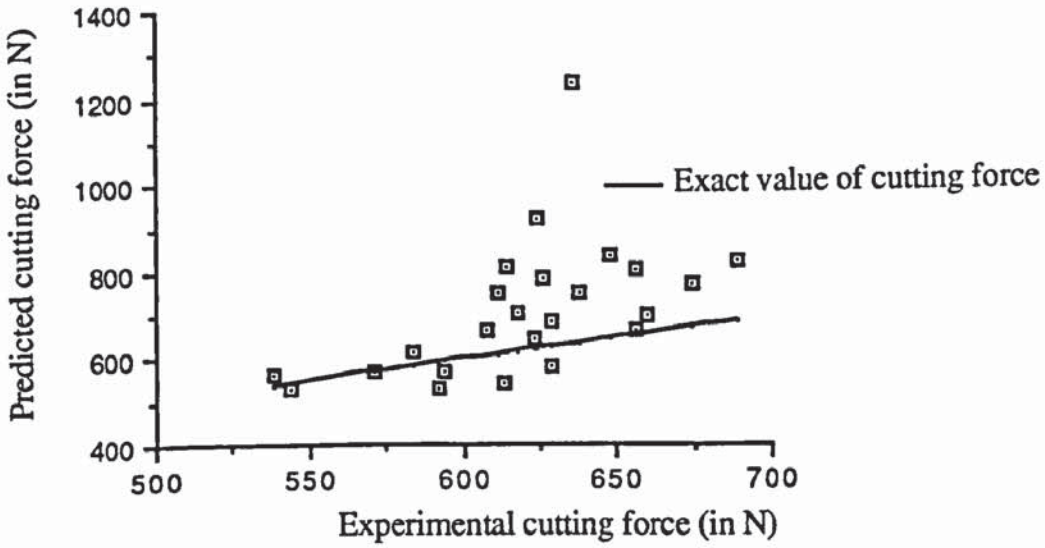

Fig. 4.15 Predicted versus experimental cutting force.

These differences can be attributed to the variations of the specific ploughing factor and tool penetration with flank wear which is not taken into account by the model.

The increase of the predicted cutting force is higher than the increase of the predicted feed force which lead to higher error of cutting force predicting at higher flank wear. Beside the effect of the flank wear upon the ploughing factor and tool penetration as mentioned above, the friction coefficient is also influenced by the tool–workpiece contact (Usui, 1984). As the temperature increases with wear the equivalent friction coefficient along the flank is decreasing. The friction coefficient associated with wear is smaller than that associated with new tool determined in Chapter 3 and therefore the ploughing part of the cutting force is less than what it is predicted by the model.

To summarise the quality of forces prediction, predicted feed and cutting forces are plotted in Fig. 4.14 and Fig. 4.15 versus corresponding experimental forces. It is shown that good prediction is provided for feed force while discrepancies are observed between predicted and measured cutting force much more for high forces corresponding to advanced flank wear. From the discussion above the model yields better prediction of feed force than cutting force. The error in feed force prediction is less than 16% whereas the error in predicting the cutting force can be up to 44%. Monitoring tool wear can be made possible based upon the prediction of feed rather than cutting force or ratio of two components. This for two reasons: (1) the feed force is more sensitive to flank wear for the range of speeds and feeds used; (2) the model is providing good prediction of this component. However, as shown by the results (Fig. 4.14 –Fig. 4.15) the error of prediction is increasing with wear. This mean that any monitoring based upon the feed force will held good only for small amounts of wear but not of practical use for advanced values of flank wear.

4.5. CONCLUSION

In this chapter, the model developed previously in Chapter 3 for steady state turning with new edge is extended to include the effect of flank wear. The present model provides explicit expressions of the feed and cutting force as function of cutting conditions, tool flank wear and some model parameters. The model parameters are determined from steady state tests developed in the previous chapter.

The developed force expressions show that both feed and cutting force are linearly increasing with flank wear for constant cutting conditions. Comparison between measured and predicted forces showed good agreement in the feed force than in the cutting force. The error in predicting the feed force is less than 16% while in cutting direction this error may reach 44%.

The error in feed force predictions are associated with the dependence that exists between flank wear and tool penetration on one hand and specific ploughing factor on the other hand. This dependency is not included in the developed model. The discrepancies observed in predicting cutting force are associated with similar reasons as in feed direction and to the decrease in the friction along the worn edge with flank wear.

Despite the good prediction of the feed force, the model can only be used for tool wear monitoring purposes for small amount of flank wear. Larger the flank wear larger the error of feed force prediction thus resulting in poor quality of monitoring.

Chapter 5

DYNAMIC MODELLING OF THE TURNING PROCESS

5.1. INTRODUCTION

This chapter outlines the development of a new model for turning machining process. In dynamic conditions, cutting process is influenced by the machine structure through the instantaneous changes in the cutting conditions (i.e. tool oscillations). The latter changes affect in their turn the machine structure behaviour through changes in the resulting forces from the cutting process as shown Fig. 5.1.

The dynamic characteristics of the machine tool are commonly represented by the receptance Loci (Fig. 5.2) resulting from the forced vibration testing of the machine under simulated working conditions. However, these dynamic coefficients turn up to be rather difficult to determine from dynamic tests (Chowdhury, 1969-1970) and therefore much more effort was made to develop models for metal cutting process where the model coefficient can be derived from steady state data (Nigm, 1977b; Klamecki, 1985). Moreover, recent models (Wu, 1985a, Endres *et al.*) have showed good qualitative correlation with the experimental charts though satisfactory quantitative agreement between the predicted and the experimental results could not be achieved. The need for forwards advances in the techniques of unmanned turning for sake of efficient productivity renders the on-line prediction of the state of the cutting

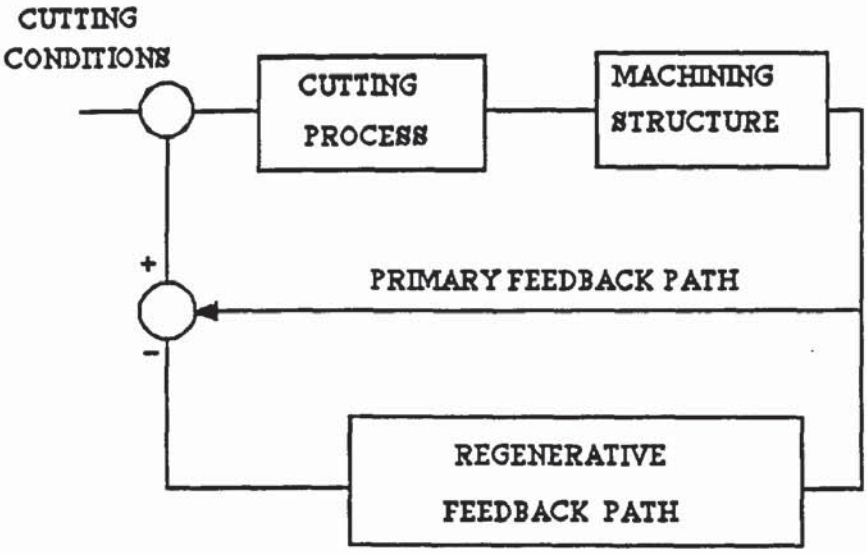

Fig. 5.1 Simplified block diagram for machining

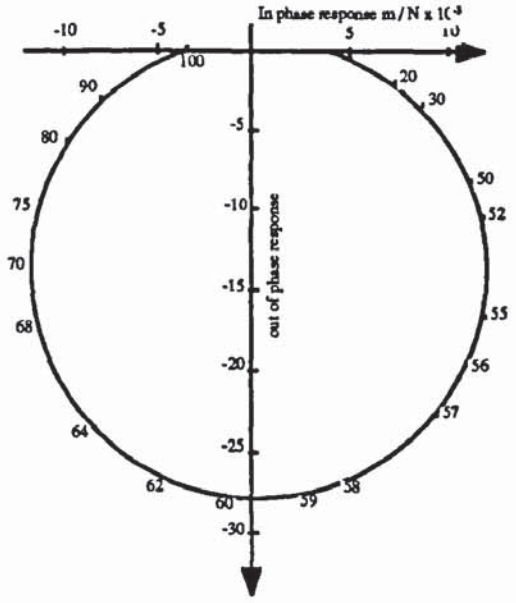

Fig. 5.2 Direct receptance of cutting process

process more and more necessary. This henceforth necessitate the study of the problem of machining in more details and on more realistic basis.

The following chapter aims to extend the basic state state model to dynamic turning. This model will be using the relationships governing the chip formation process under steady state conditions as established in chapter 3. This chapter outlines the effect of the tool vibration upon the turning forces as well as on the incremental variations of the machining force components. It discusses also the sensitivity of the shear angle, the depth of the tool penetration and the rake forces ratio and the mean frictional coefficient along the secondary face of the tool regarding to changes in the input cutting parameters.

5.2. DYNAMIC CUTTING PROCESS

Whereas in steady state conditions the cutting parameters maintain their initial values, in the floor conditions, cutting tools are excited during machining by changes in the cutting forces (Fig. 5.3 and Fig. 5.4). These variations can be generated by a hard spot in the workpiece, material clearing from a built–up edge on the tool, a chip breaking or changes in the characteristics of the cutting process. The structure responds (Fig. 5.4) to these changes by a relative displacement between the cutting tool and the workpiece. This displacement affects the values of the cutting parameters which results in a further variation of the cutting force. Hence, in dynamic cutting process the cyclic variations in the independent cutting conditions namely the variation in the chip thickness, the instantaneous cutting speed are initiated by the relative oscillation between the tool and the workpiece.

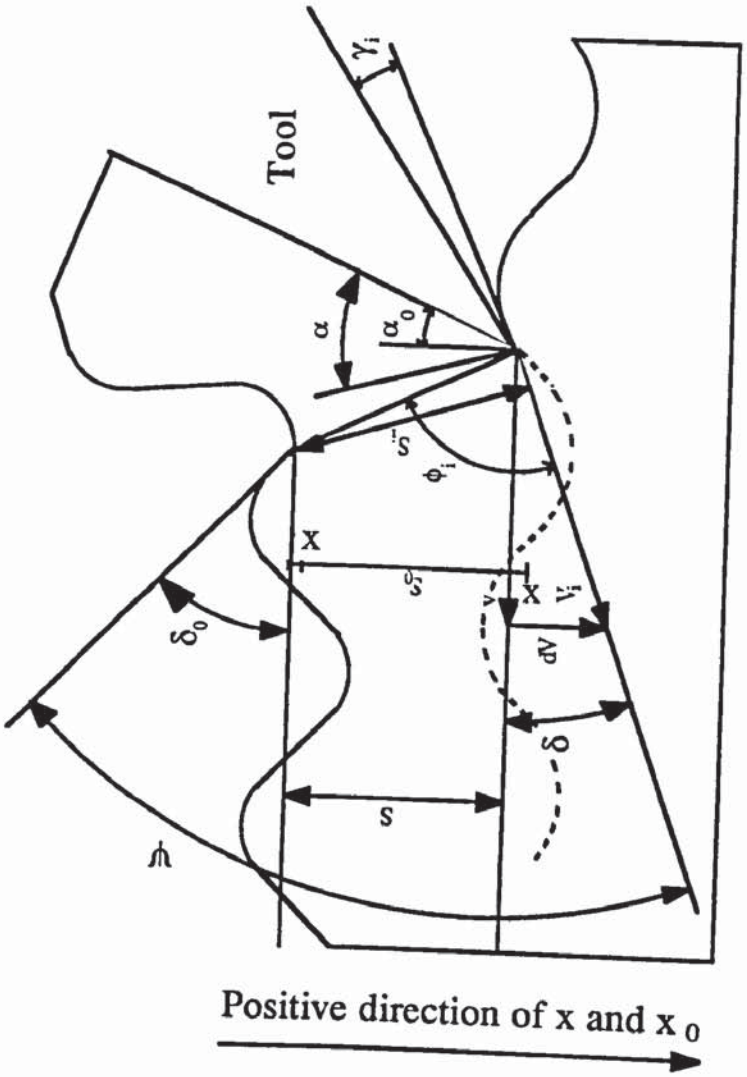

Fig: 5.3. Configuration of the dynamic cutting process

In the present study the relative displacement between the tool and the workpiece is assumed to result only from the displacement of the tool holder as the workpiece can be considered as a rigid body and does not deform in the direction perpendicular to the feed direction. The turning tool holder is clamped at one end with the tool end is free. It is furthermore supposed that the tool is only vibrating in a normal direction to the cutting direction since this motion that affects the instantaneous values of the undeformed chip thickness.

The geometry of the cutting process can be represented as shown in Fig 5.3. It can be seen as discussed above that the dynamic cutting process consists of a cutting process subsystem, tool–post and tool holder structures and a feed–back mechanism which form the link between the cutting process and the tool–post and tool–holder structure (Fig. 5.4). Thus the vibration affects the cutting process thereby the turning forces through its direct effect on the instantaneous chip thickness S_i (Fig. 5.4).

The dynamic cutting process (Fig. 5.3) is considered as a superimpose of two simple turning configurations of wave removing (Fig.5.5a) and wave generating (5.5b). The former refers to the case when the tool is held steady and moves perpendicular to the mean cutting direction when removing an undulated surface as is this might be the case after the first revolution of the workpiece. The latter refers to metal removing when the tool is vibrating perpendicular to the mean of the cutting speed and the workpiece surface is not disturbed which is the case during the first revolution of the workpiece. In real metal removing both cases are met and are referred to as regenerative cutting.

Fig: 5.4. Dynamic turning process block diagram

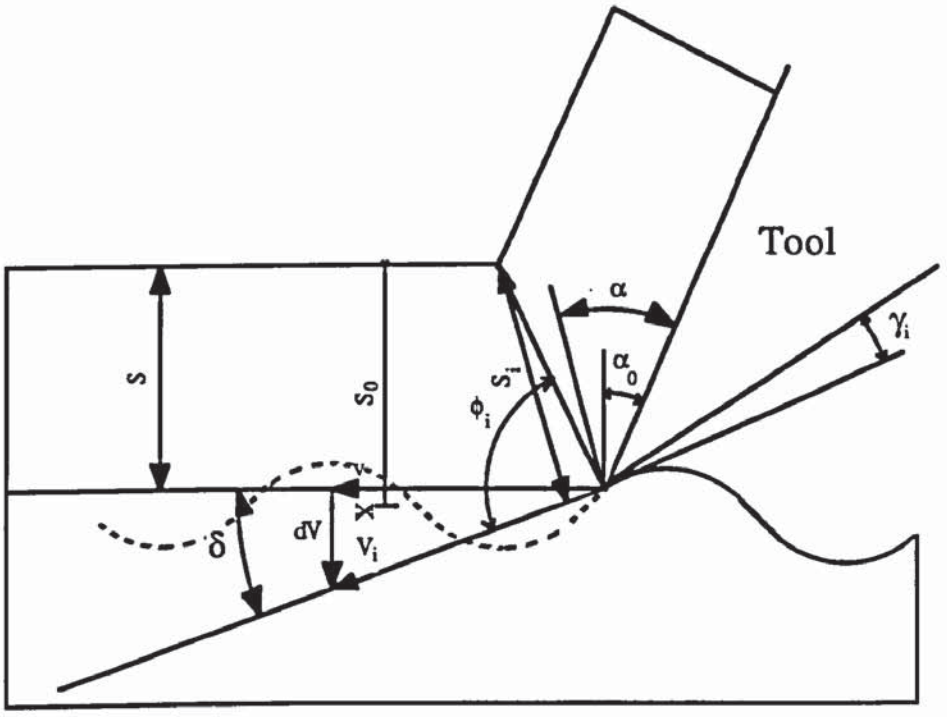

(a) wave generating

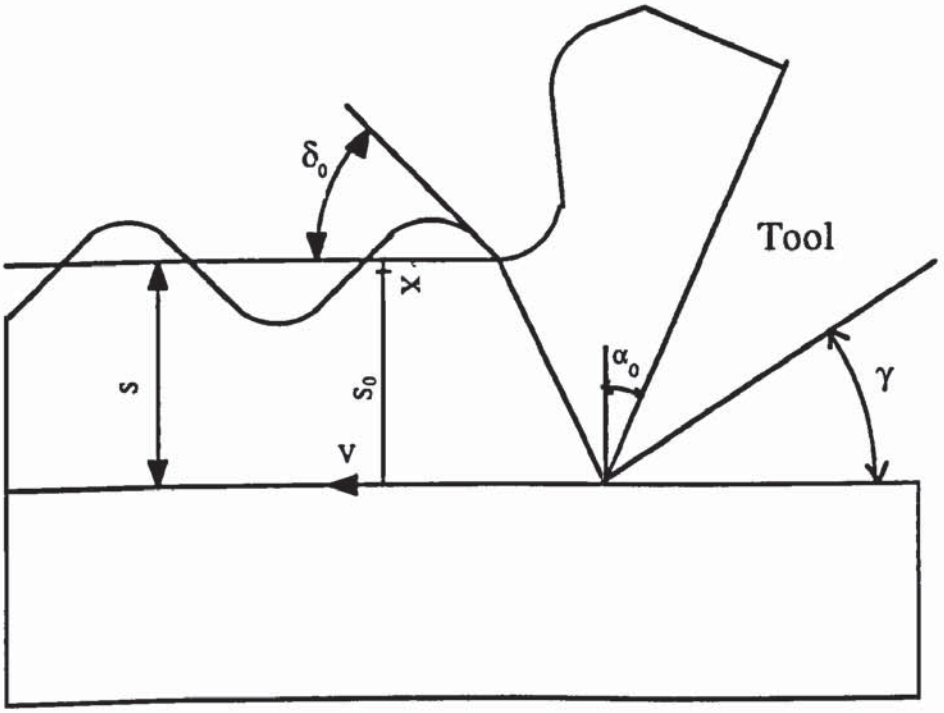

(b) wave removing

Fig. 5.5 Wave generating and wave removing during machining process

In this modelling, since the chip formation whether under oscillatory or steady state conditions is fundamentally the same (Tobias, 1965; Wu, 1985; Hamdan, 1990) (Fig.5.3), it is considered that the shear plane concept is equally valid for the dynamic cutting process (Tobias). In this modelling analysis the following assumptions are also considered:

- The cutting is carried out in orthogonal cutting conditions.
- The tool is only vibrating along the feed axis x.
- The tool is new and has a finite radius at the cutting edge.
- The dynamic variation of the clearance angle is such that the instantaneous clearance angle does not acquire a negative values allowing for rubbing to occur between the flank face and the freshly machined surface (Kegg, 1965).

It is implicitly included in the foregoing discussion that modelling the dynamic cutting process should include the dynamic modelling of the parameters influencing this process such as:

- Modelling the dynamic cutting conditions
- Modelling the dynamic cutting force
- Modelling the effect of the tool holder–tool post structure upon the cutting process.

The two first parts concerning with the modelling of the cutting conditions and the cutting process for dynamic turning are developed in the following sections, whilst the third part dealing with the effect of the structure of the machine and the tool post–tool

holder is reported in Chapter 6 dealing with the set–up and equipments used for the experimental work.

5.3. DYNAMIC CUTTING CONDITIONS

The instantaneous cutting speed is measured along the tangent to the machined surface and thereby, the instantaneous shear angle is the angle between the cutting speed vector and the position of the shear plane (Fig. 5.3). The chip thickness is measured however at the free end of the shear plane whereas the tool displacement is measured at the tool edge. There will be then a geometrical out–phase between the tool displacement and the free surface of the tool and therefore the undeformed chip thickness depends upon the mean geometrical lead of the free end of the shear plane.

Under the assumptions mentioned earlier, the following equations can be derived in accordance with the geometry of Fig. 5.3.:

– Variation in the instantaneous cutting speed

$$dV = \left(\frac{\dot{x}}{2} \right) \left(\frac{\dot{x}}{V} \right) \tag{5.1}$$

– Variation in the undeformed chip thickness

$$dS = x - x_0 + \varepsilon \left(\frac{\dot{x}}{V} \right) \tag{5.2}$$

– Variation in the instantaneous rake angle of the tool

$$d\alpha = \frac{\dot{x}}{V} \tag{5.3}$$

– Variation in the instantaneous flank angle

$$d\gamma = -\frac{\dot{x}}{V} \tag{5.4}$$

– Variation in the instantaneous cutting direction

$$d\delta = \frac{\dot{x}}{V} \tag{5.5}$$

– Variation in the free surface slope relative to the instantaneous cutting direction

$$d\psi = \frac{\dot{x} - \dot{x}_0}{V} \tag{5.6}$$

Where:

– V is the mean cutting speed.

– ε the geometric lead of the free end of the shear plane relative to the cutting edge as measured along the mean cutting direction.

– x(t) is the relative displacement between the tool and the workpiece as measured along the normal to the mean cutting speed. This displacement is generally referred to as a negative feed–back path (Fig. 5.4) because the dynamic chip thickness is decreased as the tool moves away from the workpiece.

– $x_0(t)$ is the dynamic variation of the uncut chip thickness produced in the cutting process during the previous revolution of the workpiece, thus:

$$x_0(t) = \kappa\, x(t - \frac{1}{N}) \tag{5.7}$$

N (rev/s) is the work revolution speed and κ the overlap factor (Tobias, 1965).

The overlap factor acts as a scaling factor of the residual chip undulation ($0 \leq \kappa \leq 1$). Tobias showed that chatter has more effect on the cutting process when the two inner and outer undulations of the machined surface and of the work surface respectively completely overlap, this is: $\kappa = 1$ and therefore:

$$x_0(t) = x(t - \frac{1}{N}) \tag{5.8}$$

$\dot{x}$ and $\dot{x}_0$ are the derivative functions of x and x_0

5.4. DYNAMIC TURNING FORCE

The dynamic force model considers the effect of the indentation around the nose of the cutting edge. As the tool moves into the work material, a certain amount of material deforms elastically and plastically because of the roundness of the cutting edge leading to an additional forces upon the flank face of the tool as discussed previously (Chapter 3). These forces will act as a positive damping thus increasing the stability of the machining systems (Wu, 1985a). The turning force is therefore the resultant of the turning force along the rake face of the tool responsible of the shearing process and of the ploughing force acting along the flank face of the tool. The former component of the turning force is named in this thesis the rake force. Thus turning forces F_{zi} and F_{xi} along and normal to the instantaneous cutting direction respectively can be expressed as:

$$\begin{aligned} F_{xi} &= F_{sxi} + P_{xi} \\ F_{zi} &= F_{szi} + P_{zi} \end{aligned} \tag{5.9}$$

F_{sxi}, F_{szi} are the components of the rake force and P_{xi} and P_{zi} the ploughing components along x_i and z_i axis. x_i and z_i are the instantaneous feed and cutting directions.

5.4.1. Dynamic force on the rake of the tool

Regarding to the assumptions made above, Fig. 5.3. can thus be used to derive the following expressions for the instantaneous cutting force components along and normal to the instantaneous cutting speed:

$$F_{sxi} = \frac{w\, k_i\, S_i\, C_{si}}{\sin(\phi_i)\,(\cos(\phi_i) - C_{si}\sin(\phi_i))}$$
$$F_{szi} = \frac{w\, k_i\, S_i}{\sin(\phi_i)\,(\cos(\phi_i) - C_{si}\sin(\phi_i))} \qquad (5.10)$$

Where C_{si}, k_i, ϕ_i and S_i are respectively the instantaneous rake forces ratio, shear stress, shear angle and instantaneous uncut chip thickness at the free end of the shear plane as measured normal to the instantaneous cutting speed.

5.4.2. Dynamic ploughing force

During dynamic turning, the tool is oscillating and the amplitude of its vibration remains of small order for normal machining operations compared to the undeformed chip thickness. On the other hand, these oscillations are progressively decreasing as the dynamic damping of the machining system is positive; otherwise the system is under

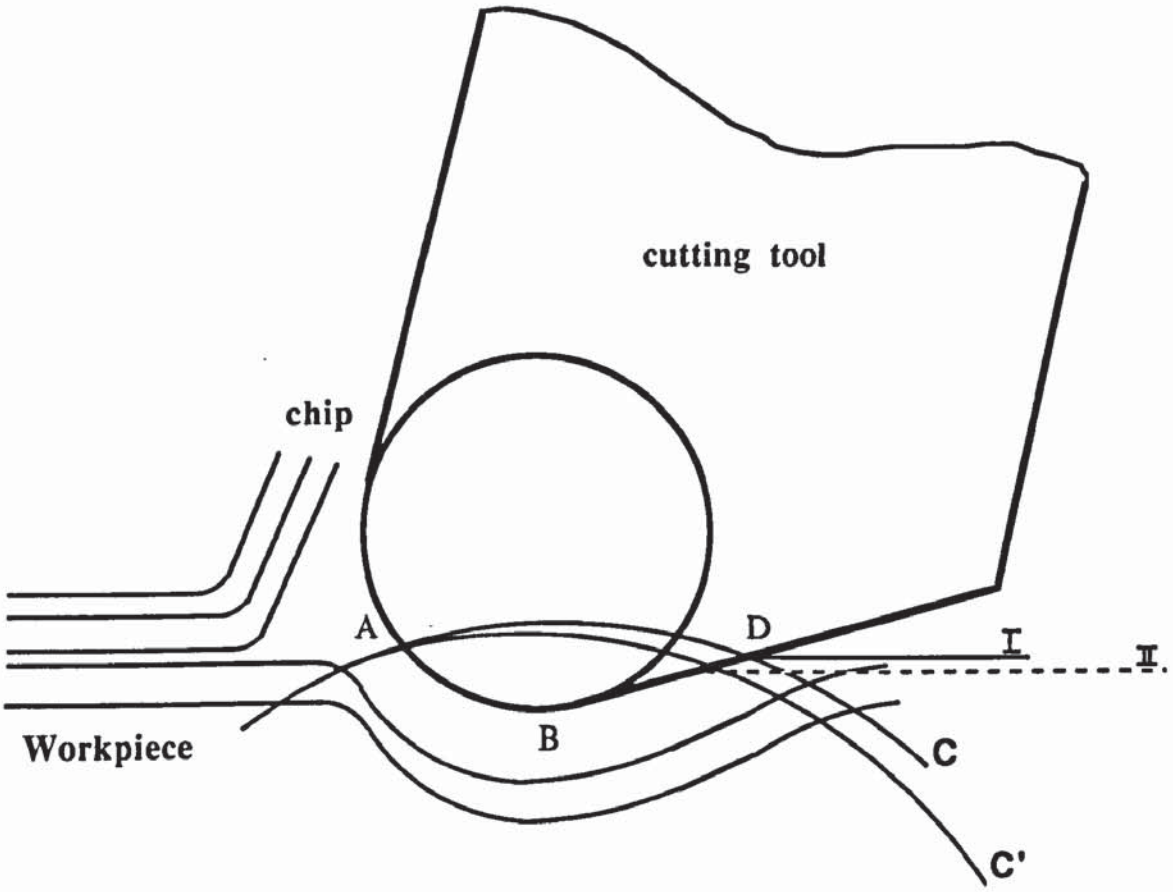

Fig. 5.6 Flow of work material around the cutting edge during oscillating turning

chattering conditions. The cutting tool remains thus in contact with the workpiece during the metal removing operation and therefore under the assumption that the tool is vibrating with an amplitude X (in m) at an angular velocity ω (rad/s), the tool displacement as well as the cut surface waviness can be described as:

$$x(t) = X e^{(j\omega t)} \qquad (5.11)$$

t: denotes the time in seconds.

As the tool moves into the work material, and because of the indentation effect (Albrecht, 1960; Wu, 1989), a part of the material below a point A (Fig. 5.6) will deform elastically and plastically and will form the upper surface of the machined surface. Whereas the material above the point A flows along the rake surface to form the removed chip. The deformation rate of the material deformed by the edge is determined by the geometry of the tool rake face. Thus the material starts to be deformed from point A (Fig. 5.6) until it reaches the maximum of deformation rate at the lower point B of the cutting edge. The depth of the material deformation under the cutting edge is continuously increasing and so is the strain in the sublayer of the work material. This period is called the loading cycle. After it passes the point B the existing strain starts to recover and so does the material under the edge. This unloading process will continue until the load is completely removed at the separation point D. When the load is released the elastic strain is released but the plastic strain still remains (Merwin *et al.*, 1963; Haslam, 1970; Rubenstein, 1985) and therefore the final level of the machined surface, shown as C' in Fig. 5.6, is lower than the partition boundary level C. For normal orthogonal cutting conditions where the process approaches the plain strain condition the plastic deformation can be neglected and the workpiece surface after machining is at the same level as that the separation between workpiece and chip

initially occurred as shown by the partition boundary C in Fig. 5.7. (Haslam, 1970). The boundary conditions at A and D are thus:

$$\xi\ (0) = 0 \qquad (5.12)$$

and

$$\xi\ (z_D) = 0 \qquad (5.13)$$

where z_D is the coordinate of the point D along the z axis.

$\xi\ (z)$ is the measure of the depth of the tool penetration at an arbitrary point E (Fig. 5.8) of coordinate z along the contact between the cutting edge and the deformed material.

In this thesis, the mean value of the maximum tool penetration at the lowest point B is assumed to correspond to the maximum depth of the material deformation in steady state conditions but where the cutting configuration is corrected to the instantaneous geometric cutting configuration (Fig. 5.3.). This is because the dynamic cutting process can be regarded as represented by a steady state geometrical configuration where the instantaneous cutting conditions are considered. Under this assumption the depth of the material deformed at B is:

$$\xi\ (z_B) = \zeta \qquad (5.14)$$

The displacement of any point E on the cutting edge can be described by a wave function (Wu, 1985) u(t, z) to introduce the time delay that exists between the tip of the tool and other point in contact with the material as follows:

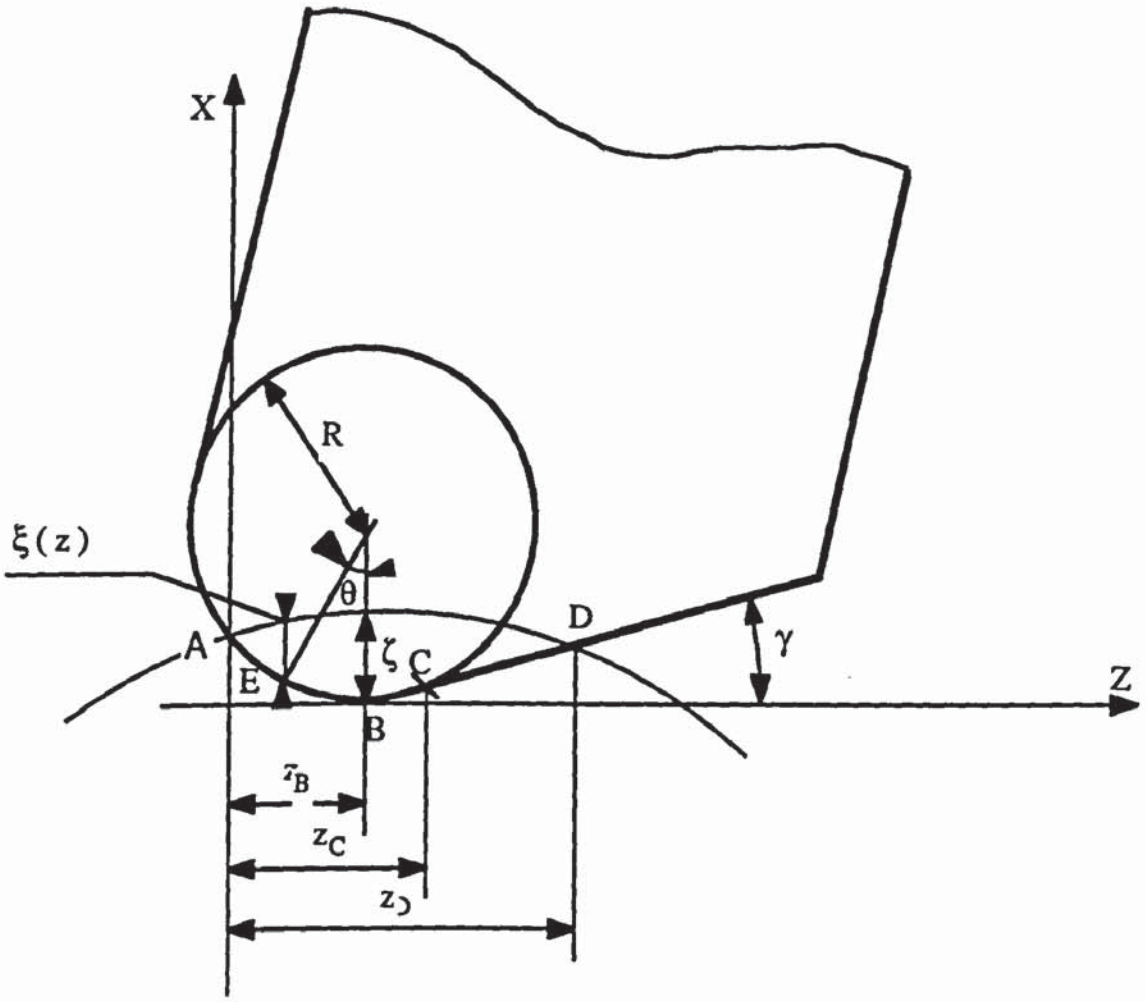

Fig. 5.7 Tool penetration during dynamic machining

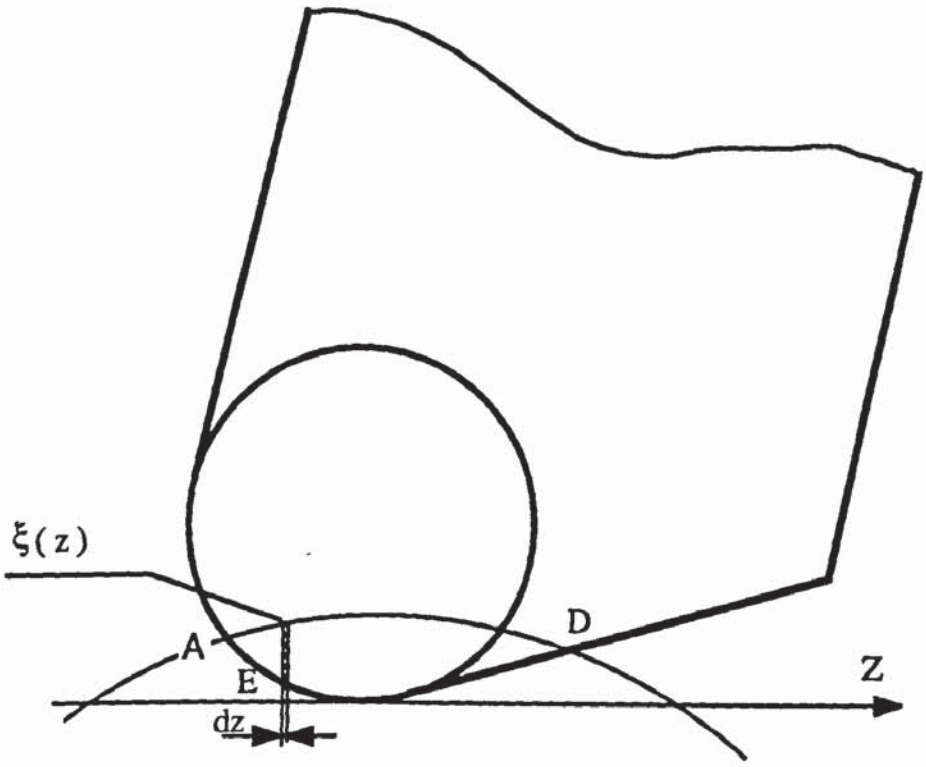

Fig. 5.8 Deformed material under an arbitrary point E of the cutting edge

$$u(t, z) = x\left(t - \frac{|z - z_B|}{V}\right) \qquad (5.18)$$

Tool penetration can therefore be expressed as given by (5.19) and (5.20).

For $0 \leq z \leq z_C$

$$\xi(z) = u(t, z) - u(t, z_B) + \zeta + \sqrt{R^2 - (z - z_B)^2} - R \qquad (5.19)$$

and for $z_C \leq z \leq z_D$

$$\xi(z) = u(t, z) - u(t, z_B) + \zeta - R(1 - \cos(\gamma)) - (z - z_C)\tan(\gamma) \qquad (5.20)$$

Where z_C is the coordinate of point C defining the point of contact between the rounded edge and the clearance face of the tool (Fig. 5.6 and Fig. 5.7).

It is noticed that $(\omega z_B) / V$ is of small order for normal cutting conditions. As a typical example of cutting at 4m/s and the tool vibratory frequency of 500Hz, the depth of the tool at point B can approximately estimated to $\zeta = R/4$ (Marui, 1983), and henceforth $z_B \leq 0.7$ R, the term $(\omega z_B) / V$ can be as small as 0.027.

Considering $(\omega z_B) / V$ is of small order and using the boundary condition of (5.12) and (5.13), the coordinates of B, C, and D are determined as:

$$z_B = \frac{-\frac{\dot{x}(R-\zeta)}{V} + \sqrt{\left(\frac{\dot{x}(R-\zeta)}{V}\right)^2 + \zeta(2R-\zeta)\left(1+\left(\frac{\dot{x}}{V}\right)^2\right)}}{1+\left(\frac{\dot{x}}{V}\right)^2} \qquad (5.21)$$

and;

$$z_D = \frac{\zeta - R(1-\cos(\gamma)) + z_C\tan(\gamma) + \frac{\dot{x}\, z_B}{V}}{\tan(\gamma) + \frac{\dot{x}}{V}} \qquad (5.22)$$

Geometric consideration yields the coordinate z_C as:

$$z_C = z_B + R\ \sin\ (\gamma) \qquad (5.23)$$

Where:

- $\dot{x}$ the velocity of the tool vibration
- ζ the depth of the tool at point B
- γ the flank angle
- V the mean cutting speed
- R the radius of the tool edge

Integrating (5.19) and (5.20) from A to D along the tool contact with the deformed material and considering that the force in the direction of the deformation is proportional to the deformed amount of material and considering a constant instantaneous equivalent mean friction angle along the contact, the ploughing components of the turning forces can be expressed as follows:

$$P_{xi} = w p_s \left\{ R(z_D - z_C)\cos(\gamma) - (R - \zeta) z_D - \frac{1}{2}\tan(\gamma)(z_D - z_C)^2 \right\}$$

$$+\frac{1}{2} w p_s \left\{ z_B \sqrt{R^2 - z_B^2} + (z_C - z_B)\sqrt{R^2 - (z_C - z_B)^2} \right\}$$

$$+\frac{1}{2} w p_s \; R^2 \left\{ \arcsin\left[\frac{z_B}{R}\right] + \arcsin\left[\frac{z_C - z_B}{R}\right] \right\}$$

(5.24)

and

$$P_{zi} = w p_s (\zeta - R) \frac{R(1+\tan^2(\tau))}{\tan^2(\tau)} \left\{ \log\left[\frac{R - z_B \tan(\tau)}{R - (z_C - z_B)\tan(\tau)}\right] + \frac{2 z_B - z_C}{\tan(\tau)} \right\}$$

$$- w p_s \frac{\dot{x}}{V} \frac{R(1+\tan^2(\tau))}{\tan^2(\tau)} \left\{ z_C + \frac{R - z_B \tan(\tau)}{\tan(\tau)} \log\left[1 - \frac{z_B}{R}\tan(\tau)\right] \right\}$$

$$- w p_s \frac{\dot{x}}{V} \frac{R(1+\tan^2(\tau))}{\tan^2(\tau)} \left\{ 2 z_C + \frac{R}{\tan(\tau)} \right\} \log\left[1 - \frac{(z_C - z_B)}{R}\right]$$

$$- w p_s \left\{ \frac{\dot{x}}{V} \frac{z_C^2 - 2(z_C - z_B)^2}{2\tan(\tau)} + \frac{3R^2}{2\tan(\tau)} \left(\arcsin\left[\frac{z_C - z_B}{R}\right] - \arcsin\left[\frac{z_B}{R}\right] \right) \right\}$$

$$+ w p_s \frac{R^2(\tan^2(\tau) - 1)}{\tan^3(\tau)} \left(\arcsin\left[\frac{z_C - z_B}{R}\right] - \arcsin\left[\frac{z_B}{R}\right] \right)$$

$$+ w p_s \frac{R^2(\tan^4(\tau)-1)}{\tan^3(\tau)\sqrt{\tan^2(\tau)-1}} \log\left[\frac{1-\frac{z_B}{R}\tan(\tau)}{1-\tan(\tau)+\sqrt{\tan^2(\tau)-1}\sqrt{1-\left(\frac{z_B}{R}\right)^2}}\right]$$

$$- w p_s \frac{R^2(\tan^4(\tau)-1)}{\tan^3(\tau)\sqrt{\tan^2(\tau)-1}} \log\left[\frac{1-\frac{z_C-z_B}{R}\tan(\tau)}{1-\tan(\tau)+\sqrt{\tan^2(\tau)-1}\sqrt{1-\left(\frac{z_C-z_B}{R}\right)^2}}\right]$$

$$+ w p_s \left\{\left[\zeta - R(1-\cos(\gamma))\right](z_D - z_C) - \frac{1}{2}\tan(\gamma)(z_D - z_C)^2\right\}\tan(\tau-\gamma) \qquad (5.25)$$

When cutting with a sharp tool of a small radius at the cutting edge nose (Appendix A1), (5.24) and (5.25) can be transformed into (5.26) and (5.27):

$$P_{xi} = w p_s \frac{\zeta^2}{\tan(\gamma) + \frac{\dot{x}}{V}}\left\{1 - \frac{1}{2}\frac{\tan(\gamma)}{\tan(\gamma)+\frac{\dot{x}}{V}}\right\} \qquad (5.26)$$

And;

$$P_{zi} = w p_s \frac{\zeta^2}{\tan(\gamma) + \frac{\dot{x}}{V}}\left\{1 - \frac{1}{2}\frac{\tan(\gamma)}{\tan(\gamma)+\frac{\dot{x}}{V}}\right\}\tan(\tau-\gamma) \qquad (5.27)$$

The above expression show that the force acting on the tool nose and along the clearance face of the tool decreases for higher clearance angle and, for a constant depth of cut, this force is decreasing as the tool vibration increases. Discussion of these observations is dealt with in 5.4.4.

5.4.3. Dynamic turning force components

Substitution of (5.10), (5.26) and (5.27) into (5.9) led to express the dynamic turning force as follows:

$$F_{xi} = \frac{w\, k_i\, S_i\, C_{si}}{\sin(\phi_i)\,(\cos(\phi_i) - C_{si}\sin(\phi_i))} + w\, p_s \frac{\zeta^2}{\tan(\gamma) + \frac{\dot{x}}{V}} \left\{ 1 - \frac{1}{2} \frac{\tan(\gamma)}{\tan(\gamma) + \frac{\dot{x}}{V}} \right\} \qquad (5.28)$$

$$F_{zi} = \frac{w\, k_i\, S_i}{\sin(\phi_i)\,(\cos(\phi_i) - C_{si}\sin(\phi_i))} + w\, p_s \frac{\zeta^2}{\tan(\gamma) + \frac{\dot{x}}{V}} \left\{ 1 - \frac{1}{2} \frac{\tan(\gamma)}{\tan(\gamma) + \frac{\dot{x}}{V}} \right\} \tan(\tau - \gamma) \qquad (5.29)$$

The first terms of (5.28) and (5.29) correspond to the instantaneous components of the force on the rake of the tool. These components have been studied extensively by many researchers. Recalling from chapter 2, the first terms are due to the dynamic variations of the uncut chip thickness S_i directly influenced by the tool displacement x(t). Furthermore, These terms are indirectly related to the effect of the cutting conditions and work material characteristics. The second terms, however, refer to the effect of the tool size related to the velocity of vibration of the cutting edge. The analytical expression of the force component accounting the tool motion in the tangential direction is newly introduced in this thesis. It is shown that the ploughing force is inversely proportional to the to the velocity of vibration of the tool.

Omitting the seconds terms of (5.28) and (5.29) and considering only the first parts that refer to the dynamic turning force components on the rake of the tool, one may consider that the dynamic force is linearly related to the tool displacement. This assumption remains valid only for small amplitudes of tool vibration and for analysis dealing with low levels of frequencies where the ratio between the velocity of the tool vibration to the mean cutting speed can be neglected compared to the flank angle of the tool. It is thus shown that ((5.28) and (5.29)) as the tool displacement increases, because of unstable cutting conditions or because of tool wear, the resulting force at the vicinity of the cutting edge is becoming smaller whilst the rake forces are larger for higher frequency range.

Therefore, the dynamic force is dependent on both the tool displacement and the velocity of the tool vibration. For low frequencies and smaller tool amplitudes of vibration the dynamic force is mostly dependent only upon the tool displacement. On the other hand, as the amplitude or the frequency of vibration increase, the effect of the ploughing force is higher and the force becomes dependent on the displacement and upon the velocity of vibration of the tool. Moreover, the expressions (5.28) and (5.29) of the turning force components show that an increase the tool rake angle results in a decrease of the effect of the velocity of the tool vibration.

The above developed turning force components only show the effect of the tool vibration and the cutting conditions but do not provide a full description of the variation of these components to any changes in the independent parameters of the cutting process. however, to single out the effect of each of the input parameters to the cutting system a detailed analysis of the dynamic component of the turning force is needed.

In the following section, a detailed analysis of the incremental variations of the cutting force is carried out. On one hand, this analysis yields a complete description of the relation between the force oscillation and the variation in the cutting process inputs. On the other hand, the theoretical results provide a better understanding of the sensitivity of the shear angle, the rake forces ratio, the tool penetration and the mean friction along the flank to the instantaneous variations of the cutting conditions.

5.5. INCREMENTAL VARIATION OF THE DYNAMIC TURNING FORCE

In order to investigate the variations of the turning forces during dynamic metal removing and give a complete description of the effect of the tool vibration upon the cutting process, incremental variations of the turning forces is considered. Thus, partial differentiations of (5.28) and (5.29) with respect to the instantaneous chip thickness S_i, instantaneous shear angle ϕ_i, instantaneous shear stress k_i, instantaneous rake forces ratio C_{si}, instantaneous tool penetration ζ_i, instantaneous mean friction angle along the flank and instantaneous clearance angle γ_i; and neglecting small terms having order higher than the first, yield the incremental dynamic variations of F_{zi} and F_{xi} in the following forms:

$$dF_{xi} = w k_e \left\{ C_s dS + C_s A_1 dk + C_s A_2 d\phi + A_3 \cot g(\phi)\, dC_s \right\}$$

$$+ w p_e \left\{ p_1 d\zeta + p_2 d\gamma \right\} \qquad (5.30)$$

$$dF_{zi} = w k_e \left\{ dS + A_1 dk + A_2 d\phi + A_3 dC_s \right\}$$

$$+ w p_e \left\{ C_p p_1 d\zeta + (p_2 C_p - p_3) d\gamma + p_3 d\tau \right\} \qquad (5.31)$$

Where:

$$k_e = \frac{k}{\sin(\phi)(\cos(\phi) - C_s \sin(\phi))} \qquad (5.32)$$

$$p_e = \frac{p_s}{\tan(\gamma) + \frac{\dot{x}}{V}} \qquad (5.33)$$

$$A_1 = \frac{S}{k} \qquad (5.34)$$

$$A_2 = \left[\frac{\sin(\phi) + C_s \cos(\phi)}{\cos(\phi) - C_s \sin(\phi)} - \operatorname{cotg}(\phi) \right] S \qquad (5.35)$$

$$A_3 = \frac{S \sin(\phi)}{\cos(\phi) - C_s \sin(\phi)} \qquad (5.36)$$

$$p_1 = 2\zeta \left\{ 1 - \frac{1}{2} \frac{\tan(\gamma)}{\tan(\gamma) + \frac{\dot{x}}{V}} \right\} \qquad (5.37)$$

$$p_2 = \frac{\zeta^2 (1 + \tan^2(\gamma))}{\tan(\gamma) + \frac{\dot{x}}{V}} \left[-\frac{3}{2} + \frac{\tan(\gamma)}{\tan(\gamma) + \frac{\dot{x}}{V}} \right] \qquad (5.38)$$

$$p_3 = \zeta^2 \left\{ 1 - \frac{1}{2} \frac{\tan(\gamma)}{\tan(\gamma) + \frac{\dot{x}}{V}} \right\} (1 + \tan^2(\tau - \gamma)) \qquad (5.39)$$

w : depth of cut

p_s : specific ploughing factor.

$$\begin{bmatrix} F_x \\ F_z \end{bmatrix} = \begin{bmatrix} \cos(\delta) & -\sin(\delta) \\ \sin(\delta) & \cos(\delta) \end{bmatrix} \begin{bmatrix} F_{xi} \\ F_{zi} \end{bmatrix} \qquad (5.40)$$

The above dynamic components of the turning force ((5.30) and (5.31)) are expressed along and normal to the instantaneous cutting direction (Fig. 5.3) and have to be resolved along and perpendicular to the mean cutting direction by using (5.40) to provide the experimentally measured dynamic components of the turning force. The primary reason for modelling the turning process is to improve the efficiency and therefore limit or even eliminate the tool vibration at an early stage to avoid chatter conditions. For this reason, it is appropriate to build the model on the assumption of small amplitude of tool vibration and henceforth for small amplitude angles δ,the dynamic turning force components can be written as:

$$dF_x = w k_e \left\{ C_s dS + C_s A_1 dk + C_s A_2 d\phi + A_3 \cot g(\phi)\, dC_s + S\, d\delta \right\}$$

$$+ w p_e \left\{ p_1 d\zeta + p_2 d\gamma + \zeta^2 C_p \left[1 - \frac{1}{2} \frac{\tan(\gamma)}{\tan(\gamma) + \frac{\dot{x}}{V}} \right] d\delta \right\} \qquad (5.41)$$

$$dF_z = w k_e \left\{ dS + A_1 dk + A_2 d\phi + A_3 dC_s - C_s S\, d\delta \right\}$$

$$+ w p_e \left\{ p_1 C_p d\zeta + (p_2 C_p - p_3) d\gamma + p_3 d\tau - \zeta^2 \left[1 - \frac{1}{2} \frac{\tan(\gamma)}{\tan(\gamma) + \frac{\dot{x}}{V}} \right] d\delta \right\}$$

(5.42)

The incremental variations of the turning force components are expressed as a function of the variations of the dependents cutting parameters. These expressions show that the dynamic turning force responds to variations in the chip thickness, shear angle, slop of the cut surface and in the mean shear stress along the shear plane. However, It is more advantageous for the analysis of the dynamic turning to express (5.41) and (5.42) as functions of the independent cutting parameters or the controllable parameters. The variation of the independent parameters can be written as given by (5.43) to (5.46); where (5.43) describes the response of the shear angle to variations in the cutting conditions and includes also the effect of the slop of the free surface of the work relative to the instantaneous cutting direction as was experimentally proved by Boothroyd (1981).

$$d\phi = T_1 \, dS + T_2 \, d\alpha + T_3 \, d\psi \qquad (5.43)$$

$$dC_s = u_1 \, dS + u_2 \, d\alpha \qquad (5.44)$$

$$d\zeta = \zeta_\alpha \, d\alpha \qquad (5.45)$$

$$d\tau = \tau_\alpha \, d\alpha \qquad (5.46)$$

Assuming that the tool vibrates accordingly to (5.11) and the cut surface varies as given by (5.7), manipulations of (5.1) to (5.6) and of (5.41) to (5.46) renders the following expressions of dF_x and dF_z in terms of x and x_0

$$dF_x = w k_e \left\{ I_1 (x - x_0) + j \left(\frac{\omega}{V}\right) \left(I_2 (x - x_0) + I_3 x \right) \right\}$$

$$+ w p_e \left\{ I_{71} + j I_{72} \right\} \frac{\dot{x}}{V} \qquad (5.47)$$

$$dF_z = w k_e \left\{ I_4 (x - x_0) + j \left(\frac{\omega}{V}\right) \left(I_5 (x - x_0) + I_6 x \right) \right\}$$

$$+ w p_e \left\{ I_{81} + j I_{82} \right\} \frac{\dot{x}}{V} \qquad (5.48)$$

where

$$I_1 = C_s \left(1 + A_1 \frac{\partial k}{\partial S} + A_2 T_1 \right) + A_3 u_1 \operatorname{cotg}(\phi) \qquad (5.49)$$

$$I_2 = C_s A_2 T_3 \qquad (5.50)$$

$$I_3 = \left(\varepsilon \left(1 + A_1 \frac{\partial k}{\partial S} \right) + A_1 \frac{\partial k}{\partial \alpha} + A_2 T_1 \varepsilon + A_2 T_2 \right) C_s$$

$$+ A_3 (u_1 \varepsilon + u_2) \operatorname{cotg}(\phi) + S \qquad (5.51)$$

$$I_4 = 1 + A_1 \frac{\partial k}{\partial S} + A_2 T_1 + A_3 u_1 \qquad (5.52)$$

$$I_5 = A_2 T_3 \qquad (5.53)$$

$$I_6 = \left(1 + A_1 \frac{\partial k}{\partial S} + A_2 T_1 + A_3 u_1 \right) \varepsilon + A_1 \frac{\partial k}{\partial \alpha} + A_2 T_2 + A_3 u_2 - C_s S \qquad (5.54)$$

$$I_7 = p_1 \zeta_\alpha - p_2 + \zeta^2 \left[1 - \frac{1}{2} \frac{\tan(\gamma)}{\tan(\gamma) + \frac{\dot{x}}{V}} \right] \tan(\tau - \gamma) \qquad (5.55)$$

$$I_8 = p_1 C_p \zeta_\alpha - p_2 C_p + p_3 (\tau_\alpha + 1) - \zeta^2 \left[1 - \frac{1}{2} \frac{\tan(\gamma)}{\tan(\gamma) + \frac{\dot{x}}{V}} \right] \qquad (5.56)$$

$$\begin{aligned} I_7 &= I_{71} + j I_{72} \\ I_8 &= I_{81} + j I_{82} \end{aligned} \qquad (5.57)$$

$$\varepsilon = S \ \mathrm{cotg}(\phi) \qquad (5.58)$$

(5.47) and (5.48) represent the variation of the dynamic turning force in the complex time domain showing thus the phase existing between the tool displacement and the dynamic force. This variation in the turning force results from dynamic variation in both variations in the rake and ploughing forces.

The real part of the rake force variation is proportional to and in phase with the chip thickness variation normal to the mean cutting direction while the imaginary consists of two parts; one proportional to the tool vibrational velocity and the other to the time rate of change of the chip thickness. Moreover, the real part of the ploughing force variation dependent upon the displacement of the tool, whereas its imaginary part is proportional to and in phase to the tool vibrational velocity.

From the above discussion, the dynamic variation of the turning force is proportional to and in phase with the chip thickness variation normal to the mean cutting direction, to the velocity of the tool vibration and to the rate of change of the chip thickness. The analysis of the dynamic cutting process and of the variation of the cutting forces has led to show that the dynamic force is increasing with the dynamic chip thickness and

decreasing with the velocity of the tool for higher frequencies while the variation of the dynamic force is proportional to the variations in chip thickness, to the velocity of tool vibration and to the rate of change in chip thickness. It is shown that the dynamic part of the ploughing force components is neither proportional to the tool vibration (Wu, 1985a) nor proportional to the tool displacement (Hamdan, 19) but it varies linearly with both the velocity and the displacement of the tool.

5.6. DYNAMIC OSCILLATIONS OF SHEAR ANGLE, RAKE FORCES RATIO, DEPTH OF TOOL PENETRATION AND FRICTION ANGLE ALONG FLANK FACE OF CUTTING TOOL

The above theoretical analysis of the dynamic turning led to express the dynamic components of the turning force as well as the dynamic variations of these components as a functions of the independent parameters together with the parameters characterising the dynamic variations of the shear angle, the rake forces ratio and the friction angle along the flank of the cutting edge of the tool. The former are considered as an input to the turning system (Fig. 5.4) whereas the latter are cutting process dependent parameters, so far not dealt with, and for which a complete determination is presented in the following section.

5.6.1. Incremental parameters for dynamic shear angle

Early study of oscillation of shear plane conducted by Hahn *et al.* (1963) showed that there is a delay period of the plastic flow behind the stress application of order of 10^{-5} sec for a typical applied stress of 689.5 N / mm^2 and accordingly, the shear plane responds almost faithfully to cyclic variations of the cutting parameters. These

theoretical conclusions were supported by the experimental findings of Hardman (1970) after using a high speed photograph camera to monitor the response of the shear angle during dynamic turning and showing that the shear plane responds to dynamic variation up to 500Hz. Moreover, an analysis of the cutting process using the slip-line field theory (Wu, 1986) led to develop an equation for dynamic variation of the shear angle in the following form:

$$\tan(\phi_i + \tan^{-1}(\mu_i) - \alpha_0) - \tan(\phi' + \tan^{-1}(\mu') - \alpha') = \frac{4}{3}(\phi' - \phi) + \frac{4}{3} d\delta_0 + \frac{2}{3} d\delta \qquad (5.59)$$

where ϕ_i and μ_i are the instantaneous shear angle and the dynamic frictional coefficient along the rake of the tool. ϕ' and μ' are the shear angle and the frictional coefficient parallel to the rake of the tool. The dynamic friction coefficient as well as μ' and ϕ' are given by the steady state functional relationships (3.6) and (3.7) of the mean friction coefficient and the mean shear angle, respectively, in terms of the cutting speed, the uncut chip thickness and the rake angle as given by (5.60) to (5.62).

$$\mu = M(V_i, S_i, \alpha_i) \qquad (5.60)$$

$$\mu' = M(V', S', \alpha') \qquad (5.61)$$

$$\phi' = \Phi(V', S', \alpha') \qquad (5.62)$$

The instantaneous cutting conditions V_i, S_i and α_i are determined from the dynamic cutting process (Fig. 5.3) by:

$$V_i = \frac{V}{\cos(\delta)} + \frac{\dot{x} \cos(\alpha_0) \cos(\phi_i - \alpha_0)}{\sin(\phi_i + \delta)} \qquad (5.63)$$

$$S_i = \frac{(S_0 - x + x_0)\sin(\phi_i + \delta)}{\sin(\phi_i)} \qquad (5.64)$$

$$\alpha_i = \alpha + \delta \qquad (5.65)$$

The cutting speed when the cutting process is carried out with fixed clearance angle is expressed as:

$$V' = \frac{V}{\cos(\delta)} \qquad (5.66)$$

Furthermore, the incremental coefficient T_1, T_2 and T_3 of (5.43) are determined by a direct partial differentiation of the dynamic shear angle as:

$$T_1 = \frac{\partial\phi}{\partial S_0} \qquad (5.67)$$

$$T_2 = \frac{\partial\phi}{\partial\alpha} \qquad (5.68)$$

$$T_3 = \frac{\partial\phi}{\partial\psi} \qquad (5.69)$$

Partial differentiations of (5.59) to (5.65) led to determine the shear angle incremental parameters express by (5.67) to (5.69) in the following forms:

$$\begin{bmatrix} T_1 \\ T_2 \\ T_3 \end{bmatrix} = \begin{bmatrix} \frac{\partial \phi'}{dS_0} & -\frac{1}{1+\mu^2}\frac{\partial \beta}{dS_0} & \frac{1}{1+\mu'^2}\frac{\partial \mu'}{dS_0} - 1 \\ \frac{\partial \phi'}{d\alpha} & -\frac{1}{1+\mu^2}\frac{\partial \mu}{d\alpha} & \frac{1}{1+\mu'^2}\frac{\partial \mu'}{d\alpha} - 1 \\ \frac{\partial \phi'}{d\psi} & -\frac{1}{1+\mu^2}\frac{\partial \mu}{d\psi} & \frac{1}{1+\mu'^2}\frac{\partial \mu'}{d\psi} - 1 \end{bmatrix} \begin{bmatrix} \frac{\frac{7}{3} + \tan^2(\phi' + \tan^{-1}(\mu') - \alpha')}{\frac{7}{3} + \tan^2(\phi + \tan^{-1}(\mu) - \alpha)} \\ \frac{1 + \tan^2(\phi + \tan^{-1}(\mu) - \alpha)}{\frac{7}{3} + \tan^2(\phi + \tan^{-1}(\mu) - \alpha)} \\ \frac{1 + \tan^2(\phi' + \tan^{-1}(\mu') - \alpha')}{\frac{7}{3} + \tan^2(\phi + \tan^{-1}(\mu) - \alpha)} \end{bmatrix} \quad (5.70)$$

Detailed expressions of the partial differentiation of ϕ', μ and μ' with respect to the uncut chip thickness S_0, the rake angle α and the slop of the free surface to the instantaneous cutting speed ψ are reported in Appendix A2.

5.6.2. Incremental parameters for rake forces ratio, tool penetration and friction coefficient along the clearance face

The dynamic variations of the rake forces ratio C_s, the tool penetration ζ and the mean friction coefficient μ_f along the flank face correspond to the variation of the dynamic values of cutting parameters. The latter are determined from the steady state equations (Chapter 3) where the instantaneous cutting conditions are used. Thus:

$$u_1 = \frac{\partial C_s}{\partial S}(V_i, S_i, \alpha_i) \quad (5.71)$$

$$u_2 = \frac{\partial C_s}{\partial \alpha}(V_i, S_i, \alpha_i) \quad (5.72)$$

$$\zeta_{\alpha} = \frac{\partial \zeta}{\partial \alpha}(V_i, S_i, \alpha_i) \qquad (5.73)$$

$$\mu_{f\alpha} = \frac{\partial \mu_f}{\partial \alpha}(V_i, S_i, \alpha_i) \qquad (5.74)$$

The instantaneous cutting conditions V_i, S_i, and α_i are given by (5.63) to (5.65).

5.6.3. Discussion

The incremental parameters (5.70) – (5.74) are used to determine the dynamic oscillations of the turning force in the mean cutting speed and the feed directions. Furthermore, these parameters yield informations on how much the dynamic components of the turning forces are sensitive to the changes in the cutting conditions. The theoretical results of the actual incremental parameters are shown in Fig. 5.9 to Fig. 5.24 inclusive, for eight cutting speeds ranging from 0.43 to 8.33 m/s, feeds from 0.10 to 0.30 mm/rev.

Theoretical investigation of the cutting process conducted by Field *et al.* (1949) and Albrecht (1965) showed that the incremental parameters of the shear angle relative to the angles α and ψ are as $T_2 = T_3 = 0.5$. Furthermore, Oxley (1963) showed that $T_3 = 0.2$ and analysis of Eggleston's (1959) results yields T_2 between 0.56 and 0.72. The equality obtained between T_2 and T_3 (Field, 1949) is based upon the analogy between the incremental variation in the rake angle $d\alpha$ and in the slope of the free surface of the workpiece $d\psi$. This analogy arose from the fact that $d\alpha$ defines the variation in the angle between the instantaneous cutting direction and that of the chip departure, while $d\psi$ represents the variation in the angle between the instantaneous

cutting direction and that of the metal surface approaching the tool edge (Fig. 5.3). This assumption is only valid for the case of wave removing turning which is mostly the case during the first revolution of the workpiece. After the first revolution of the work, the tool is also removing the waviness of the work surface and then, as can be seen from (5.6), ψ responds also to the variations of the slope of the workpiece surface. Moreover, when the tool is maintained steady and is removing the wave generated during the previous work–revolution, the rake angle remains constant whereas ψ is oscillating due to variations in the upper surface of the workpiece.

Examining Fig. 5.11 to Fig. 5.12 it can be seen that, in accordance with the findings of Oxley, Albrecht and Field, the amplitude of T_2 is varying between 0.05 and 0.8. T_2 is oscillating at the same frequency of the tool vibration and its amplitude increases with feed rate for cutting speeds up to 3.40 m/s and decreases with the cutting speed, and as the cutting speed increases above 3.40 m/s, the amplitude of oscillation of T_2 becomes rather decreasing with an increase in the feed. However, the phase becomes stable as the feed is increased. It can be concluded that the sensitivity of the shear angle to changes in the rake angle is decreasing with the cutting speed and, increasing with feed for low range of speeds up to 2.28, but this sensitivity becomes decreasing with the feed for higher cutting speed above 3.40 m/s. Contrary, the sensitivity of the shear angle to changes in the variation of the slope of the cut surface ψ is however increasing with the cutting speed (Fig. 5.13 to Fig. 5.14) and decreasing with the feed rate for higher speeds above 2.28m/s but is almost unaffected by feed for a relatively low speeds. It is also shown that the amplitude of the dynamic oscillation of the shear angle with the oscillation of the cut surface is decreasing with the cutting speed and therefore is dynamically less sensitive to variations of the angle ψ. The increase of the sensitivity of the shear angle with the cutting speed explain the experimental findings of Minis *et*

al. (1990a, 1990b, 1990c), of Wu (1985b) and of Tobias (1965) showing that the stability limit of the turning process is decreasing with the cutting speed.

Because no published data is available concerning T_1, analysis of the published experimental results obtained by Eggleston (1959) shows that for steady state turning the mean values for T_1 is 1029 rad/m for machining SAE1112. The values of the amplitude of T_1 are found to be between 550 and 2000 rad/m for all the range of cutting speeds under investigation. As can be seen from Fig. 5.9 to Fig. 5.10 and Fig. 5.16, the amplitude of response of the shear angle to variations in the feed rate decreases with the cutting speeds up to 5.2m/s and starts to decrease when the speed is increased from 7.27 to 8.33m/s. Moreover, the amplitude of T_1 increases with the feed rate for low speeds up to 2.28 m/s and decreases with feed for higher speed above 3.40 m/s. When the cutting speed is increased from 0.43 to 5.20m/s, the sensitivity of the shear angle to variations in the chip thickness decreases by 22% for feed of 0.10 mm/rev and by 38% for feed of 0.30 mm/rev (Fig. 5.16). Nevertheless, for higher speeds than 5.20 m/s, the amplitude of T_1 increases by about 60% for 0.10 mm/rev and when the speed is varied from 5.20 to 8.33 m/s but, for the same increase of speed, it only increases by about 44% for a feed of 0.30 mm/rev.

Concerning the variations of the of the rake forces ratio characterising the frictional state in the secondary shear zone, Fig. 5.17 shows that the dynamic rake forces ratio is increasing with the amplitude of the tool vibration and decreasing the frequency of tool vibration. This decrease is attributed to the decrease in the temperature of the chip–tool interface T_{int} with the frequency of oscillation. This decrease of T_{int} can be explained by the findings of Zorev (1963), Bailey (1975) and Oxley (1989) showing that the friction force on the tool rake face mainly due to the internal shearing of a thin chip layer adjacent to the tool face (secondary shear zone). Consequentially, the

average tangential stress σ_t on the tool rake depends mainly upon the shear strength of this layer contrary to the average normal stress σ_n which depends only on the properties of the whole chip. Therefore, it is expected that the variation of the chip–tool interface temperature T_{int} will have a greater effect on σ_t than that it has on the normal stress σ_n. Moreover, owing to the large heat capacity of the tool relative to that of the chip (Kannatey–Asibu, 1985), the incremental dynamic variation $d\alpha$ and dS will result in a corresponding change in T_{int} smaller than that occurring under steady state cutting process which will result in a similar attenuation of σ_t without much affecting σ_n. This will, in turn, result in an attenuation in the dynamic variation of C_s as can be seen from the simple relation $C_s = \sigma_t / \sigma_n$.

The dynamic variation of the rake forces ratio with the dynamic chip thickness and the rake angle is shown in Fig. 5.17 to Fig. 5.18 and in Fig. 5.19 to Fig. 5.20 respectively. It is shown that the variation of the rake forces ratio with the chip thickness undulation is almost not sensitive to any changes in the feed rate and that its amplitude is decreasing with the cutting speeds ranging from 0.43 to 3.40 m/s but is increasing with speeds higher than 5.20 m/s. Furthermore, the amplitude of oscillation of the rake forces ratio to the instantaneous rake angle is decreasing with the cutting speed on the one hand, increasing with feed for speeds smaller than 3.40 m/s and becomes decreasing with a tendency to stabilise for speeds greater than 5.20 m/s on the other.

The decrease of u_1 and u_2 with the cutting speeds up to a speed of 3.40 m/s can be explained by the fact that the dynamic variation of the chip–tool interface temperature dT_{int} is expected to decrease as the specific heat of the tool increases, since the increase in the latter will cause a corresponding increase in the heat capacity or the thermal inertia of the tool. Moreover, dT_{int} decreases as the frictional process upon the tool

rake approaches the diabetic conditions since this allows less percentage of the heat generated to be transferred to the tool to change its temperature (Shaw, 1960). Both the increase of the specific heat of the tool and the decrease of the percentage of heat transferred to the tool can result from an increase of the cutting speed. This is confirmed by the theoretical and the experimental results of Shaw (1960) showing that, in metal cutting, the percentage of the generated heat energy transferred to the tool decreases as the cutting speed increases. Therefore, an increase in the cutting speed will result in a decrease in the amplitude of oscillation of the rake force ratio with the chip undulation and the oscillation of the rake angle. However, above 5.20 m/s and because the amplitude of oscillation of u_1 and u_2 is increasing with speed, it appears that the specific heat of the tool decreases with speed at high cutting speed range. This will allow thus more heat to be transferred to the cutting tool in contrast to that occurring in relatively low cutting speed range. Unfortunately, no published data is available in this matter and these trends at high speeds can explain the increase in the rate of the crater wear at high levels of cutting speed because of the decrease of the tool strengths with the temperature.

Similar conclusions are brought about by analysing the variation of the instantaneous mean friction angle along the flank of the tool shown in Fig. 5.21 to Fig. 5.22. It is found that the dynamic variation of the mean friction angle along the flank of the tool is less sensitive to changes in the feed and that its amplitude is decreasing with the cutting speed for speeds smaller than 3.40 m/s and becomes increasing with speed when the cutting speed is larger than 5.20 m/s. This shows that similar phenomenon regarding to the friction is occurring along the rake and the flank of the tool.

The sensitivity of the depth of the tool penetration (Fig. 5.23 and Fig. 5.24) to changes in the rake angle is not affected by the chip undulation but is decreasing with

the cutting speed up to 3.40 m/s and becomes oscillating at small amplitudes at high speeds. For speeds up to 3.40 m/s, a decrease of the cutting speed will increase the sensitivity of the depth of the tool penetration to the variations of the rake angle and therefore more amount of material is deformed under the cutting edge at low cutting speeds.

5.7. CONCLUSION

A dynamic model describing the turning process as a dynamic system for which the tool vibration is considered as input and the turning forces as output was developed in this chapter. Analysis of the theoretical expressions of the dynamic turning forces did not yield a full description of the effect of the independent cutting parameters upon the cutting process and revealed the need for considering the dynamic incremental variation of the turning forces components. This, however, allows to single out the effect of each input parameters upon the outputs of the process.

Furthermore, analytical expressions of the variation of the shear angle, the rake forces ratio, the tool penetration and the mean friction angle along the flank of the tool is provided. Theoretical analysis of the latter parameters gives a good agreement with the published results in this field and provides a better interpretation of the experimental finding for turning process. It is generally shown that there is generally a tendency for better stability and low amplitudes of oscillation in medium range of cutting speeds that is about 3.40 and 5.20 m/s (204 and 312 m/min).

The developed model will be used in Chapter 7 to predict the dynamic turning forces for different cutting conditions when the measured tool vibration is fed as input into

this model. Experimental set–up and effect of the machine tool–post and tool–holder on the dynamics of the cutting is reported in Chapter 6.

PAGE

NUMBERING

AS ORIGINAL

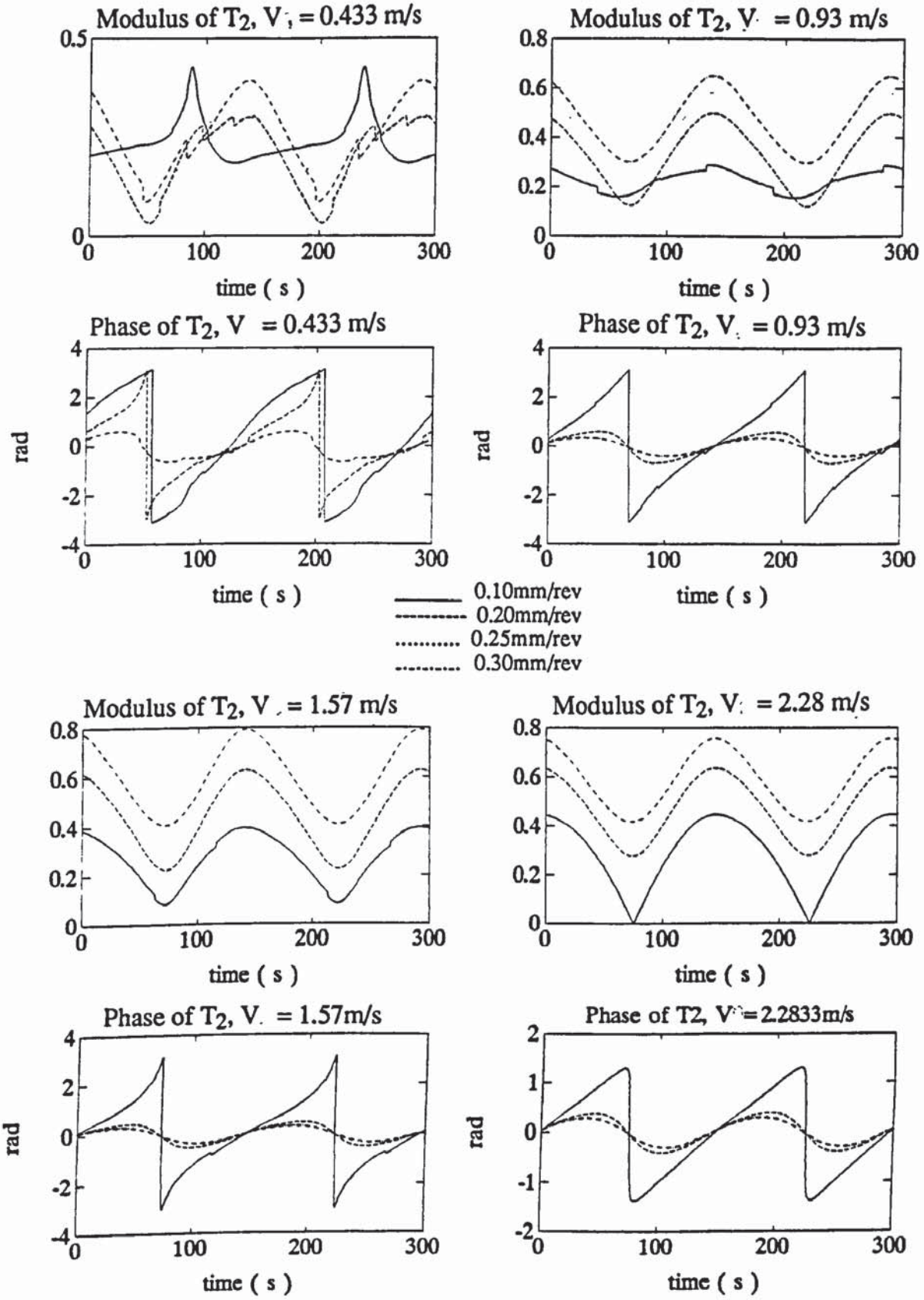

Fig. 5.11 Dynamic oscillation of shear angle with instantaneous rake angle, V_0 = 0.43, 0.92, 1.57 and 2.28 m/s.

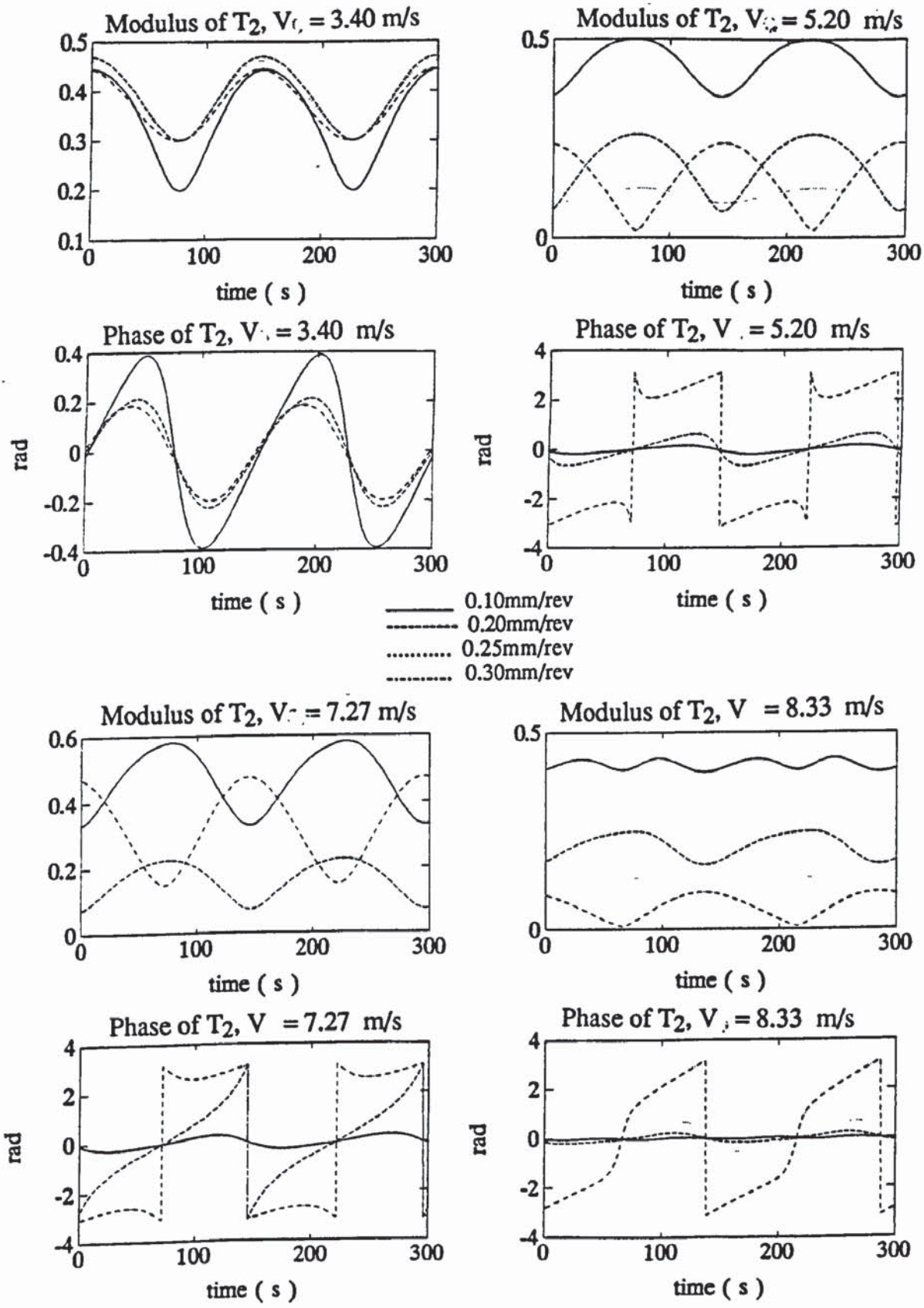

Fig. 5.12 Dynamic oscillation of shear angle with instantaneous rake angle, V_0 = 3.40, 5.20, 7.27 and 8.33 m/s.

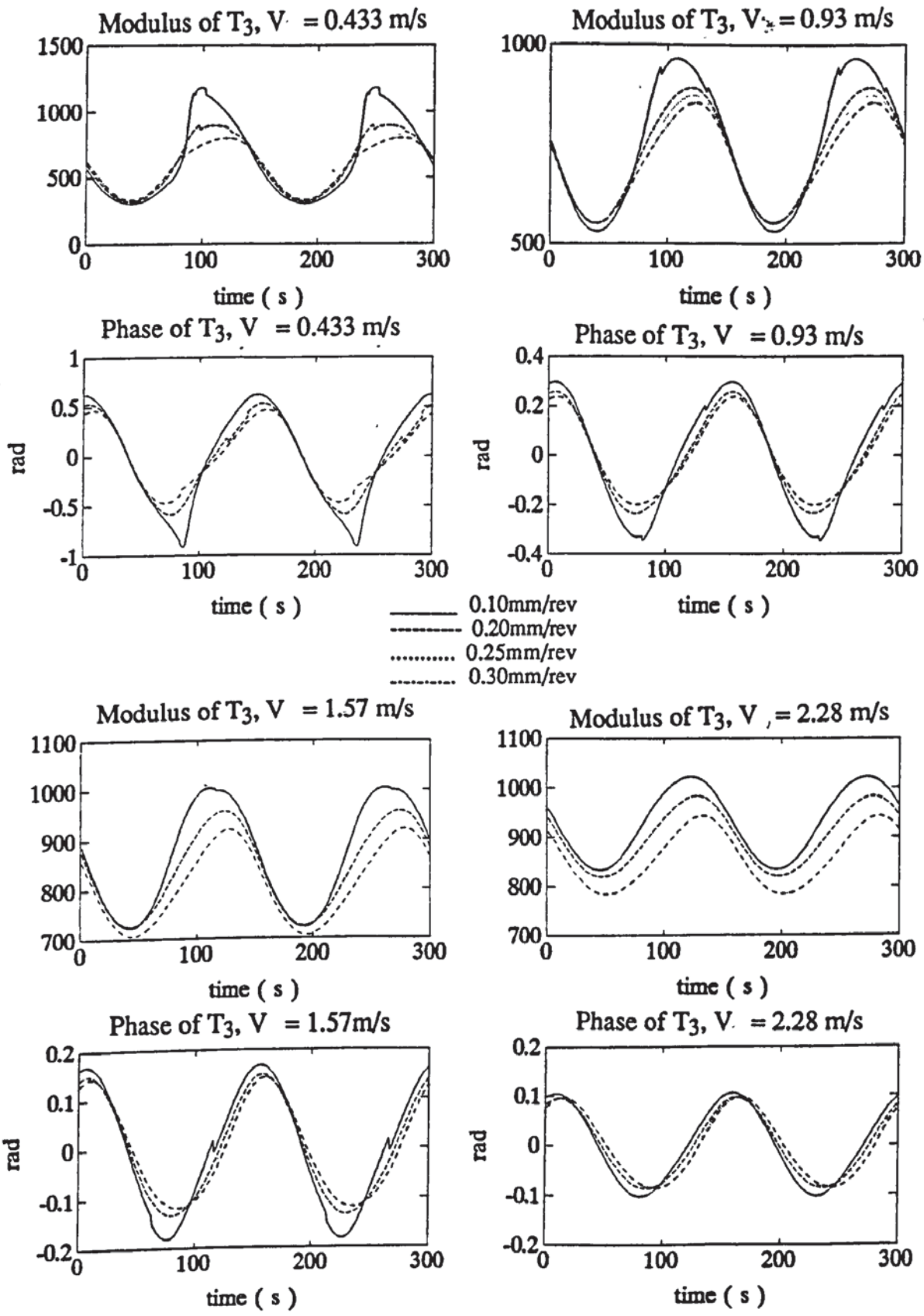

Fig. 5.13 Dynamic oscillation of shear angle with instantaneous slope of cut surface, V_0 = 0.43, 0.92, 1.57 and 2.28 m/s.

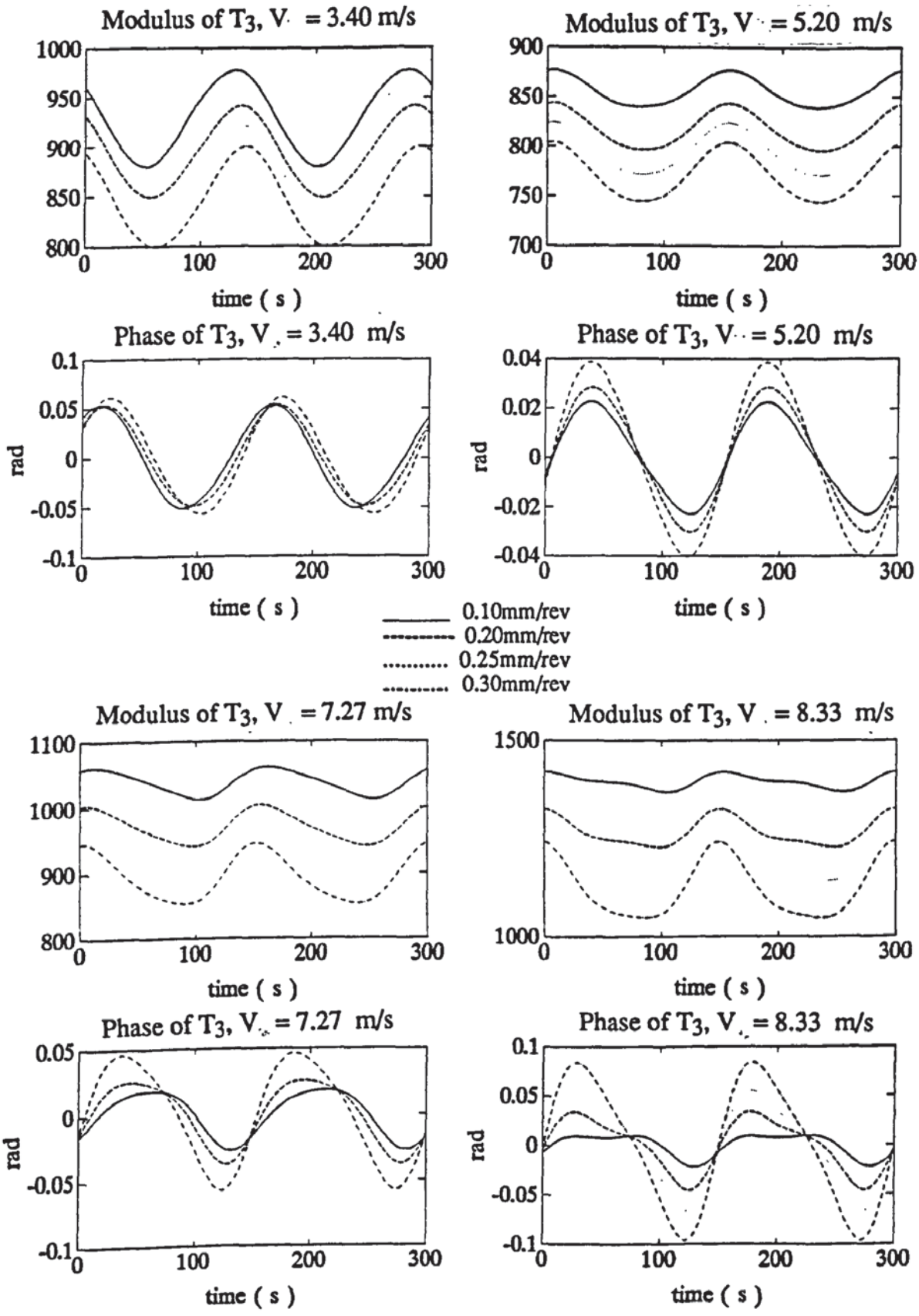

Fig. 5.14 Dynamic oscillation of shear angle with instantaneous slope of cut surface, V_0 = 3.40, 5.20, 7.27 and 8.33 m/s.

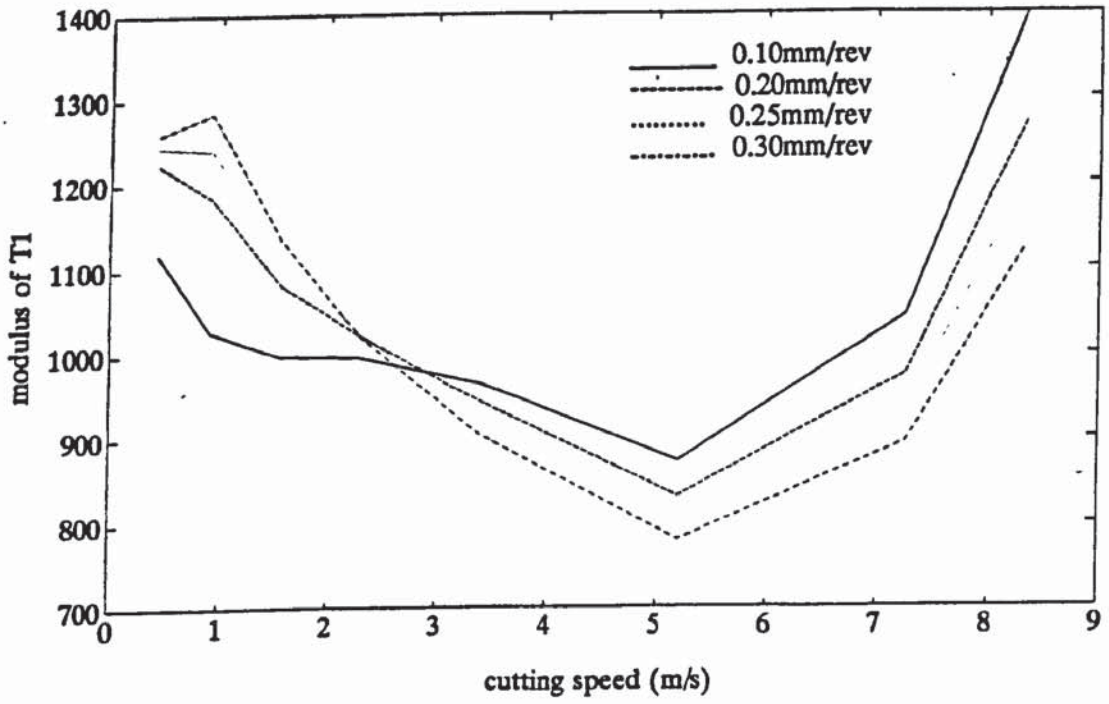

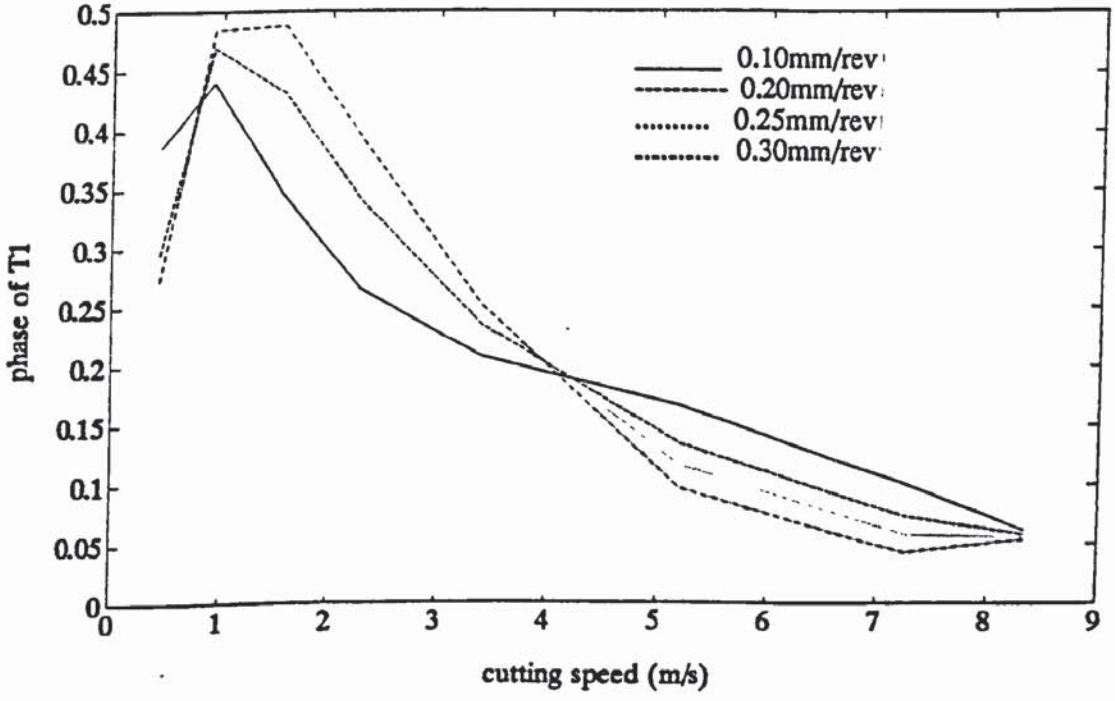

Fig. 5.15 Dynamic variation of the mean shear angle with cutting speed.

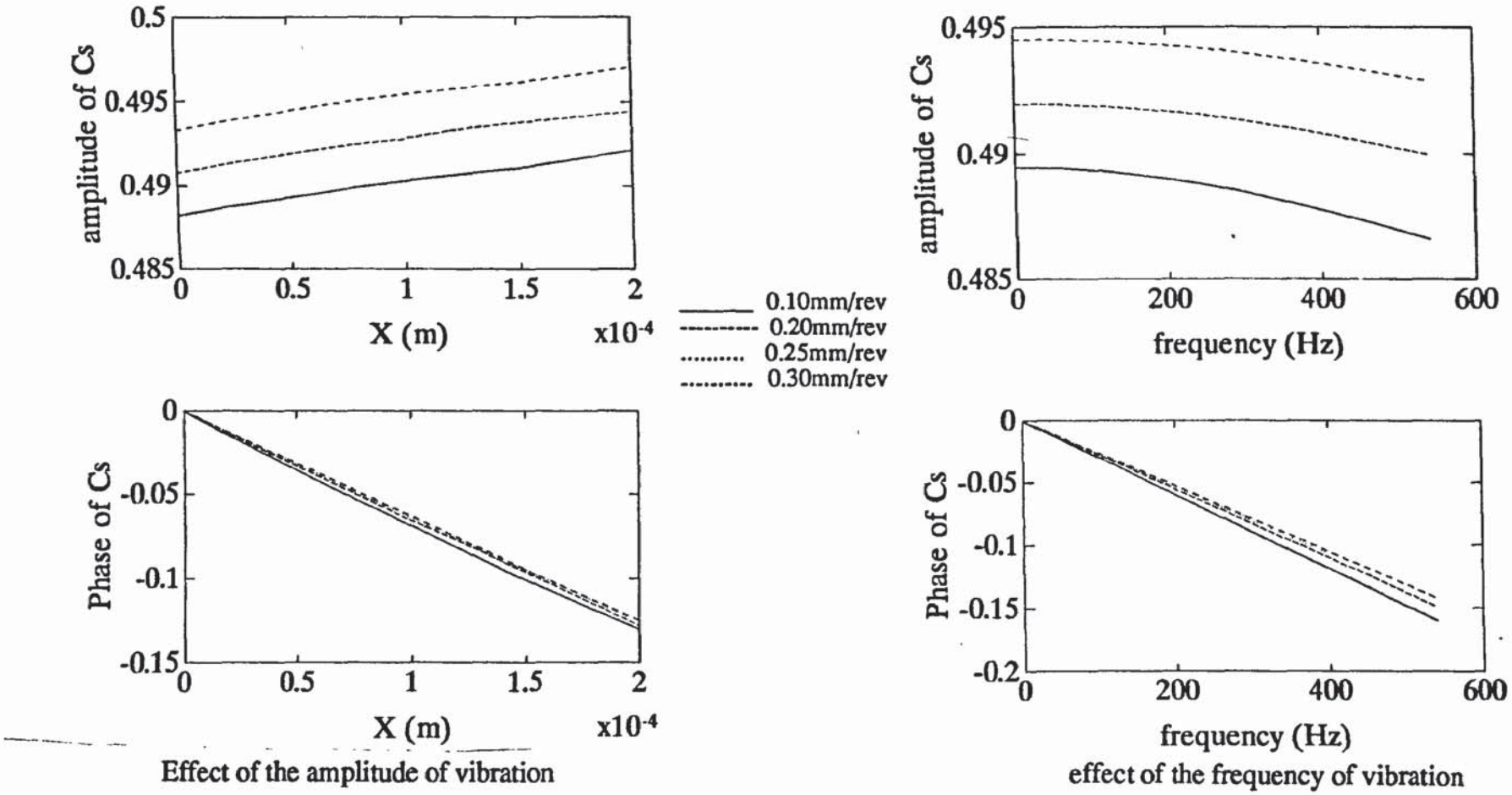

Fig. 5.16 Variation of rake forces ratio C_s with amplitude and frequency of tool vibration

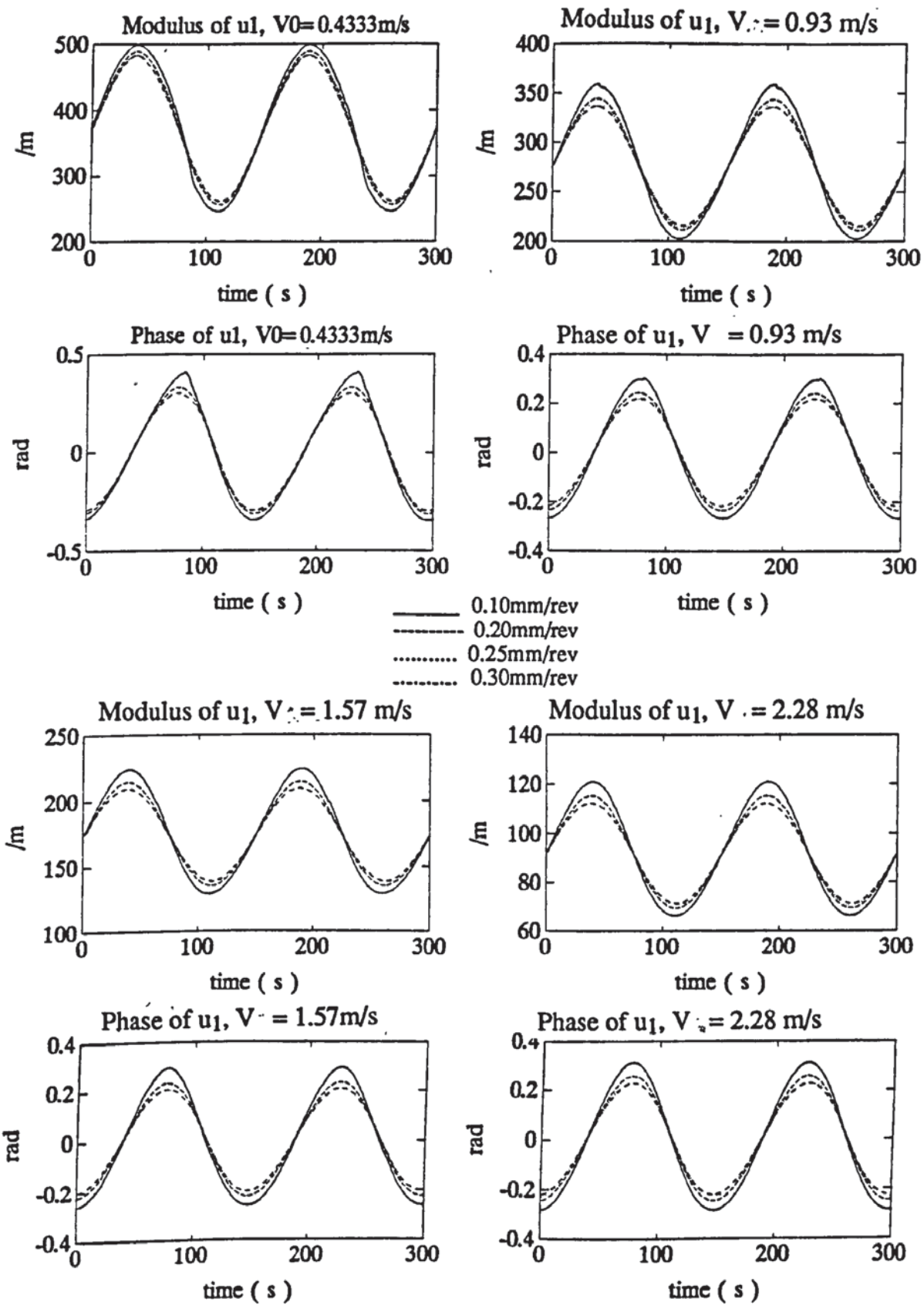

Fig. 5.17 Variation of rake forces ratio with instantaneous chip thickness, V_0 = 0.43, 0.92, 1.57 and 2.28 m/s.

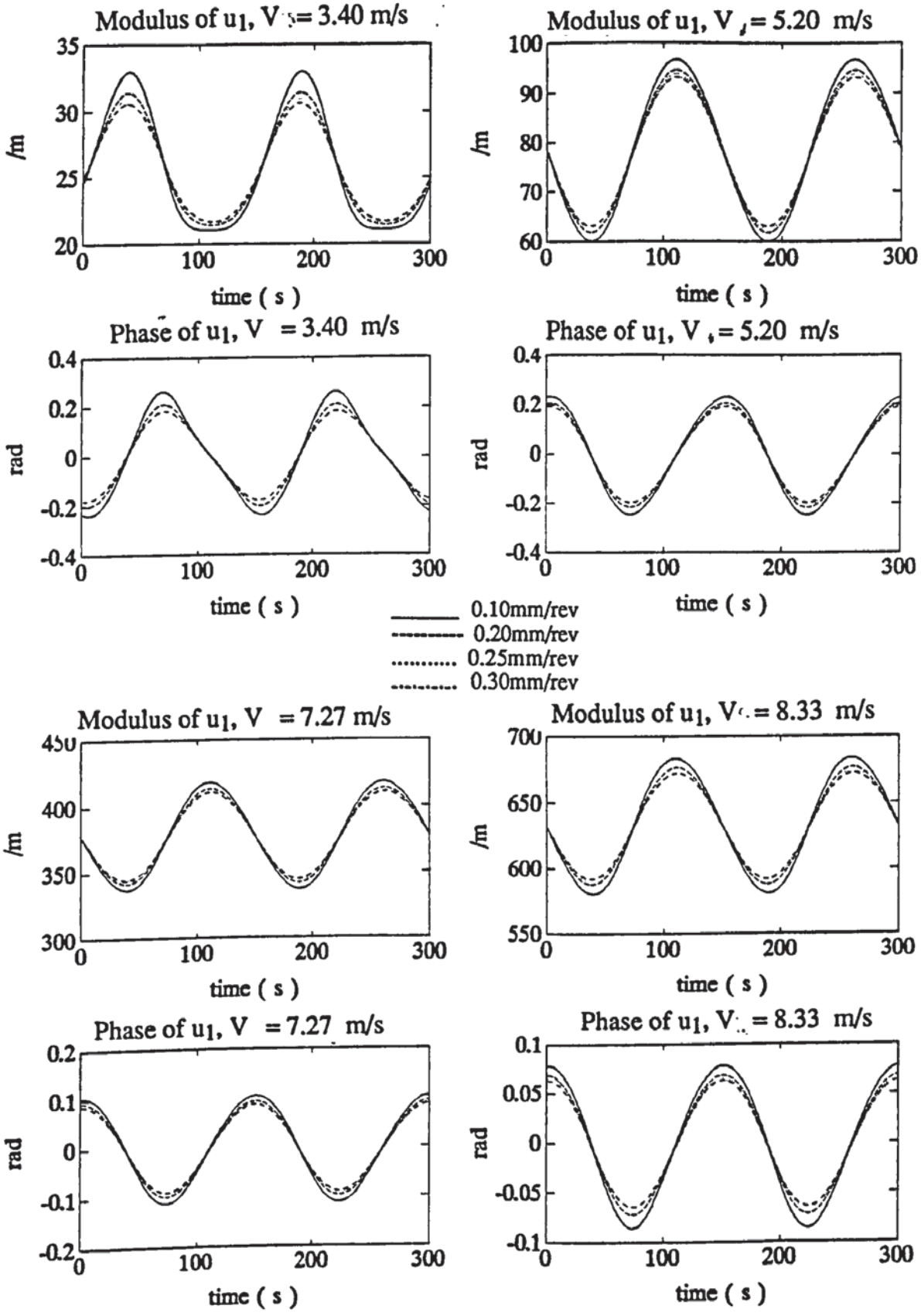

Fig. 5.18 Variation of rake forces ratio with instantaneous chip thickness, V = 3.40, 5.20, 7.27 and 8.33 m/s.

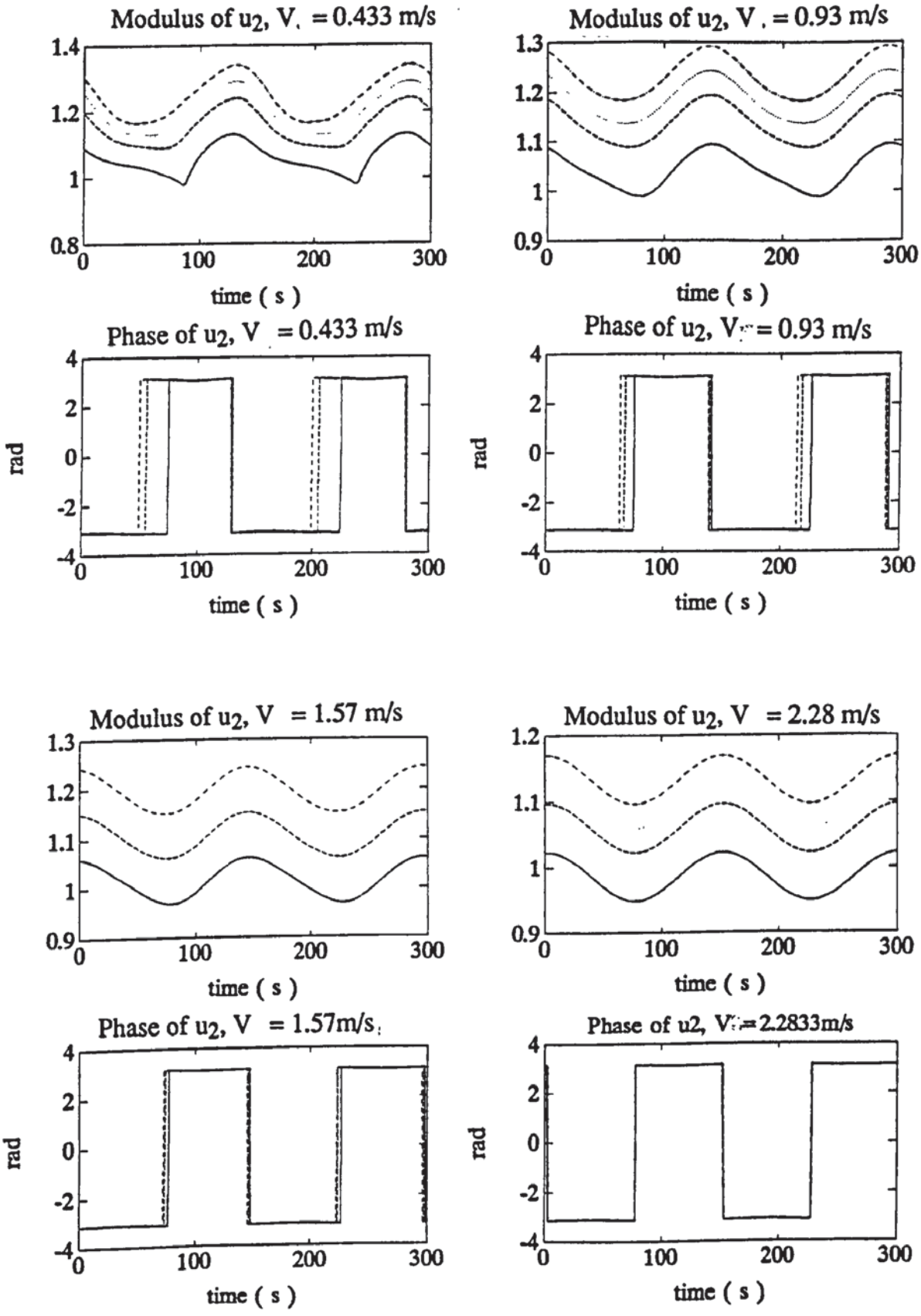

Fig. 5.19 Variation of rake forces ratio with instantaneous rake angle, $V_0 = 0.43$, 0.92, 1.57 and 2.28 m/s.

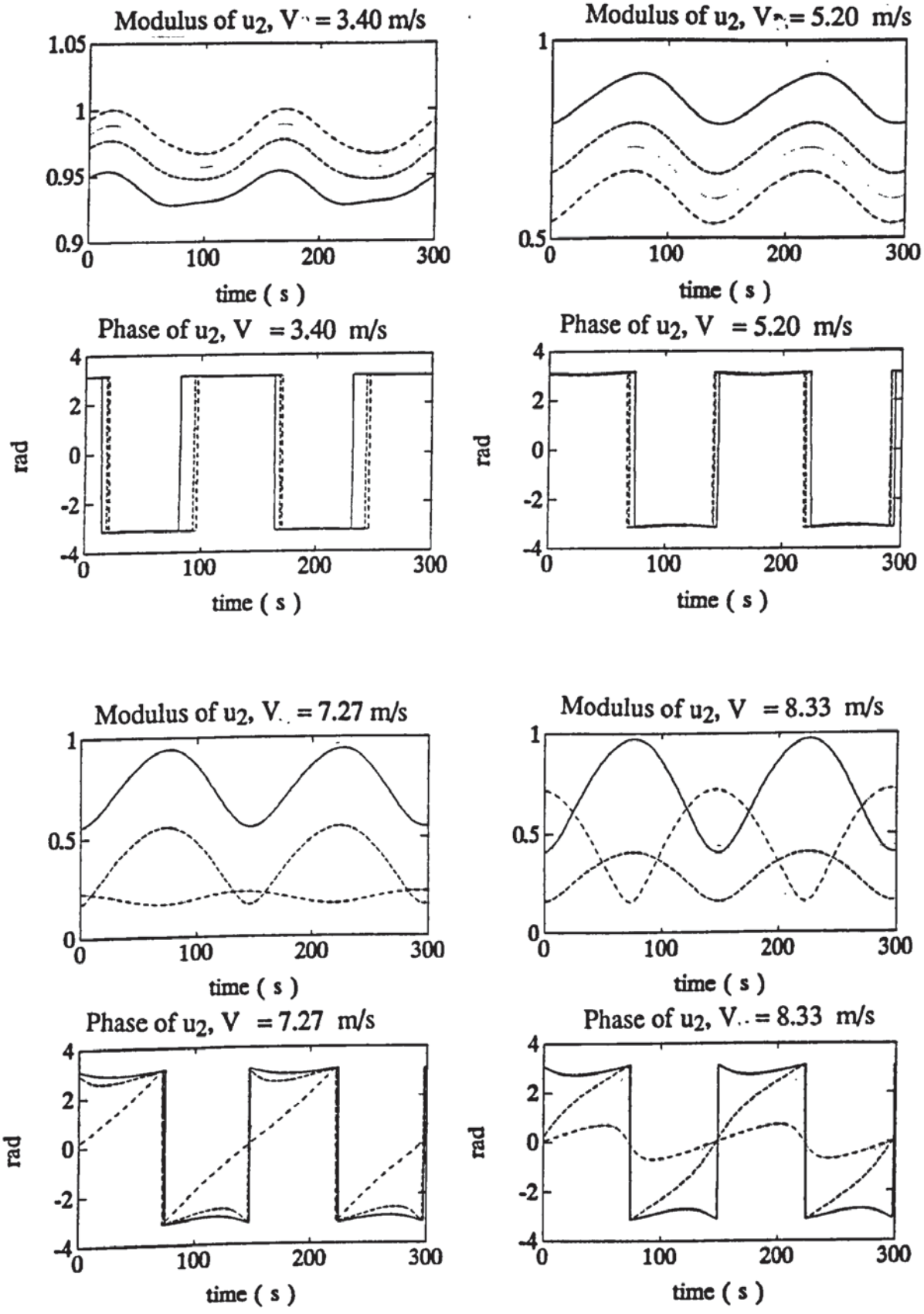

Fig. 5.20 Variation of rake forces ratio with instantaneous rake angle, $V_0 = 3.40$, 5.20, 7.27 and 8.33 m/s.

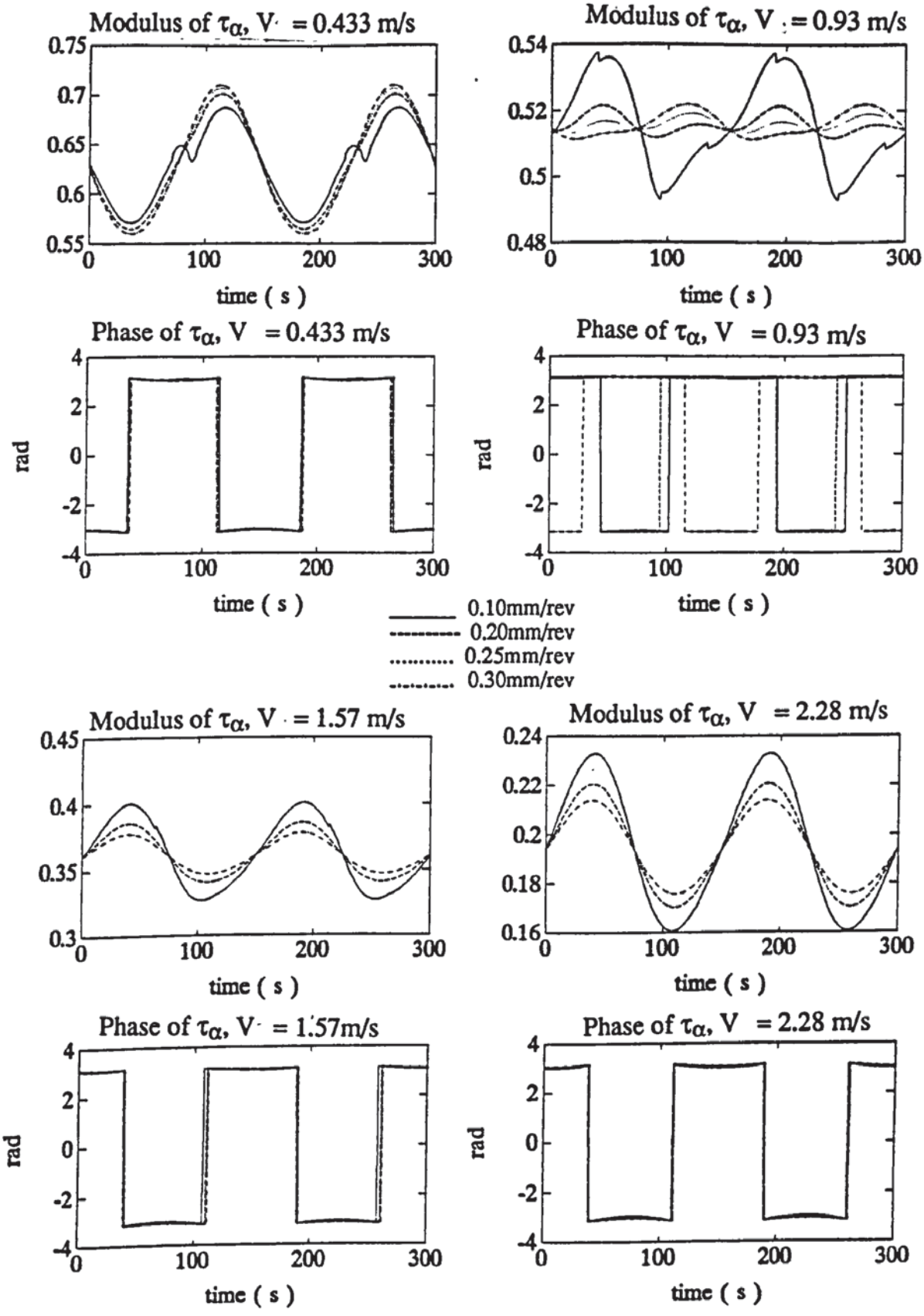

Fig. 5.21 Variation of mean flank friction angle with instantaneous rake angle, $V_0 = 0.43$, 0.92, 1.57 and 2.28 m/s.

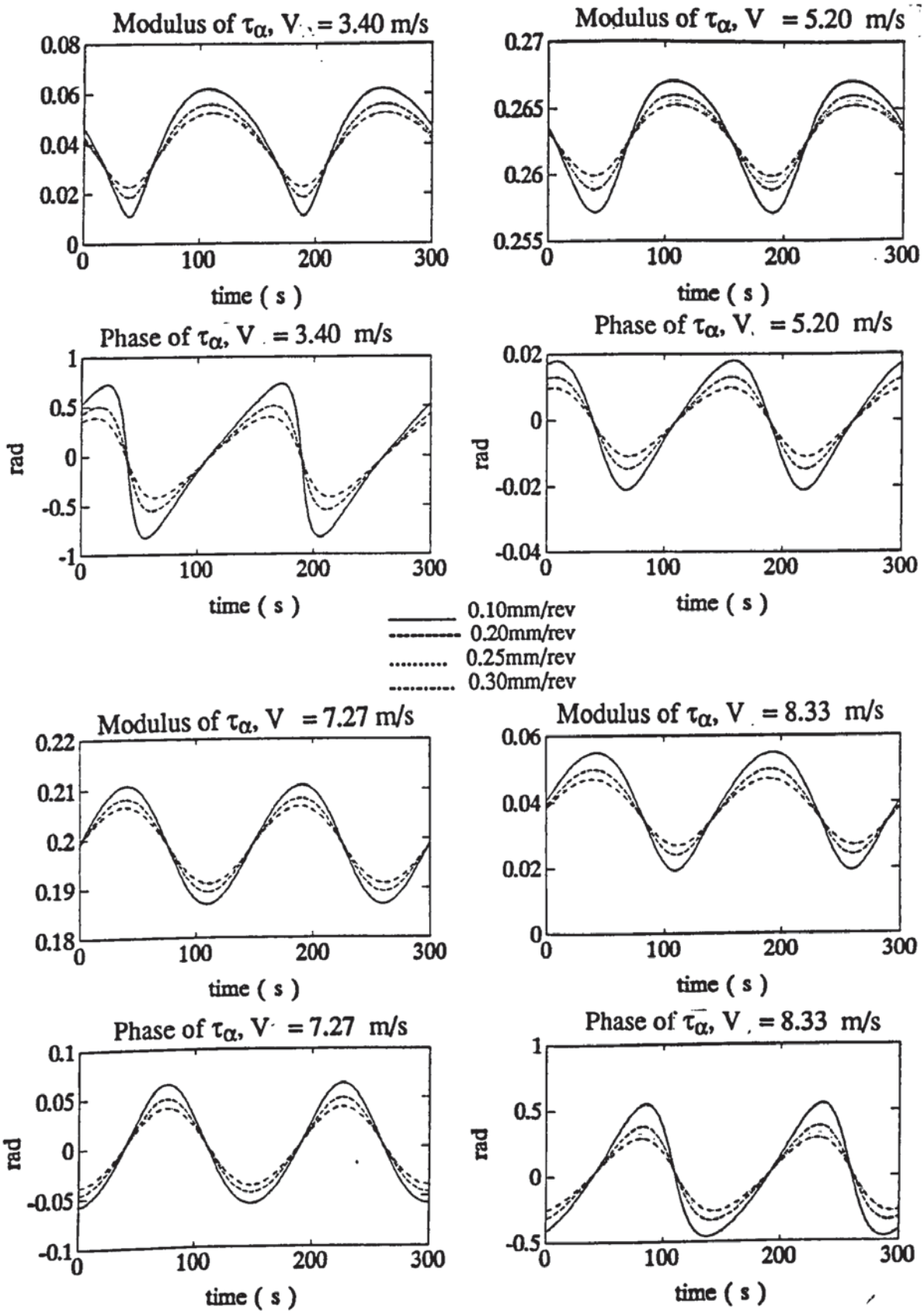

Fig. 5.22 Variation of mean flank friction angle with instantaneous rake angle, V_0 = 3.40, 5.20, 7.27 and 8.33 m/s.

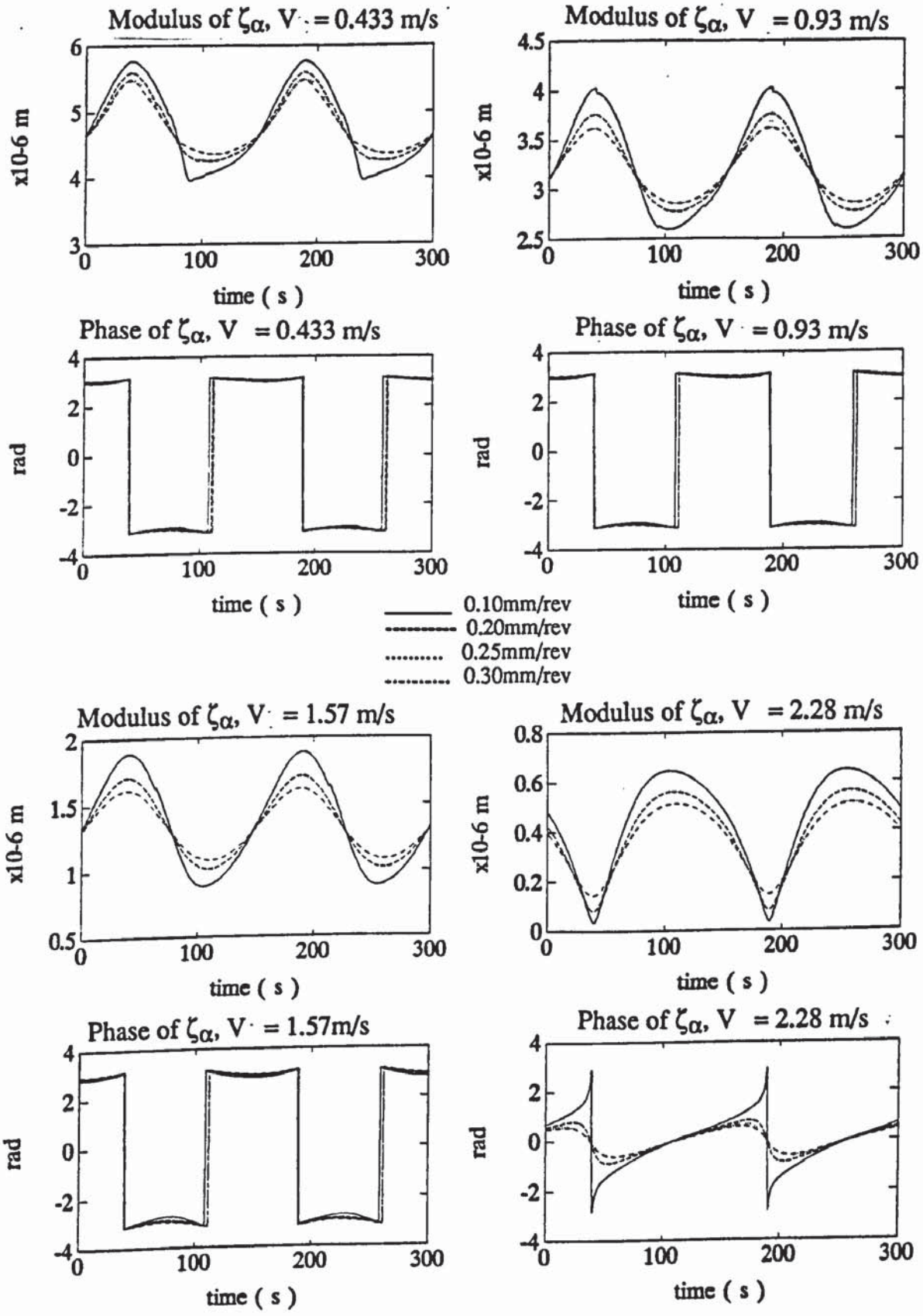

Fig. 5.23 Variation of depth of tool penetration with instantaneous rake angle, V_0 = 0.43, 0.92, 1.57 and 2.28 m/s.

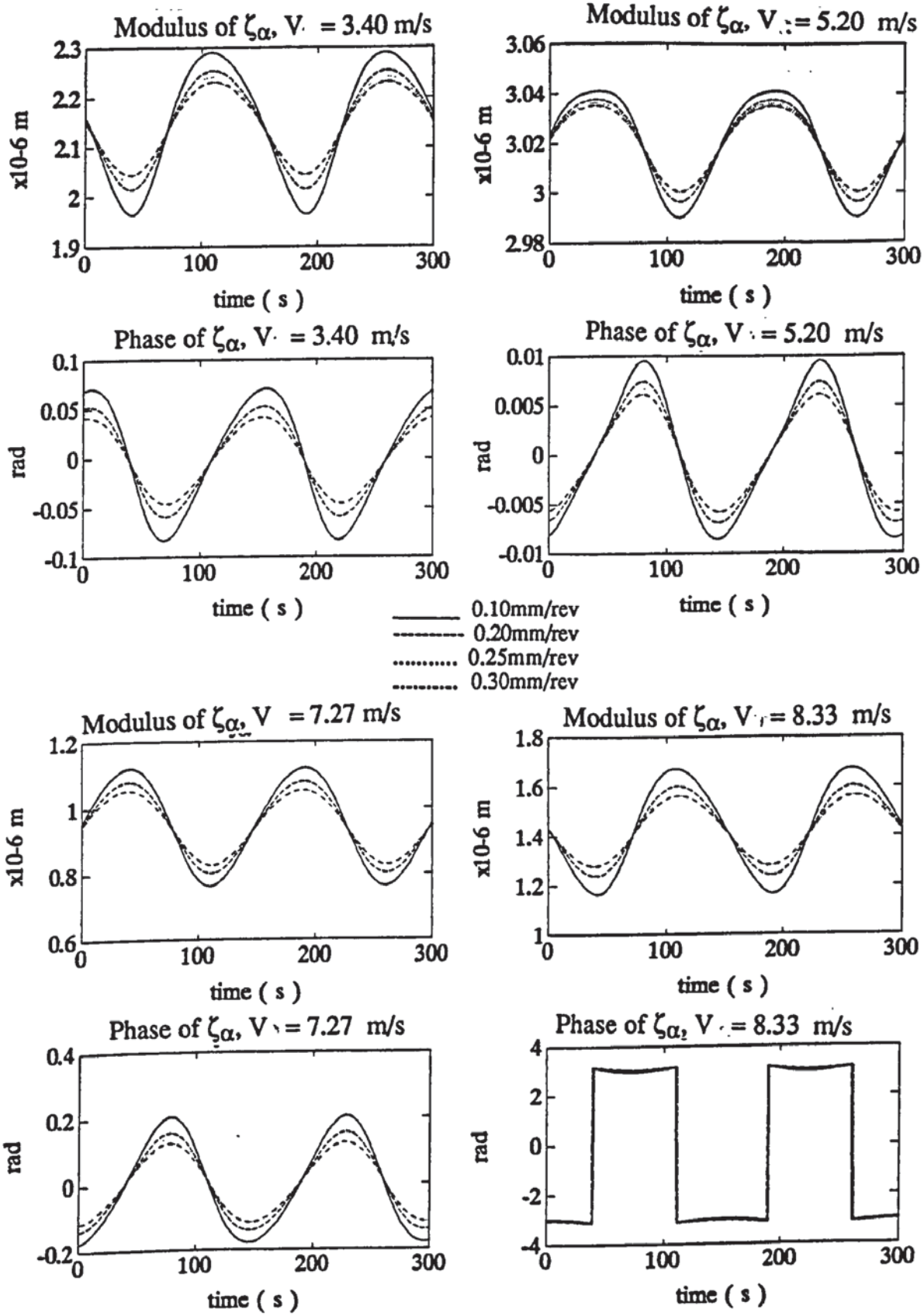

Fig. 5.24 Variation of depth of tool penetration with instantaneous rake angle, V_0 = 3.40, 5.20, 7.27 and 8.33 m/s.

Chapter 6

DYNAMIC MACHINING TESTS: Instrumentation and test rig

6.1. INTRODUCTION

A dynamic turning model for turning process with new cutting edge have been developed in Chapter 5. From the chatter point of view, the cutting process is considered as a dynamic system, the input of which is the chip thickness modulation and the output is the turning force. The chip modulation is initiated by chatter in the cutting test rig thus providing the energy of vibration from the cutting process itself. This undulation is represented by the tool vibration at the tip in the feed direction. The following sections discuss the design of the experimental rig and the instrumentation used in the experimental tests. These also discusses some of the frequency characteristics of the tool and the dynamometer that influence the measurements of the tool vibration and the dynamic turning force components.

The experimental rig used in this investigation for orthogonal dynamic tests is shown in Fig. 3.3. The test rig basically promises a single edge cutting tool, force dynamometer mounted on a rigid block fixed on the cross slide of the turret of the machine tool. The tool has a throw–away carbide tip (TPUN160304) which is mounted to the dynamometer through a tool holder and clamp as shown in Fig. 6.2. The tool holder was machined to present a circular cross section so that the rake angle can be varied as required (steady state experiments, Chapter 3). The cutting test rig

is suitable for orthogonal cutting of tubular workpiece along the longitudinal axis of the lathe, as shown in Fig. 3.3.

6.2. FORCE MEASUREMENT

The cutting and feed force components of the turning force are measured by a three components piezo–electric dynamometer. The dynamic response of this dynamometer with the tool mounted is determined using impact test.

This dynamic analysis of the dynamometer in working conditions, i.e. tool and upper block mounted, aims to determine the transfer function of the system dynamometer and all the neighbouring blocks mounted on the dynamometer or on which the dynamometer is fixed. This transfer function H_d will be used to correct the measured force in order to determine the real cutting force. The real turning force is applied on the tool tip where no access is possible to measure its value and therefore the measure of the force is made far away from the point of application of the force. In steady state conditions, the steady value of the force on the tool is the same as that sensed by the dynamometer, whilst in dynamic analysis the measured dynamic force is influenced by the structure of all the mechanism between the point of measurement and the point where the force is applied. If a force F_{input} is applied on the tool tip, and its measure is done at the output of the dynamometer as F_{output}, the ratio between these two forces defines in frequency domain the transfer function of the dynamometer as given below:

$$H_d = \frac{F_{output}}{F_{input}} \qquad (6.1)$$

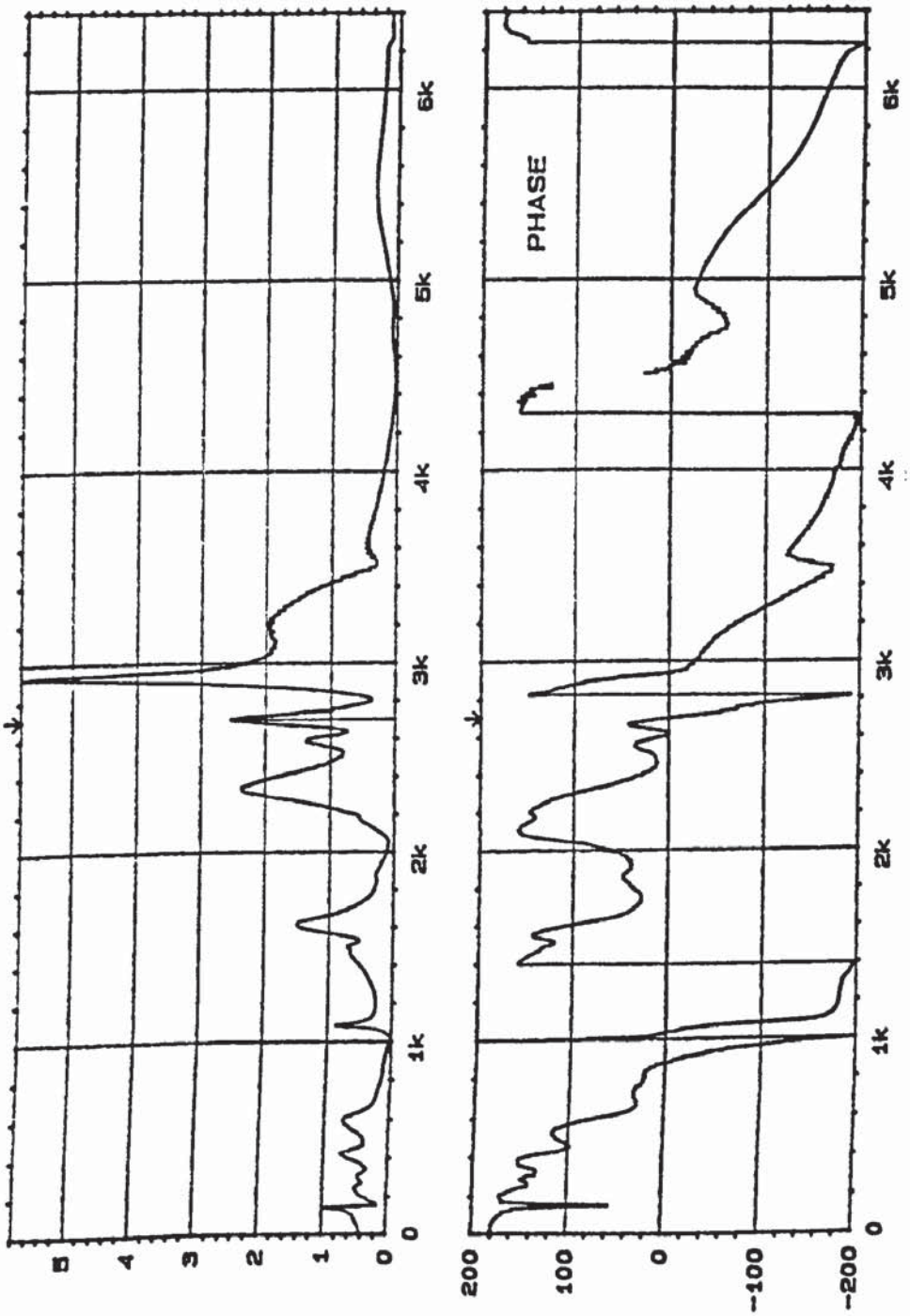

Fig. 6.1 Transfer function of the dynamometer / machine system.

As the model predicts the force upon the tool tip when the tip acceleration is known, it is a sine qua non condition to use (6.1) to determine the model predicted force as output from the dynamometer.

An impact test was carried out by impacting the tool tip in the feed direction and measuring the output feed force output from the dynamometer. The determined transfer function is shown in Fig. 6.1. The impact test showed that, along the feed direction, the dynamometer / machine system has a flat response up to 2.2kHz and a major mode of vibration between 2.2 and 3.5kHz while the natural frequency along the feed direction occurs at 2928 Hz. The cross responses between the vertical and the horizontal directions are found to be less that 1% up to 1.6 kHz and less than 2.4% up to 6 kHz. Therefore for the frequency range under investigation, the cross sensitivity is neglected.

The data of the transfer function H_d is stored in the hard disk of the computer and will be used as given by (6.1) in the model program to determine the dynamic turning force components.

6.3. TOOL VIBRATION MEASUREMENT

Preliminary trials to measure the tool vibration with accelerometer mounted on the dynamometer showed that this is not adequate. This is because the output of the accelerometer is contaminated with high level of noise. It was decided, therefore, to

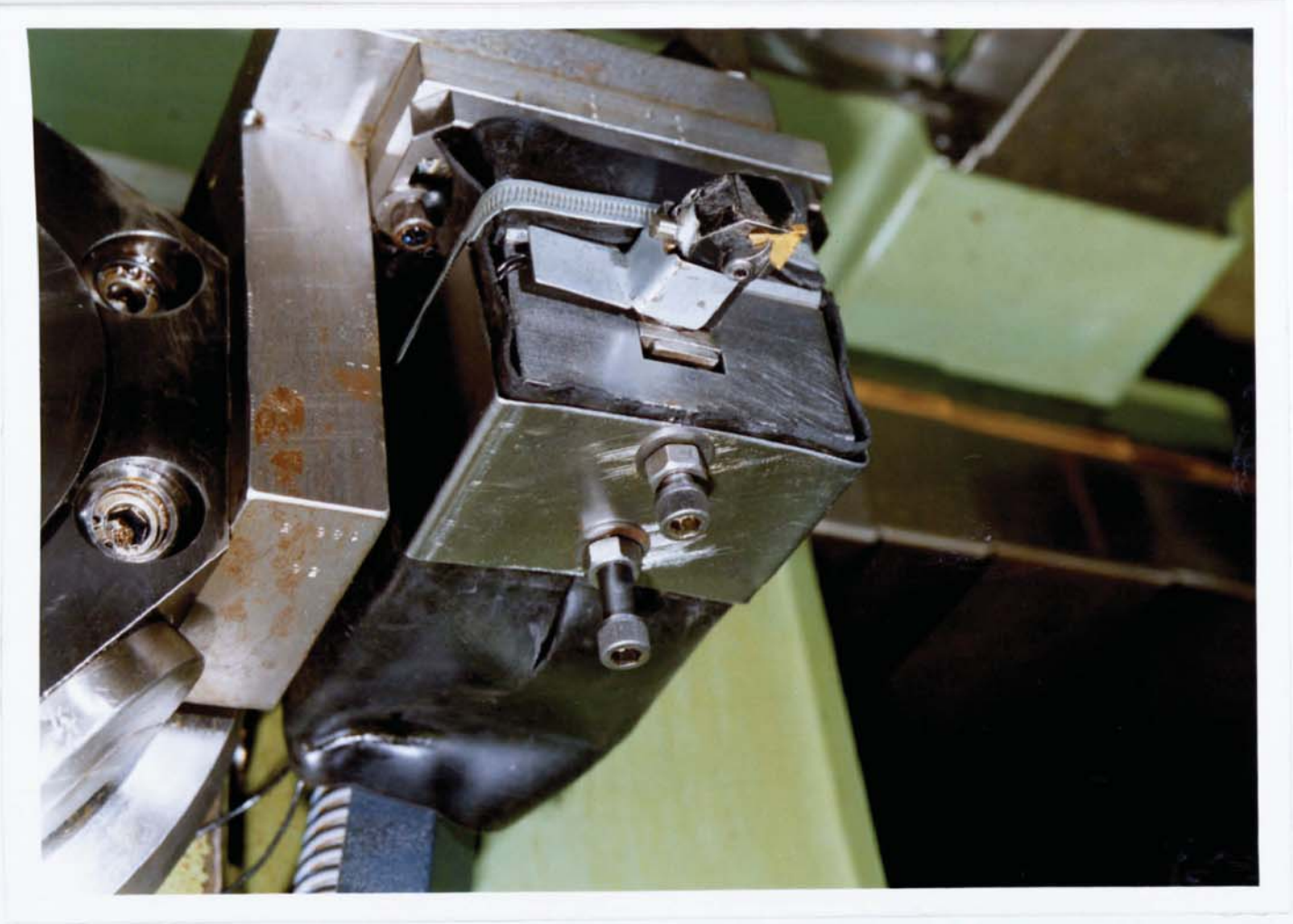

Fig. 6.2 Tool holder and tool post.

measure the tool vibratory acceleration along the feed direction by accelerometer glued on the tool holder as near as possible to the tool tip as shown in Fig. 6.2. This mode of fixation using the glue is suitable for frequency analysis up to 10kHz (Ewins, 1984). Fig. 6.2 shows the tool holder mounted on the dynamometer with the tip on and the accelerometer sensing the acceleration of the tool in the feed direction. The wire of the accelerometer is protected so it will not be damaged by the chip clearing away from the tool.

The tool can be considered as a rigid beam clamped in one end and free in the other end. Under this assumption, the wave length for the highest frequency of the range investigated is found to be 12 times the the maximum distance between the accelerometer and the point where the acceleration is wanted to be measured and therefore it is justifiable to assume that the signal out of the accelerometer represents the actual vibratory acceleration of the tool tip up to 6.4 kHz.

6.4. RELIABILITY OF RECORDING DYNAMIC DATA

The reliability of the magnetic tape recorder is assessed prior performing actual cutting tests. The aim of this is to investigate the gain and phase distortion encountered in different channels of the tape recorder for the analogue signals recorded on the magnetic tape. The tape recorder has four channels connected to the same recording and playing back heads mounted on the same stack.

A sine wave of different frequencies and 1V peak to peak is simultaneously recorded on the four channels of the tape recorder. A sample of the input signals is given in Fig. 6.3 for a frequency of 504 Hz. The four recorded signals are then played back

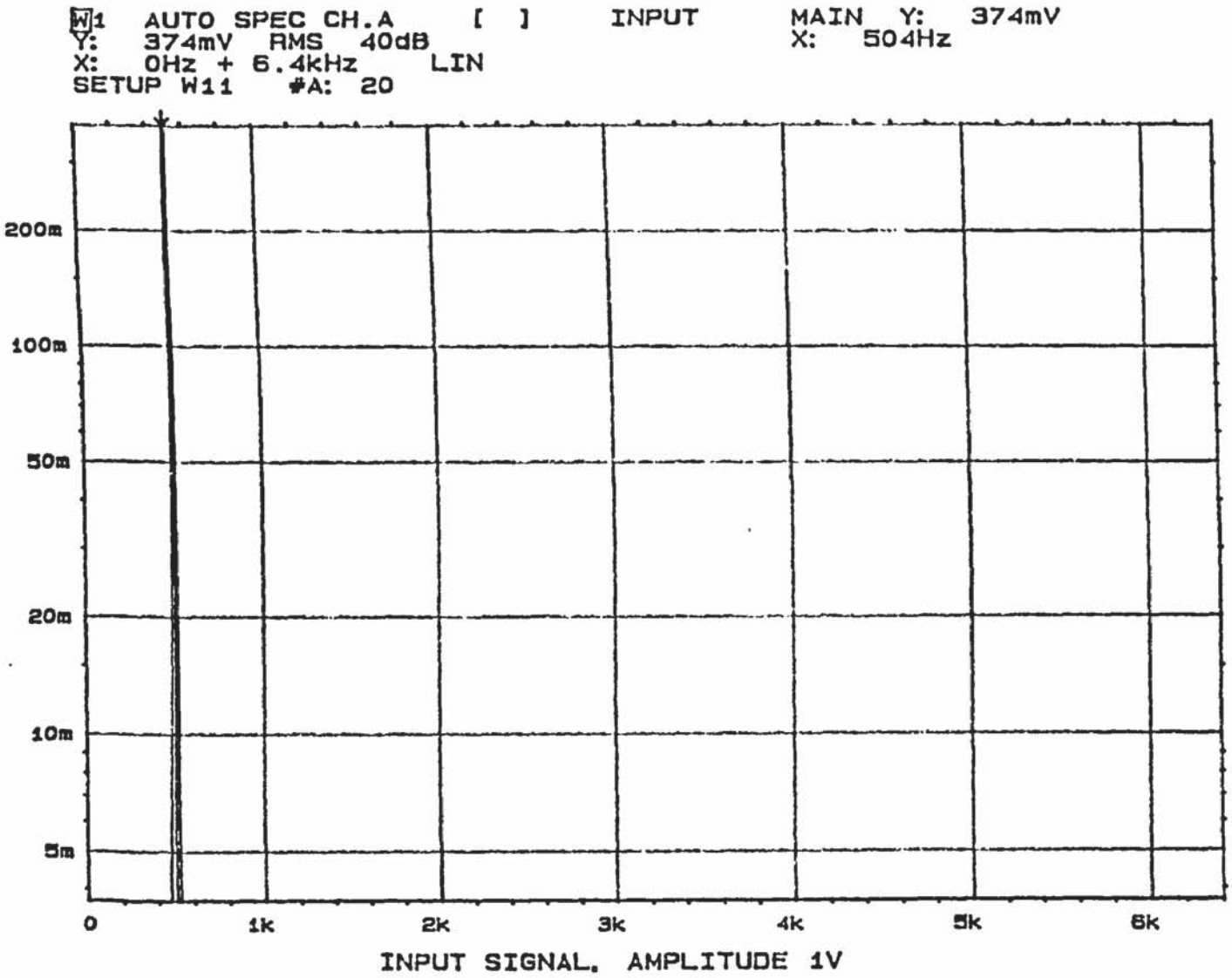

Fig. 6.3 In–put signal to the four channels of the tape recorder.

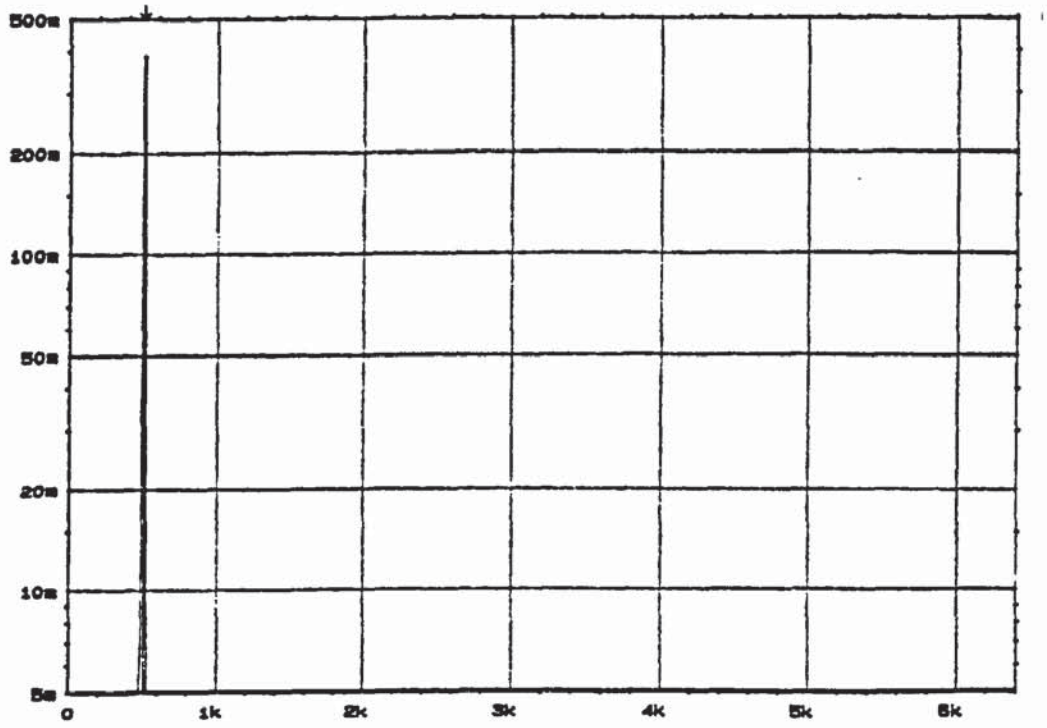

Fig. 6.4 Out–put signal from channel 1 of the tape recorder.

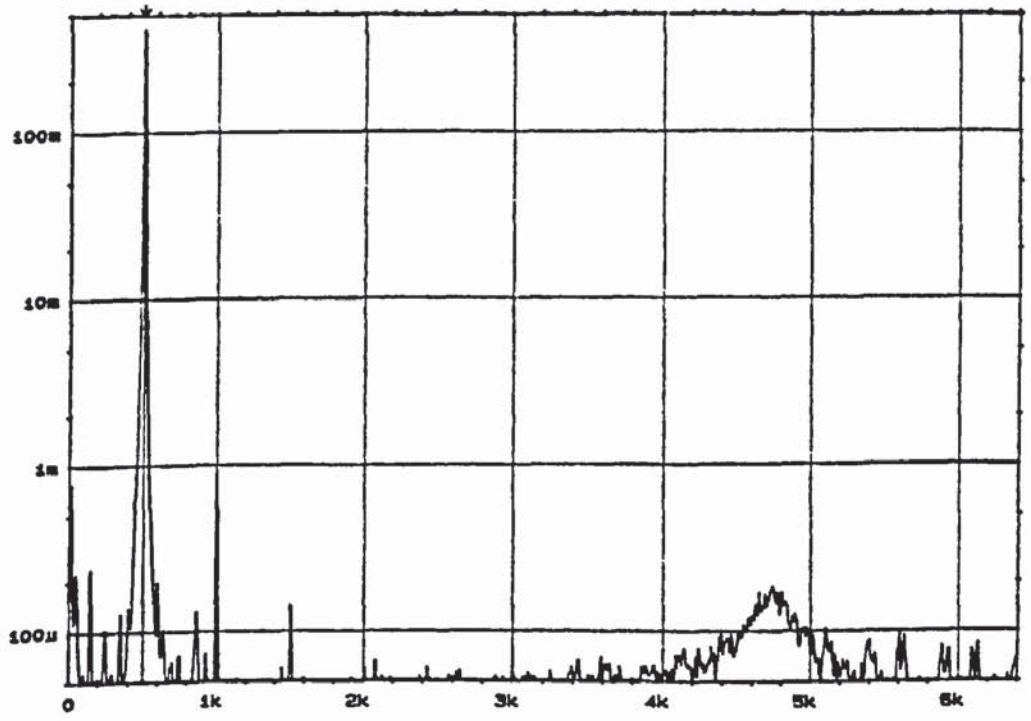

Fig. 6.5 Out–put signal from channel 2 of the tape recorder.

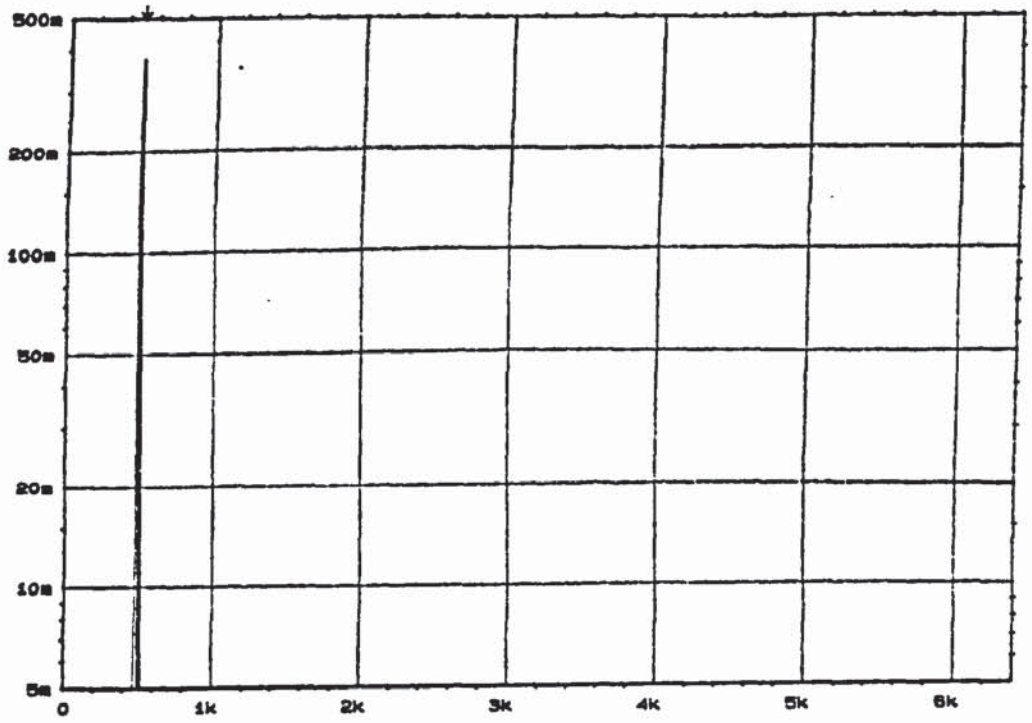

Fig. 6.6 Out–put signal from channel 3 of the tape recorder.

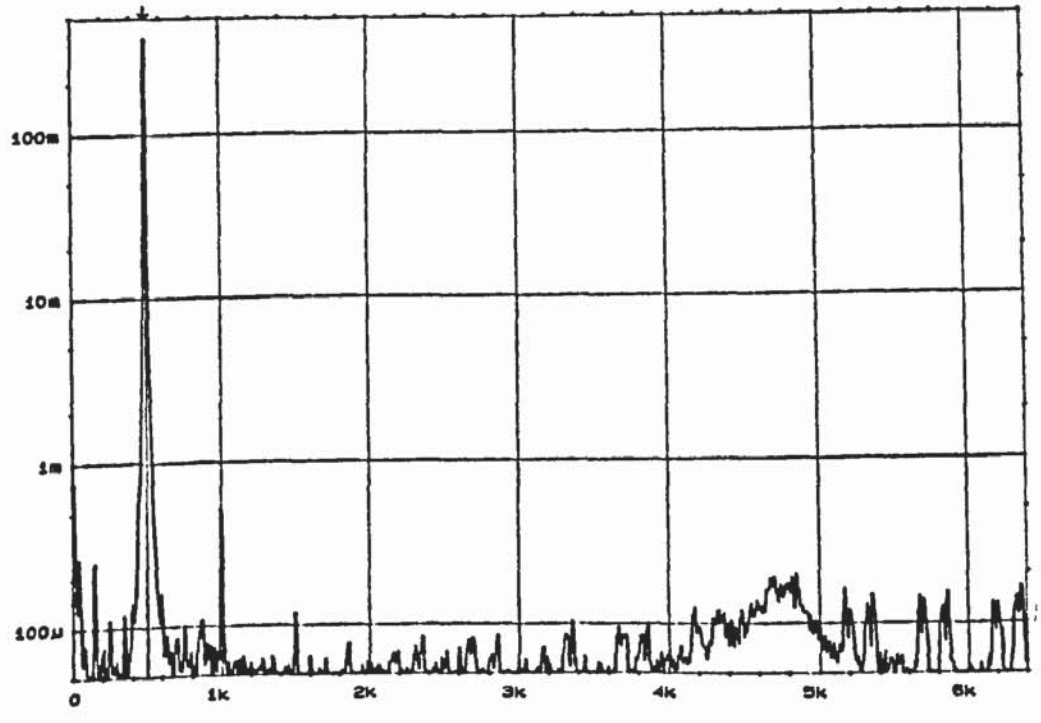

Fig. 6.7 Out–put signal from channel 4 of the tape recorder.

into a FFT–analyser and each test is repeated three times to check the repeatability of the results. The frequency analysis showed that for each channel the gain is constant and is about 1.0348 and 1.0882 for channel 1 and channel 2 respectively and that this gain is 1.011 for both channel 3 and channel 4. Moreover, the phase shift between the four channels channels is found to be at 504 Hz as follows (Fig. 6.4 to Fig. 6.7):

– Between channel 1 and channel 2, the phase shift is – 0.7 deg.
– Between channel 1 and channel 3, the phase shift is – 1.3 deg.
– Between channel 1 and channel 4, the phase shift is – 0.6 deg.

This shift, however, is frequency dependent according to the relationships:

– Between channel 1 and channel 2, the phase shift is – 0.00139 f (deg).
– Between channel 1 and channel 3, the phase shift is – 0.00258 f (deg).
– Between channel 1 and channel 4, the phase shift is – 0.00119 f (deg).

This shifts in phases may be attributed to an imperfect synchronization between the different channels.

It is concluded that the recording tape is accurate within a 8% magnitude and can reach up to 15.5 deg phase at the upper frequency of interest. This led to consider the correction in magnitude and phase of the played–back signals according to the gains and phase shifts determined above.

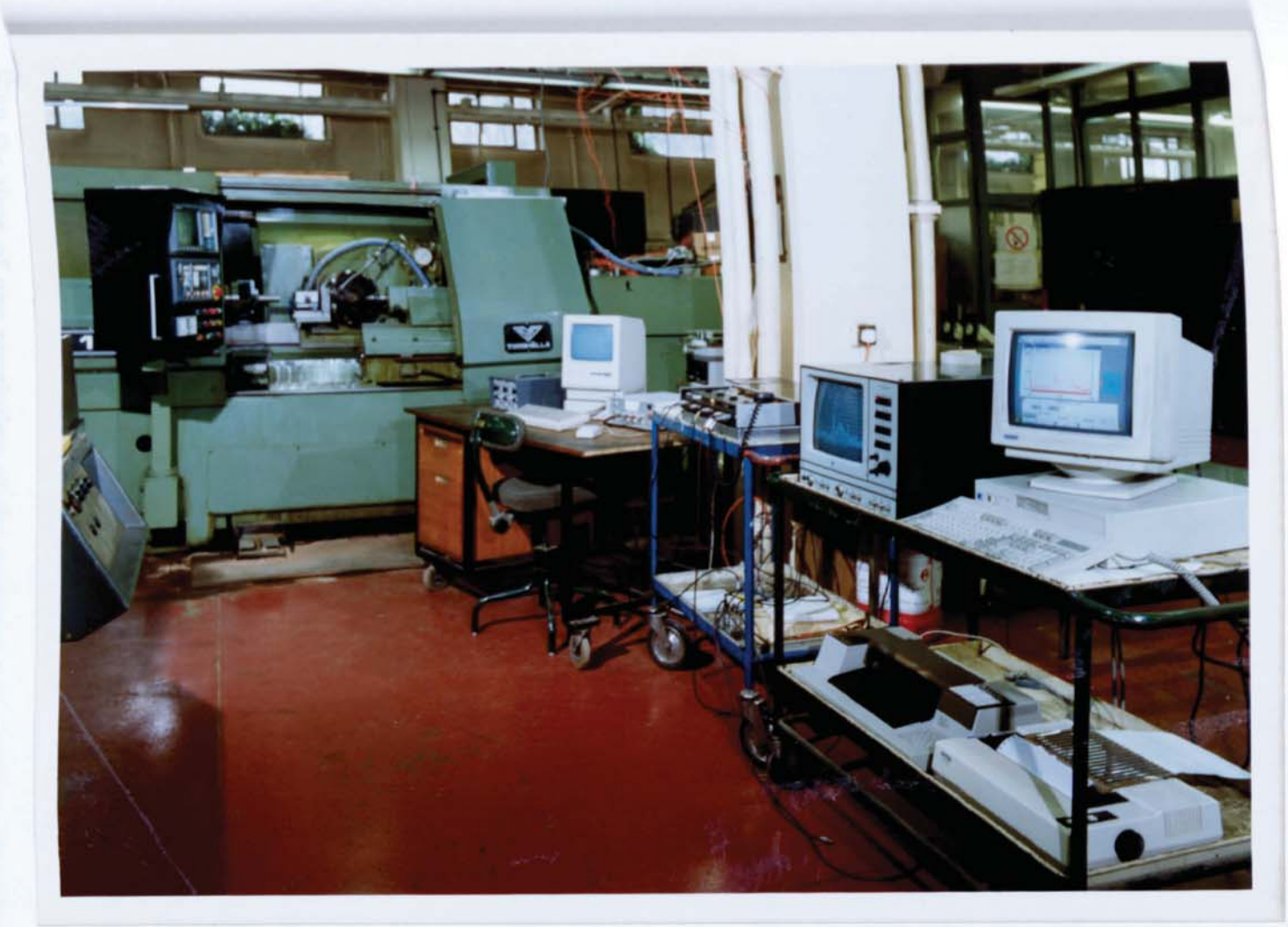

Fig. 6.8 General view of the experimental set–up.

6.5. EXPERIMENTAL PROCEDURE

The experimental procedure compromise between setting the test rig, carrying out the test, sampling the data by the FFT analyser and the Macintosh computer and recording the results on the magnetic tape.

The output signals from the dynamometer and the accelerometer are amplified through a Kistler and a B&K amplifiers respectively (Fig. 6.8). The Kistler output is thereafter fed to the FFT analyser (Channel B for the feed force), to the tape recorder and to Macintosh computer to measure steady state components of turning force. The output of the B&K amplifier of tool acceleration is fed into type recorder (Channel 1) and Channel A of the FFT analyser. The feed force is recorded on channel 2 of the tape recorder while cutting force is recorded on channel 2.

The data recorded on Macintosh by the Maclab hardware is used for steady state values of turning force components. The maclab software provides the average value of the measured forces.

The dynamic analysis of the recorded data on the tape is carried out off–line by transferring the data of the tape recorder to PC computer using a 1401–plus hardware. The software used with the 1401–plus has the ability of sampling the data at a desired rate and storing it as sweeps each of a given duration. In this analysis the sampling rate is set to 15151.51Hz and the reading from the tape lasts for ten sweeps each of 0.0337925 seconds and 512 points of measurements. The duration of a sweep is less than the time of one revolution of the workpiece for cutting speed less or equal to

7.2666 m/s which allow therefore to determine the tool acceleration within one revolution of the workpiece. This enables to determine the determine the actual oscillation of the tool and the undulation of the free surface of the workpiece.

For each of the dynamic tests, the workpiece used is a 1045 carbon steel bar with the following chemical composition:

– Carbon	0.40 – 0.45 %
– Manganese	0.70 – 0.90 %
– Phosphorous	< 0.06 %
– Silicon	0.05 – 0.35 %
– Sulphur	< 0.06 %

The workpiece is 600mm long.76.2mm of diameter. The hardness is about 225 Hv and was found to be similar for all the batch of workpieces used. All the tests are carried out on the same diameter.

Carbide tool tips similar to those used in steady state cutting tests are used in these tests. For tests with new cutting edge, tool tip is changed for every test and the measurements are taken about 5s after starting machining.

To study the tool wear examination were conducted using Scan electron microscope. It was found that tips wear only on the flank face and no important wear is observed on the rake. In some condition of low cutting speeds nose wear is important compared to flank wear. It was decided then to consider always flank wear as the average between nose wear and measured flank wear. Moreover, flank wear is considered as the average between the measured wear before and after each test.

Furthermore, SEM observations showed that the worn land on the flank of the tool is not perfectly flat and is not parallel to the mean cutting speed. The worn land forms a slightly negative and these finding are used in Chapter 4 and Chapter 8 to simulate flank wear.

Chapter 7

PREDICTION OF DYNAMIC TURNING FORCE COMPONENTS

7.1. INTRODUCTION

In this chapter, cutting analysis is based upon the experimental measures and the predicted feed and cutting forces at various cutting conditions. The present study of the dynamic turning seeks a verification of the mathematical model developed in Chapter 5 which describes the relation between dynamic forces and tool motion. Orthogonal dynamic cutting tests covering different cutting conditions are carried out when turning a bar workpiece. Simultaneously, dynamic turning force components as well as tool acceleration in feed direction are recorded on a four channels tape recorder for off–line analysis. Moreover, a comparison between predicted and experimental turning force components is carried out and in the light of the experimental results a monitoring method for tool wear is introduced but will be dealt with in the following chapter.

7.2. EXPERIMENTAL TESTS

7.2.1. Experimental conditions

The experimental work is conducted on TORSHALLA CNC–lathe as in Chapter 3 and Chapter 4 under cutting conditions as summarised in Table 7.1 when turning an SAE steel bar.

work material	S.A.E. 1045 steel
out side diameter (mm)	38.10
Cutting configuration	Orthogonal dry bar turning
Uncut chip thickness (mm)	0.10, 0.15, 0.20, 0.25, 0.30
Cutting speed (m / s)	2.31, 3.40, 5.20, 7.27, 10.22
Depth of cut (mm)	1.5
Cutting tool	Standard steel cutting Grade tungsten carbide tools: TPUN 160304 edge radius less than 0.004 mm
Flank angle (deg)	5
Rake angle (deg)	6

Table 7.1 Experimental cutting conditions for dynamic bar turning.

7.2.2. Collect of cutting data

The recorded data is transferred in time domain to a computer using a 1401–plus multi–channel hardware. During turning process, the vibrating tool leaves an undulated surface behind which is being cut by the tool the following revolution. As discussed in Chapter 5, this produced undulating surface, represented by a function x_0 which is treated as a residual chip load acting as a second input to the system model. As the dynamic ploughing model uses the tool displacement x and x_0 during the actual and the previous revolution of the workpiece respectively, there is a need to record the data by samples of one revolution duration. The software with the 1401–plus has the facility of sampling the data at high rate of frequency and saving it as a chosen number of sweeps each of a specified duration. For the actual investigation, the sampling rate was set to

15151.52 Hz so the frequency analysis can be done up to 7575.76 Hz and each sample of the data consists of ten sweeps of 0.0337925s each.

The impact between tool edge and workpiece at the beginning of machining affects the instantaneous cutting force significantly. However, under non–chattering conditions this effect will be progressively damped. Because the actual model do not consider the effect of the first impact between the tool and the workpiece, it was decided to use sweep 5 as the surface undulation function x_0 and the sweep 6 as actual acceleration of the cutting tool. The data of sweeps 5 and 6 is then transferred to a matlab software format and thereafter integrated once and twice to determine the tool velocity and displacement for the two successive workpiece revolutions. Together with tool displacement and tool velocity, cutting conditions are fed to a developed Matlab–programme to determine dynamic cutting force on tool tip using the results from Chapter 3 together with the relationships (5.21) to (5.23) and (5.30) to (5.74) of Chapter 5.

The model provides the actual dynamic force on the tool tip and therefore the calculated forces are modified by the tool poste–tool holder transfer function H_d to yield the forces out–put of the dynamometer which then are compared to measured forces. The results of experiments and predictions are presented and discussed in the following sections.

7.3. EXPERIMENTAL RESULTS

A Matlab programme is used to transform the recorded signals from time domain to frequency domain using the Welch method of power spectrum estimation together with a hanning window function where the corrections in phase are introduced as mentioned

in Chapter 6. The obtained results for tool acceleration in feed direction, feed force and transfer function are shown in Fig. 7.1 to Fig. 7.8 for the cutting conditions mentioned above.

The study of the steady state turning process (Chapter 3) showed two distinguishable cutting speed regions. At the low cutting speed region, the magnitudes of the cutting force components fluctuate following a certain pattern as the cutting speed increases. This is due to the presence of the B.U.E during machining. At the low cutting speed region, the fluctuation pattern of the measured force are actually dominated by the fluctuation pattern of the height of the B.U.E versus the cutting speed. At the high cutting speed region, B.U.E disappears and the magnitude of the turning force components decreases as the cutting speed increases owing to the effect of the temperature which softens the workpiece material flowing through the cutting zone. The obtained dynamic turning force components however show different tendencies with the cutting conditions from what was shown by the steady state forces.

7.3.1. Effect of feed and speed on tool acceleration spectra

Examining Fig. 7.1 to Fig. 7.2 it is observed that acceleration spectra exhibit a broad peak at about 5kHz. It is worth noticing that this peak is shifted towards low frequencies as the feed is increased. Moreover, for all the frequency range under investigation, the tool acceleration increases as the feed increases from 0.10 to 0.25 mm/rev for low speed as 2.28 m/s, but decreases as the feed is increased up to 0.30 mm/rev. The tool acceleration is more sensitive to the feed variations within 4 to 6kHz than what it is for lower or higher frequencies.

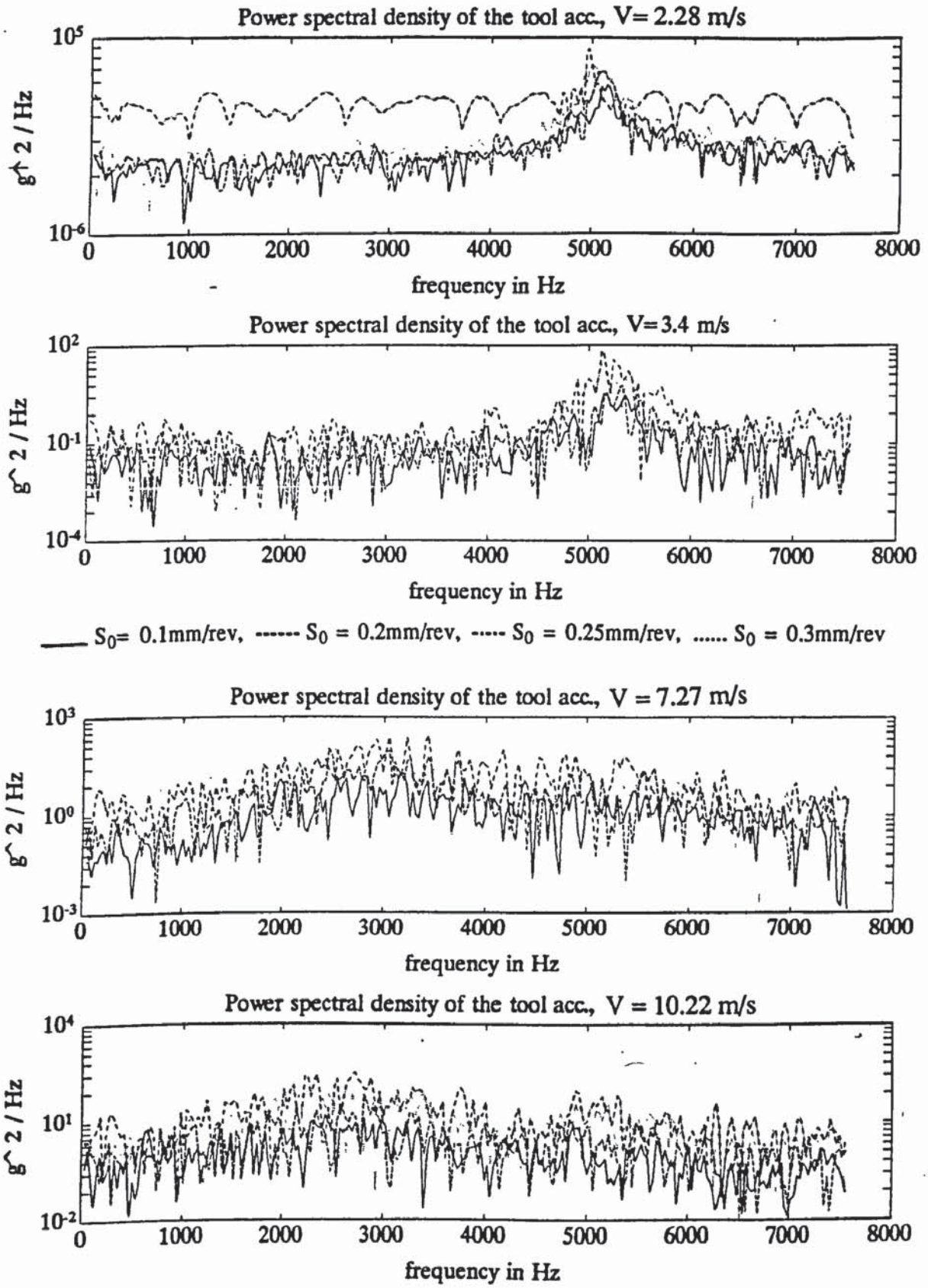

Fig. 7.1 PSD of tool acceleration in feed direction

V = 2.28, 3.40, 7.27, 10.22 m/s.

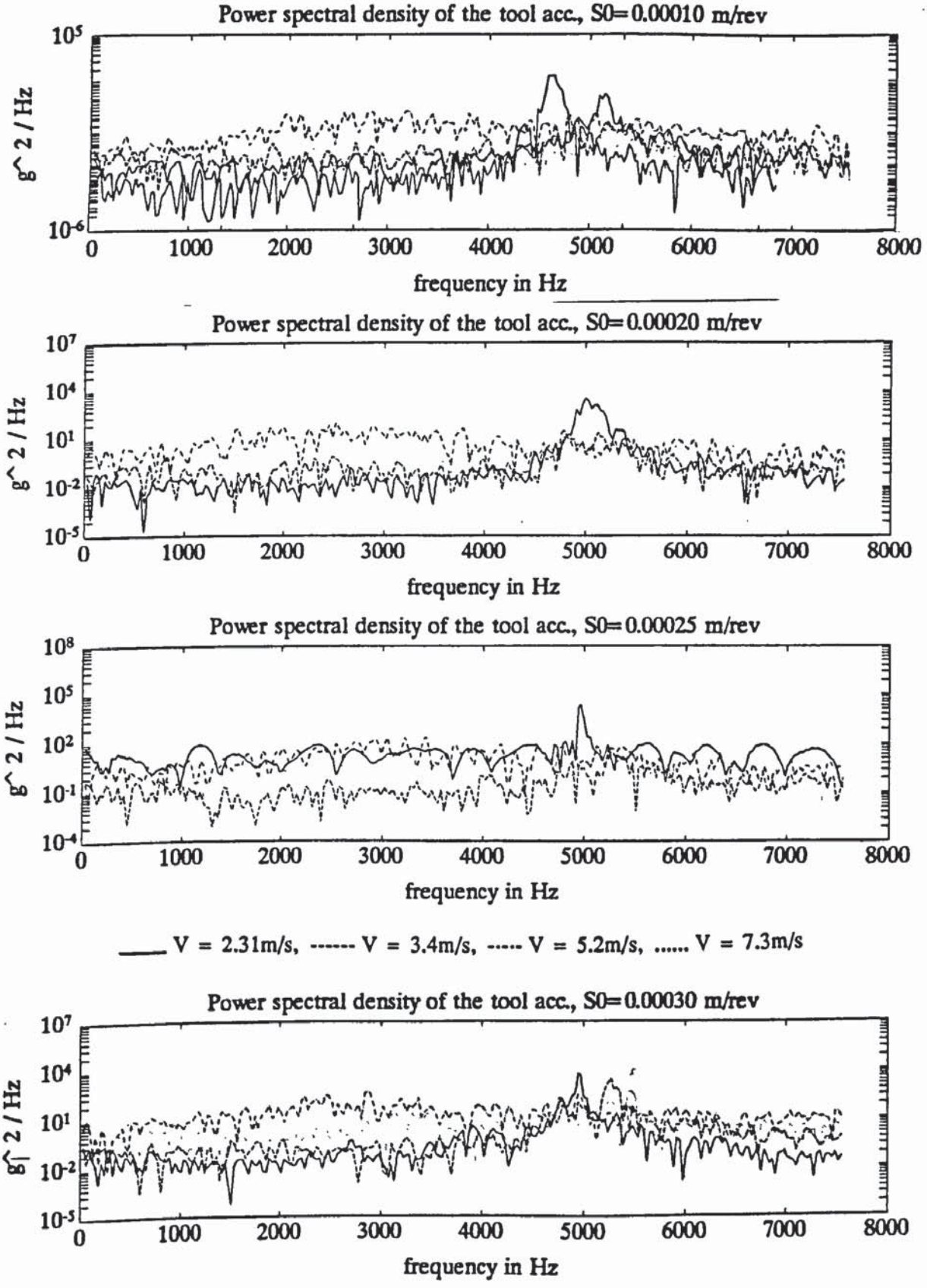

Fig. 7.2 PSD of tool acceleration in feed direction

S_0 = 0.10, 0.20 0.025, 0.30 mm/rev.

The amplitude of tool acceleration is increasing with the cutting speed more rapidly for low frequencies up to 4kHz and above 6kHz. Therefore, the peak exhibited around 5kHz tends to vanish as the cutting speed and feed are increased.

The acceleration spectra show that low frequencies are more dominating for higher cutting conditions which is more associated with the effect of the machine structure. These spectra show that the effect of the machine tool structure is more affecting the cutting process through its effect upon the tool frequency for higher cutting conditions and tends to hide the effect of the tool and tool holder system. However, for relatively lighter cutting conditions, the tool structure has more effect upon the cutting process at around the natural frequency of this system.

Regarding to the Root Mean Square (RMS) value of tool acceleration up to 7.5kHz, Fig. 7.3 shows that the RMS of acceleration increases with feed for higher speeds than 3.4 m/s whereas for low speeds (2.28 m/s) it reaches a maximum at a feed of 0.20 mm/rev after which the RMS of the tool acceleration is decreasing with the feed. It is noticed also that except for the lowest speed and the highest feed investigated, the RMS of the tool acceleration is increasing with speed and that rate of its variation with the latter decreases as the feed increases.

The singularities shown for the lowest speed of 2.28 m/s shown in Fig. 7.3 and Fig. 7.4 can be attributed to the effect of the built–up edge on the rake face of the tool. In fact, as earlier mentioned in Chapter 3, a built–up edge was shown to exist for cutting speed up to 1.57 m/s but vanishes for higher speeds.

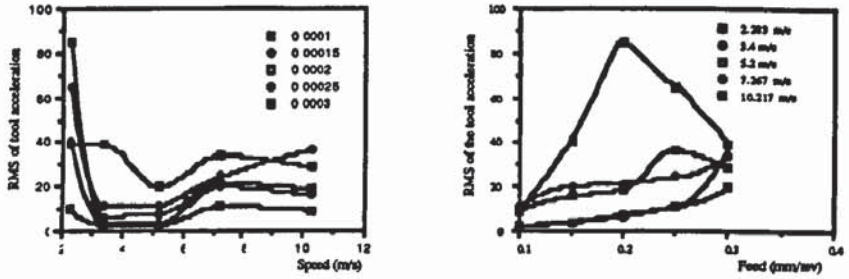

Fig. 7.3 Variation of the RMS of tool acceleration with speed and feed.

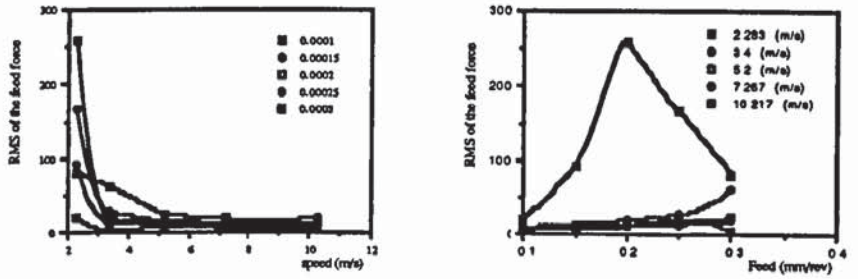

Fig. 7.4 Variation of the RMS of feed force with speed and feed.

Therefore, the range of speeds between these two values of speed can be considered as an unstable region for the existence of the built–up edge and therefore is starts to increase in size but it is rapidly torn away by the chip flowing along the rake of the tool. This existence and vanishing phenomenon lead to an internal disturbances in the cutting process responsible for higher amplitudes of the tool vibration at low speeds.

7.3.2. Effect of feed and speed on feed force spectra

Similar remarks can be drawn after analysing the feed force spectra shown in Fig. 7.5 and Fig. 7.6. Indeed, the feed force amplitude increases with feed over all the frequency range up to 7.5kHz with an important increase for frequencies lower than 3.4kHz and above 5.7kHz. A peak is exhibited around 5.2kHz, as is the case for the acceleration spectra, and whose frequency is decreasing with feed. The sensitivity of

feed force to the variations of feed rate decreases as the cutting speed increases but is nevertheless more sensitive to feed and speed changes within 3.5 to 6kHz.

As expected, the RMS value of feed force shown in Fig. 7.4 is decreasing with cutting speeds higher than 2.29 m/s and increasing with feed. Similar tendencies are observed in the force as in the tool acceleration for the same reasons as discussed above.

7.3.3. Effect of cutting conditions upon transfer function of cutting process

The transfer spectra for cutting process are shown in Fig. 7.7 to Fig. 7.8 when the system considered is cutting process, tool post and tool holder and where the input is tool acceleration and the output is the measured feed force.

For low cutting speeds (Fig. 7.7) the transfer function varies slightly with feed and becomes independent of feed rate as cutting speed increases above 3.40m/s. The variation of system transfer function with feed at low speed show that the system considered is a non–linear system regarding to the feed. An increase of the transfer function with feed at low speeds means that small variations in tool vibration lead to an important force increment increasing with feed rate. It can be concluded that at low speeds, the cutting process is responding in non–linear fashion to tool vibration and that this non–linearity phenomenon is increasing with feed.

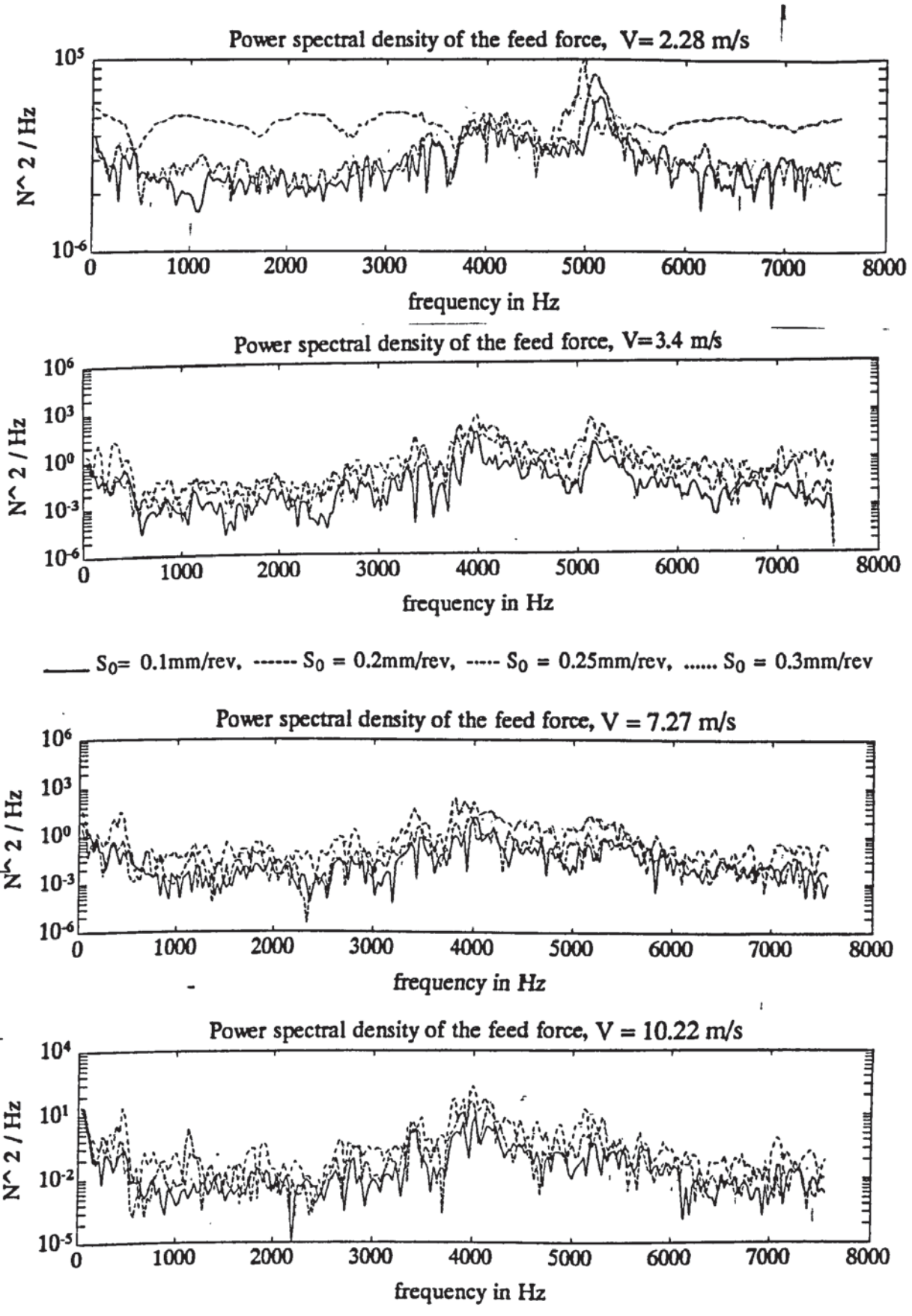

Fig. 7.5 PSD of feed force

V = 2.28, 3.4, 7.27, 10.22 m/s.

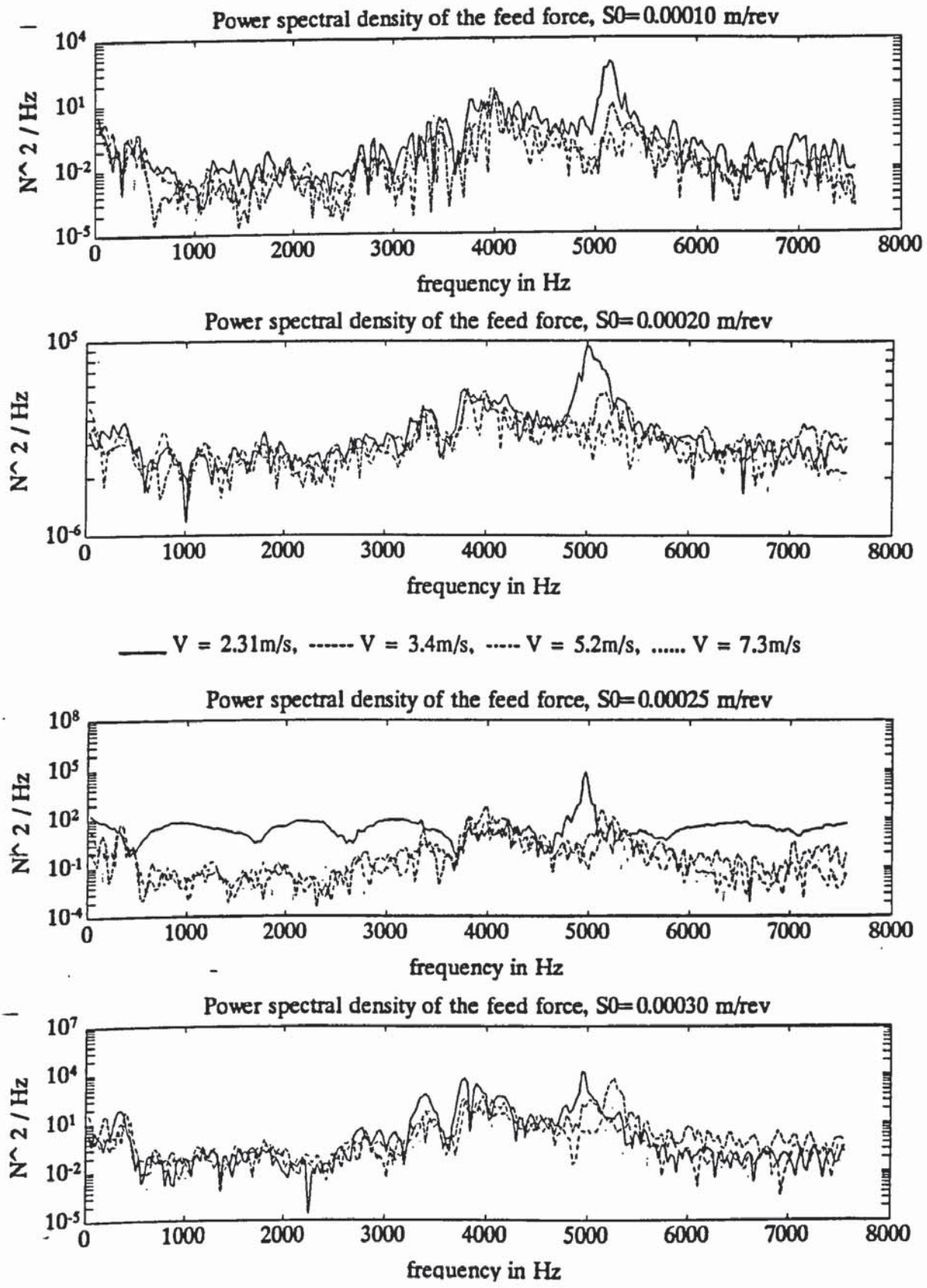

Fig. 7.6 PSD of feed force

S_0 = 0.10, 0.20, 0.25, 0.3 mm/rev.

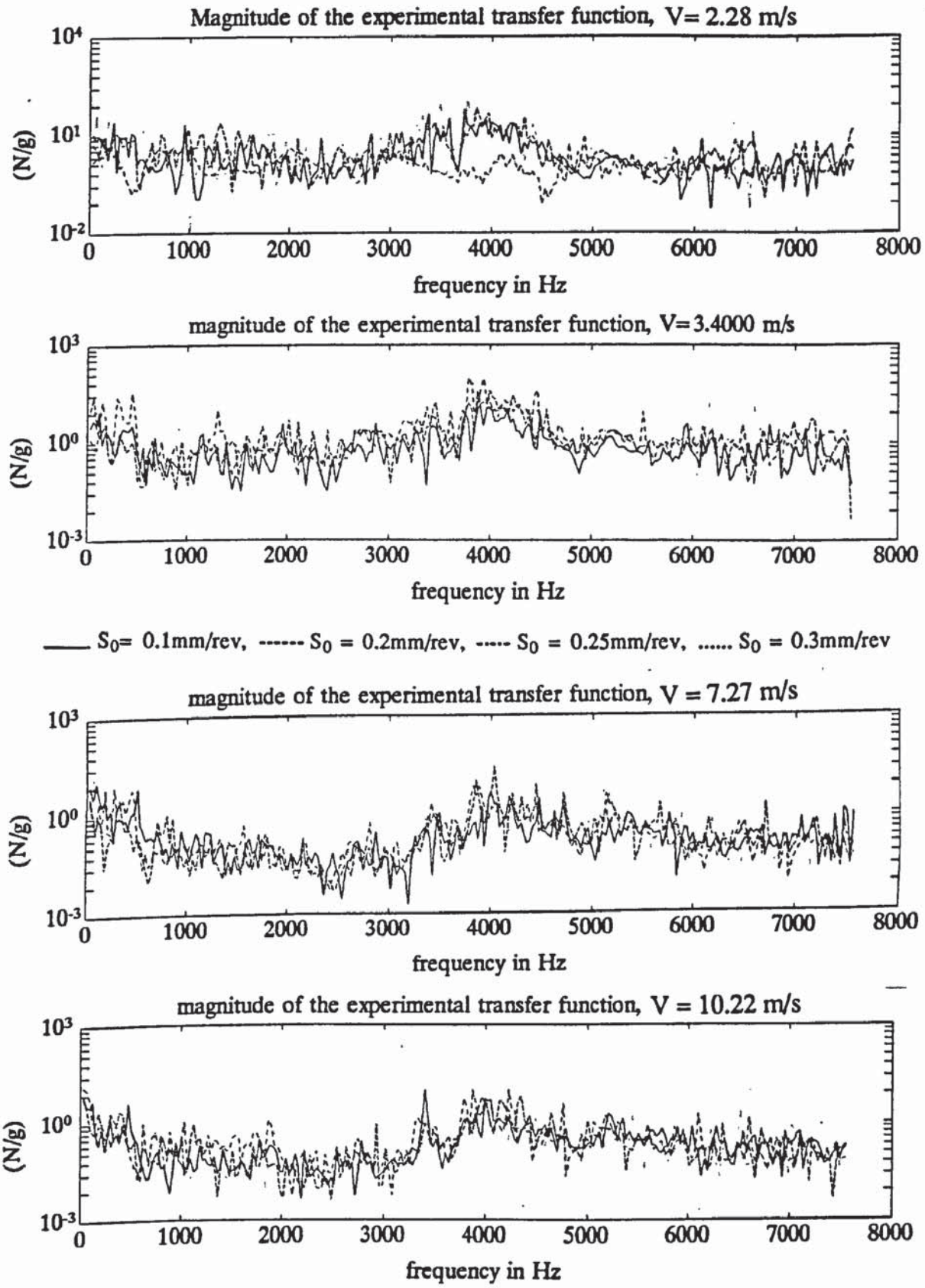

Fig. 7.7 Transfer function of cutting process

V = 2.28, 3.4, 7.27, 10.22 m/s.

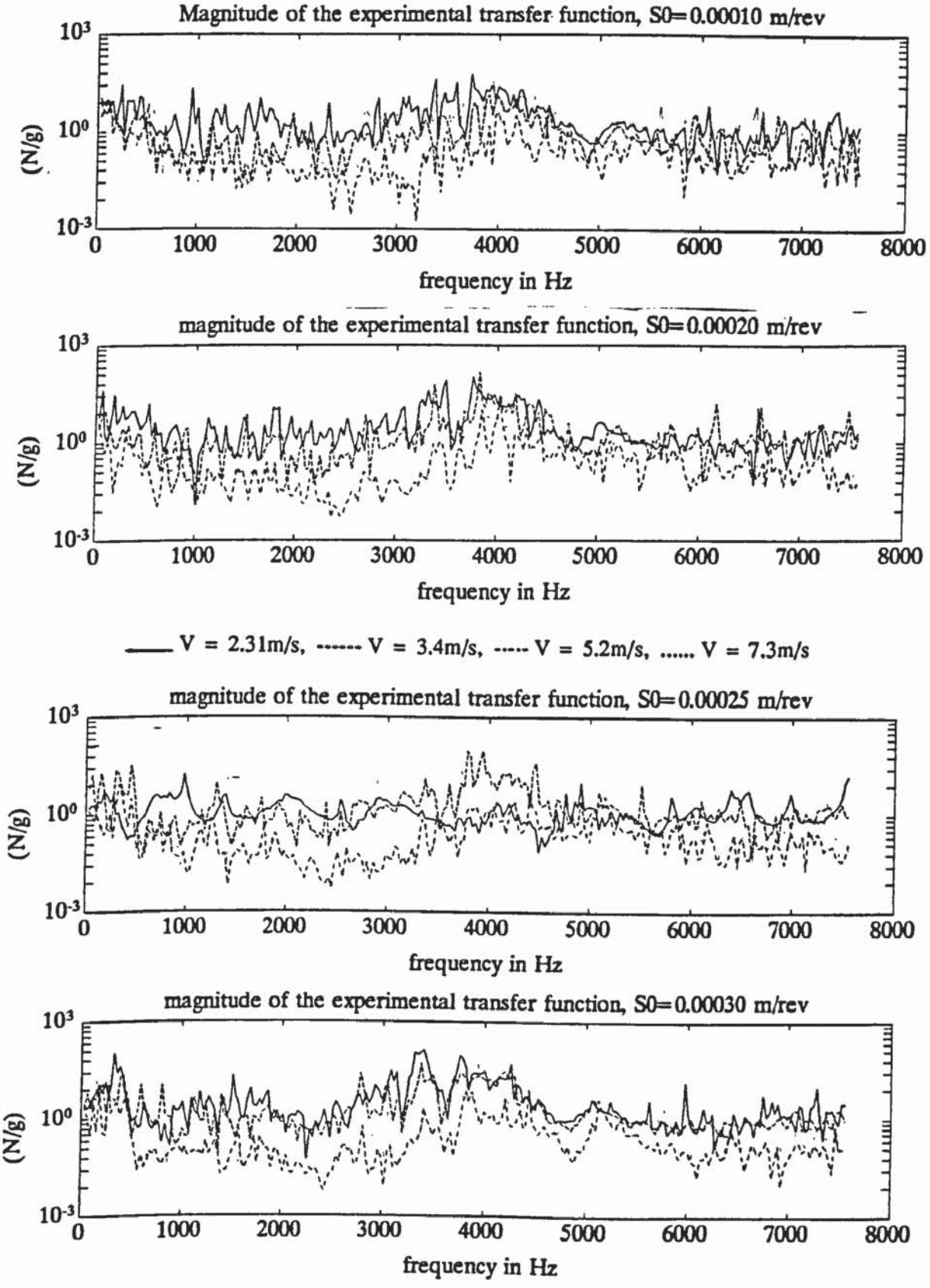

Fig. 7.8 Transfer function of cutting process

S_0 = 0.10, 0.20, 0.25, 0.30 mm/rev.

Considering Fig. 7.8, the spectra show that the transfer function is decreasing with the cutting speed up to 7.27m/s for all the feeds investigated and over all the range of frequency considered. Above 7.27m/s the magnitude of the transfer function is decreasing with speed. An increase in the cutting speed up to 7.27m/s lead to a decrease of the sensitivity of the feed force to vibration, however, above this speed the cutting process is increasing of sensitivity of the feed force to the tool vibration. These observations show that there is a tendency towards better cutting conditions in medium region of cutting speeds as predicted theoretically by the analysis of the incremental parameters in Chapter 5. For higher speeds, small perturbations of the tool in the feed direction will results in a large changes in the feed force. This will therefore lead to chattering conditions.

The transfer function spectra (Fig. 7.7 to Fig. 7.8) exhibit a peak around the natural frequency of the tool holder–tool post at about 4kHz. It is also noticed that there is some dominant peaks below 500Hz corresponding to the influence of the machine structure. However, the dominant region is found to be between 3 to 5kHz and that is for all the cutting conditions under investigation.

7.4. PREDICTION OF DYNAMIC TURNING FORCE COMPONENTS

The significance to predict the instantaneous dynamic turning force is to clearly present the time history of the dynamic machining force during turning operations. This information would be most valuable for diagnosing the characteristics of turning tool vibration because the instantaneous dynamic feed force is the major driving force to excite the cutting tool during machining. Furthermore, the instantaneous dynamic feed

force may be one of the best candidates being the process variable for on–line manipulation in adaptive control turning systems.

Fig. 7.9 to Fig. 7.12 represent a some of predicted and the measured dynamic turning force components for the cutting conditions summarised in Table 7.1. The random changes of magnitude of turning force components can be considered to represent the random fashion in which the cutting edge meets hard or soft spots in the workpiece material. The maximum variation is approximately 20% of the nominal cutting force. Upon careful examination of the mean level a variation about the mean level may be observed. The shift of the mean level represents the shift from static equilibrium of the tool to the dynamic equilibrium owing to the presence of the nominal cutting force during turning. The dynamic variation of cutting force is due to the presence of the residual load through the regenerative feedback path. Examination of instantaneous cutting force generated during machining reveals that dynamic variation of the instantaneous cutting force is mainly contributed to by both cutting mechanism and interaction between cutting mechanism and structural dynamics of the machine tool. This confirms the conclusions drawn by Tobias (1965) and Tlusty (1978) that the cutting process and the machine tool structure are the two basic linked elements of the closed chatter loop (Fig. 2.3).

It can be seen that the model provides a good prediction of the form of the force components spectra for the cutting conditions under investigation. Regarding to the magnitude of the dynamic oscillation of the machining force components, the predicted components correspond fairly well to the experiments (Fig. 7.9 to Fig. 7.12).

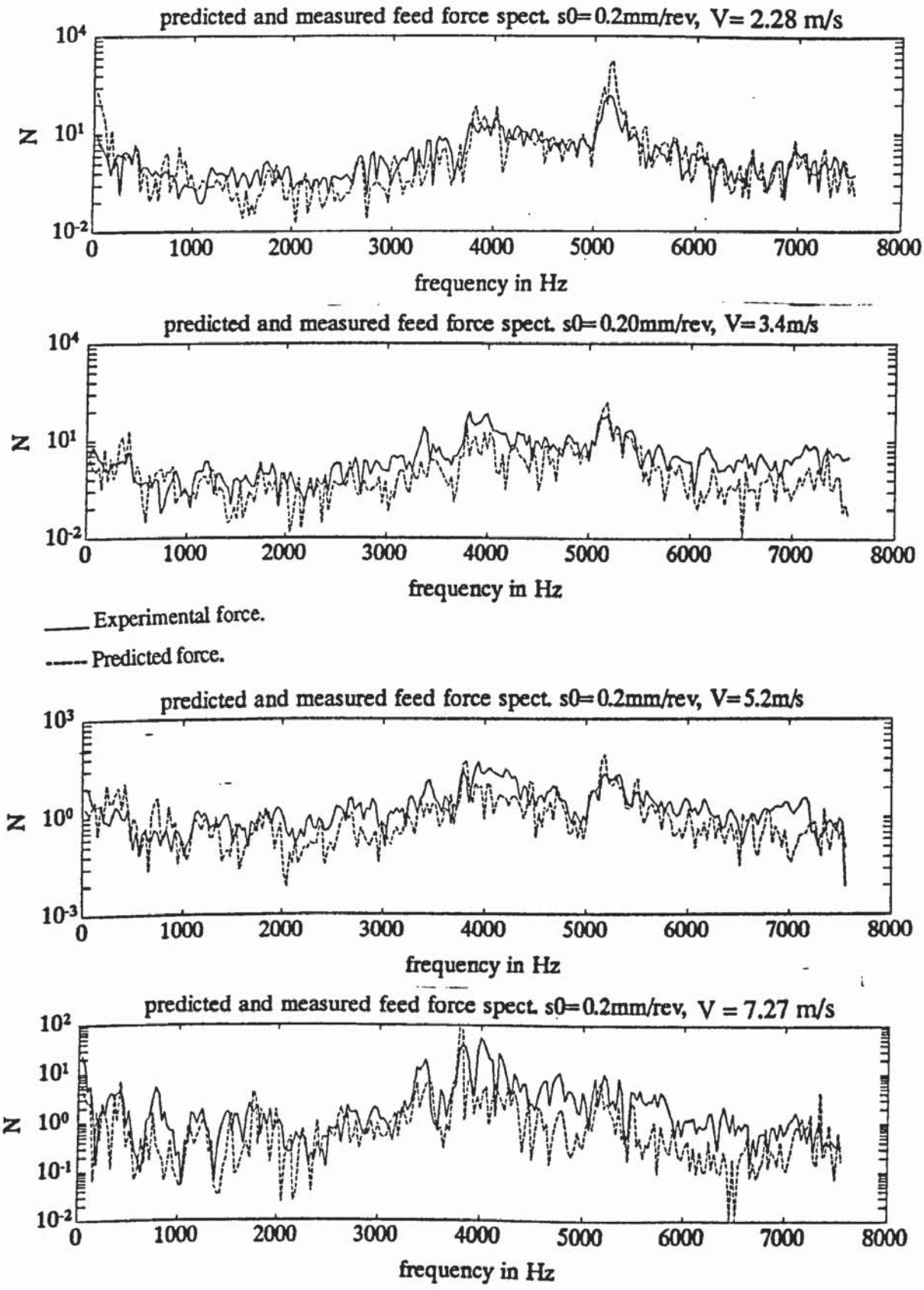

Fig. 7.9 Predicted and experimental feed force, S_0 = 0.20 mm/rev

V = 2.28, 3.40, 5.20, 7.27 m/s.

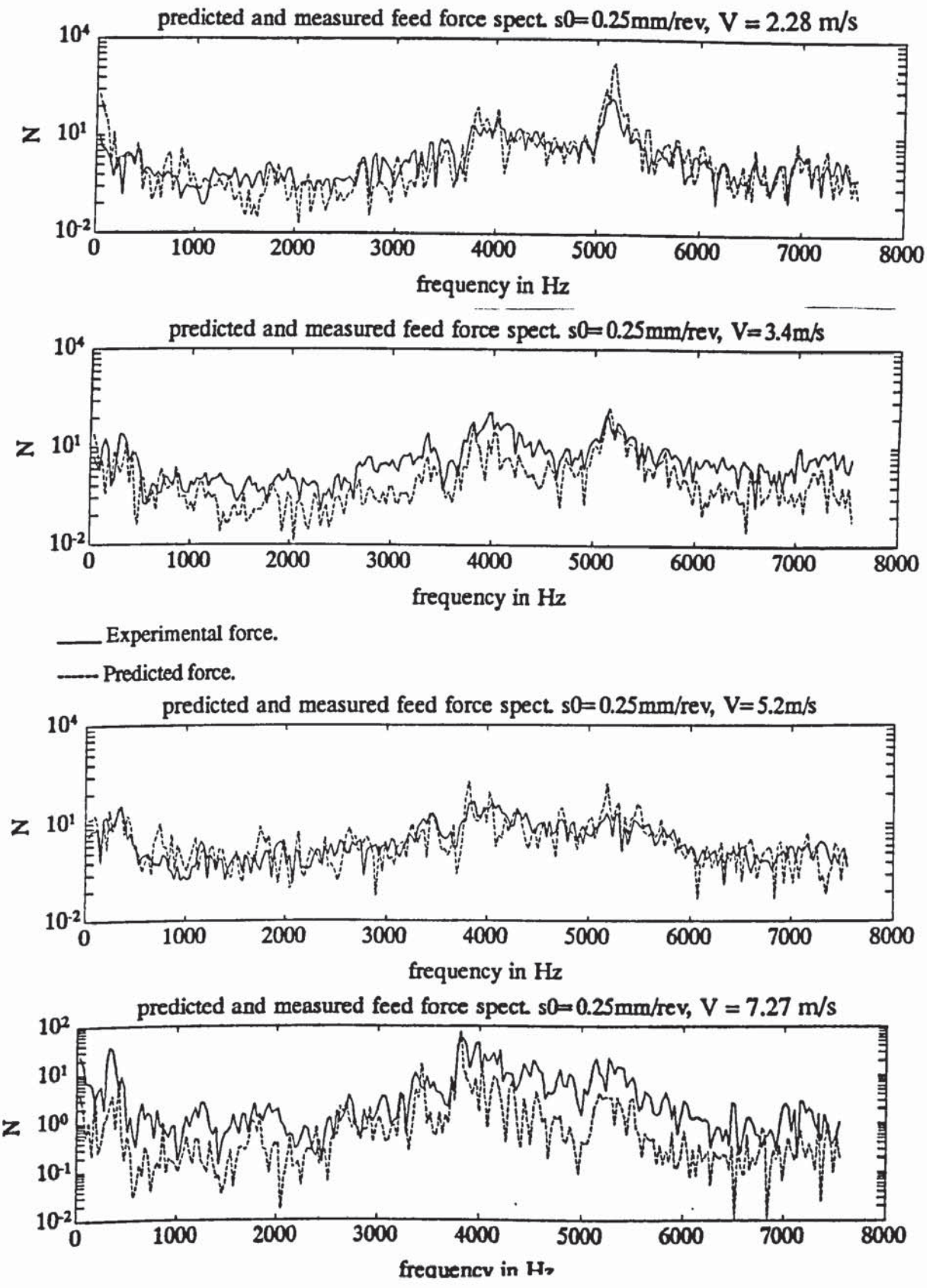

Fig. 7.10 Predicted and experimental feed force, $S_0 = 0.25$ mm/rev

V = 2.28, 3.40, 5.20, 7.27 m/s.

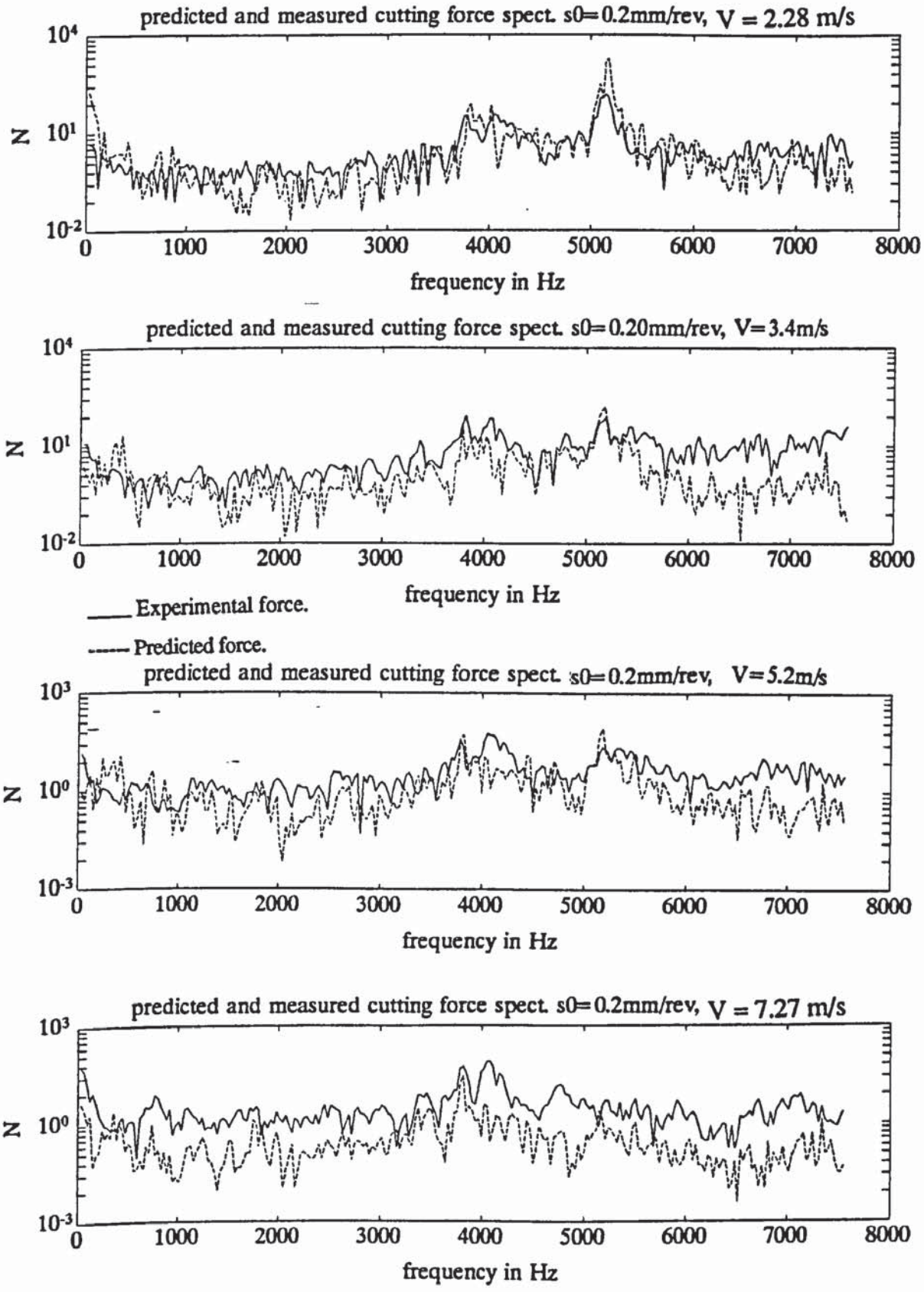

Fig. 7.11 Predicted and experimental cutting force, S_0 = 0.20 mm/rev

V = 2.28, 3.40, 5.20, 7.27 m/s.

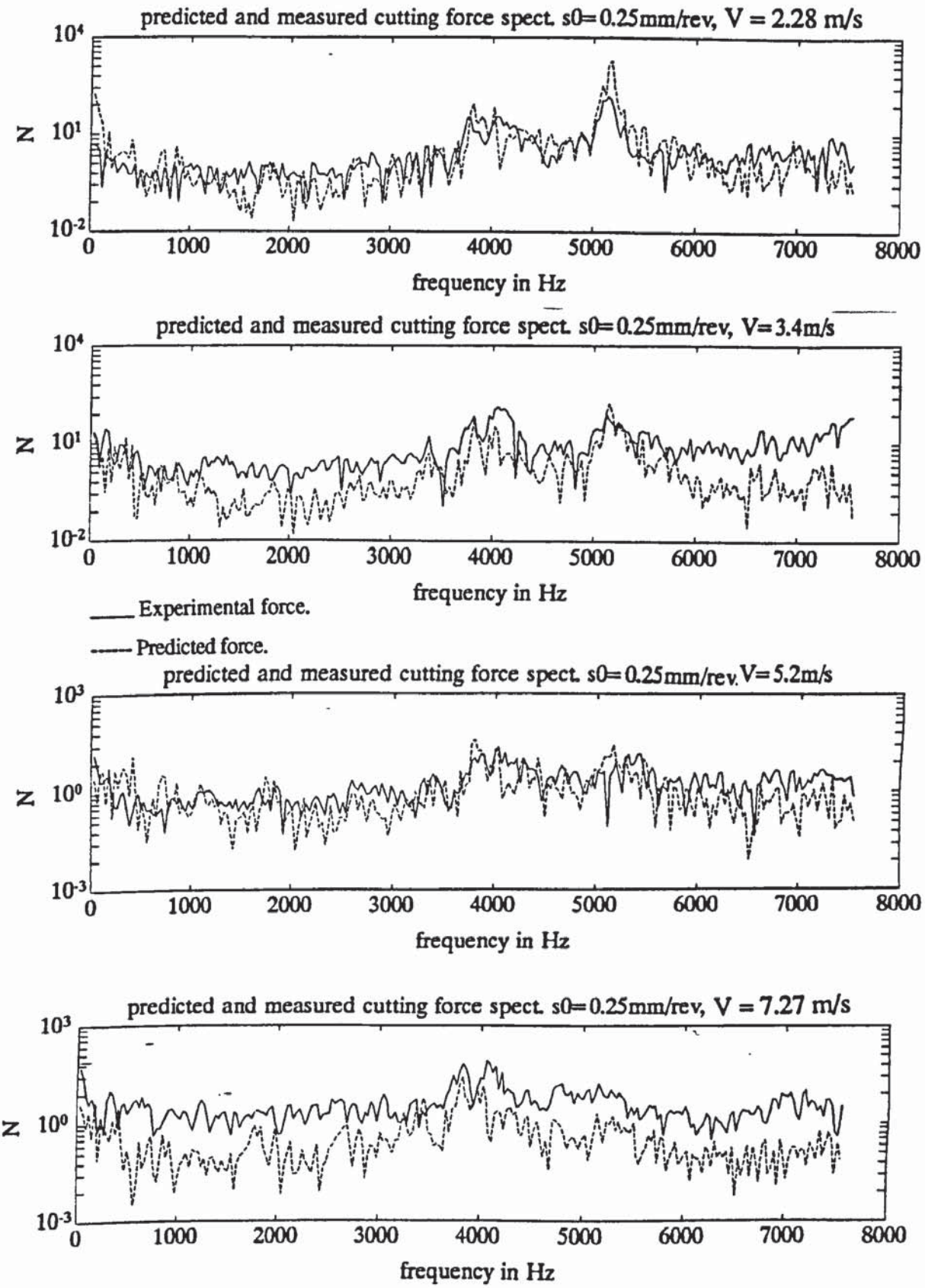

Fig. 7.12 Predicted and experimental cutting force, S_0 = 0.25 mm/rev

V = 2.28, 3.40, 5.20, 7.27 m/s.

Discrepancies are mostly observed at high frequencies but for frequencies up to 5.2kHz, the model predict well the dynamic components of the cutting forces. From the theoretical analysis of the cutting process through analysis of the variations of the dynamic incremental coefficients, it was shown that there is different tendencies in changes of these coefficients according to the cutting conditions. It was shown for instance that the amplitude of response of the shear angle to variations in feed rate increases with speed for medium range, up to 5.20m/s and it decreases when speed is above 7.27m/s. Similar variations were observed for the other parameters such as flank friction incremental coefficient, rake forces ratio and tool penetration. Moreover, it was discussed that all these parameters are together influencing the cutting process and lead to better stability and low initial amplitudes of oscillation in medium range of cutting speeds. This conclusion is put in evidence when predicting the dynamic turning force components where results are much better up to 5.20m/s. Therefore, the discrepancies observed in predicting the cutting force components for higher speed particularly around 5kHz can be attributed to the perturbation affecting the cutting process resulting in higher amplitudes of oscillations. These perturbations can be initiated and/or supplied by the chattering conditions.

At low cutting speeds, it is well known that a built–up edge is increasing in size and after reaching a maximum of size this part of workpiece metal is torn away by the flowing chip and a new edge starts to build–up on the rake of the cutting tool. Moreover, it is also well known that the machining force components are decreasing with the size of the B.U.E. The instantaneous variation of the size of the B.U.E will lead therefore to important perturbations in the dynamic turning force through its effect upon the instantaneous rake angle. In steady state conditions however, this is not of great effect since the measurements and the predictions are only dealing with the average values of the different cutting parameters and therefore a small variations will

affect the results by may be less than 10% which is still within the range of the acceptable predictions. These perturbations explain the noticeable decrease in the amplitude of dynamic force oscillations as the speed is increased from 2.28 to 3.40m/s.

It has been long known that one way to avoid chatter is to use low cutting speeds. The called "process damping" was introduced by Tobias (1965) where it was shown that there is loss of the damping as the cutting speed increases. When the cutting tool is vibrating during machining, the effective flank angle varies throughout the vibratory cycle as discussed in Chapter 5. It is minimum in the middle of the downward slope and this causes an increase of the feed force as can be derived from the relationship (5.41) established earlier in Chapter 5. The effective flank angle is maximum in the middle of the upward motion (Tobias, 1965). Obviously, the incremental force along the flank of the cutting tool is out of phase (Chapter 5) with the displacement and therefore it acts as a damping force whose amplitude is increasing with the slope δ of tool vibratory displacement (5.41). This slope increases with the decrease of the wave-length defined as a ratio of the cutting speed to the frequency of the tool vibration.

For chatter vibration, the frequency is closed to the natural frequency of the workpiece–tool–machine structure system. For shorter wave-lengths (lower speeds) the process damping becomes more significant, however, for long wave-lengths (higher speeds) the process damping gradually loses its influence. Therefore, as the cutting speed becomes more important, the cutting process enters chattering conditions where the condition of small vibration is no longer valid. Therefore the established relationships in Chapter 5 cannot be considered as representing the cutting process leading to poor prediction of the dynamic force components.

For speeds ranging from 2.28m/s to 5.20m/s and for feeds from 0.10 to 0.30 mm/rev, the model provides a good prediction of the dynamic turning force components but, nevertheless, however the difference between the prediction and the experiments for low and very high cutting speeds, the model still provides a good prediction of the general shape of variation of the force components under these conditions. This is of great importance for tool wear monitoring where more interest is given to the relative changes in the cutting parameters and not to their actual values.

Analysing Fig. 7.9 to Fig. 7.12 it can be observed that dynamic variations in the measured as well as predicted feed and vertical turning force components are almost similar after which the idea of considering the ratio between the dynamic parts has emerged. Similarly to the force component ratio C_s, the ratio of the dynamic parts of the cutting force components can be considered as representing a dynamic angle representing the phase between the vertical and the feed dynamic forces. It can therefore refer to the lead angle between the dynamic force components.

By this definition, the tool lead angle is formed by the tool cutting edge and the direction of the feed which becomes variable in cases where the cutting edge itself is no longer a straight line but an arc. This is due to the fact that the position of the cutting edge at every point along the arc varies. Under the assumptions of small amplitudes of vibration and single degree of freedom cutting tool system the tool edge must remain straight and therefore this ratio is maintained constant.

Examining the experimental results and the model predictions an important observation can be found that the obtained ratios are almost independent of feed and cutting speed. This ratio is slightly affected by the cutting conditions at low frequencies and is almost constant for frequencies between 2.5 and 5.5kHz. This variation at low frequencies

may be physically explained by the following fact. Beside the shear process occurring in the cutting zone, contacting deformation of the workpiece material and the tool also occurs in the contacting area between the tool and the workpiece as a result of the ploughing process. Because the hardness of the workpiece material is relatively low with respect to the hardness of the tool material, the occurrence of the contacting deformation is mostly on the workpiece side (Chapter 3 and Chapter 5). The turning force components affected by the contacting deformation is the feed force, the magnitude of which can be increased because of the material work hardening during the ploughing process. The degree of of the ploughing process affects more the turning force components at low frequencies as the deformation can be considered as a relatively slow process. The study of variations of this ratio with respect to the cutting conditions is reported in Chapter 8 where the effect of the flank wear is also introduced. The above conclusions render the so–defined lead ratio between the dynamic parts of the turning force component an important candidate for tool wear monitoring.

7.5. CONCLUSION

From the above results and discussions it can be concluded that the steady state relationships governing the cutting forces can be utilised for dynamic turning process with a modified process configuration as developed in Chapter 3 and Chapter 5. The prediction of the dynamic turning force components relies entirely on the steady state cutting data and considers only the tool vibration in the feed direction as input to the cutting process.

The major contribution of the present model is that it predicts the cutting forces by only measuring the tool vibration. Usually it is difficult and expensive in practical conditions

to design a machine tool with force dynamometer because it is not convenient particularly for turning machines and also because it reduces the stiffness of the machine structure and thus the range of efficiency of the machine. Generally speaking, the efficiency of a machine tool is usually limited by the power or the chatter. The effect of chatter is directly related to the quality of the surface finish of the machined surfaces while the limit in power is related to the rate of the material removal. Both are affected by the introduction of a deformable or flexible parts between the tool and the machine saddle. The former is introduced by decreasing the the machine stiffness and the latter by the limit of the maximum load upon the dynamometer. Beside, a dynamometer cannot be used for the case of machine with turret revolver as the CNC controller can change the cutting tool as required by the manipulator through the machining programme. This model has therefore the advantage of predicting the cutting force components when the tool vibration is known which is easier and more convenient for measurements.

As far as the prediction of the model is concerned, this is in very good agreement with the experimental results of this investigation for medium range of the cutting conditions. The discrepancies observed for high speeds and low frequencies are associated with the introduction of chatter while the large existence of higher oscillations of the dynamic force are attributed to the simultaneous existence and disappearance of the built–up edge.

Experimental observation, which are also predicted by the model showed that, in contrast to the steady state force components, the ratio between the dynamic turning force components is almost independent of the cutting conditions despite small variations for some cases at low frequencies which can be related to the effect of the work hardening and the ploughing deformations. However, for higher frequencies

than 2kHz, this ratio is maintained constant and will be dealt with in more details in the following chapter.

Chapter 8

MODELLING OSCILLATORY TURNING WITH WORN TOOLS AND FLANK WEAR MONITORING

8.1. INTRODUCTION

A model for dynamic turning was developed in Chapter 5 and experimental results in Chapter 7 showed that this ploughing model provides a good prediction of the dynamic turning force components. Furthermore, experimental findings which are also predicted theoretically, were made towards tool wear predictions. In–process tool wear monitoring has a great significance to giving full play of machine tool, preventing workpiece and tool from damage and increasing economical benefit. It is also one of the essential prerequisites for cutting process optimisation and adaptive control; in CNC machines and flexible manufacturing systems. Therefore, it is aimed in this chapter to develop a model that describes the dynamic turning with worn cutting tools. This model is a direct extension of the dynamic ploughing model developed in Chapter 5 and considers the flank wear as the most important type of wear affecting the tool life and the quality of the turned surfaces as in Chapter 4. Experiments with different tool flank wear levels are carried out to validate the applicability of the present model. Furthermore, root mean square value and frequency composition of the vibration and force signals and the changes in their pattern during tool wearing is experimentally and theoretically investigated, then criteria for in–process tool wear monitoring is proposed.

8.2. MODEL FOR DYNAMIC TURNING WITH WORN TOOL

As discussed in Chapter 5, different factors such as the existence of soft or hard particles in the work material and the machine structure are responsible for the tool oscillation during machining. When the tool wear is introduced the metal cutting configuration becomes more complicated and demanding for close analysis. As the flank wear is usually modelled by a flat surface, corresponding to zero degrees of flank angle, the trace of the work surface will be geometrically the same as the geometry of the cutting edge (*Fig. 5.3*).

Because the tool is moving upwards or downwards in the work material in the direction of feed, and because the contact between the tool and the workpiece is along the worn flank of the tool, an increase in the resisting force to the tool penetration should be observed as the flank wear increases. This results from the fact that the smaller the flank angle the larger the surface of contact between the tool and the work material. It was observed by Marui *et al.* (1983a, 1983b) that the smaller the rake angle the larger the rate of increase of the chatter vibration amplitude with the depth of cut and that a negative damping is introduced by the resistive force which is then increasing with wear.

At the lowest point of the tool displacement (Fig. 8.1) the contact of the tool and the workpiece will leave a flat B–C on the machined surface. The workpiece surface generated therefore by a worn tool is schematically represented by Fig. 8.1. It is easy to understand that as the tool wears and/or the cutting speed increases the length of the flat part increases. Moreover, at constant speed, the larger the tool wear the larger the time for the tool to finish a vibration cycle and henceforth larger wear decreases the

frequency of the tool vibration. The decrease of the frequency and the increase of the amplitude of the tool vibration lead to a large decrease in the quality of the turned surface.

It is assumed that the experimental sampling rate during the experiments is fast enough to consider that the effect of tool wear on tool vibration amplitude and frequency is negligible and the hypothesis of 5.4.2. remains valid. The boundary limit C between the tool and the deformed material is shown in Fig. 8.1 and Fig. 8.2. The separating point D can be within the worn area (Fig. 8.2) or along the flank face of the cutting tool (Fig. 8.1).

The condition of having D along the flank and not between B and C can be determined, by (4.4) and (4.5), as:

$$\dot{x} \leq \frac{\zeta V}{z_B + VB} \qquad (8.1)$$

Using similar considerations as in Chapter 4 and Chapter 5, the instantaneous turning force components can be expressed as:

$$F_{xi} = \frac{w\, k_i\, S_i\, C_{si}}{\sin(\phi_i)\,(\cos(\phi_i) - C_{si}\sin(\phi_i))}$$

$$+ \frac{1}{2} w\, p_s \left\{ 2\, z_B (\zeta - R) + z_B \sqrt{R^2 - z_B^2} + R^2 \arcsin\left(\frac{z_B}{R}\right) \right\}$$

$$+ w\, p_s \left\{ \zeta\, VB + \zeta\,(z_D - z_B) - \frac{1}{2}(z_D - z_C)^2 \tan(\gamma) \right\} \qquad (8.2)$$

$$F_{zi} = \frac{w\, k_i\, S_i}{\sin(\phi_i)\,(\cos(\phi_i) - C_{si}\sin(\phi_i))}$$

$$- w\, p_s \frac{\dot{x}}{V} \frac{R\,(1+\tan^2(\tau))}{\tan^2(\tau)} \left\{ z_B + \frac{R - z_B \tan(\tau)}{\tan(\tau)} \log\left[1 - \frac{z_B}{R}\tan(\tau)\right] \right\}$$

$$+ w\, p_s \frac{R^2(\tan^4(\tau) - 1)}{\tan^3(\tau)\sqrt{\tan^2(\tau) - 1}} \log\left[\frac{1 - \frac{z_B}{R}\tan(\tau)}{1 - \tan(\tau) + \sqrt{\tan^2(\tau) - 1}\sqrt{1 - \left(\frac{z_B}{R}\right)^2}} \right]$$

$$- \frac{w\, p_s}{\tan(\tau)} \left\{ \frac{\dot{x}}{V} \frac{z_B^2}{2} - R^2 \left(\frac{3}{2} - \frac{\tan^2(\tau) - 1}{\tan^2(\tau)} \right) \arcsin\left(\frac{z_B}{R}\right) \right\}$$

$$+ w\, p_s (\zeta - R) \frac{R\,(1+\tan^2(\tau))}{\tan^2(\tau)} \log\left| 1 - \frac{z_B}{R}\tan(\tau) \right|$$

$$+ w\, p_s \left\{ \zeta\, VB \tan(\tau) + (z_D - z_C) \left(\zeta - \frac{1}{2}(z_D - z_C)\tan(\gamma) \right) \tan(\tau - \gamma) \right\} \qquad (8.3)$$

Where z_B, z_C and z_D are given by (3.13), (4.4) and (4.5) respectively.

In the case of large velocity of the tool vibration where conditions (8.1) is not satisfied, the separation point D is between B and C (Fig. 8.2). Therefore, the contact between the workpiece and the active flank of the tool is not along all the worn area but rather limited to a part BD as shown in Fig. 8.2. and the coordinate z_D of point D is given by:

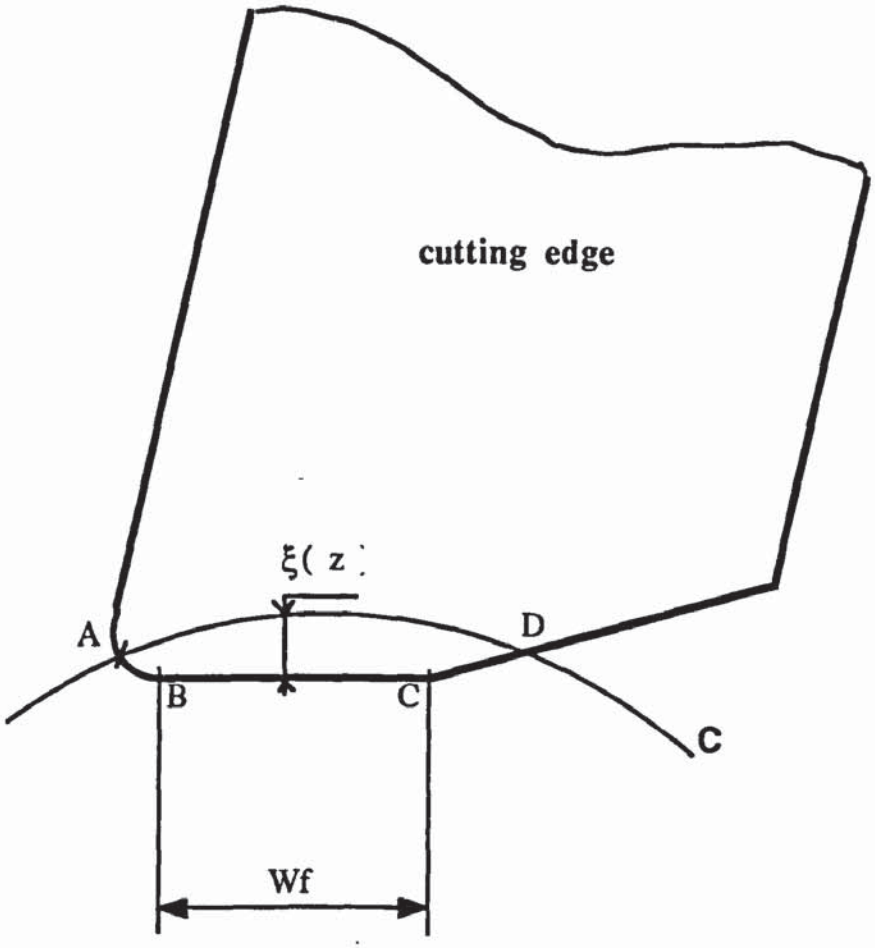

Fig. 8.1 Tool penetration during low velocity of tool vibration.

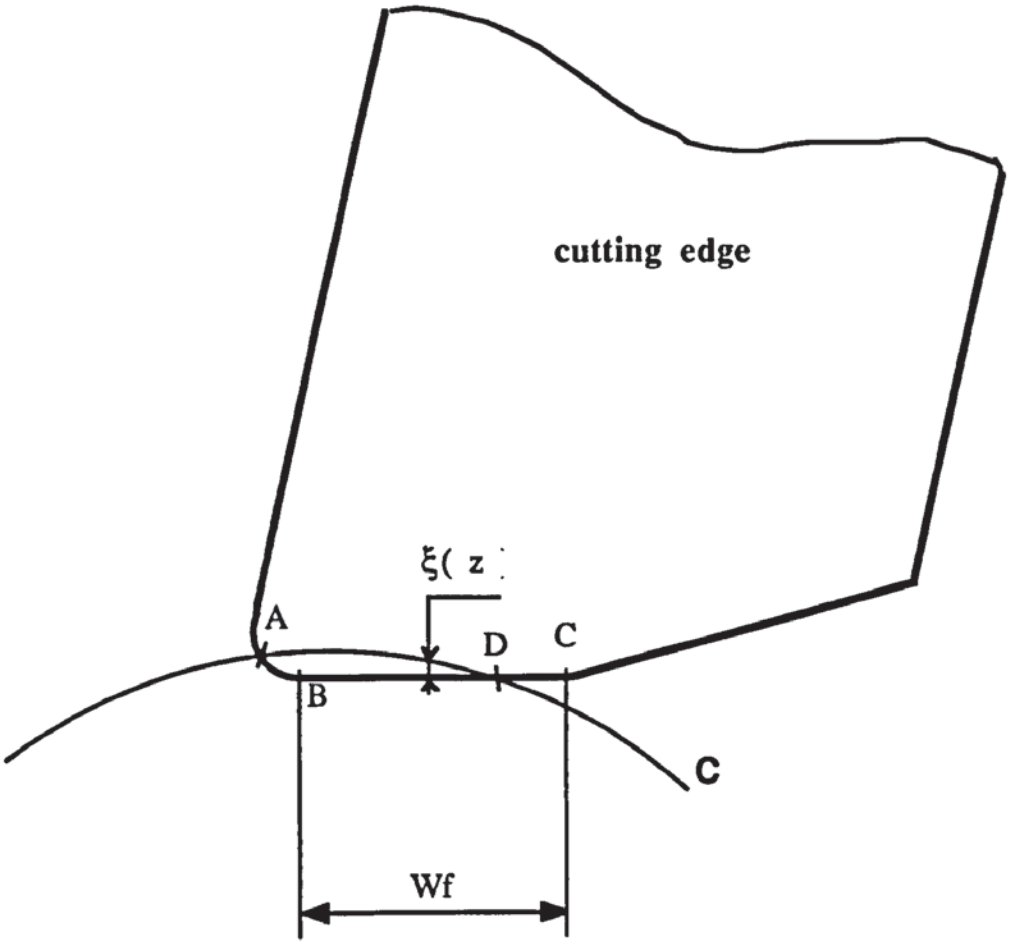

Fig. 8.2 Tool penetration during high velocity of tool vibration.

$$z_D = z_B + \frac{\zeta V}{\dot{x}} \qquad (8.4)$$

The dynamic turning force components in case of large amplitudes of vibration are as:

$$F_{xi} = \frac{w\, k_i\, S_i\, C_{si}}{\sin(\phi_i)\,(\cos(\phi_i) - C_{si}\sin(\phi_i))}$$

$$+ \frac{1}{2} w\, p_s \left\{ 2\, z_B (\zeta - R) + z_B \sqrt{R^2 - z_B^2} + R^2 \arcsin\left(\frac{z_B}{R}\right) \right\}$$

$$+ w\, p_s\, \zeta \left(\frac{\zeta V}{\dot{x}} - z_B \right) \qquad (8.5)$$

and

$$F_{zi} = \frac{w\, k_i\, S_i}{\sin(\phi_i)\,(\cos(\phi_i) - C_{si}\sin(\phi_i))}$$

$$- w\, p_s \frac{\dot{x}}{V} \frac{R\,(1 + \tan^2(\tau))}{\tan^2(\tau)} \left\{ z_B + \frac{R - z_B \tan(\tau)}{\tan(\tau)} \log\left[1 - \frac{z_B}{R} \tan(\tau) \right] \right\}$$

$$+ w\, p_s \frac{R^2(\tan^4(\tau) - 1)}{\tan^3(\tau)\sqrt{\tan^2(\tau) - 1}} \log \left[\frac{1 - \frac{z_B}{R}\tan(\tau)}{1 - \tan(\tau) + \sqrt{\tan^2(\tau) - 1}\sqrt{1 - \left(\frac{z_B}{R}\right)^2}} \right]$$

$$- \frac{w\, p_s}{\tan(\tau)} \left\{ \frac{\dot{x}}{V} \frac{z_B^2}{2} - R^2 \left(\frac{3}{2} - \frac{\tan^2(\tau) - 1}{\tan^2(\tau)} \right) \arcsin\left(\frac{z_B}{R}\right) \right\}$$

$$+ w\, p_s (\zeta - R) \frac{R(1+\tan^2(\tau))}{\tan^2(\tau)} \log\left(1 - \frac{z_B}{R}\tan(\tau)\right)$$

$$+ w\, p_s\, \zeta \left(\frac{\zeta V}{\dot{x}} - z_B\right) \tan(\tau) \qquad (8.6)$$

The cutting edge of worn tool is deformed during machining to a finite but small radius, and henceforth (8.2) and (8.3) can be reduced, in case of small velocity of vibration (8.1), to:

$$F_{xi} = \frac{w\, k_i\, S_i\, C_{si}}{\sin(\phi_i)\,(\cos(\phi_i) - C_{si}\sin(\phi_i))}$$

$$+ w\, p_s \left[\zeta\, VB + \frac{\zeta - \frac{\dot{x}}{V} VB}{\tan(\gamma) + \frac{\dot{x}}{V}} \left\{ \zeta - \frac{1}{2} \frac{\zeta - \frac{\dot{x}}{V} VB}{\tan(\gamma) + \frac{\dot{x}}{V}} \tan(\gamma) \right\} \right] \qquad (8.7)$$

$$F_{zi} = \frac{w\, k_i\, S_i}{\sin(\phi_i)\,(\cos(\phi_i) - C_{si}\sin(\phi_i))}$$

$$+ w\, p_s \left[\zeta\, VB \tan(\tau) + \frac{\zeta - \frac{\dot{x}}{V} VB}{\tan(\gamma) + \frac{\dot{x}}{V}} \left\{ \zeta - \frac{1}{2} \frac{\zeta - \frac{\dot{x}}{V} VB}{\tan(\gamma) + \frac{\dot{x}}{V}} \tan(\gamma) \right\} \tan(\tau - \gamma) \right] \qquad (8.8)$$

When the velocity of the tool vibration is important with large wear land VB, (8.1) is not satisfied and the instantaneous turning force components for small radius of the cutting tool are as follows:

$$F_{xi} = \frac{w\, k_i\, S_i\, C_{si}}{\sin(\phi_i)\,(\cos(\phi_i) - C_{si}\sin(\phi_i))} + w\, p_s\, \zeta^2 \frac{V}{\dot{x}} \qquad (8.9)$$

and

$$F_{zi} = \frac{w\, k_i\, S_i}{\sin(\phi_i)\,(\cos(\phi_i) - C_{si}\sin(\phi_i))} + w\, p_s\, \zeta^2 \frac{V}{\dot{x}} \tan(\tau) \qquad (8.10)$$

The relationships developed above show that the dynamic turning force components depend upon the width of wear land for medium range of wear i.e. where condition (8.1) is satisfied. As flank wear increases and velocity of cutting tool increases so that (8.1) is not satisfied the dynamic feed and cutting forces as shown by (8.9) and (8.10) become not directly dependent upon the flank wear. An increase in tool wear lead to an increase in tool vibration amplitude thus resulting in a decrease in dynamic ploughing forces. In other words, at high values of flank wear the dynamic turning force components are expected to decrease with subsequent flank wear. Lee *et al.* (1989) analysed the dynamic feed and cutting forces when the flank wear is varied up to 700μm. In their experimental results the dynamic components of turning force were found to decrease rapidly for flank wear above 500μm. Because no analytical modelling of the cutting process was provided, this decrease was attributed to the chipping of the cutting edge. No explanation to this decrease was provided by Lee *et al.*. In fact a chipping phenomenon will result in higher damping and thus smaller amplitudes of vibration which will result in smaller dynamic force. However, beside the chipping of the cutting edge, as the flank wear was as high as 700μm the relationship (8.1) may not be any longer respected and thus the resulting dynamic turning force components become decreasing with flank wear.

Adopting the same method as explained in 5.5 of Chapter 5, the instantaneous turning force components in the direction and normal to the instantaneous cutting speed, when machining with worn, tool can be determined by manipulating (8.9) and (8.10), as follows:

– Small velocity of vibration ((8.1) satisfied):

$$dF_{xi} = w\,k_e\Big\{ C_s\,dS + C_s\,A_1\,dk + C_s\,A_2\,d\phi + A_3\,\mathrm{cotg}(\phi)\,dC_s\Big\}$$

$$+ w\,p_e\left\{\left(p_4 + Wf\left[\tan(\gamma) + \frac{\dot{x}}{V}\right]\right)d\zeta + p_5\,d\gamma\right\} \qquad (8.11)$$

$$dF_{zi} = w\,k_e\Big\{ dS + A_1\,dk + A_2\,d\phi + A_3\,dC_s\Big\}$$

$$+ w\,p_e\left\{\left(p_4\,C_p + Wf\tan(\tau)\left[\tan(\gamma) + \frac{\dot{x}}{V}\right]\right)d\zeta + \left(p_5\tan(\tau - \gamma) + p_6\right)d\gamma\right\}$$

$$+ w\,p_e\left\{\zeta\,Wf\left(1 + \tan^2(\tau)\right)\left(\tan(g) + \frac{\dot{x}}{V}\right) - p_6\right\}d\tau \qquad (8.12)$$

– Large velocity of vibration ((8.1) not satisfied):

$$dF_{xi} = w\,k_e\Big\{ C_s\,dS + C_s\,A_1\,dk + C_s\,A_2\,d\phi + A_3\,\mathrm{cotg}(\phi)\,dC_s\Big\} + 2\,w\,p_s\,\zeta\,\frac{V}{\dot{x}}\,d\zeta \qquad (8.13)$$

$$dF_{zi} = w\,k_e\Big\{ dS + A_1\,dk + A_2\,d\phi + A_3\,dC_s\Big\}$$

$$+ w\, p_s\, \zeta \frac{V}{\dot{x}} \left(2 \tan(\tau)\, dz + \zeta \left(1 + \tan^2(\tau) \right) d\tau \right) \qquad (8.14)$$

Where:

$$p_4 = \zeta + \frac{\zeta - \frac{\dot{x}}{V} Wf}{\tan(\gamma) + \frac{\dot{x}}{V}} \frac{\dot{x}}{V} \qquad (8.15)$$

$$p_5 = \frac{\left(\zeta - \frac{\dot{x}}{V} Wf \right) \left(1 + \tan^2(\gamma) \right)}{\tan(\gamma) + \frac{\dot{x}}{V}} \left\{ 0.5 \left(3\zeta - \frac{\dot{x}}{V} Wf \right) + \frac{\zeta - \frac{\dot{x}}{V} Wf}{\tan(\gamma) + \frac{\dot{x}}{V}} \tan(\gamma) \right\} \qquad (8.16)$$

$$p_6 = -\left(\zeta - \frac{\dot{x}}{V} Wf \right) \left\{ \zeta - \frac{1}{2} \frac{\zeta - \frac{\dot{x}}{V} Wf}{\tan(\gamma) + \frac{\dot{x}}{V}} \tan(\gamma) \right\} \left(1 + \tan^2(\tau) \right) \qquad (8.17)$$

The instantaneous dynamic feed and cutting forces are determined from the (8.13) to (8.14) above and the matrix transformation (5.40). These expressions together with (5.40), (8.15) to (8.17) are used further to predict the dynamic feed and cutting force for different cutting conditions and flank wear levels.

8.3. TOOL WEAR CHARACTERISATION IN FREQUENCY DOMAIN

Different methods were developed in the past for tool wear monitoring and tool failure detection (Tlusty, 1983). When the degree of tool wear is reflected by the cutting force,

power or temperature, the average value model is often adopted (Chapter 3, Sata *et al.*, 1973; Ridley, 1982), where the average value of the signal is considered to be related to the tool wear (Chapter 4). This model is easily interfered by various random factors in cutting process which often results to great statistical errors. Thereby to improve the monitoring accuracy, some kind of low pass filters are applied to filter out the fluctuation components in signals and to obtain as pure as possible the average value. This is the case of Chapter 3 and Chapter 4 where the force component signals are filtered using Kistler amplifier to 10Hz low pass to investigate the steady state components. From the signal processing point of view, a great amount of useful information is lost on the model. Particularly, the average value component of the signal is not so sensitive to some important characteristics before rapid tool wear appears, large change in the average value component may take place but it is too late to send out an alarm signal.

It is therefore necessary to measure and analyse the fluctuation component of the signal to search out the characteristic parameters in different wear stage of cutting tools. The method commonly used is spectral analysis (Sata *et al.*, 1973), which means in case of one signal to evaluate the power spectral density (PSD) function which represent the energy distribution of the signal over frequency domain. Every spectrum peak represents the energy of the definite sine component in that frequency point, while the average value is only a spectrum peak at the frequency of 0 Hz in the PSD diagram.

In the present investigation, the developed model provides the dynamic force components when the feed vibration of the cutting tool is sensed. In the following sections, RMS and PSD spectra of the tool vibration and turning force components are used to develop an approach for tool wear monitoring after which experimental findings are used to validate the prediction of this tool wear monitoring criteria.

8.4. EXPERIMENTAL TESTS

In this chapter, similar cutting tests as in Chapter 4 are carried out (Table 4.1). While in Chapter 4 interest was given to the steady state value of feed and cutting forces when turning under different cutting conditions and values of flank wear, in the foregoing chapter, emphasis is given to the dynamic components of the turning force. The cutting tests are run on a TORSHALLA lathe to cut an SAE 1045 material using tools at different flank wear levels. The tool acceleration in feed direction is sensed by an accelerometer mounted on the tool as near as possible to the cutting tip while the turning force components are measured by a piezo–electric dynamometer. The data analysis is conducted in a same procedure as presented in section 7.2.

Results of these tests are used as first step to validate the theoretical predictions of the developed model and highlight a tool wear monitoring procedure, furthermore, these are used. In the last section, the model is used to predict the defined tool wear monitoring factor and predictions are compared with experimental findings.

8.5. EXPERIMENTAL RESULTS

The experimental tool acceleration, feed and cutting forces spectra are shown in Fig. 8.3 to Fig. 8.14. These are obtained by off–line analysing the replay signal of the four channels tape recorder through the 1401–plus hardware. In each figure flank wear on is varied from 0μm as new tool to 230μm as a maximum of wear level. It is noticed that beyond this level the tool chips rapidly and breaks afterwards. Moreover, in Fig. 8.3 to Fig. 8.5, Fig. 8.7 to Fig. 8.9 and Fig. 8.11 to Fig. 8.13, representing tool acceleration, feed force and cutting force respectively, the feed is

maintained constant (0.20 mm/rev) and the cutting speed is varied from 2.28m/s to 7.27m/s in three steps. While in Fig. 8.6, Fig. 8.10 and Fig. 8.14, feed of 0.25 mm/rev and cutting speed of 3.4 m/s are used. It can be seen from Fig. 8.3 to Fig. 8.14 that there are several regularities that the PSD of the tool vibration, feed and cutting forces vary with tool wear as discussed below.

When new cutting edge is used to start cutting, the average energy in tool acceleration, feed and cutting force is high over all the range of frequency under investigation, this is to say that the level of background noise is high. No dominant frequency range is usually observed (Fig. 8.3).

As the cutting speed increases, the peaks observed in the acceleration spectra (Fig. 8.3 to Fig. 8.6) at low frequency range up to 2kHz become smaller and a broad increase is is then observed between 2 and 4.5kHz. This band of frequency is narrower higher the speed or the feed. It is worth noticing that at a feed of 0.0002m/rev (Fig. 8.3 to Fig. 8.5), the amplitude of tool acceleration remains small for the range of speed investigated. However, as the feed is increased up to 0.25 mm/rev the process becomes unstable with rapid increase in the amplitude of acceleration (Fig. 8.6). In this chattering condition the tool acceleration has increased by about 7times.

Similar variations as in tool acceleration are observed in feed force oscillations as the speed varies from 2.28 m/s to 7.27 m/s and feed from 0.20 to 0.25 mm/rev. The cutting process is unstable at speed of 2.28m/s and feed of 0.25mm/rev. While the acceleration is increased by about 7times, the dynamic component of the feed force increases by about 10times and the cutting force by about 15times within 2 to 4.5kHz. This amount of increase do not concern all the range of frequency but is confined to frequencies close to the natural frequency of the system tool holder–tool post

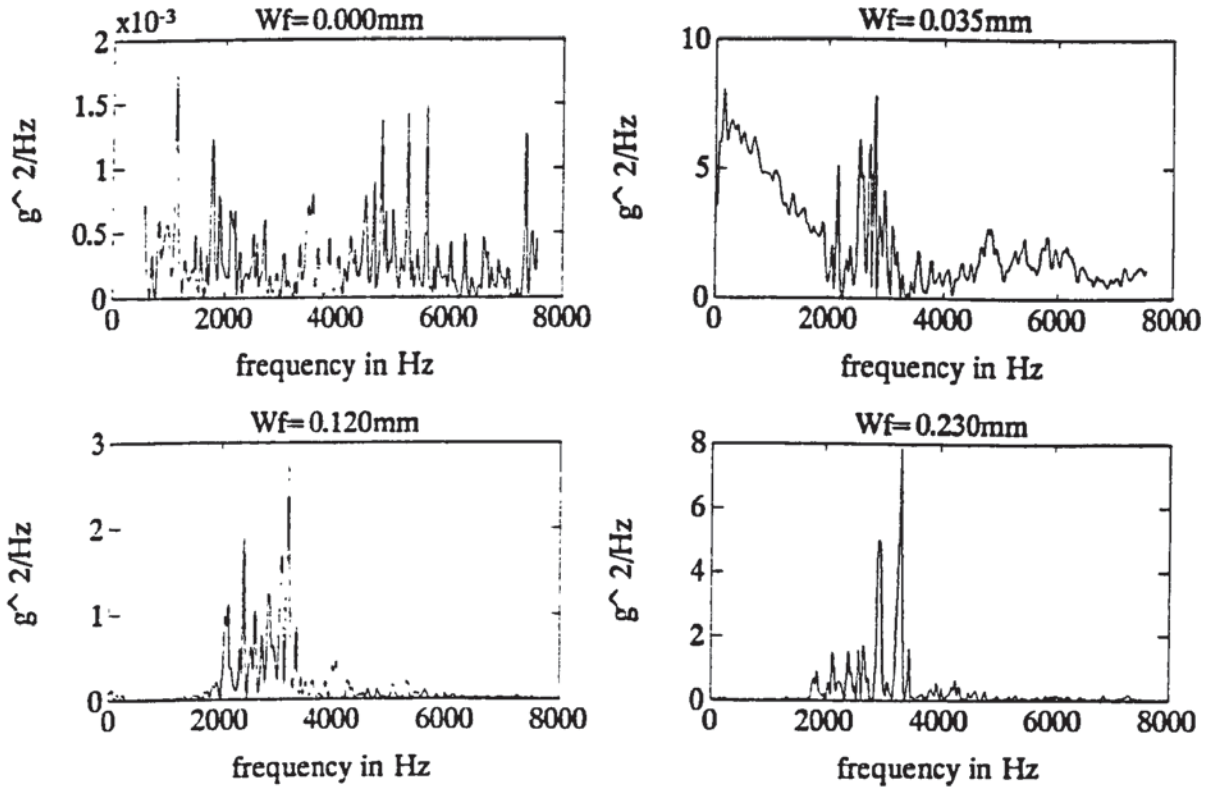

Fig. 8.3 PSD of tool acceleration: S_0 = 0.2mm/rev, V = 2.2833m/s.

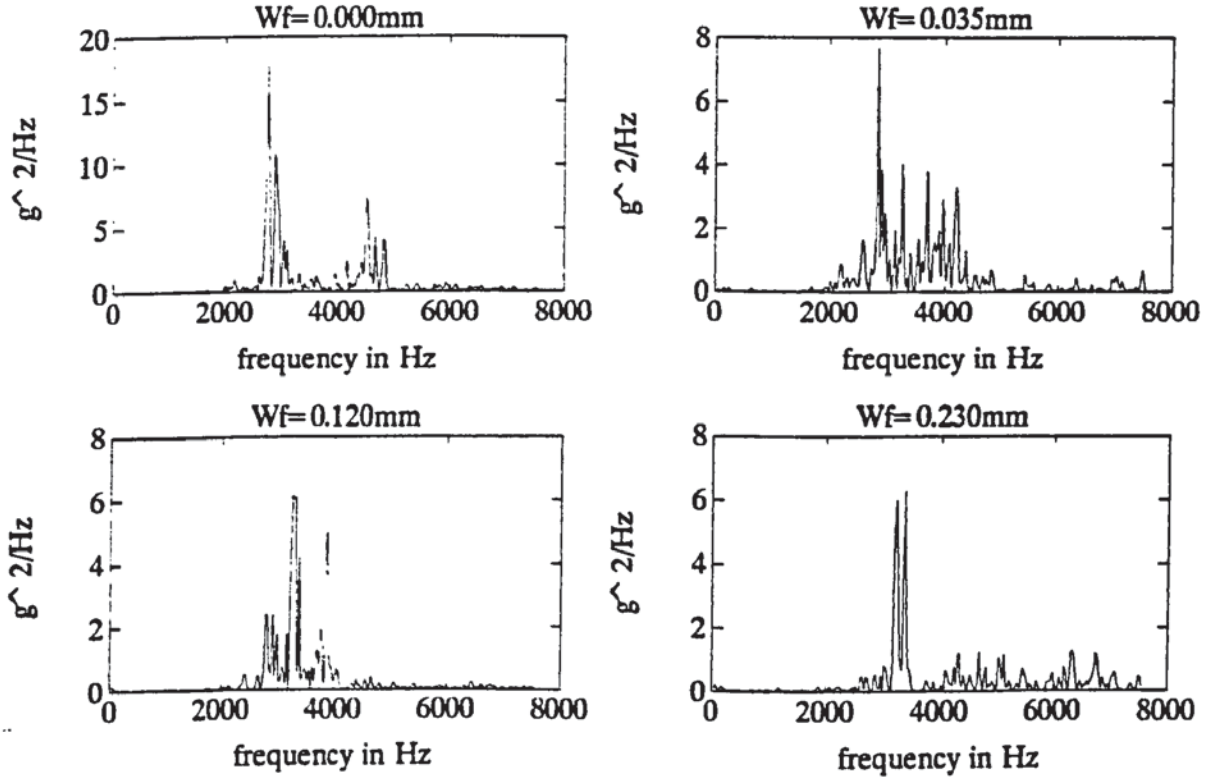

Fig. 8.4 PSD of tool acceleration: S_0 = 0.2mm/rev, V = 3.4m/s.

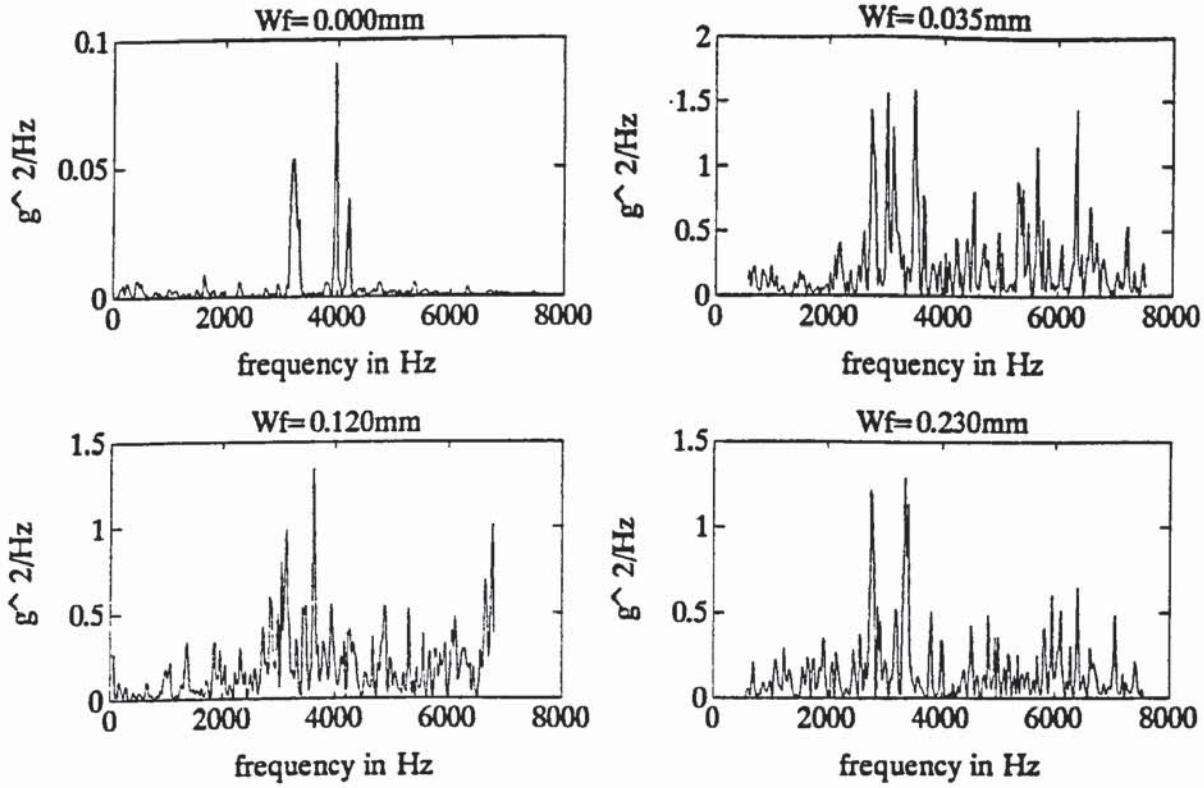

Fig. 8.5 PSD of tool acceleration: S_0 = 0.2mm/rev, V = 5.2m/s.

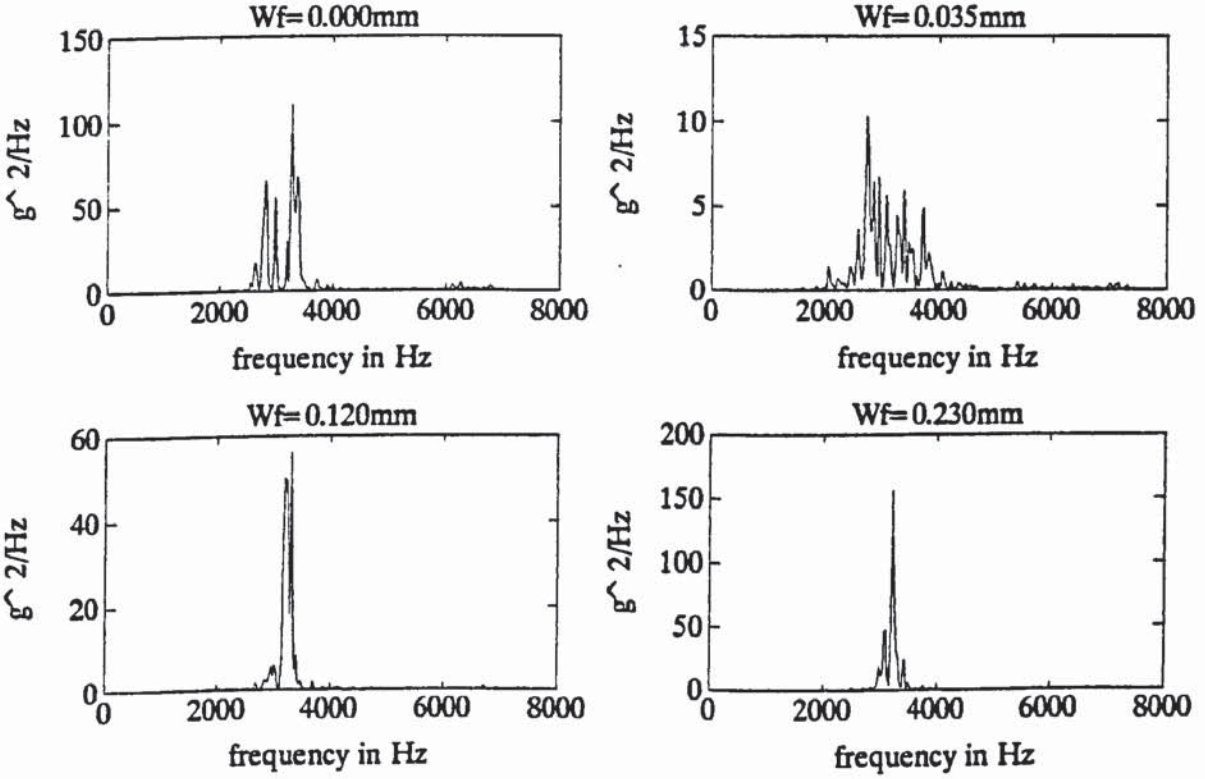

Fig. 8.6 PSD of tool acceleration: S_0 = 0.25mm/rev, V = 3.4m/s.

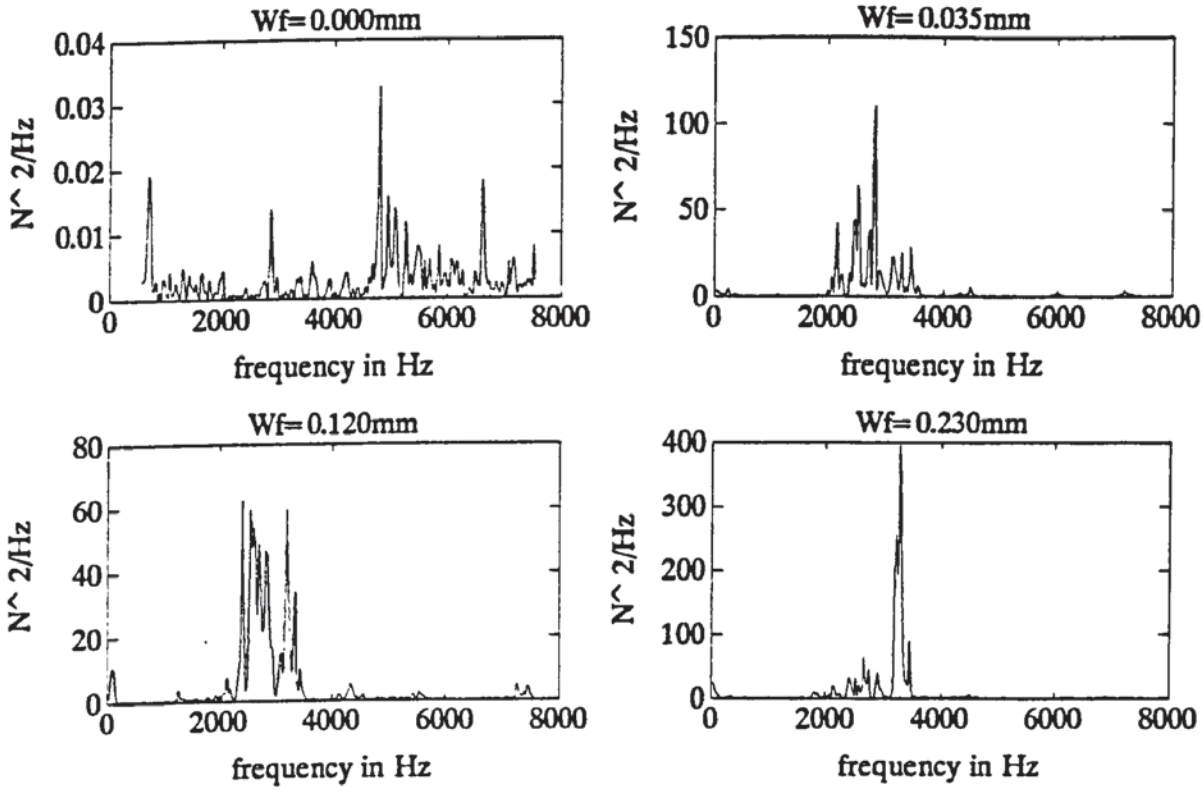

Fig. 8.7 PSD of feed force: S_0 = 0.2mm/rev, V = 2.2833m/s.

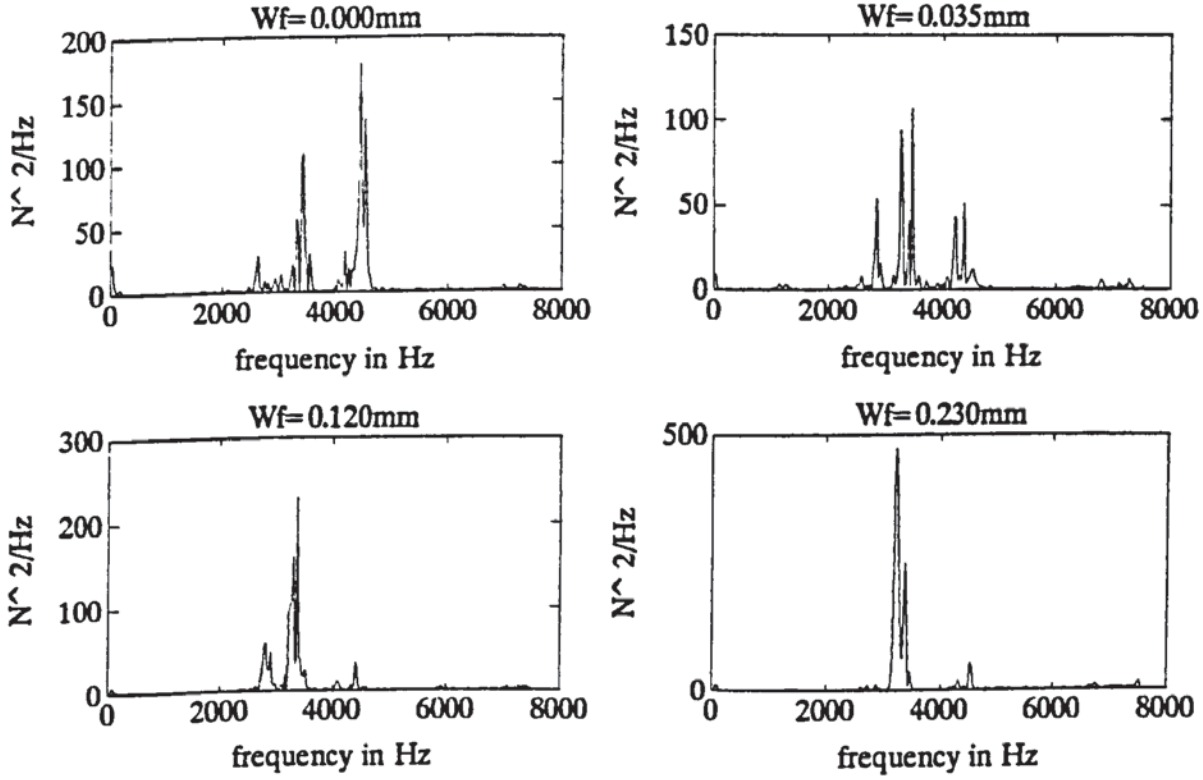

Fig. 8.8 PSD of feed force: S_0 = 0.2mm/rev, V = 3.4m/s.

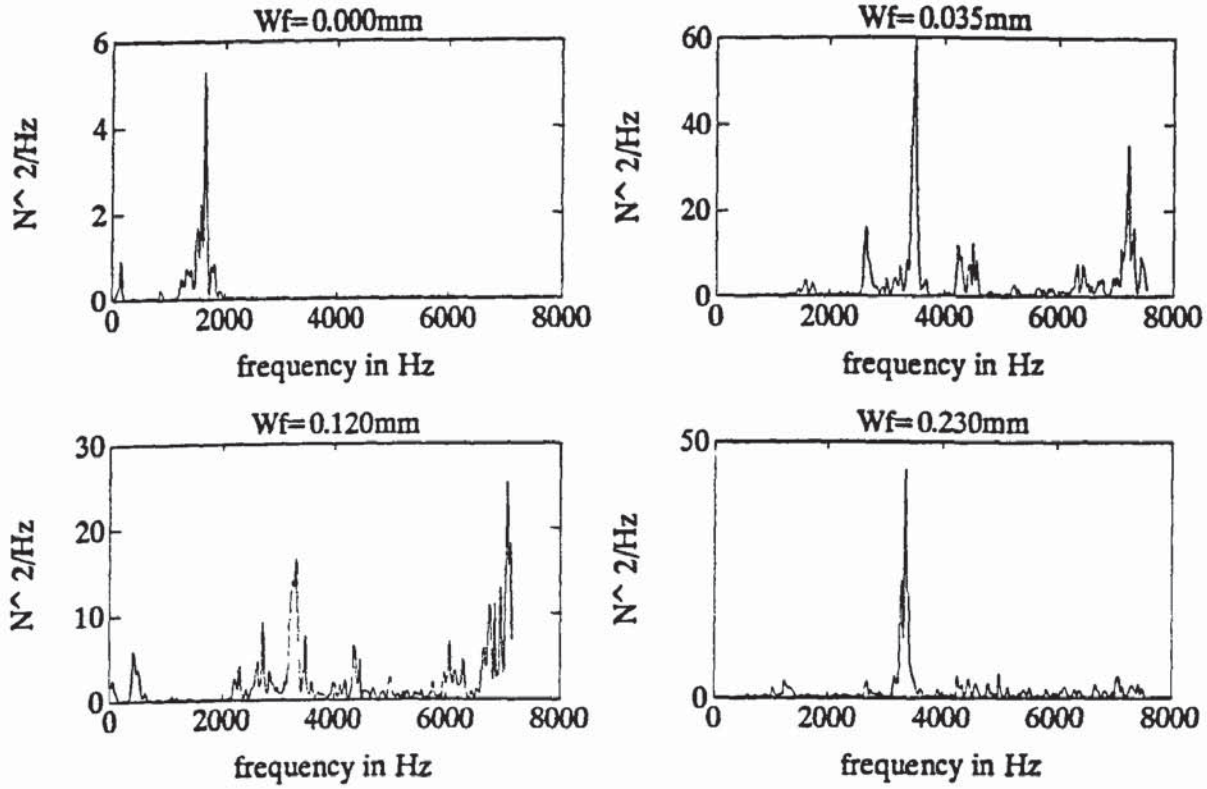

Fig. 8.9 PSD of feed force: S_0 = 0.2mm/rev, V = 5.2m/s.

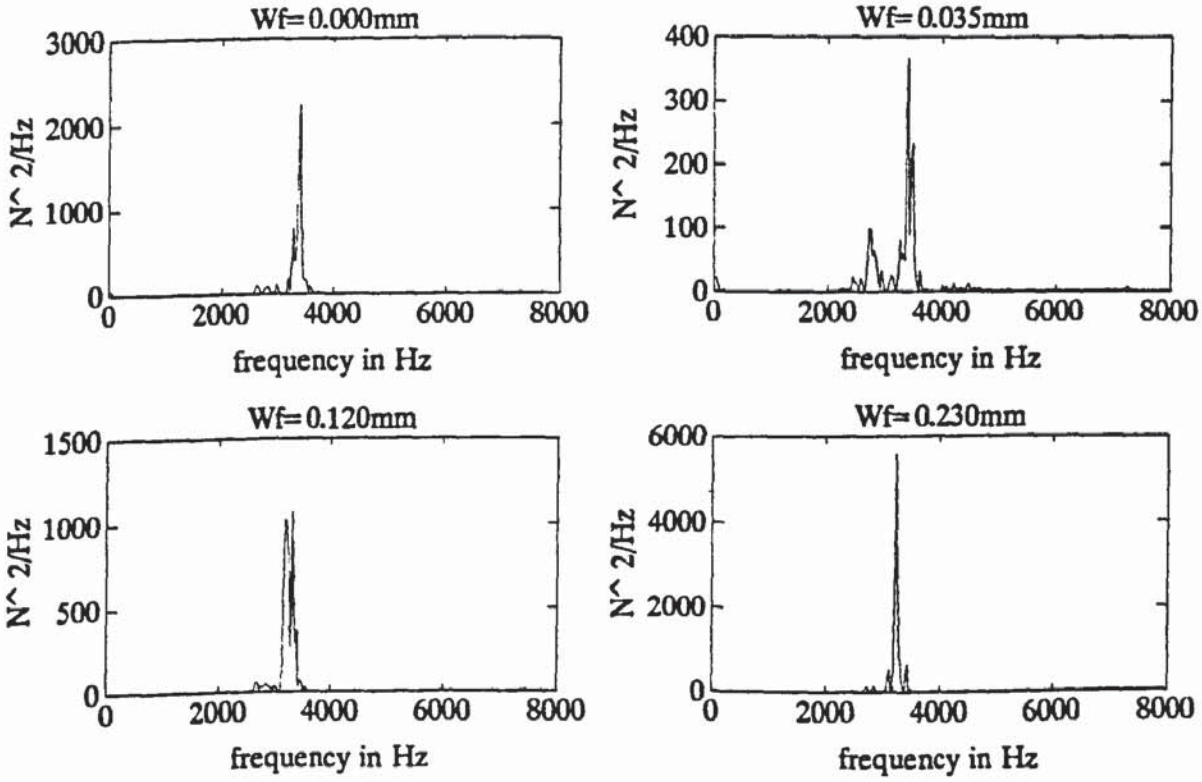

Fig. 8.10 PSD of feed force: S_0 = 0.25mm/rev, V = 3.4m/s.

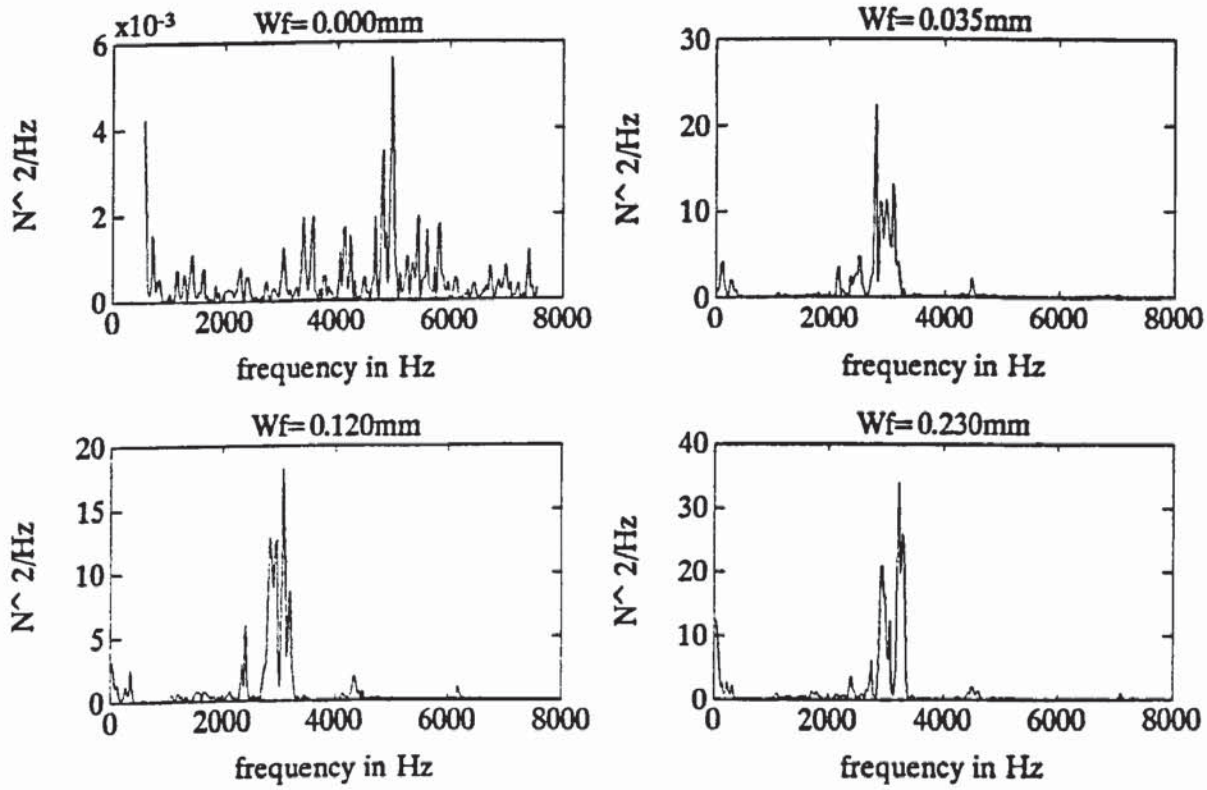

Fig. 8.11 PSD of cutting force: S_0 = 0.2mm/rev, V = 2.2833m/s.

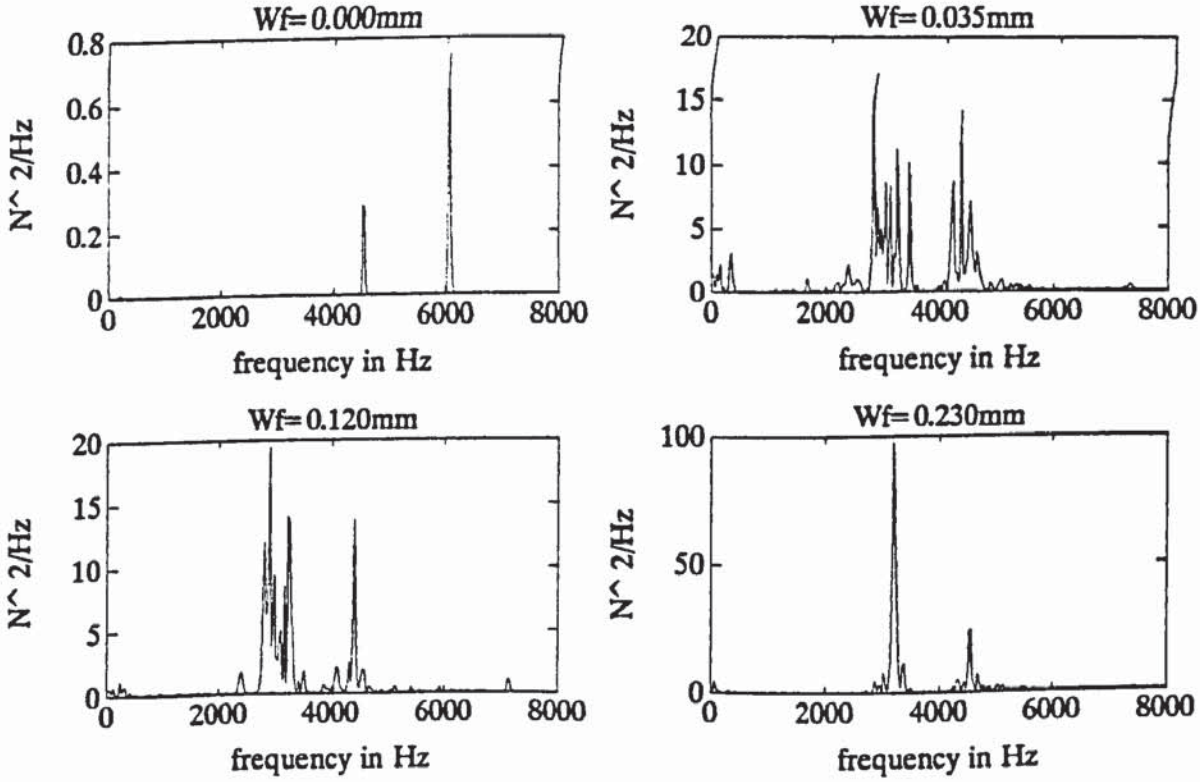

Fig. 8.12 PSD of cutting force: S_0 = 0.2mm/rev, V = 3.4m/s.

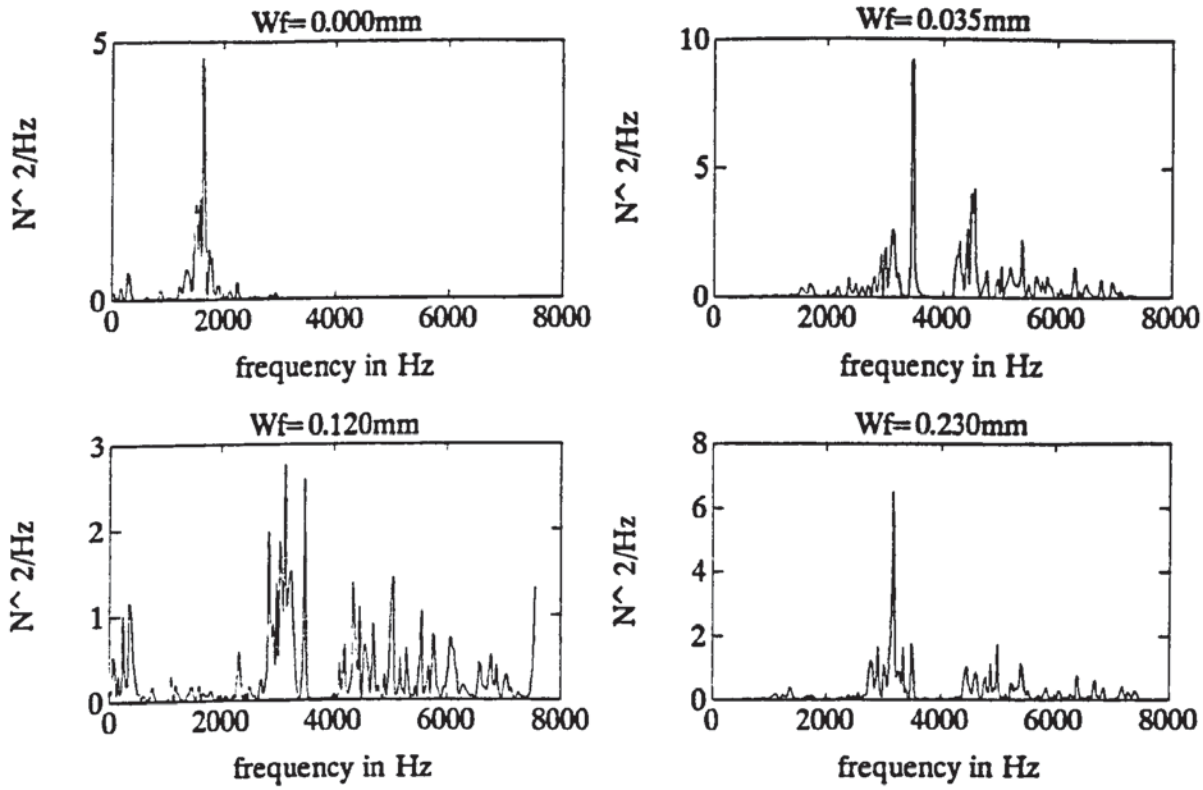

Fig. 8.13 PSD of cutting force: S_0 = 0.2mm/rev, V = 5.2m/s.

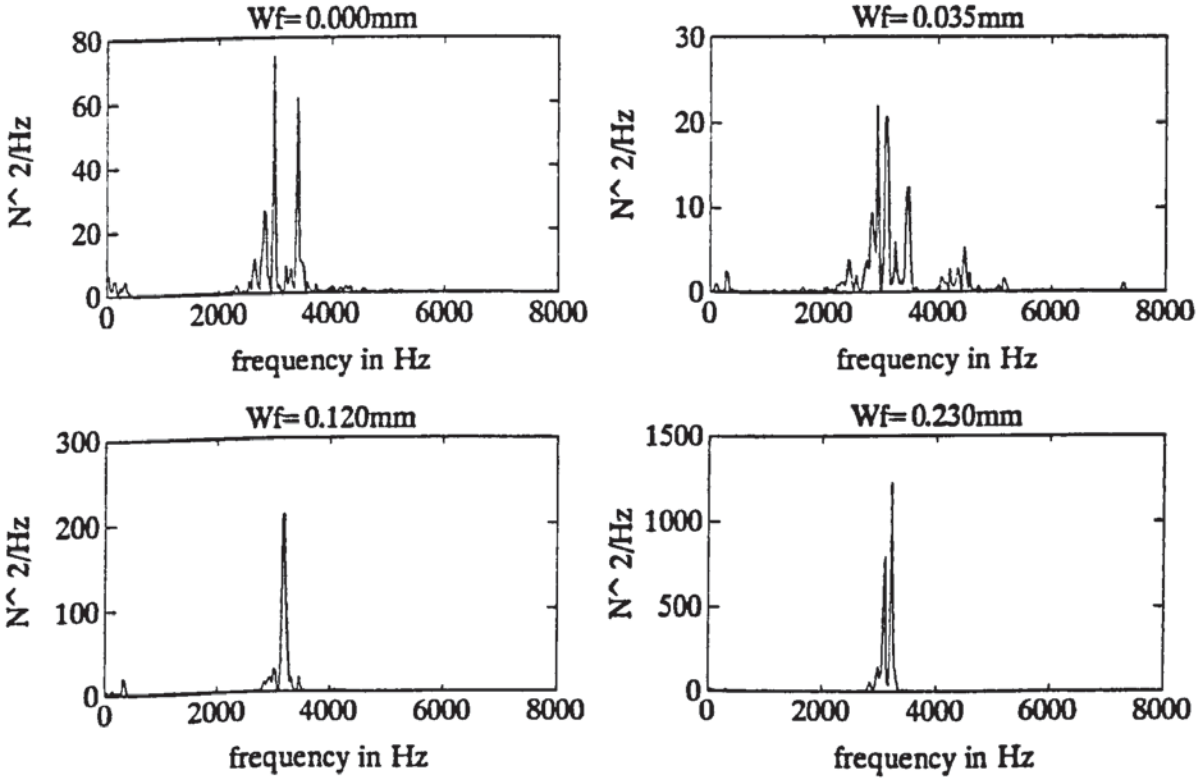

Fig. 8.14 PSD of cutting force: S_0 = 0.25mm/rev, V = 3.4m/s.

(Chapter 6). From the above results it is seen that the effect of the machine structure at low frequencies is decreasing with cutting speed while the effect of the tool post system becomes more important.

In the initial wear stage (Wf=350μm), the energy level in lower frequency range 0–2kHz gradually decreases, while the energy level of background noise in acceleration, feed and cutting force spectra has little variation. Some peaks appear around 4kHz in early stage of wear but die out as the flank wear increases. Analysis of the low frequency of the spectra show that some peaks at low frequency correspond to the workpiece revolution speed and its harmonics.

In normal wear stage without chipping, the energy below 2kHz in acceleration and forces spectra decreases to a relatively low level and keeps rather stable during whole normal wear stage. Some peak appear above 4kHz (Fig. 8.12 and Fig. 8.13) but the energy is small compared to the energy of the whole signal.

As can be seen from Fig.8.3 to Fig. 8.14 peaks are dominating in acceleration, feed and cutting force spectra which are closer to the natural frequency of the cutting system according to the results of impact test in Chapter 6. The energy in these spectrum peaks increases step by step in normal wear stage, but their frequency positions are not changed throughout the wearing tests. This increase however do not seem to be easily correlated with the amount of flank wear.

During the experimental tests some tool are chipped or broken while machining is in progress. It was found that when the tool is starting to chip, which is considered as failure of the tool in the present study, the energy below 2kHz in the acceleration spectrum increases evidently more than the increase in the feed or the cutting force.

However the energy near the resonant frequency peaks is almost unchanged. Furthermore, at the moment when the tool breaks, almost all higher peaks in the PSD of acceleration and forces spectra disappear in a short time, the level of background noise is rather high, which indicates that the total energy of the corresponding signal increase rapidly. The obtained spectra are nearly a horizontal line and no any definite component occupies a dominant position. This is a typical characteristics of the white noise of random vibration.

The case of tool chipping and tool breakage is not well developed in the following work and the reason is that from the point of view of the present thesis the tool fails when the surface quality is not at the standard of the desired turned surfaces. On the other hand, It was observed that when the tool starts to chip the roughness of machined surface is deteriorating gradually and some small sparks appear near the tool tip. Evidently, in this case, it is appropriate to send out the alarm signal to change the cutting tip.

From the above discussion it can be summarised that tool acceleration, dynamic feed and cutting forces are increasing with flank wear and that the amount of increase depends upon the cutting conditions. The spectra of tool acceleration, feed and cutting forces show that low frequencies are dominating for new cutting edge, while as the flank wear increases a broad increase is observed near the natural frequency of the cutting system. Despite the existence of some peaks at high frequency (4kHz) in the first stage of the flank wear, the energy contained is small compared to the energy of whole signal. These peaks are further vanishing as the flank wear increases.

8.6. PREDICTION OF TURNING FORCE DURING MACHINING WITH WORN TOOL

The developed model for flank wear turning is used to predict turning force components under different wear levels and cutting conditions. The input to the model are cutting conditions, tool displacement and tool velocity during the actual and previous workpiece revolutions. The tool displacement and velocity are obtained by integrating the tool acceleration twice and once respectively.

A typical spectra of predicted and experimental spectra of feed and cutting forces are shown in Fig. 15 to Fig. 20 for cutting speeds ranging from 2.28m/s up to 5.20m/s and feeds from 0.20mm/rev up to 0.25mm/rev. It is shown that the model yields reasonable predictions of turning force components for different wear levels and cutting conditions used.

Analysing the obtained spectra, the following conclusions can be drawn:

– In general good predictions are obtained at high frequencies above 3kHz for new cutting edge. Though as the flank wear increases, better predictions are obtained at low frequency than frequencies above 5.5kHz. This is because, as discussed above, when tool edge is still new low frequencies are dominants which introduces more disturbances thus resulting in less accuracy in theoretical predictions. However, as the tool wears higher frequencies become more dominants and therefore discrepancies between prediction and experiments are at high frequencies.

– It is noticed that the accuracy of predicting feed and cutting forces is less sensitive to flank wear in medium range of frequencies between 2.5 to 5.5kHz than in lower or

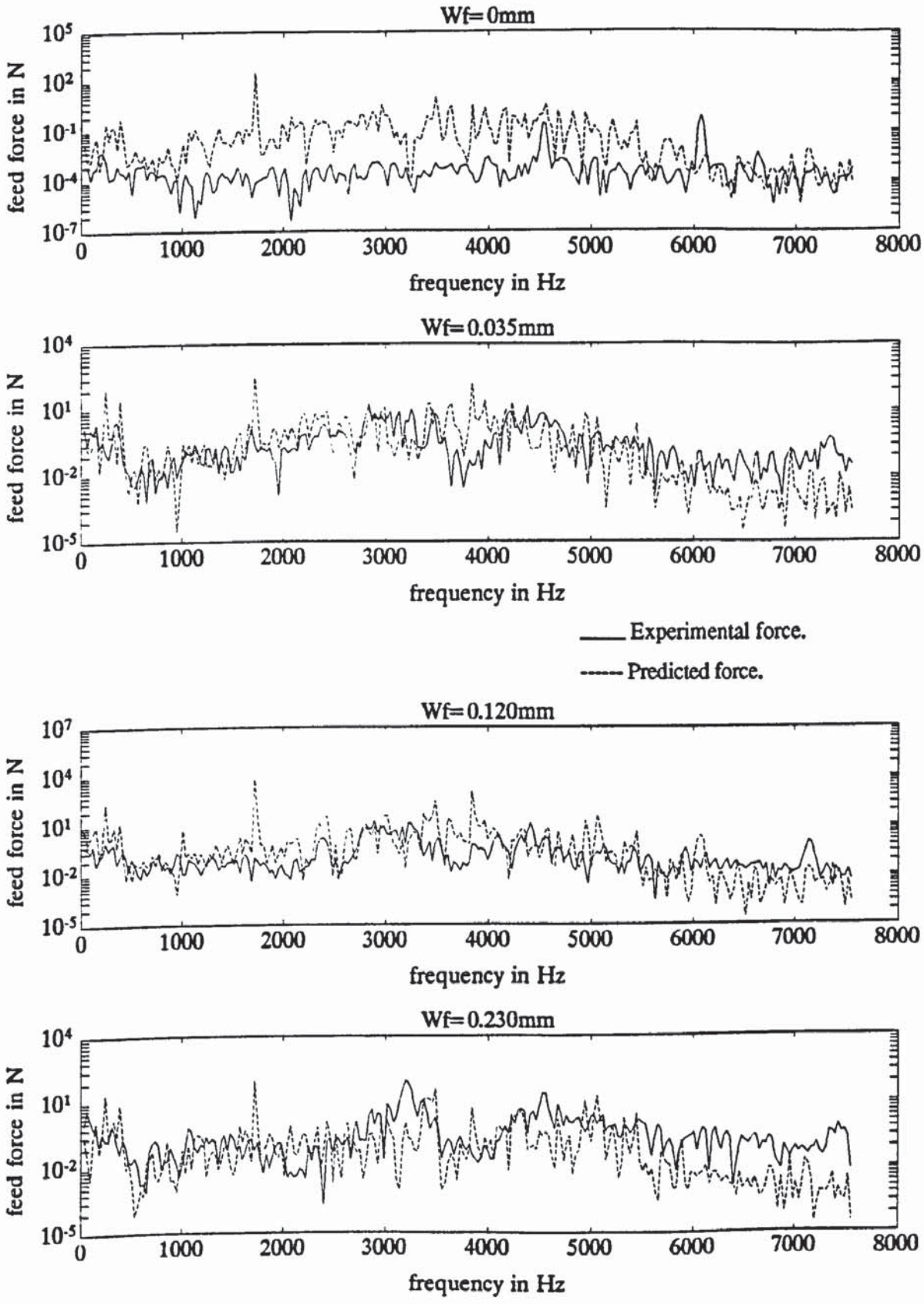

Fig. 8.15 Predicted and experimental amplitude of feed force autospectrum, S_0 = 0.2mm/rev, V = 3.4m/s.

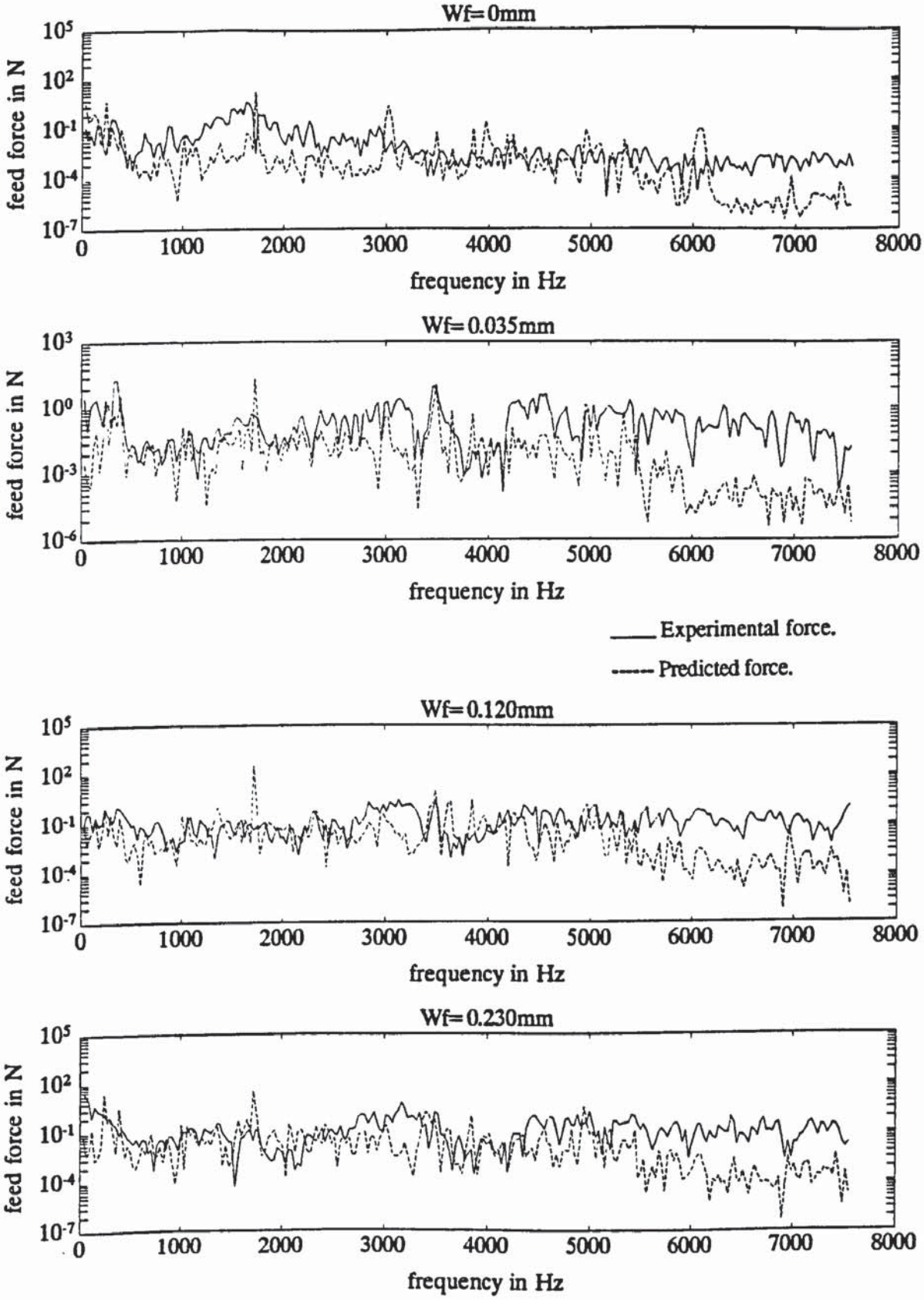

Fig. 8.16 Predicted and experimental amplitude of feed force autospectrum, S_0 = 0.2mm/rev, V = 5.2m/s.

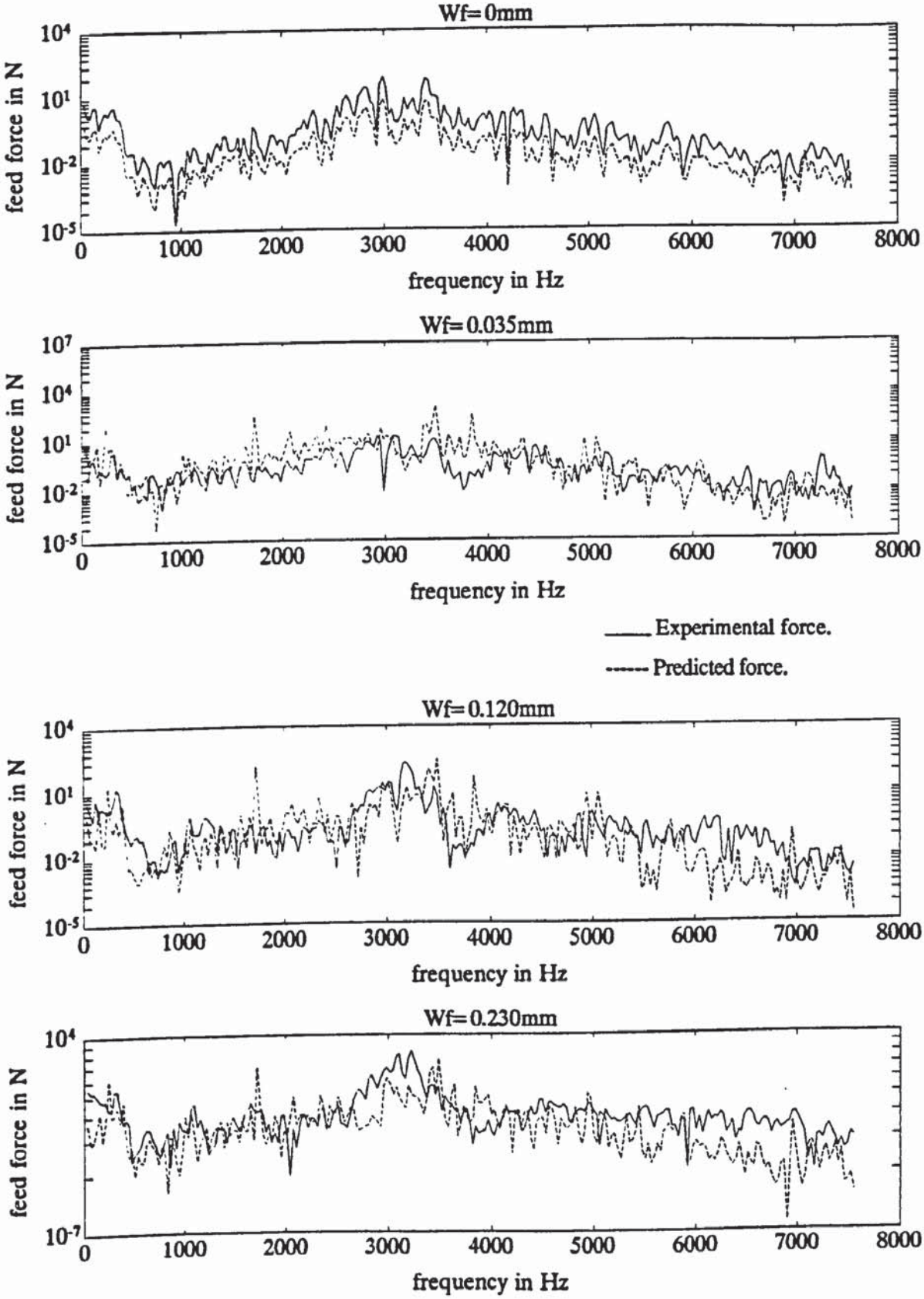

Fig. 8.17 Predicted and experimental amplitude of feed force autospectrum,

S_0 = 0.25mm/rev, V = 3.4m/s.

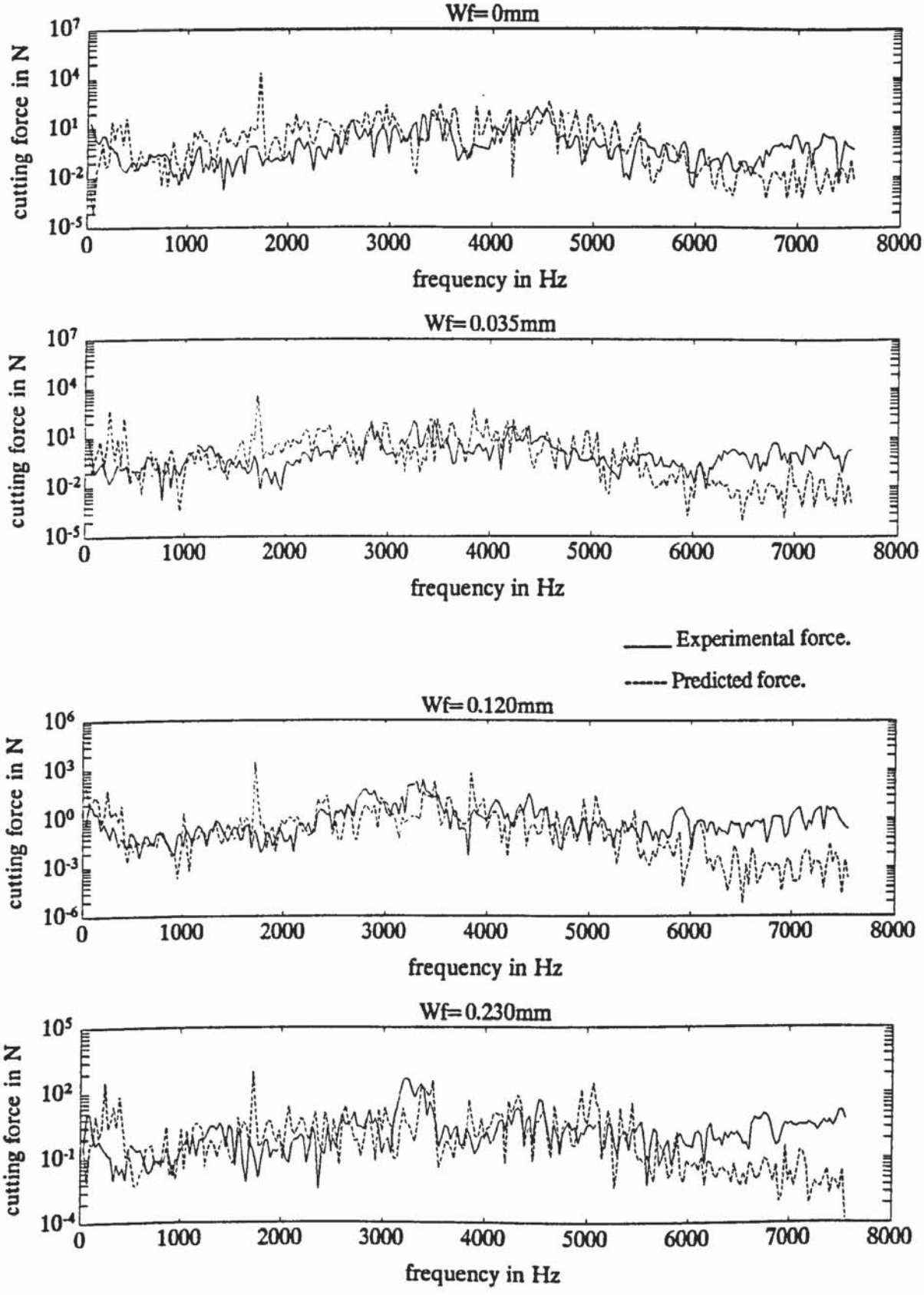

Fig. 8.18 Predicted and experimental amplitude of cutting force autospectrum, S_0 = 0.2mm/rev, V = 3.4m/s.

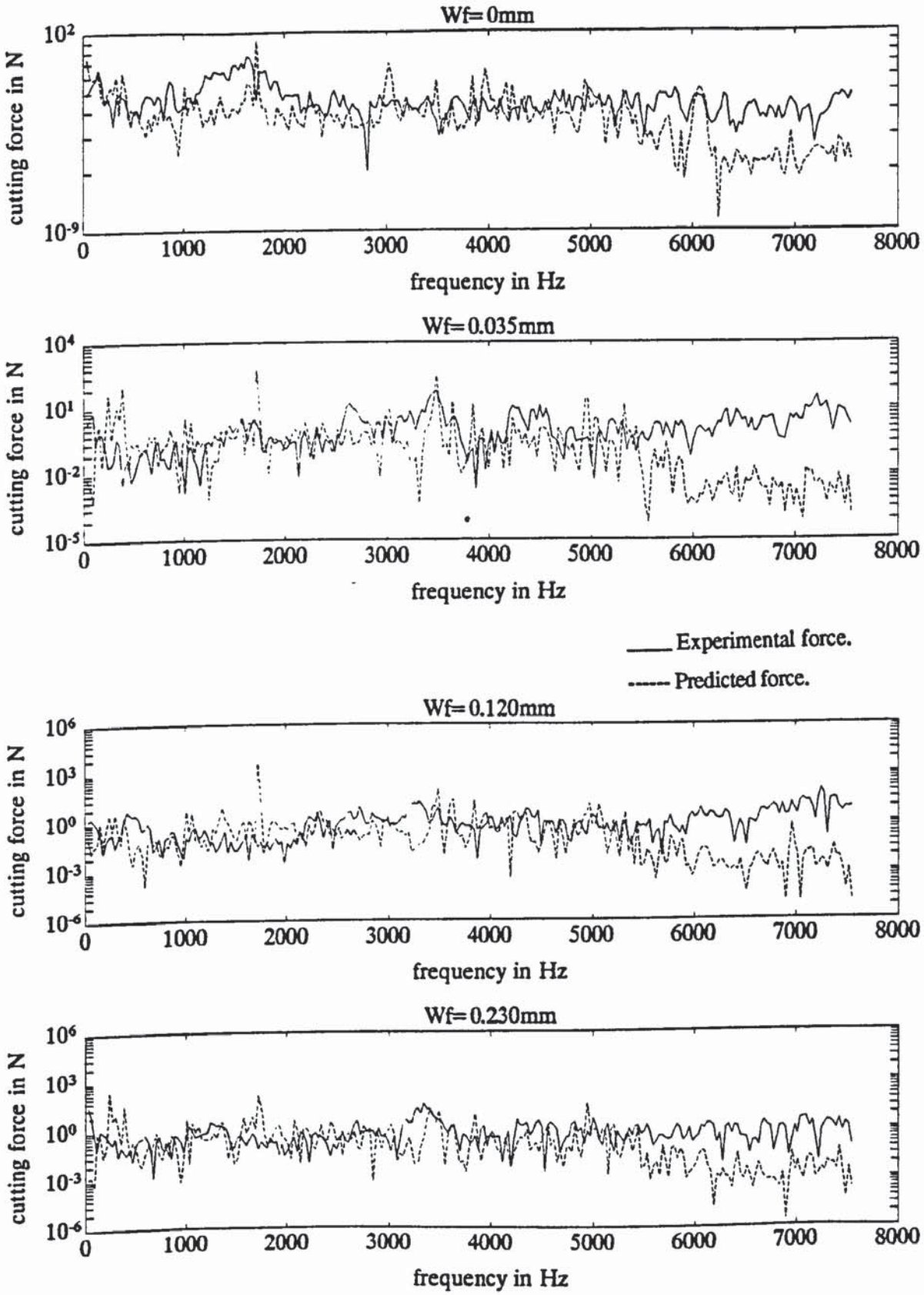

Fig. 8.19 Predicted and experimental amplitude of cutting force autospectrum, S_0 = 0.2mm/rev, V = 5.2m/s.

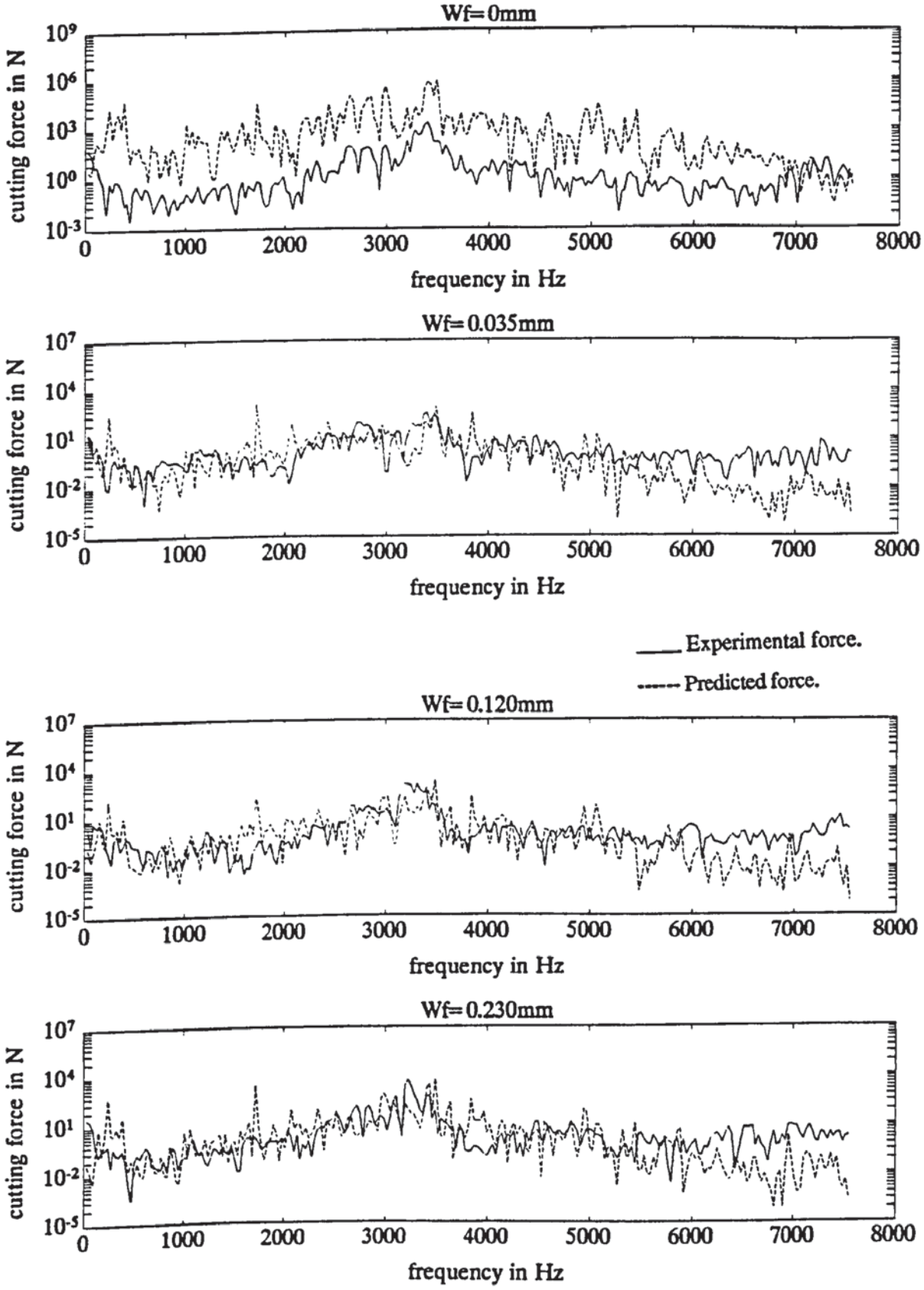

Fig. 8.20 Predicted and experimental amplitude of cutting force autospectrum, S_0 = 0.25mm/rev, V = 3.4m/s.

higher frequencies. Because of this consistent observation and because of the large increases with wear in the force and acceleration spectra within this band of frequency, more emphasis will be given to this range of frequency in order to develop a criteria for flank wear monitoring.

– It is worth mentioning that all the spectra points used in this work satisfy (8.1). The cutting tests were run under the conditions of small amplitudes of vibration and not high flank wear level. The former is a sine qua none condition in the development of the present model (Chapter 5) and was achieved by selection of conditions where chatter is avoided. While the latter was limited by the brittleness of the cutting tips used.

8.7. FLANK WEAR MONITORING CRITERIA

In the development of a flank wear monitoring criteria, the steady state forces were considered in Chapter 4, while in the foregoing section tool acceleration, dynamic component of the turning force together with their corresponding spectra. The spectral analysis of cutting force, feed force and tool tip vibration are carried out up to 6.510kHz. The choice of this frequency range resulted from the frequency resolution used (29.523Hz) and from the band of frequency that bears good informations about the magnitude of the tool wear and is adopted after analysing different spectra which showed good correlation with wear between 2 and 5kHz.

Analysis of the steady state turning force components in Chapter 4 showed that feed force is more sensitive to wear than cutting force. Yet, the predicted feed forces were found to be closely coinciding with the measured forces but nevertheless, the increase of feed force with wear is highly dependent upon the cutting conditions and

furthermore the accuracy in the force prediction decreases with flank wear. Furthermore, the range of repeatability of feed force measurement as well as the error in force prediction render any criteria of wear monitoring insensitive to any small variations in flank wear. Thus, for the sake of flank wear monitoring, dynamic analysis of turning has become necessary.

As mentioned above dynamic feed force, cutting force and tool vibration are considered. In the following section, these component are separately analysed in order to develop a criteria for tool wear monitoring.

8.7.1. Vibration of turning tool

In order to correlate tool vibration to flank wear, the root mean square of tool acceleration was measured for different cutting conditions and flank wear levels. A sample of the obtained results is represented in Fig. 8.21. As represented in Fig. 5.21, the RMS of tool acceleration decreases as the tool starts to wear because when the tool is still new the contact area is too small resulting in small damping and henceforth is higher average amplitude of vibration. However, as the flank wear increases, the contact between the work material and the cutting edge increases accordingly and resulting higher RMS of tool acceleration. In fact when the flank wear increases under no chipping the contact area increases and the force within this contact increases as well which lead to a decrease in the dynamic damping. This is can be better understood by analogy between the tool and workpiece and joints in mechanical parts.

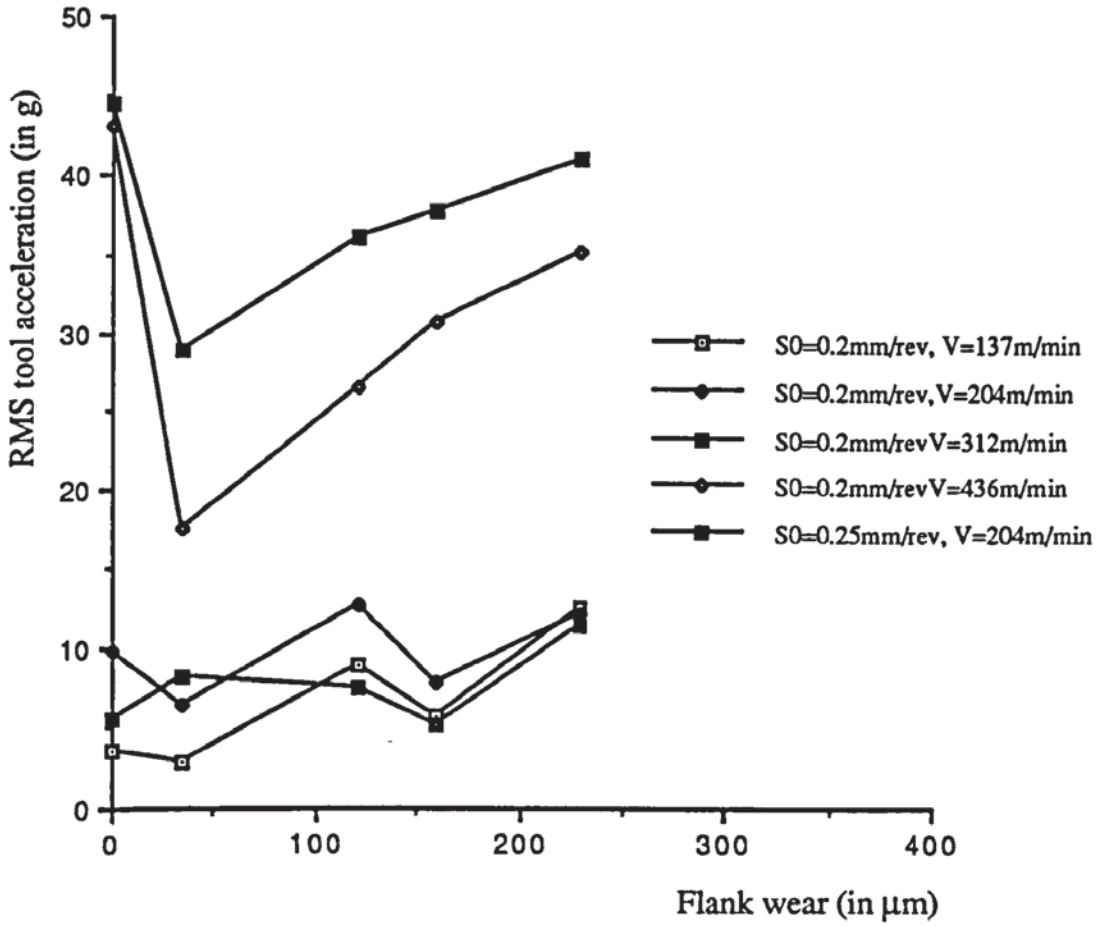

Fig. 8.21 Variation of the RMS of tool acceleration with flank wear.

In every mechanical system, different parts can be joined by different possibilities and the commonly and widely used one is the bolted joint. In this particular design which can represent the situation in metal cutting with cutting tool and workpiece are the two parts and the contact is the flank wear area. The ploughing force is the force applied by the bolts. When the joining force is small, corresponding to new tool, the actual damping is high whereas the stiffness is small. In contrast, as the tool wears, the joining forces are higher providing smaller damping and higher stiffness henceforth

higher vibration amplitudes. This analogy explains thus the shift towards higher frequencies and the increase in the vibration amplitude observed in the spectra as the tool wears.

The experimental results of Fig. 8.21 show that except for higher feed and speed the increase of amplitude of tool acceleration is not significant with flank wear. The RMS of tool acceleration is rather increasing and decreasing with flank wear. This is attributed to the existence of some micro–chipping on the flank of the cutting tool. Using the same analogy as above, when the tool edge chips away by a small amount this can be regarded as the existence of loose bolt in mechanical joint which leads to higher damping and smaller stiffness. Therefore the amplitude of vibration is damped.

However, under unstable cutting conditions corresponding to V=7.27m/s, S_0=0.20mm/rev and V=3.40m/s, S_0=0.25mm/rev an important increase in the RMS of the acceleration signal is observed. Under these conditions the effective damping is too small thus leading to higher amplitudes of vibrations.

The pattern of too vibration helps to detect the existence of chattering conditions whereas the fluctuation and variations observed in RMS of acceleration render it difficult to relate to flank wear. In the next step, the dynamic components of the turning force are considered.

8.7.2. Dynamic components of turning force

The experimental dynamic feed and cutting forces are shown in Fig. 8.22 and Fig. 8.23 for cutting conditions as summarised in Table 7.1. It can be seen that the amplitude of the dynamic components of the turning force are decreasing with speed

and increasing with feed rate under stable conditions. However when the cutting speed is increased from 5.2 up to 7.27m/s the amplitude of turning force components becomes higher with cutting speed.

In Chapter 4 the steady state components of the turning forces was found to present an upward trend with respect to flank wear. The dynamic components however show considerable fluctuations but exhibit a relatively sharp increase towards the end of the tool life. Experimental results for a large set of cutting conditions showed that the trends depicted by Fig. 8.22 and Fig. 8.23 are consistent.

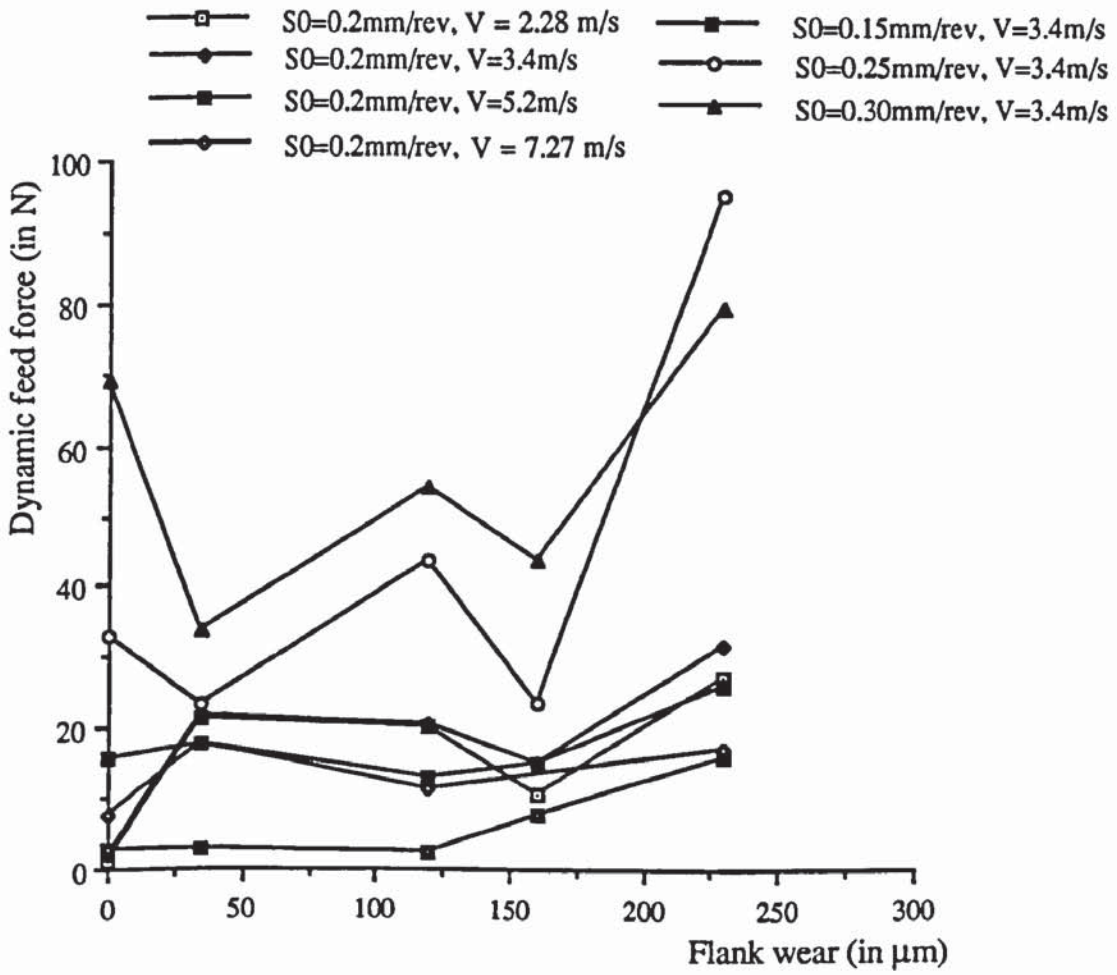

Fig. 8.22 Dynamic feed force versus flank wear.

Moreover, Analysis of the results obtained from a comprehensive test programme (Table) showed that the RMS of the dynamic turning force components bear little informations to the magnitude of the flank wear.

Because the feed and cutting dynamic forces as depicted by Fig. 8.22 and Fig. 8.23 exhibit similar trends with respect to flank wear one may suggest the ratio of these two components as a possible tool wear monitoring factor.

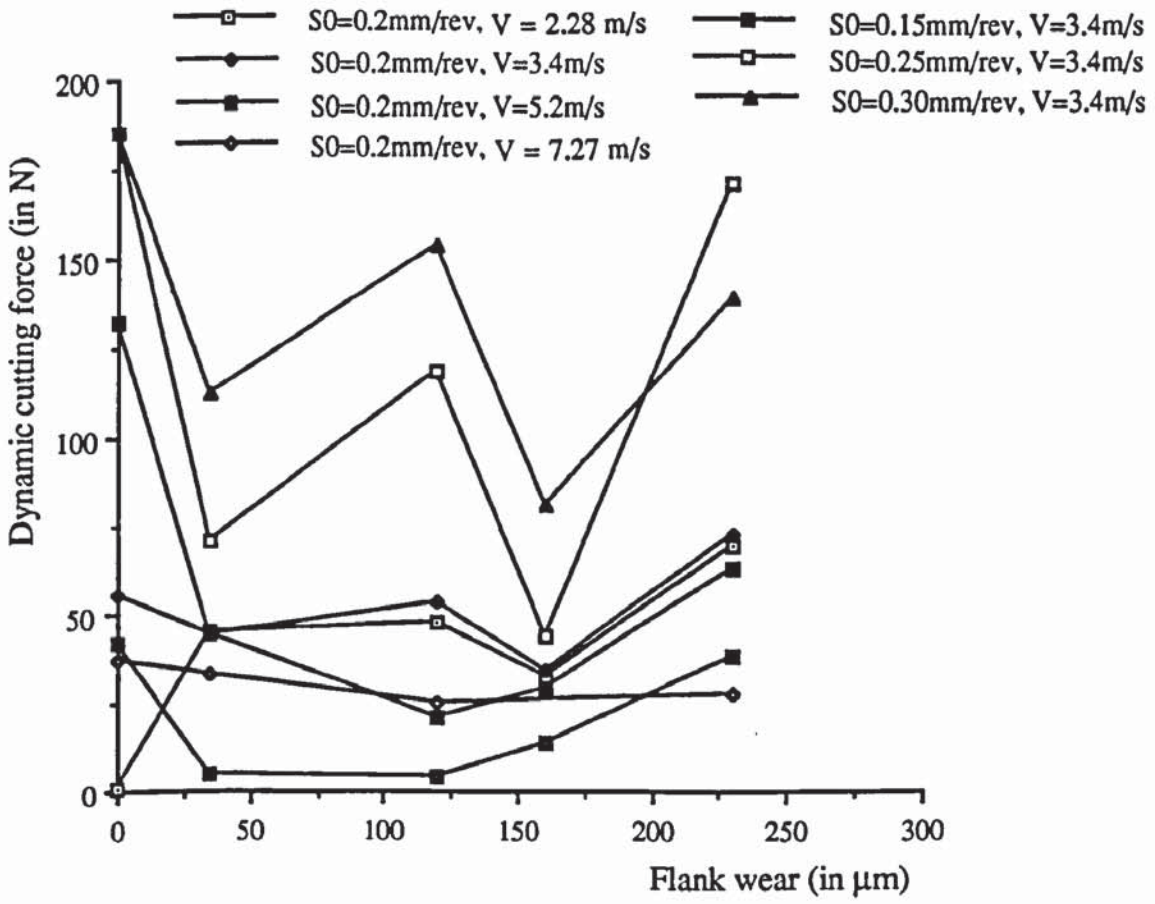

Fig. 8.23 Dynamic cutting force versus flank wear.

The dynamic forces ratio in Fig. 8.18 is defined as ratio between the RMS of dynamic feed force to the RMS of dynamic cutting force. In steady state machining process the shear force ratio C_s and ploughing forces ratio C_p are directly related respectively to the equivalent friction coefficient parallel to the rake and flank of the tool (3.8) and (3.23) respectively. The dynamic ratio however do not present any consistent variation with cutting conditions. As the tool wears, the dynamic forces ratio is varying between 0.3 and 0.6. This shows therefore that both feed and cutting force oscillations are varying by similar proportions with flank wear. No consistent variations with wear are found and thus the dynamic forces ratio is not suitable for tool wear monitoring.

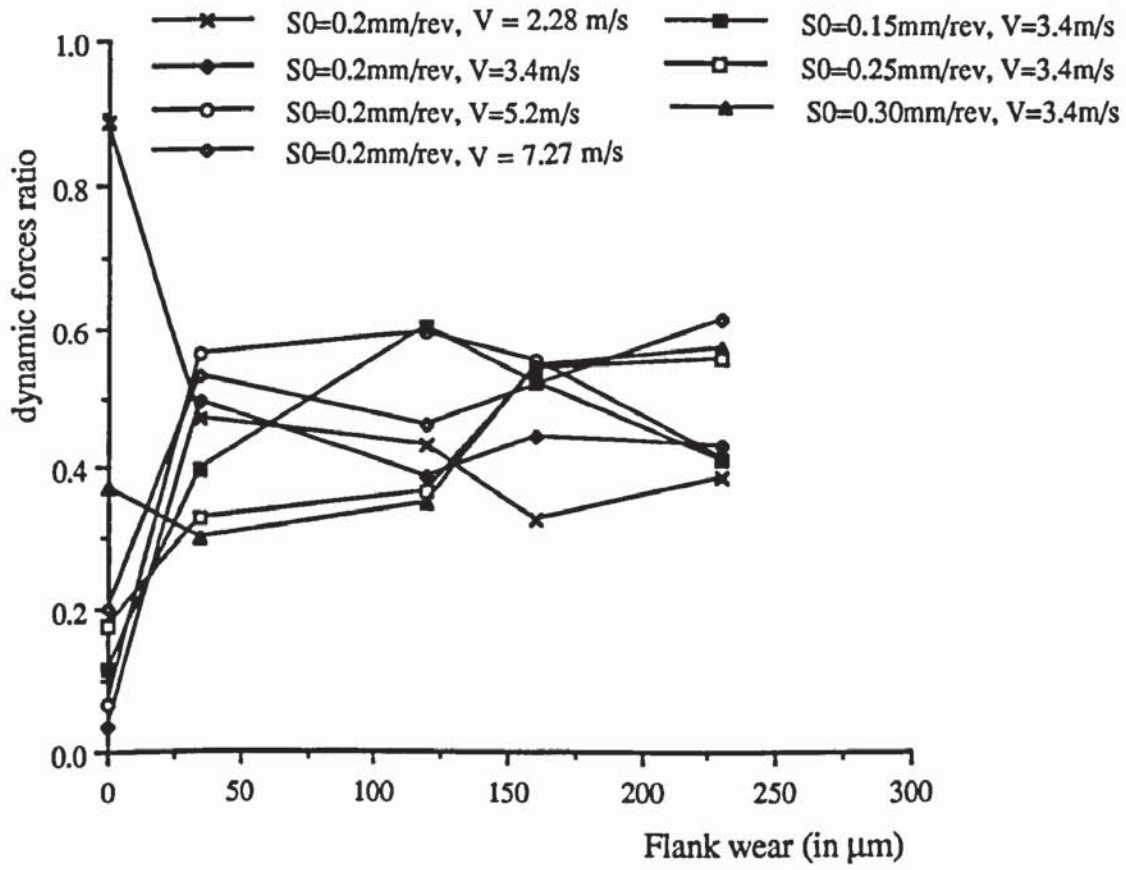

Fig. 8.24 Dynamic forces ratio versus flank wear.

The results discussed above showed that neither the RMS of tool vibration nor the RMS of dynamic turning force components nor dynamic forces ratio are suitable for an on–line flank wear monitoring system. Similar conclusions regarding to the relationship between dynamic force and tool wear were drawn by Lee *et al.* (1989) and Guang *et al.* (1984). The variations in dynamic components of turning forces may be attributed to the random fashion in which the tool meets hard spots in work material. Furthermore, when the tool wear is increased the cutting configuration is changed accordingly and other phenomenons like changes in dynamic damping and stiffness of the machining system are taking place in same time. The dynamic damping has received more attention by several workers than dynamic stiffness even though in practice it is much easier to act on stiffness than damping. It is known that the regenerative effect as well as tool wear act as negative feedback to the system thus leading the machining instability. This is attributed to the introduction of negative damping by these factors which results in smaller effective damping of the cutting system.

8.7.3. Frequency response function (FRF) of the cutting process

The frequency response of cutting process is defined as the ratio between the output and the input in frequency domain. Here the input to the cutting system is the tool acceleration whereas the output is the measured turning force components. The measured forces are the output of the piezo–electric dynamometer. Several studies were concerned with the analysis of the frequency response of the cutting process. Rao (1986) defined a ratio between the amplitude of the dynamic force and the tool displacement at the tool holder natural frequency as an index to monitor flank wear. Moreover, Lee *et al.* (1989) found that the component of the dynamic cutting force at natural frequency of the tool holder bears useful information about tool wear and tool

chipping. In both analyses no informations were reported about the resolutions used in determining these components. In practical conditions to measure a component at given frequency is remote to be possible and any reading is done with definite resolution depending on the number of reading points and band of frequency of interest.

In additions as the tool wear increases the contact area between the cutting edge and workpiece material is increasing. This increase in contact surface results in a variations in the effective damping and stiffness. The forces on the guide-lines are increasing with flank wear which can lead to higher stiffness and smaller damping. The decrease in damping increases the amplitude of tool vibration while an increase in effective stiffness decreases the effective natural frequency of the machining system. This is to say that the effective natural frequency of the machining is affected by flank wear.

Analysis of the experimentally measured acceleration and forces in 8.5 showed a frequency band of interest around the natural frequency of the tool holder–tool post system. Further detailed analysis of cross spectrum of acceleration and force signals and cepstrum showed no correlation with flank wear. However the transfer function was found to bear good informations about flank wear. In stead of using only one frequency component which may lead to errors because of any shift in frequency, in this thesis the area under the FRF function or in other word the power contained in the FRF is considered in a band of frequency. If f_{min} and f_{max} are respectively the minimum and maximum frequency of interest, the power contained in frequency response function $H_{\gamma F}$ within this band is determined as:

$$\text{Power between } f_{min} \text{ and } f_{max} = \int_{f_{min}}^{f_{max}} H_{\gamma F}\, df = \Delta F \sum_{f_{min}}^{f_{max}} H_{\gamma F} \qquad (8.18)$$

Where $H_{\gamma F}$ is the the FRF of the cutting process in which the acceleration γ is the input and the force (F_x or F_z) is the output. ΔF is the frequency resolution.

Two bands of frequency were considered; the first is for the full range which is from 0 up to 6.5kHz and the second concentrate upon the region of the natural frequency of the cutting system which is defined between 3166 and 3403Hz.

(8.18) is used to determine the energy of the FRF for both frequency bands and sample of the obtained results is shown in Fig. 8.25 to Fig. 8.28.

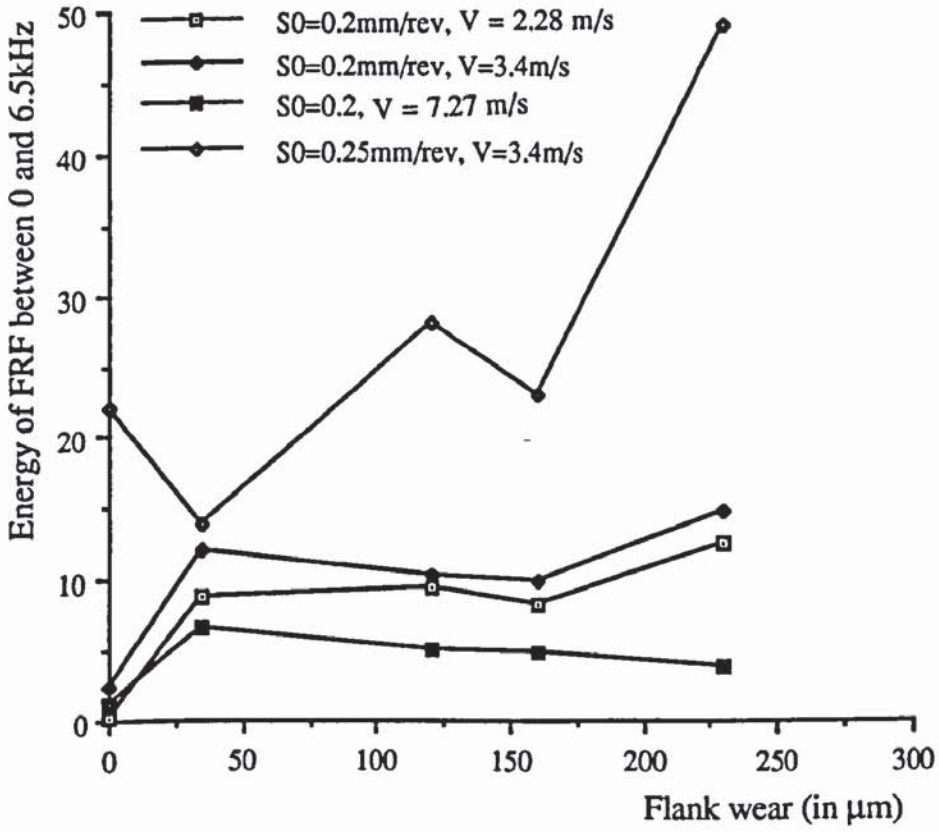

Fig. 8.25 Energy of the FRF in feed direction between 0 and 6.5kHz.

It is shown that the energy contained in the FRF tends to increase with flank wear. However oscillations are most observed at medium range of flank wear values and a sharp increase is exhibited near the life end of the cutting tool. It is worth noticing that the variations observed in the signals are similar between 0 and 6.5kHz or 3.16 and 3.4kHz. This shows that the variation in the energy of the FRF is dominated by the band of frequency near the natural frequency of the cutting system.

Under stable cutting conditions the oscillations in the FRF energy are relatively small whereas under unstable conditions (V=3.40m/s, S_0=0.25mm/rev) there is these oscillations become much higher.

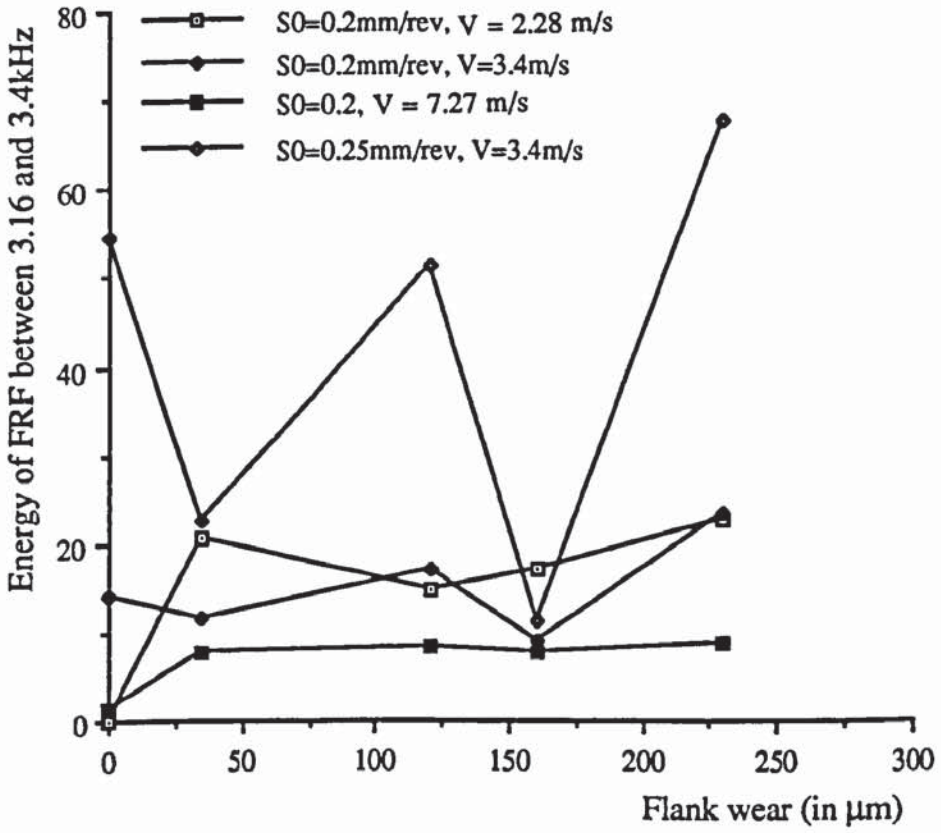

Fig. 8.26 Energy of the FRF in cutting direction between 0 and 6.5kHz.

Comparison between Fig. 8.25 and Fig. 8.27 and between Fig. 8.26 and Fig. 8.28 shows that the energy contained between 3.16 and 3.4kHz represents about 20% of the energy contained in the FRF between 0 and 6.5kHz when the cutting edge is new. As the tool wear increases the increase in the energy of the FRF is much higher within 3.16–3.4kHz and can reach up to 92% of the energy of FRF over 0 to 6.5kHz band.

An increase in the FRF with flank wear means that when the flank wear is increased the cutting system becomes sensitive to tool acceleration and any small increase in the latter results in large increase in the turning force components. Therefore, when the

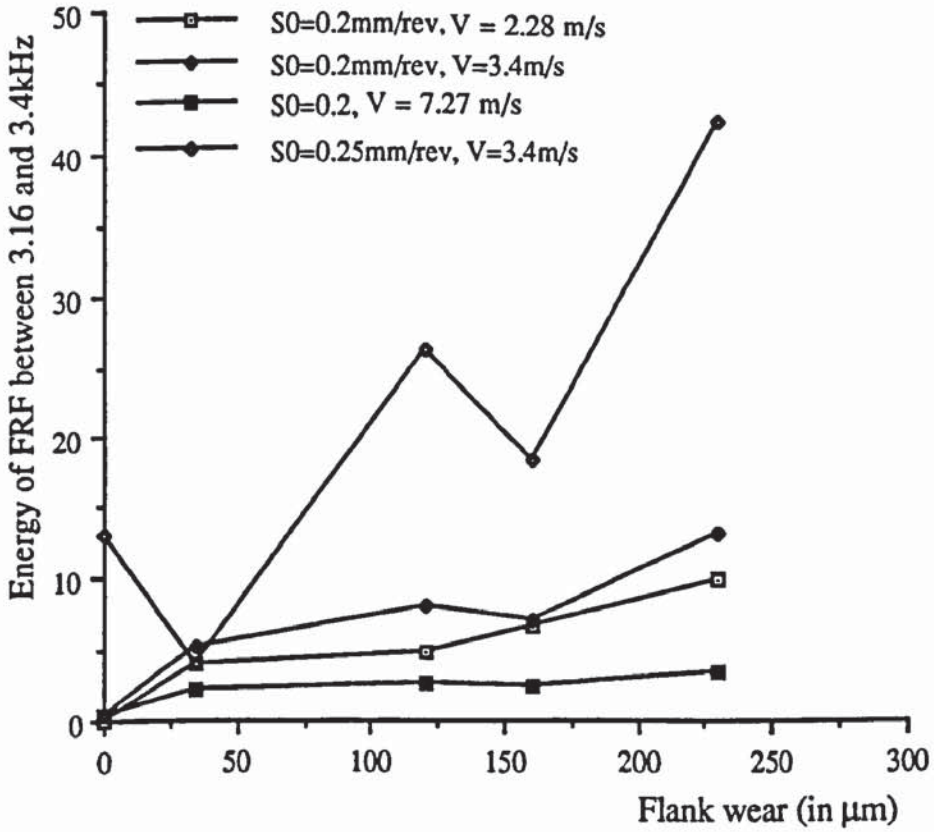

Fig. 8.27 Energy of the FRF in feed direction between 3.16 and 3.4kHz.

tool is affected by tool wear the contribution of tool vibration to machining forces is higher and more emphases is to be given to tool vibration. Steady state feed and cutting forces are predicted basically on geometric considerations and thus the error of prediction because of neglecting the effect of tool vibration is higher for advanced wear levels. This henceforth shows the advantage of considering the dynamic turning process for wear monitoring rather than steady state considerations.

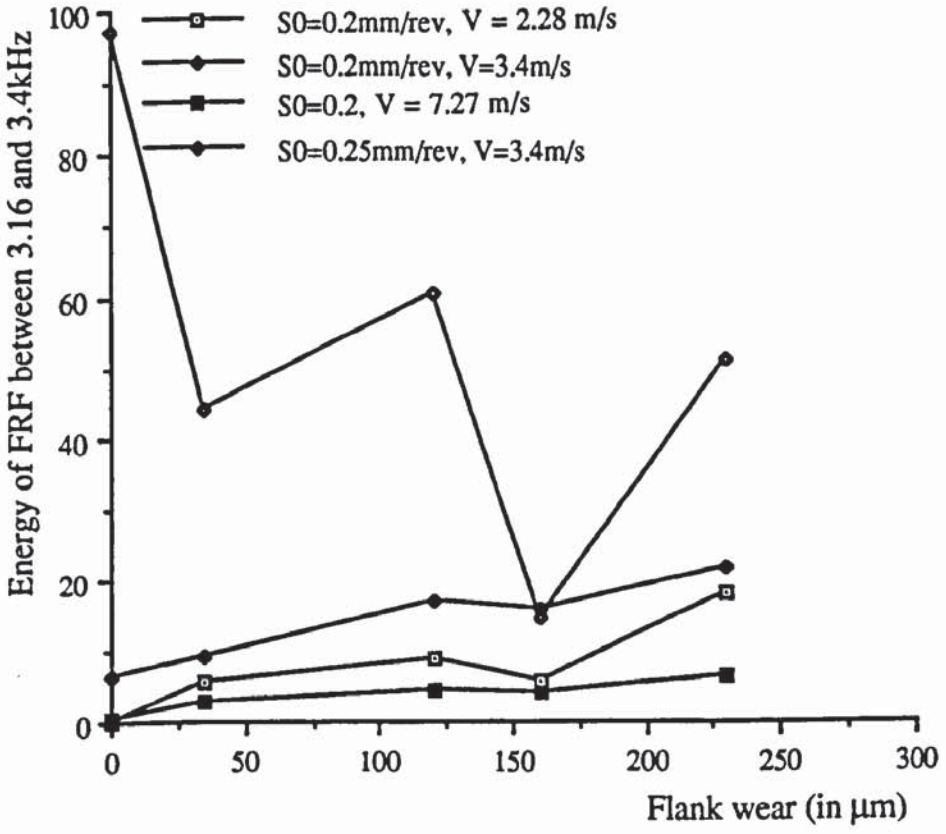

Fig. 8.28 Energy of the FRF in cutting direction between 3.16 and 3.4kHz.

The rapid increase observed between 3.16 and 3.4kHz than over the full range of frequency of interest together with the similar variations observed in these bands led to consider the ratio of the FRF energy within 3.16–3.4kHz to the energy of FRF between 0 and 6.5kHz in both feed and cutting direction. This ratio is called in this thesis IPR (Inertance Power Ratio) and is proposed as tool wear monitoring factor as is discussed in the following section.

8.7.4. Flank wear monitoring factor

Spectral analysis of the tool vibration and turning force components led to define a flank wear monitoring factor named inertance power ratio (IPR). This parameter represents the ratio between the power of the inertance signal contained in 3.16–3.4 kHz to that contained in 0 – 6.5kHz (8.19). The IPR obtained for the cutting direction showed no consistent relationship with flank wear as depicted in Fig. 8.30. In vertical direction (Fig. 8.22) this ratio varies in random fashion with flank wear whereas in the feed direction it shows good correlation with flank wear. The IPR in feed direction increases monotonically with flank wear from about 0.2 to 0.9 when the flank wear is varied from 0 up to 230μm. For worn tool the energy of the FRF signal is almost contained between 3.16 and 3.4kHz.

The IPR in feed direction is therefore proposed as flank wear monitoring factor. It is also noticed that this ratio showed similar tendencies when different dynamometer was used. Prior tests conducted using a different piezo–electric dynamometer showed that tool wear can be monitored by means of the IPR defined above at around the natural frequency of that dynamometer.

$$IPR = \frac{\text{power contained in the FRF between 3.16 and 3.40kHz}}{\text{power contained in the FRF between 0 and 6.50kHz}} \qquad (8.19)$$

When tool cutting edge is still new, the contact between work material and cutting tool is very small compared to worn tool. The increase of contact surface increases the amount of deformed material around the tool nose and the ploughing forces thus offering higher amount of resistance to the oscillations. It was shown in Chapter 5 that

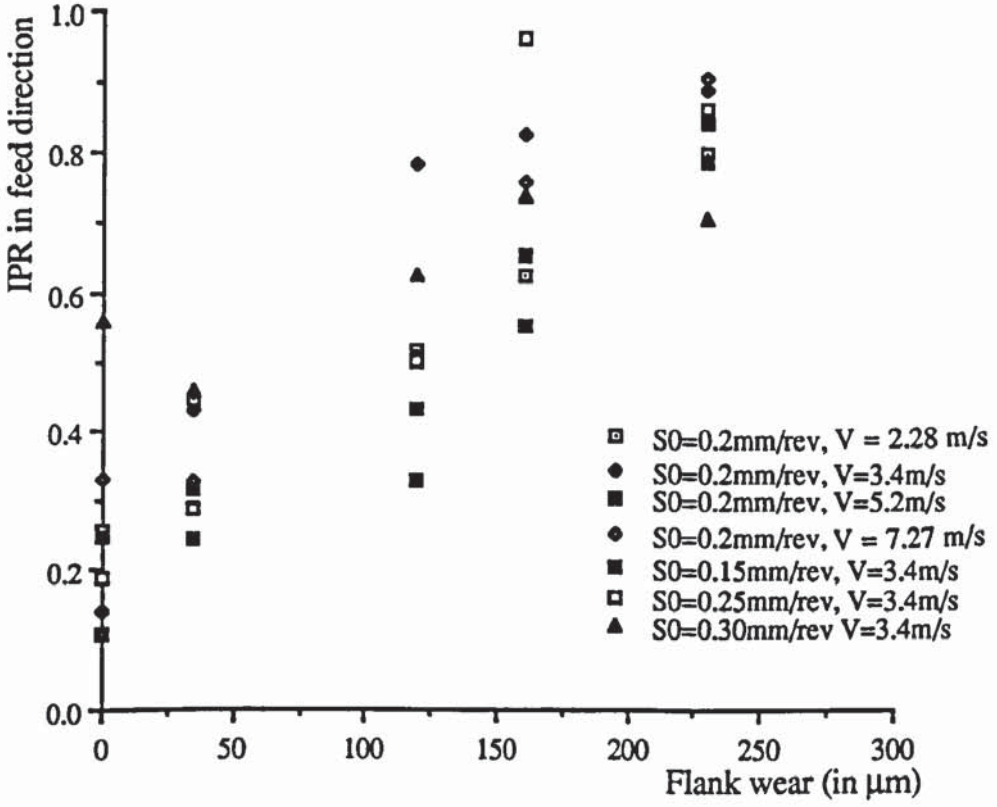

Fig. 8.29 IPR in feed direction.

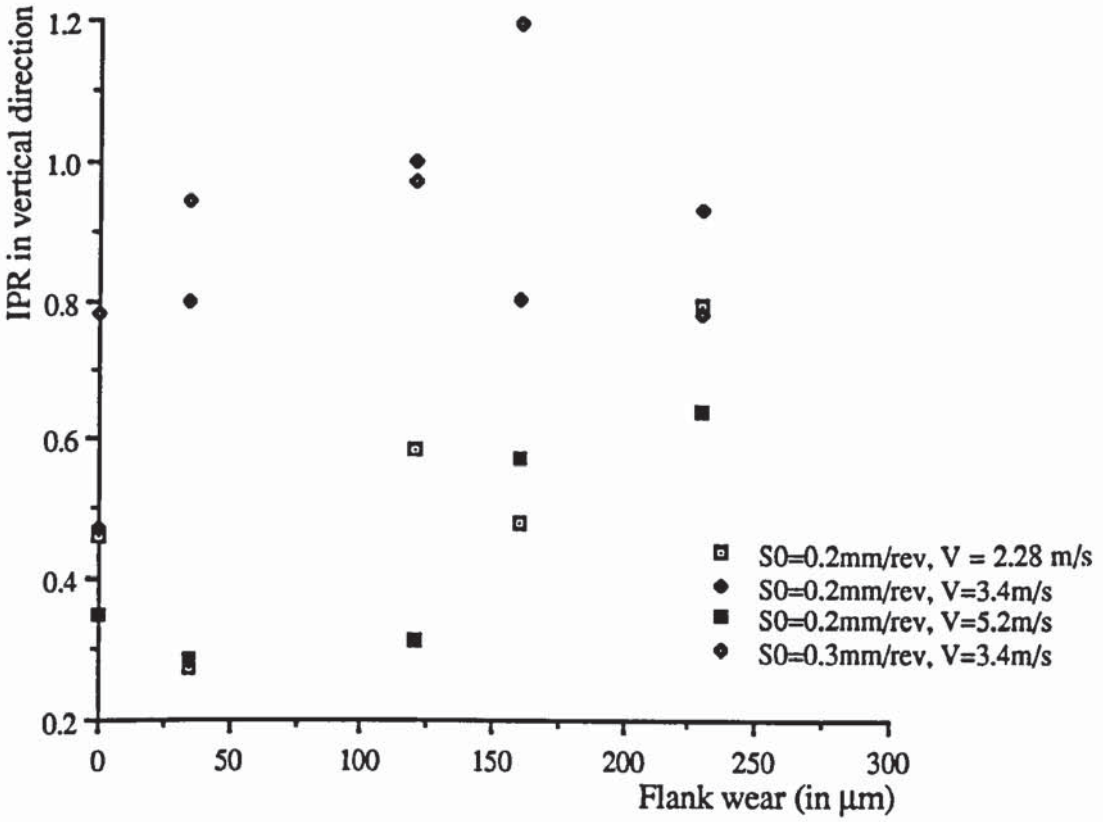

Fig. 8.30 IPR in vertical direction.

a force lagging the shear forces by 90º is introduced by the ploughing process which can be identified as damping force. The increase in the damping introduced by the ploughing forces increases the resistance to the oscillations which causes the dynamic force as measured by the dynamometer to increase more rapidly than the vibration amplitude.

It worthy to notice that the IPR defined above is increasing with wear even under unstable conditions for medium range of tool wear. However as the flank wear

becomes higher a sharp fall is observed. This observation can be used to set a limit for flank wear under lightly unstable conditions.

This ratio has the advantage of being less dependent upon the transfer function of tool holder–tool post system. On the other hand, as shown in Fig. 8.23, the IPR is about 0.9 at the end of the tool life for all the cutting conditions under investigation.

As this work aims to predict the end of tool life, the following section discusses the theoretical prediction of the defined IPR and the

8.8. THEORETICAL PREDICTION OF FLANK WEAR MONITORING FACTOR

As stated in the introductory part of this thesis, the purpose of performing steady state and dynamic cutting analysis, as done from Chapter 3 up to the forgoing chapter, is to provide a tool wear monitoring factor and a model which is able to predict tool life from this factor thus ensuring a satisfactory machining performance of turning operations. The definition of the word "satisfactory" may be associated with machining cost, productivity, surface finish, etc.... As shown shown above, the IPR is increasing with flank wear, but because the tool life is function of the surface quality required, the maximum values of IPR is to be determined by the operator for each different working conditions.

In this section, the developed model is used to predict the the defined IPR for different cutting conditions and predictions are compared to experimental findings. For four speeds and four feeds as summarised in Table 4.1, the IPR is determined as a function of flank wear. Fig. 8.31 to Fig. 8.37 present the corresponding calculated and

experimentally determined IPR. In these figures the solid curves represent the predictions and the signs 'x' the experimental points.

The basic pattern of these curves clearly indicates that the predicted and experimentally determined "inertance power ratio" is increasing with flank wear. This ratio increases significantly from 0.2 up to 0.9 when flank wear increases from 0 to 230μm. Most of the cases the model over estimates the value of IPR which can be attributed to the error in measuring flank wear and accuracy of the model predictions. For the cutting conditions investigated, from the point of view of this thesis, the cutting edge reaches the end of its life when the IPR is above 0.9. This limit can be considered as an alarm for stopping the cutting and changing the tool tip.

For constant feed 0.20mm/rev, the IPR prediction error is observed generally to decrease with cutting speed (Fig. 8.31 to Fig. 8.34). This error reaches its maximum of 29% for cutting speed of 3.40m/s and for flank wear of 120μm. However, the prediction error is decreases as flank wear increases. It is observed, furthermore that this error is decreasing with feed for constant speed of 3.40m/s (Fig. 8.32, Fig. 35 to Fig. 8.37). The maximum error of 16% is obtained for cutting speed of 3.40m/s and feed of 0.15mm/rev.

Again it should be point out that however the discrepancies observed between the experiments and the theoretical predictions, the model is providing satisfactory results for maximum error of 29%. More importantly this error is decreasing with wear which the most critical and important to predict. At advanced level of wear, above 120μm, the error in predicting the IPR does not exceed 16% and most cases is less than 8%.

It can be summarised that the model developed for worn turning tool satisfactorily predicts the dynamic components of the turning force as well as the "inertance power ratio" defined as a parameter to monitor flank wear. For turning with carbide tips, flank wear in normal cutting conditions can be limited to 300μm and therefore an error of 10% will results in a maximum error of 30μm of flank wear. Practically this error is acceptable and in severe cases like in case of expensive workpieces the maximum allowed flank wear can be set to introduce the effect of errors in model predictions.

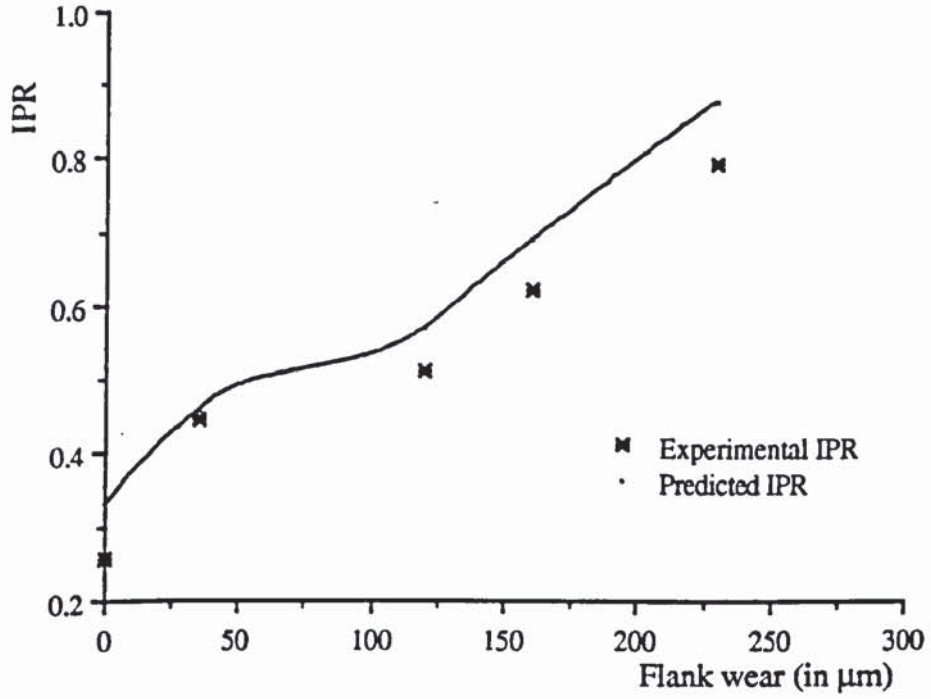

Fig. 8.31 IPR versus flank wear, cutting speed 2.38m/s, feed 0.20mm/rev.

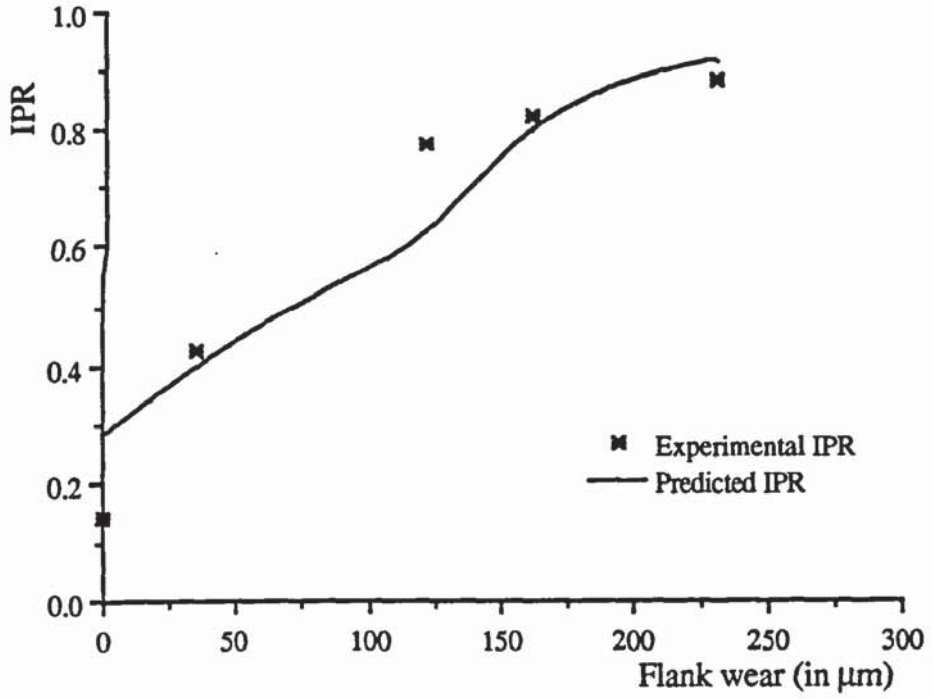

Fig. 8.32 IPR versus flank wear, cutting speed 3.4m/s, feed 0.2mm/rev.

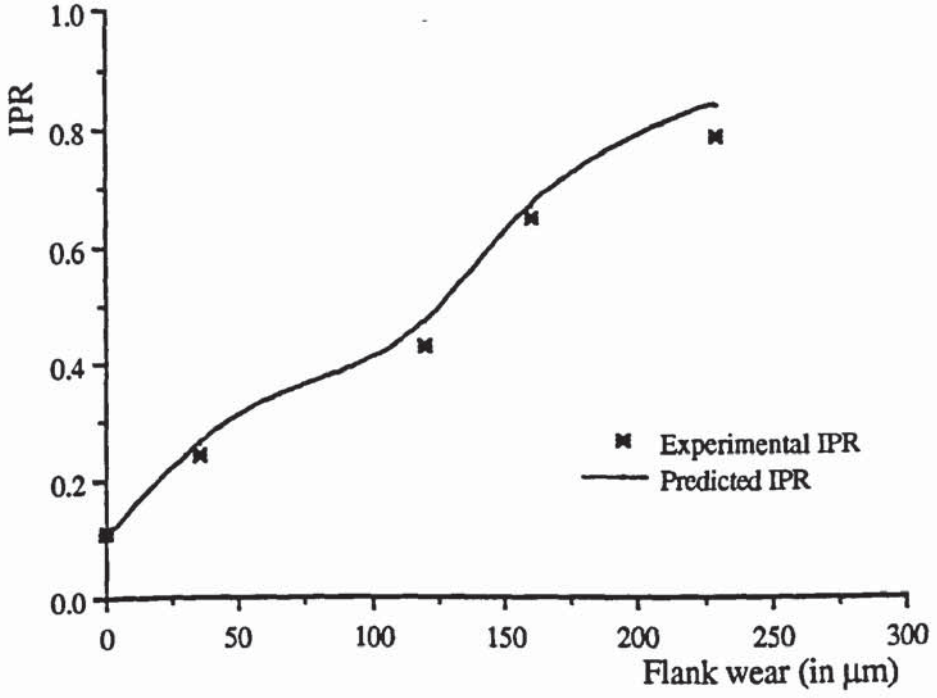

Fig. 8.33 IPR versus flank wear, cutting speed 5.2m/s, feed 0.2mm/rev.

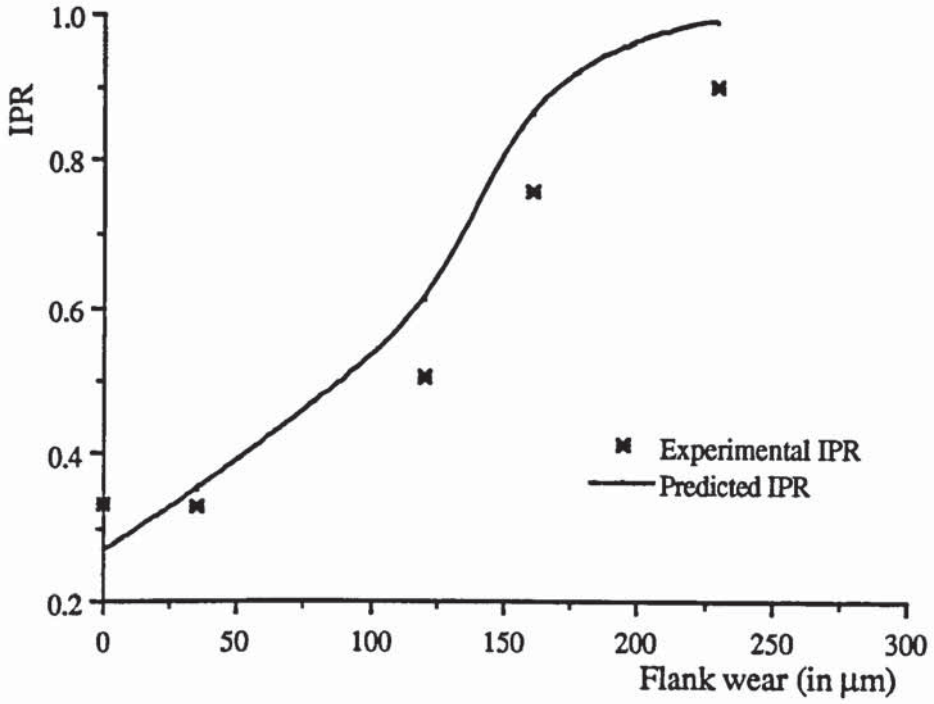

Fig. 8.34 IPR versus flank wear, cutting speed 7.2667m/s, feed 0.2mm/rev.

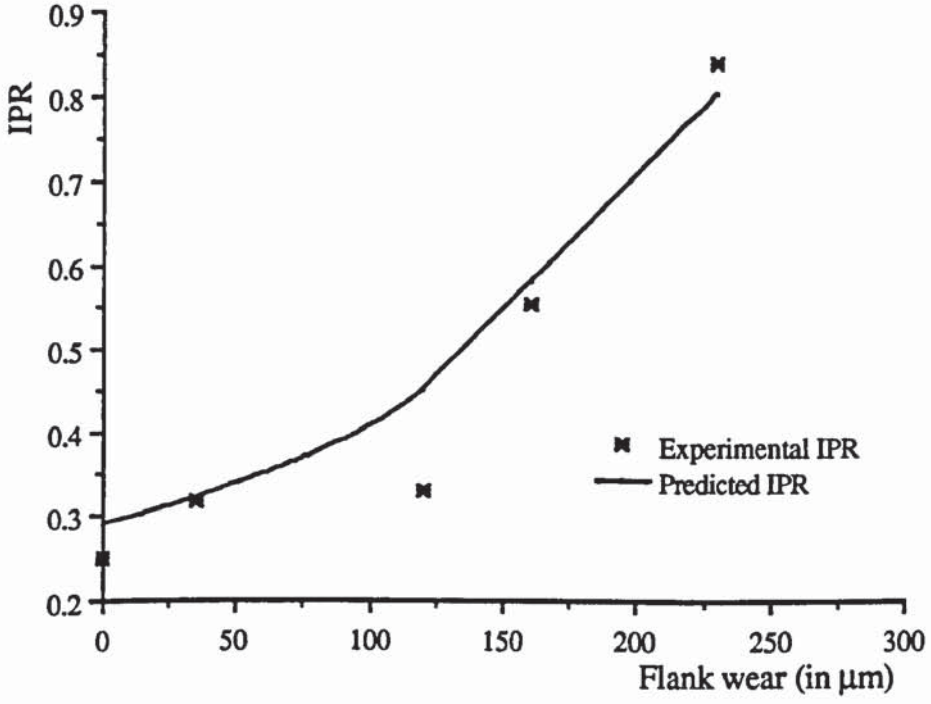

Fig. 8.35 IPR versus flank wear, cutting speed 3.4m/s, feed 0.15mm/rev.

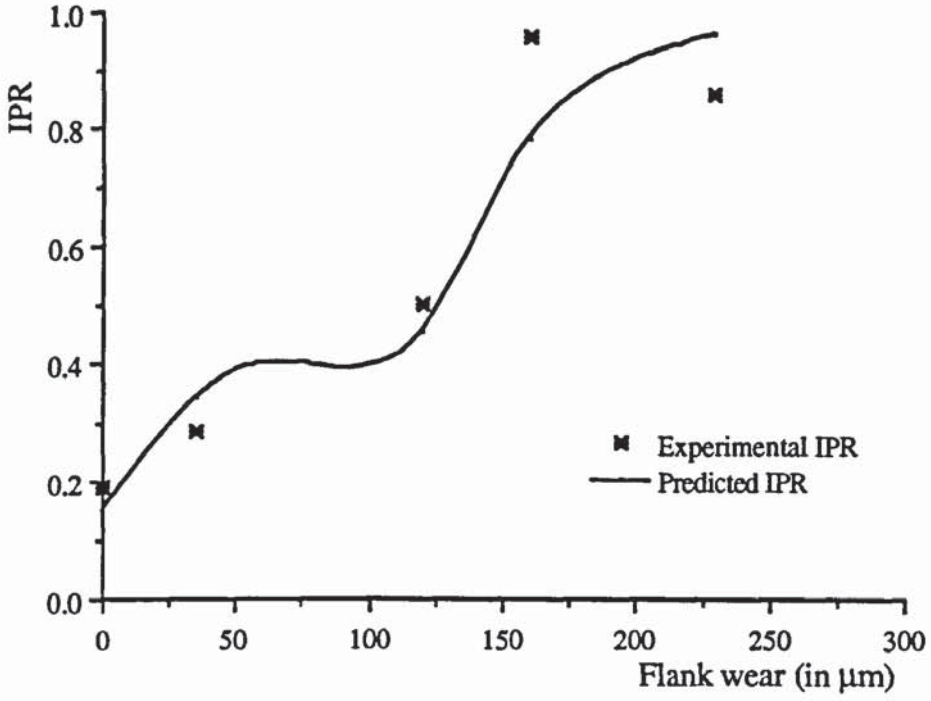

Fig. 8.36 IPR versus flank wear, cutting speed 3.4m/s, feed 0.25mm/rev.

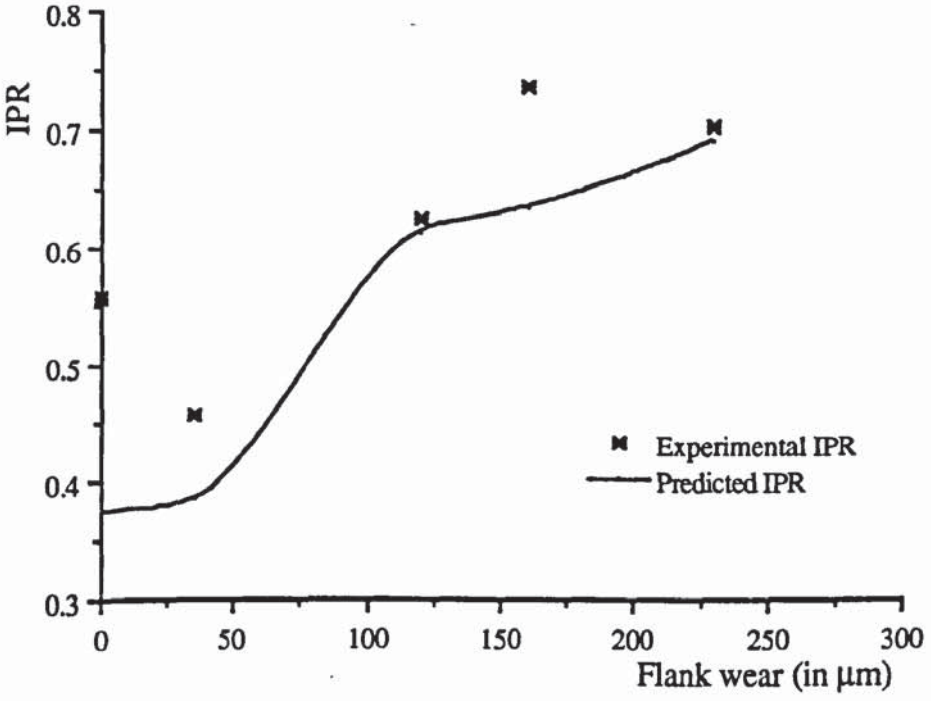

Fig. 8.37 IPR versus flank wear, cutting speed 3.4m/s, feed 0.3mm/rev.

Experimental and predicted results of IPR strongly support the validity of the assumptions made in the development of the present model. In the following section, a flank wear monitoring procedure is presented. This show how the present model and the proposed monitoring factor can be used in practice to monitor flan wear during turning.

8.9. FLANK WEAR MONITORING PROCEDURE

In this chapter a model for turning with worn tool is developed and experimentally tested for a set of feeds and cutting speeds. The model also provides good prediction of the defined factor for flank wear monitoring. However, to determine either the dynamic turning force components or the IPR the flank wear must be known beforehand. Therefore the above results cannot be implemented directly for an on–line flank wear monitoring. It should be pointed out that the present thesis has two major achievement:

– Dynamic modelling of turning.
– Development of flank wear criteria.

The dynamic turning model contributes to a better understanding of metal cutting process and enables to determine the dynamic machining forces only from tool acceleration and cutting conditions. This has the major advantage of not using any dynamometer to measure forces which turns inadequate and expensive. While the flank wear monitoring criteria IPR provides a tool which satisfactorily can be used to predict the end of tool life.

The findings of this work can therefore be applied to the study of the dynamic of machine tools. The model can be directly applied to investigate the behaviour of the

machine structure under different cutting conditions and flank wear levels. However, in tool wear monitoring applications the model considers flank wear as an input parameter rather than an output and henceforth and intermediate processing is necessary.

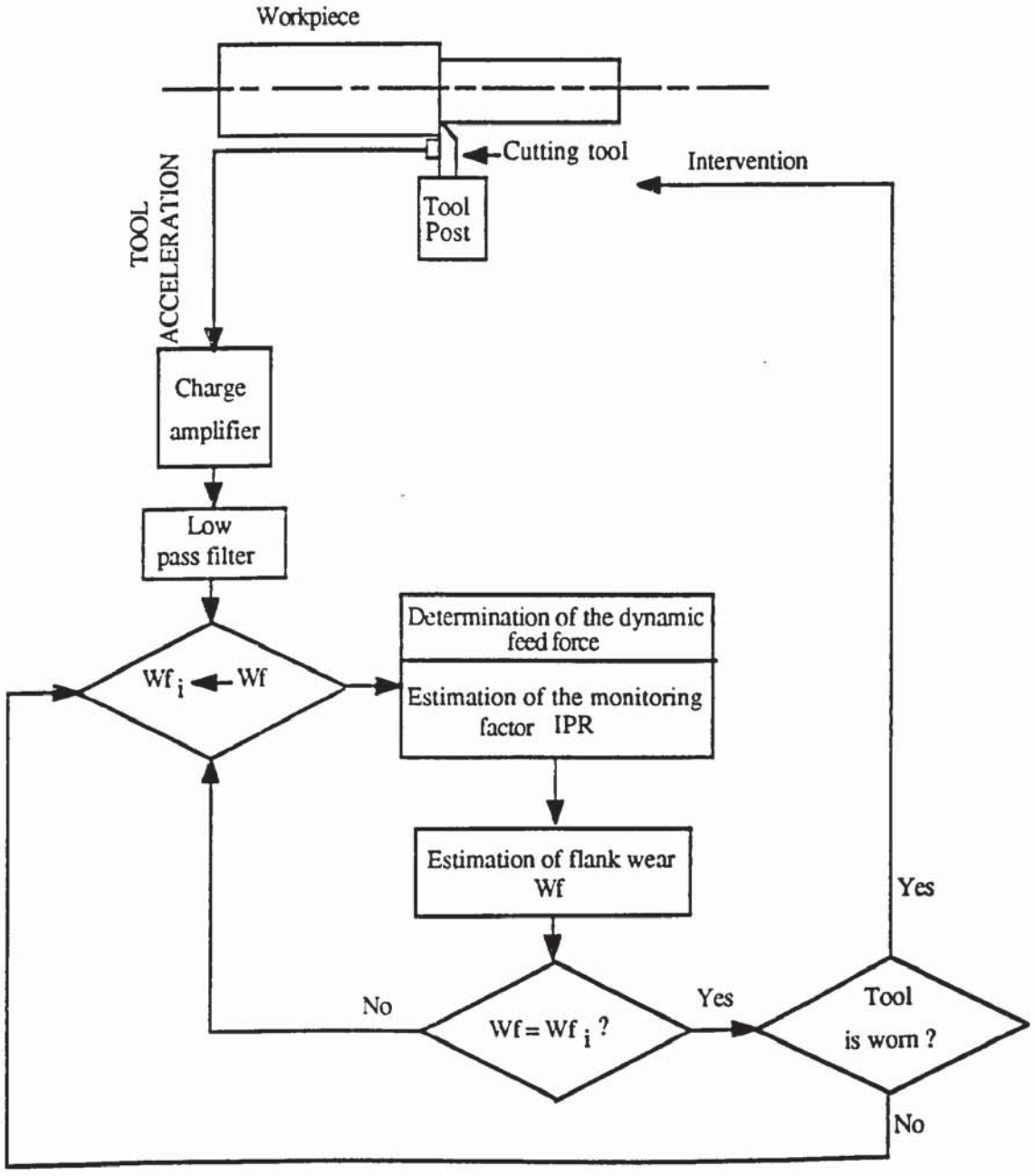

Fig. 8.38 Block diagram for tool flank wear monitoring.

The block diagram shown in Fig. 8.38 outlines the methodology to perform on–line monitoring based on signal detection of tool acceleration and model determination of IPR. Assume that the set of cutting conditions and surface finish for which the wear monitoring system is to be set are known beforehand. For these conditions the IPR can easily be correlated to tool flank wear: IPR = IPR(Wf). This expression can be used to determine flank wear given the value of IPR.

At the beginning of machining process, *the tool is new and then* $Wf_i = 0$ thus the first estimation of the IPR is possible. As the machining progresses, Wf increases and last known value of flank wear is considered to determine the IPR and thereafter the actual flank wear Wf. When the calculated flank wear Wf is equal to the initial value Wf_i used in the IPR determination, the comparison is made with the maximum wear allowed. When this maximum is not yet achieved the cutting process is carried out, otherwise the cutting is interrupted for changing the tool tip.

As the rate of increase of flank wear is too small compared to the rate of sampling, the initial value of flank wear will be close to its real value and therefore the iteration will be fast.

As seen form the block diagram, this monitoring procedure do not involve the use of sophisticated or powerful equipments and is easy to install for practical conditions.

8.10. CONCLUSION

In this chapter, four major subjects involved in the dynamic cutting analysis have been discussed. These are the development of dynamic model for turning and taking account

of flank wear, analysis of dynamic force variations with flank wear, development of criteria of flank wear monitoring and presentation of its monitoring procedure.

From the experimental results some conclusions can be drawn:

– low frequencies are dominating when the cutting edge is still new. However, as the tool wears, more important increase in vibration and turning forces spectra is observed around the natural frequency of the cutting system and higher frequencies become more dominant.

– Analysis of the RMS of the feed, cutting forces and tool acceleration showed no consistent trends with flank wear.

– By considering the cutting process as a system where tool acceleration is the input and machining force components are the output, the FRF was found to bear useful informations about flank wear. Broad increase with wear was found within 3.16–3.4kHz than in any other frequency band between 0 and 6.5kHz. This observation forms the basis of the proposed tool flank wear monitoring factor.

– A ratio between the power of the inertance over 0–6.5kHz to the energy within 3.16–3.4kHz is proposed as monitored factor and named in this thesis inertance power ratio (IPR). The power here is considered as a summation of the magnitude of each harmonic component of the system transfer function (inertance) times the frequency resolution at a specified band of frequency.

– IPR was shown to correlate well with flank wear in the feed direction than in the cutting direction. The feed direction is therefore more suitable for wear monitoring than vertical direction which is in agreement with several previous worker's results (Rao, 1986).

– The major advantage of the IPR is that it is not very influenced by the dynamics of the tool holder and tool post.

– The developed ploughing model for dynamic turning with worn tool yields good predictions of the turning forces components as well as of the monitoring factor. This model can therefore be used for tool flank wear monitoring by predicting the IPR during machining.

– Major contribution of this work is to render possible the determination of the transfer function of the cutting process only be measuring the acceleration at the tool tip. This is turns to be more convenient for practical conditions as it is much more convenient, easier and cheaper to measure tool vibrations than forces in turning.

The developed model showed satisfactorily predictions of dynamic cutting force components and the defined IPR. In work floor conditions the IPR can easily be related by simple expression to flank wear. This enables to determine flank wear which will be used on one hand as input to the model and on the other for deciding wether the tool tip is to be changed or continue machining.

Chapter 9

CONCLUSIONS AND SUGGESTIONS FOR FURTHER WORK

9.1. CONCLUSIONS

The overriding goal of this research has been the modelling of turning process for the purpose of better understanding of cutting process and developing a criteria for tool wear monitoring. The developed model considers, in addition to the shearing process and the forces along the tool rake, the effect of the ploughing mechanism introduced by the work material flowing around the nose of the cutting edge.

This model permits the study of steady state and dynamic turning with new and worn cutting tools. A system tool wear monitoring has been introduced by considering the dynamic oscillations of the turning forces components. It was showed, however that despite the good prediction of force in steady state turning with worn tool, steady state parameters are not of good precision as dynamic parameters where tool wear is more easily and accurately detected. Experiments to built and justify the validity of the model were carried out.

Results from theoretical prediction from the model, for steady state as well as for dynamic turning with new and worn tools, together with experimental and published data are well matched. Therefore, the validity of the present theoretical modelling is confirmed. Important findings and practical significances of this thesis are as follow:

1. In the absence of built–up edge, the metal machining dependent parameters resulting from dry orthogonal steady state cutting of a number of steel grades can be expressed as a mathematical functions of tool geometry and cutting conditions. These expressions, can be determined from few number of steady state tests. As a result of these tests in where cutting force components and chip thickness are measured, steady state cutting data is established over a wide range of cutting conditions. Henceforth, the flow of the work material along the rake and around the tool nose is fully described and the quality of the modelling is justified by the good prediction of turning force components.

2. The flank wear can be modelled as a rubbing surface which introduces more deformations of the work material at the vicinity of the cutting edge.

3. The developed system model has been shown to be very flexible since it includes the effect of cutting conditions, tool geometry and work material upon the dynamic turning process system. As demonstrated in this thesis work, when the relevant time–invariant system parameters are replaced by time–varying system parameters, the resulting system model can be used to investigate the dynamic characteristics of turning with new as well as with worn cutting tools.

4. Analysis of steady state forces showed that steady state feed and/or cutting forces are not suitable for tool wear monitoring. This is attributed to the large variation in the measure of these forces for similar tests.

5. In addition to steady state cutting forces, dynamic components of turning force showed no consistent variation with flank wear that can be used for on–line wear monitoring. However, analysing the transfer function of cutting process, a criteria for

flank wear monitoring is developed. This criteria named "Inertance Power Ratio" (IPR) is defined as a ratio between the power contained in the inertance signal between 3.16 and 3.4kHz and that contained between 0 and 6.5kHz. The latter band of frequency is found to contain the natural frequency of the tool post–tool holder system. The inertance is strongly dependent upon the transfer function between the tool tip and the out–put of the dynamometer. The defined IPR is function of the selected cutting conditions, machine structure, workpiece material being cut and tool geometry. Nevertheless, because almost 80% of the inertance power is contained between 3.16 and 3.4kHz the defined IPR is much less dependent upon the dynamics of the machine structure. Good agreement between predicted and experimentally determined IPR were obtained.

6. A procedure for on–line flank wear monitoring was presented. The IPR is monotonically increasing with flank wear and an expression of flank wear as function of IPR can be easily obtained.

The major contribution of the present work is a development of model which predicts dynamic and steady state forces for new as well as for worn tool when tool vibration is measured. The modelling of the dynamic turning process based upon random vibration of cutting tool thrown a new light on microscopic aspects of cutting mechanics by bringing together vibration and turning forces.

9.2. RECOMMENDATIONS

Recommendations for future consideration can be directed towards the following areas:

1. In the development of the model coefficients, the ploughing factor p_s was considered as constant. Knowledge of this factor is significant in the formulation of the ploughing force components and thus its determination deserves special attention in the future work. Considering that the slop of feed and cutting forces versus flank wear are (w p_s) and (w p_s tan(τ)) similar analysis as conducted in Chapter 3 can be carried out to determine expressions of ploughing factor p_s as function of the cutting conditions.

2. The most significant achievement of the current research is a deeper understanding of the interactions between tool vibration, cutting process and turning forces. As a matter of fact, the cutting tool is considered here as a single degree of freedom which supported by experimental results and other researchers. In bar turning, the tool is vibrating down and upwards in the plan normal to the feed direction resulting in instantaneous variation in the depth of cut.

In order to further study the dynamic characteristics of the cutting process by including the dynamic variation of the uncut chip thickness and of the depth of cut a model of tool holder and tool post system with two degrees of freedom is needed. In this analysis the effect of the side angle of the tool can also be included. Modal analysis techniques can be used to determine the dynamic characteristics of such system.

3. Expression of flank wear as function of IPR is to be developed in future work. A tool wear system can be implemented based on the corresponding chart in Chapter 9.

REFERENCES

– Albrecht, P. (1960), "New Developement in the Theory of the Metal-Cutting Process. Part1: The ploughing Process in Metal Cutting", *Transaction of the ASME, Journal of Engineering for Industry*, 348–358.

– Albrecht, P. (1965), "Dynamics of Metal Cutting Process" , *Transaction of the ASME, Journal of Engineering for Industry*, **87B**,429–431.

– Altintas, Y. (1992), "Prediction of Cutting Forces and Tool Breakage in Milling From Drive Current Measurements", *Transaction of the ASME, Journal of Engineering for Industry*, **114**, 386–392.

– Arnold, R.N. (1946), "Mechanism of Tool Vibration in Cutting of Steel" *Proceedings Institution of Mechanical Engineers*, **154**, 261–284.

– Aesecularatne, J.A., Hinduja, S. & Barrow, G. (1992), "Optimum Cutting Conditions for Turned Components", *Proc. Instn Mech. Engrs*, **206**, 15–31.

– Bailey, J.A. (1975) " Friction in Metal Machining - Mechanical Aspect", *Wear*, **31**, 243–275.

– Barker, R.W., Klutke, G. & Hinich, M.J. (1993), "Monitoring Rotating Tool Wear Using Higher–Order Spectral Features", *Transaction of the ASME, Journal of Engineering for Industry*, **115**, 23–29.

– Barrow, G., Graham, W., Kurimoto, T. & Leong, Y.F. (1982) "Determination of the Rake Stress Distribution in Orthogonal Machining", *Int. J. M. T. D. R.*, **22**, 75–85.

– Bhaoyal, B.C. (1988), "Vibration Analysis and Monitoring Techniques", *J. Institution of Eng. India*, **68**, 132–137.

– Bitans, K. & Brown, R.H. (1965) "An Investigation of the Deformation in Orthogonal Cutting", *Int. J. Mach. Tool Des. Res.*, **5**, 155–165.

– Boothroyd, G. (1963), "Temperatures in Orthogonal Metal Cutting", *Proceeding IME*, **177**, 789–795.

– Boothroyd, G. (1981), *Fundamentals of Metal Machining and Machine Tools*, International student edition: McGraw-Hill International Book Company.

– Chowdhury, I., Sadek, M.M. & Tobias, S.A. (1969), "Determination of the Dynamic Characteristics of Machine Tool Structure", *Proceeding of Int. Mech. Eng.*, **184**, 69–70.

– Clifton, R.J., (1983) "Dynamic Plasticity" *Transaction of the ASME, Journal of Applied Mechanics* , **50**, 941–952.

– Cook, N.H. (1959), "Self Excited Vibrations in Metal Cutting", *Transaction of the ASME, Jounal of Engineering for Industry*, **81**, 183–186.

– Danai, K. & Ulsoy, A.G. (1987), "A Dynamic State Model for On–Line Tool Wear Estimation in Turning" *Transaction of the ASME, Journal of Engineering for Industry*, **109**, 396–399.

– Das, M.K. & Tobias S.A. (1967), "The Relation Between the Static and the Dynamic Cutting of Metals", *Int. J. Mach. Tool Des. Res.*, **7**, 63–89.

– Dewhurst (1978) "On the Non–Uniqueness of the Machining Process" *Proc. R. Soc.*, London, series A360, 587–610.

– Doi, S. & Kato, S. (1956) "Chatter Vibration of the Lathe Tools", *Transaction of the ASME, Jounal of Engineering for Industry*, **78**, 1127–1134.

– Eggleston D.M., Herzog R. & Thomsen E.G. (1959), "Observations on the Angle Relationships in Metal Cutting", *Transaction of the ASME, Journal of Engineering for Industry* , 263–279.

– Eggleston, D.M., Kobayashi, S., Herzog, R.P. & Thomsen, E.G. (1960), "A Critical Comparison of Metal-Cutting Theories with New Experimental Data", *Transaction of the ASME, Journal of Engineering for Industry* , 333–347.

– Enahoro, H.E. & Oxley, P.L.B. (1966), "Flow Along Tool–chip Interface in Orthogonal Metal Cutting", *Journal of Mechanical Engineering Science*, **8**(1), 36–41.

– Endres, W.J., Sutherland, J.W., DeVor, R.E., & Kapoor, S.G. (1991) "A Dynamic Model for the Cutting Force System in the Turning Process" *Transaction of the ASME, Journal of Engineering for Industry*, 193–212.

– Ernest, H. & Merchant, M.E. (1941) "Chip Formation, Friction and High Quality Machined Surfaces: Surface Treatment of Metals", *American Society of Metals, N.Y.*, **29**, 299–328.

– Evans, L. (1987), "Monotoring of Wear of High Speed Steel end Mills-- Some Practical considerations", *Carbide tool Journal*, 19–23.

– Ewins, D.J. (1984), "*Modal Testing– Theory and Practice*", Research Studies Press.

– Field, M., & Merchant, M.E., (1949) "Mechanics of Formation of the Discountineous Chip in Metal Cutting" *Transaction of the ASME, Journal of Engineering for Industry*, **71**, 421–432.

– Finnie, I. & Shaw, M.C. (1949) "The Friction in Metal Cutting", *Transaction of the ASME*, 1649–1657.

– Friedman, R. (1963), "Theory and Practice of Adaptive Control in Drilling", *Rocketdyne North America Aviation, Inc. SAE Reprints* Nº650763.

– Goforth, R.E. & Kulkanni, A. (1983), "In Process Tool life Evaluation by Force Ratio Analysis", *Proc. of the ASME*, Winter annual meeting, Boston, Mass.

– Hahn, R.S. & Worcester, M. (1953), "Metal Cutting Chatter and Its Elimination", *Transaction of the ASME, Jounal of Engineering for Industry*, **75**, 1073–1080.

– Hamdan, M. N. & Bayoumi, A.E. (1989), "An Approach to Study the Effects of Tool Geometry on the Primary Chatter Vibration in Orthogonal Cutting", *Journal of sound and vibration*, **128**(3), 451–469.

– Haslam D. & Rubenstein C. (1970), "Surface and Subsurface Workhardening Produced by the Planning Operations", *Annals of the CIRP*, **17**, 369-372.

– Hebingotham, W.B., Gogia, S.L. (1961), "Metal Cutting and the Built–up Nose", *Proc. Instn. Mech. Engrs.* **175**(18), 892–902.

– Hinduja S., Petty D.J. & Barrow, G. (1985), "Calculation of Optimum Cutting Conditions for Turning Operations", *Proc. Instn Mech. Engrs*, **199**(2), 81–92.

– Hsu, T. (1967), "Some Aspect of the Dynamic Similarity in Metal Cutting", *Transaction of the ASME, Journal of Engineering for Industry* , 525–529.

–Inasaki, I., Aida, S. & Fukuoka, S. (1987), "Monitoring System for Cutting Tool Failure Using an Acoustic Emission Sensor", *JSME International Journal*, **30**(261), 523–528.

– Iwata, K., Osakada, K. & Terasaka, K. (1984) "Process Modelling of Orthogonal Cutting by the Rigid Plastic Finite Element Method" *Transaction of the ASME, Journal of Engineering for Materials and Technology*, **106**, 132–138.

– Jang, D.Y., Siereg, A. (1992), "Machining Parameter Optimization for Specified Surface conditions", *Transaction of the ASME, Jounal of Engineering for Industry*, **114**, 254–257.

– Jelty, S. (1984), "Measuring Cutting Tool Wear On–line: Some Practical Considerations", *Manufacturing Engineering*, 55–60.

– Jelty, S.K. & Sunny, A. (1987), "A Radiometric Sensor for Untended Turning" Strategies for Automation of Machining: Material & Process, *Proceeding of an Int. Conf.*, Orlando, Florida USA, 5–7 May, 15–23.

– Johnson, G.R., Hoegfeldt, J.M., Lindolm, U.S. & Nagy, A. (1983a) "Response of Various Metals to Large Tortional Strains Over a Large Range of Strain Rates, Part1: Ductile Metals" *Transaction of the ASME, Journal of Engineering for Material Technology*, **105**, 42–47.

– Johnson, G.R., Hoegfeldt, J.M., Lindolm, U.S. & Nagy, A. (1983b) "Response of Various Metals to Large Tortional Strains Over a Large Range of Strain Rates, Part2: Less Ductile Metals" *Transaction of the ASME, Journal of Engineering for Material Technology*, **105**, 48–53.

– Kaneto, T., Sato, H., Tani, Y. & O-hori, M. (1984) "Self-Excited Chatter and its Marks in Turning", *Transaction of the ASME, Jounal of Engineering for Industry*, **106**, 222–228.

– Kannatey–Asibu, E. (1985) "A Transport–diffusion Equation in Metal Cutting and Its Application to Analysis of the Rate of Flank Wear", *Transaction of the ASME, Journal of Engineering for Ind.*, **107**, 81–89.

– Kasahara, N., Sato, H. & Tani, Y. (1992), "Phase Characteristic of Self– Excited Chatter in Cutting", *Transaction of the ASME, Jounal of Engineering for Industry*, **114**, 393–399.

– Kegg, R. L. (1965) "Cutting Dynamics in Machine Tool Chatter: Contribution to Machine–tool Chatter Research", *Transaction of the ASME*, **87B**, 464–470.

– Kegg, R.L. (1978), "Production Experience with Adaptive Control", Cincinnati Milaccon USA, *3rd NC–Robot Automation Conference*, Milan, 20–24.

– Klamecki, B.E. (1985) "Experimental Investigation of a catastroohe Theory Model of Metal Chip Formation", *Transaction of the ASME, Jounal of Engineering for Industry*, **107**, 77–79.

– Knight W.A. (1968) "Application of Universal Machinability Chart to the Prediction of Machine Tool Stability", *International Journal of Machine Tool Design and Research*, **8**, 1–14.

– Kolarits, F.M. & DeVries, W.R. (1991), "A Mechanistic Dynamic Model of End Milling for Process Controller Simulation",*Transaction of the ASME, Jounal of Engineering for Industry*, **113**, 177–183.

– Kopalinsky, E.M. & Oxley, P.L.B. (1984) "An Investigation of the Influence of Feed and Rake Angle on the Ratio of Feed Force to Cutting Force when Machining with Negative Rake Angle Tools", *Annals of the CIRP*, **33**(1), 43–46.

– Koren, Y. (1979) "Design of Computer Control for Manufacturing Systems" *Transaction of the ASME, Jounal of Engineering for Industry*, **101**, 326–331.

– Lau, W.S. & Rubenstein, C. (1972), "The Influence of Flank Wear, Cutting Speed and Cutting Fluid on the Surface and Sub-surface Workhardening Produced in an Orthogonal Planing Operation", *Int. J. Mach. Tool Des. Res.*, **12**, 311–323.

– Lee, E.H. & Shaffer, B.W. (1951) "The Theory of Plasticity Applied to a Problem of Machining", *Journal of Applied Mechanics*, 405–413.

– Lee, L.C., Lee, K.S., & Gan, C.S. (1989), "On the Correlation Between Dynamic Cutting Force and Tool Wear", *Int. J. Mach. Tools Manufact.*, **29**(3), 295–303.

– Liu, C.R. & Barash, M.M. (Nov. 1976), "The Mechanical State of the Sublayer of a Surface Generated by Chip-removal Process, Part 1: Cutting with a Sharp Tool", *Transaction of the ASME, Jounal of Engineering for Industry*, 1192–1203.

– Liu, C.R. & Liu, T.M. (1985), "Automated Chatter Suppression by Tool Geometry Control", *Transaction of the ASME, Jounal of Engineering for Industry*, **107**, 95–98.

– Machinability Data Center (1980), "Machining Data Handbook", Third edition.

– Mackinnon, R. & Wilson, G.E., and Wilkinson, A.J. (1986), "Tool Condition Monitoring Using Multi-component Force Measurements", *Machine Tool Design and Research Conference*, Manchester 17th - 18th Sept., 317–324.

– Malvurn, L.E., (1969), *Introduction to the Mechanics of a Contineous Medium*", Prentice–Hall, Englewood Cliffs, N.J.

– Martin, P., Mutel, B. & Drapier, J.P. (1974), "Influence of Lathe Tool Wear On the Vibrations Sustained in Cutting", *Machine Tool Design and Research Conference*, Manchester, 251–257.

– Marui, E., Ema, S. & Kato, S. (1983a), "Chatter Vibration of Lathe Tools. Part 1: General Characteristics of Chatter Vibration", *Transaction of the ASME, Journal of Engineering for Industry*, **105**, 100–106.

– Marui, E., Ema, S. & Kato, S. (1983b), "Chatter Vibration of Lathe Tools. Part 2: On the Mechanism of Exciting Energy Supply", *Transaction of the ASME, Journal of Engineering for Industry*, **105**, 107–113.

– Masuko M., (1953), "Fundamental Researches on the Metal Cutting. 1- A New Analysis of Cutting Forces", *Transaction Society of Mechanical Engineers*, **19**, 32–39.

– Matias, R.A., Book, W. & Weich, A. (1980), "Adaptive Control: Monitoring and Control of Metal Process", *Proceedings of the Machine Task Force Conf.*, **4**(13), 1–8.

– Matsushima, K., Bertok, P. & Sata, T. (1982), "In-process Detection of Tool Breakage by Monitoring the Spindle Motor Current of a Machine Tool", *ASME Winter Annual Meeting*, 145–153.

– Merchant, M.E. (1945) "Mechanics of Metal Cutting Process", *J. of Appl. Physics*, **16**(5), 267-275.

– Merritt, H.E. (1965), "Theory of Self–Excited Machine Tool Chatter", *Transaction of the ASME, Journal of Engineering for Industry*, **87**, 447–454.

– Merwin, J.E. & Johnson, K.L., (1963) "An Analysis of Deformation in Rolling Contact" *Proc. Inst. Mech. Eng.*, **117**(27), 276–284.

– Minis, I.E., Magrab, E.B. & Pandelidis, I.O., (1990a) "Improved Methods for the Prediction of Chatter in Turning, Part1: Determination of Structural Response Parameters", *Transaction of the ASME, Journal of Engineering for Ind*, **112**, 12–20.

– Minis, I.E., Magrab, E.B. & Pandelidis, I.O., (1990b) "Improved Methods for the Prediction of Chatter in Turning, Part2: Determination of Cutting Process Parameters", *Transaction of the ASME, Journal of Engineering for Ind*, **112**, 21–27.

– Minis, I.E., Magrab, E.B. & Pandelidis, I.O., (1990c) "Improved Methods for the Prediction of Chatter in Turning, Part3: A Generalized Linear Theory", *Transaction of the ASME, Journal of Engineering for Ind*, **112**, 28–35.

– Moriwaki, T. (1984), "Sensing and Prediction of Tool Failure", *Bulletin of the Japan Society of Precision Engineering*, **18**(2), 90–96.

– Moriwaki, T. (1980), "Detection of Cutting Tool Fracture by Acoustic Emission Measurement", *Annals of CIRP*, **29**(1), 35–40.

– Nachtigal, C.L. & Cook, N.H. (1970), "Active Control of Machine –Tool Chatter", *Transaction of the ASME, Journal of Engineering for Industry*, **92**, 238–244.

– Nakajima, K., Ohgo, K. & Owano, T. (1968), "Formation of Built–up Edge During Machining", *Wear II*, 369–379.

– Nigm, M.M., Sadek, M.M. & Tobias, S.A. (1972a) "Prediction of Dynamic Cutting Coefficients from Steady State Cutting Data", *Proceeding Thirteenth International MTDR*, 3–12.

– Nigm, M.M., Sadek, M.M. & Tobias, S.A. (1972b) "Prediction of Dynamic Cutting Coefficients from Steady State Cutting Data", *Annals of the C.I.R.P.*, **21**(1), 97–98.

– Nigm, M.M. & Sadek, M.M. (1977a) "Experimental Investigation of the Characteristics of Dynamic Cutting Process", *Transaction of the ASME, Jounal of Engineering for Industry*, **99**, 410–418.

– Nigm, M.M., Sadek, M.M. & Tobias, S.A. (1977b) "Determination of Dynamic Cutting Coefficients from Steady State Cutting Data", *Int. J. Mach. Tool Des. Res.*, **17**, 19–37.

– Nigm M. M., Sadek M. M., & Tobias S. A. (1977c), "Dimentional Analysis of the Steady State Orthogonal Cutting Process", *Int. J. of Mach. Tool Des. and Res.*, **17**, 1–18.

– Ohgo, K. (1978), "The Adhesion Mechanism of The Built–up Edge and Layer of the Rake Face of a Cutting Tool", *Elsevier Sequoia S.A.*, Lausane, 117–126.

– Okushima, K. & Hitomi, K. (1961) "An Analysis of the Mechanism of Orthogonal Cutting and Its Application to Discontinuous Chip formation", *Transaction of the ASME, Journal of Engineering for Industry* , 545–556.

– Oxley, P.L.B., (1963) "Mechanics of Metal Cutting for a Material of Variable Flow Stress" *Transaction of the ASME, Jounal of Engineering for Industry*, **85B**, 339–342.

– Oxley, P.L.B., (1989), "*The Mechanics of Machining: An Analytical Approach to Assessing Machinability*", John Wiley & Sons, Published by Ellis Hordwood Ltd.

– Rahman, M. & Ito, Y. (1986), "Detection of the Onset of Chatter Vibration", *Journal of Sound and Vibration*, **109**(2), 193–205.

– Rahman, M. (1988), "In Process Detection of Chatter Threshold", *Transaction of the ASME, Jounal of Engineering for Industry*, **110**, 44–50.

– Rao, S.B. (1986), "Tool Wear Monitoring Through the Dynamics of Stable Turning", *Transaction of the ASME, Journal of Engineering for Industry*, **108**, 183–190.

– Rapier, A.C. (1954), "A Theoretical Investigation of the Temperature Distribution in the Metal Cutting process", *Journal of Appl. Phys.*, **5**(11), 400–407.

– Ridley, R.O. (1982), "A Review of the Use of the Power / Torque / Force Measurements for Monitoring Production Cutting Process", *Proceeding MTIRA*, Seminar on Techniques for Unmanned Machining.

– Rubenstein, C.(1976a), "an Analysis of Tool Life Based on Flank–Face Wear, Part 1: Theory", *Transaction of the ASME, Jounal of Engineering for Industry*, 221–225.

– Rubenstein, C.(1976b), "an Analysis of Tool Life Based on Flank–Face Wear, Part 2: Comparison of Theory with Experimental Observations", *Transaction of the ASME, Jounal of Engineering for Industry*, 227–231.

– Rubenstein, C., Lau, W.S. & Venuvinod, P. K. (1985), " Flow of Workpiece Material in the Vicinity of the Cutting Edge", *Int. J. Mech. Tool Des. Res.*, **25**(1), 91–97.

– Sata, T., Matsushima, K., Nagakura, T. & Kono, E. (1973), "Learning and Recognition of the Cutting States by Spectrum Analysis", *Annals of the C.I.R.P.*, **22**(1), 41–42.

– Shaw, M.C., (1984), "*Metal Cutting Principles*", Oxford University Press, Oxford.

– Shi, T. & Ramalingam, S. (1990), "Real–Time Flank Wear Sensing", *Fundamental Issues in Machining*, PED–Vol. 43, Presented at the Winter Annual Meeting of the ASME, Dallas, Texas, nov. 25–30th, 157–170.

– Shi, T. & Ramalingam, S. (1991), "Slip–Line Solution for Orthogonal Cutting with a Chip Breaker and Flank Wear", *Int. J. Mech. Sci.*, **33**(9), 689–704.

– Shield, B.H.L., & Oven, M. (1987), "Gain Selection for Turning Variable Gain Adaptive Control System For Turning", *Transaction of the ASME, Journal of Engineering for Industry*, **109**, 399–403.

– Sisson, T. R., & Kegg R. L. (1969), "An Explanation of Low Speed Chatter Effects", *Transaction of the ASME, Journal of Engineering for Industry*, **91**(4), 951–958.

– Stephensen, D.A. & Wu, S.M. (1988a), "Computer Models for the Mechanics of Three–Dimentional Cutting Process – Part I: Theory and Numerical Method. *Transaction of the ASME, Journal of Engineering for Industry*, **110**, 32–37.

– Stephensen, D.A. & Wu, S.M. (1988b), "Computer Models for the Mechanics of Three–Dimentional Cutting Process – Part II: Results for Oblique End Turning and Drilling. *Transaction of the ASME, Journal of Engineering for Industry*, **110**, 38–43.

– Stevenson, R., (1992) "The Morphology of Machining Chips Formed During Low Speed Quasi–Orthogonal Machining of CA360 Brass and Model for their Formation", *Transaction of the ASME, Jounal of Engineering for Industry*, **114**, 404–411.

– Taibi, S., Penny, J.E.T., Maiden, J.D. & Bennouna, M. (1990), "Monitoring Tool Wear During the Turning Process", Comadem Conference, London, July 16th–19th, 74–79.

– Taraman, K., Swando, R. & Yumauchi, W. (1974), "Relationship Between Tool Forces and Flank Wear", *SME Technical paper*, Nº MR74.

– Titpon, H. (1982), "Techniques of Unmanned Machining" *The Machine Tool Industry Research Association*, One–day Seminar on Techniques of Unmanned Machining, MTIRA, Macclesfield, Cheshire, U.K.

– Tlusty, J. & Andrews, G.C. (1983), "A Critical Review of Sensors for Unmanned Machining", *Annals of the CIRP*, **32**(2), 1–10.

– Tlusty, J. (1985), "Machine Dynamics", Handbook of High Speed Machining Technology, R.I. King, edition Chapman and Hall.

– Thomsen, E. G., Mac Donald, A. G., & Kobayashi, S. (1962), "Flank Friction Studies With Carbide Tools Reveal Sub-layer Plastic Flow", *Transaction of the ASME, Journal of Engineering for Industry*, **84**, 53-62.

– Tobias, S.A., (1965), "*Machine Tool Vibration*", Blackie.

– Tobias, S.A. & Fishwick, W. (1956) "The Vibration of Radial Drilling Machines Under Test and Working Conditions" *Proceeding I. Mech. Eng.*, **170**, 232–250.

– Tomita, N., Cristina, B. (1988), "On–Condition Maintenance of Machinery Based on Vibration Measurement and Frequency Analysis", *Bultinal Institutlui Politechnic*, Bucurasti Seria Macanica, **50**, 97–100.

– Uehara, K. & Kanda, Y. (1984), "Idetification of the chip Formation Mechanism Through Acoustic Emission Measurement", *Annals of CIRP*, **33**(1), 71–74.

– Usui, E. & Shnakashi, T. (1984), "Analytical Prediction of Cutting Tool Wear", *Wear*, **100**, 129–151.

– Venuvinod, P.K., Lan, W.S. & Rubenstein, C. (1990), "Tool Life in Oblique Cutting as a Function of Computed Flank Contact Temperature", *Transaction of the ASME, Journal of Engineering for Industry*, **112**, 307–312.

– Wallace, P. W. & Boothroyd G. (1964), "Tool Forces and Tool-Chip Friction in Orthogonal Machining", *J. of Mech. Eng. Sci.*, **6**(1), 74–87.

– Weller, E.J., Schrier, H.M. & Weichbroot, B. (1969), "What Sound Can Be Expected From a Worn Tool?", *J. of Engineering for Industry*, 525–534.

–Weston, R.H., Harisson, R., Booth, A.H. & Moore, P.R. (1989)."A New Approach to Machine Control", *Computer Aided Eng. Journal*, **6**(1), 27–32.

– William, H.P., Brian, P.F., Saul, A.T. & William, T.V. (1986), *Numerical Recipes: The Art of Scientific Computing*, Cambridge University Press.

– Wolf, W. & Magadanaz, P. (1981), "Feed Force Monitoring for Operation Security and Reliability", *SME Technical Paper*, Sandvik Coromant, Inc., IQ, **81**, Society of Manufacturing Engineers.

– *Wu, D.W. & Liu, C.R. (1985a), "An Analytical Model of Cutting Dynamics. Part* 1: Model Building", *Transaction of the ASME, Jounal of Engineering for Industry*, **107**, 107–111.

– Wu, D.W. & Liu, C.R. (1985b), "An Analytical Model of Cutting Dynamics. *Part 2: Verification", Transaction of the ASME, Jounal of Engineering for Industry*, **107**, 112–118.

– Wu, D.W. (1986), "Governing Equations of the Shear Angle Oscillation in Dynamic Orthogonal Cutting", *Transaction of the ASME, Jounal of Engineering for Industry*, **108**, 281–287.

– Wu, D.W. (1989), "A New Approach of Formulating the Transfer Function for Dynamic Cutting Processes", *Transaction of the ASME, Jounal of Engineering for Industry*, **111**, 37–47.

– Wu, D.W. & Matsumoto, Y. (1990), "The effect of Hardness on Residual Stresses in Orthogonal Machining of AISI 4340 Steel", *Transaction of the ASME, Jounal of Engineering for Industry*, **112**, 245–252.

– Yamazaki, K., Yamada, A. & Sawai, N. (1974), "A Study on Adaptive Control in an N.C. Milling Machine", *Annals of the CIRP*, **23**(1), 153–154.

– Yee, K.W., Blomquist, D.S., Dornfeld, D.A. & Pan, C.S. (1986), "An Acoustic Emission Chip–Form Monitor for Single Point Turning", 26th *MTDR Conf.*, Manshester 17th–18th september, 305–312.

– Yellowley, C.T. & Attintas, Y. (1987), "Strategies and Sensors for the Regognition of Tool Failure and Real Time Identification of Cutting Conditions in Milling and Turning Operations", Strategies for Automation of Machining: Material & Process, *Proceeding of an Int. Conf.*, Orlando, Florida USA, 5–7 May, 181–189.

– Yen, D.W. & Wright, P.K. (1983), "Adaptive Control In Machining – A New Approach Based On The Physical Constraints of Tool Wear Mechanism", *Transaction of the ASME, Journal of Engineering for Industry*, **105**, 31–38.

– Zakaria, A.A. & Elgomayel, I.I. (1975), "On The Reliability of the Cutting Temperature for Monitoring Tool Wear", *Int. J. Mach. Tool Des. and Res.*, **15**, 195–208.

– Zorev, N.N. (1963), "Inter–relation between Shear Process Occuring alomg Tool Face and Shear Plane in Metal Cutting", *Proc. Int. Prod. Eng. Res. Conf. ASME*, Pittsburgh, 42–49.

– Zorev, N.N. (1966), "*Metal Cutting Mechanics*", English edition, Pergamon Press Ltd.

Appendix A1

EFFECT OF TOOL NOSE ON TURNING FORCE COMPONENTS

Albrecht (1960) conducted an extensive experimental work to relate the radius to the rake and flank angles of the cutting edge of an high speed steel (HSS) tool. He showed that even with a very careful grinding, the sharpness of the tool is limited and a finite radius exists at the cutting edge. Experimental results led to express an analytical expression between the geometry of the tool and the tool nose as:

$$R = 13.208\ 10^{-6} \tan^2\left(\frac{\frac{\pi}{2} - \alpha - \gamma}{2}\right) \qquad (A1.1)$$

R is the tool nose radius (in m).

For an HSS tool with similar geometry as the carbide tools used in this research (α = 5º and γ = 6º) the expected sharpness as determined by A1.1 is: R = 9 µm. For carbide tools this sharpness is smaller than that of an HSS tool because of the accuracy of the manufacturing process used for carbide tools.

In Chapter 3 a complete expression of the force acting on the flank of the tool is developed ((3.19) and (3.20)). These expressions are used to determine the variation of the ploughing force with tool nose R. Fig. A1.1 represents the variation of

the ploughing force components ($P_x - P_{x0}$) and ($P_z - P_{z0}$) as the radius of the cutting edge is increased from 0 to 3.5μm. Where: P_x and P_z are the ploughing forces in feed and cutting direction respectively. P_{x0} and P_{z0} are ploughing forces in feed and cutting direction on a tool with nil nose.

Fig. A1.1 show that ploughing force increases more rapidly with the radius of cutting edge than in cutting direction. The ploughing force in cutting direction is almost unaffected by tool nose. The broad increase of ploughing force in feed direction is because the material deformation is in the direction of feed. Because of the accuracy in measurements and repeatability of the forces measure, It is however shown that, for small radius of tool nose, the ploughing force can be represented by its limit when R tends to 0 as given by (3.21) and (3.22).

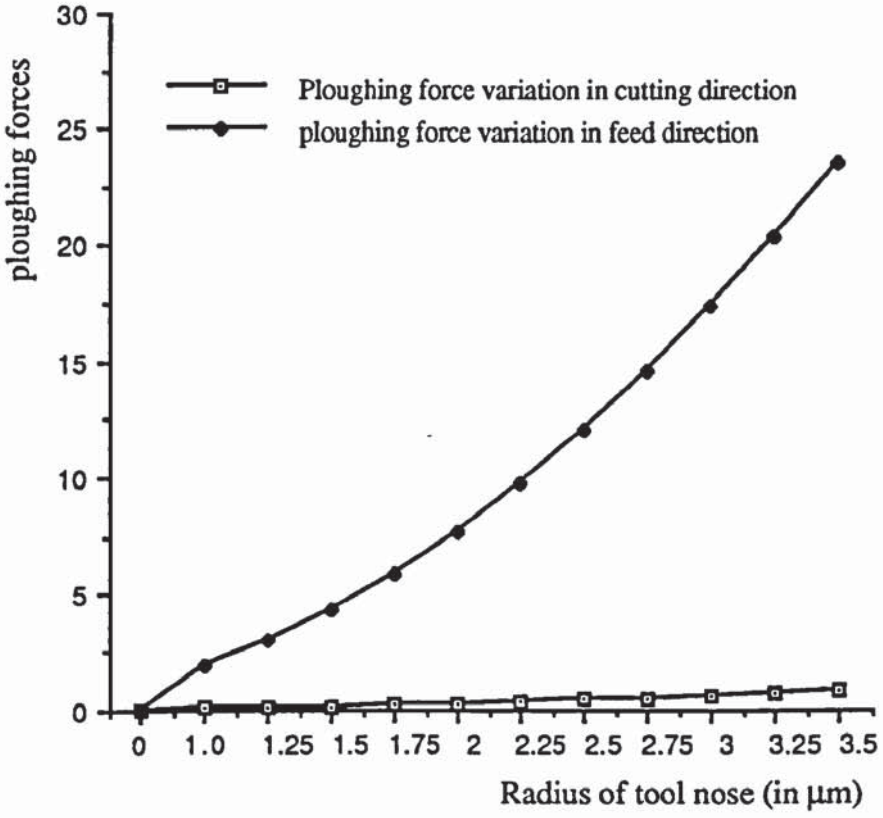

Fig. A1.1 Variation of ploughing force components with tool nose radius.

Appendix A2

VARIATION OF THE DYNAMIC CUTTING PARAMETERS

The following appendix describes a detailed expressions for the variations of the dynamic equivalent mean friction coefficient μ, the friction coefficient μ' and the shear angle ϕ' during dynamic turning with a constant rake angle with respect to the variation of chip thickness, cutting speed and rake angle.

In chapter 5 ((5.61) to (5.64)), the above expressions were established:

$$\mu = M(V_i, S_i, \alpha_i) \qquad (A2.1)$$

$$\mu' = M(V', S_i, \alpha_i) \qquad (A2.2)$$

$$\phi' = \Phi(V', S_i, \alpha_i) \qquad (A2.3)$$

Where V', V_i, S_i and α_i are given as:

$$S_i = (S_0 + x - x_0) \frac{\sin(\phi + \delta)}{\sin(\phi)} \qquad (A2.4)$$

$$V_i = \frac{V}{\cos(\delta)} + \frac{\dot{x} \cos(\alpha) \cos(\phi - \alpha)}{\sin(\phi + \delta)} \qquad (A2.5)$$

$$V' = \frac{V}{\cos(\delta)} \qquad (A2.6)$$

$$\alpha_i = \alpha + \delta \qquad (A2.7)$$

The functional relationships M and Φ of the mean friction angle and the mean shear angle in terms of the cutting speed, the chip thickness and the rake angle are given as was developed in chapter 3 as:

$$M(V, S, \alpha) = \frac{C_s(V, S, \alpha) + \tan(\alpha)}{1 - C_s(V, S, \alpha)\tan(\alpha)} \qquad (A2.8)$$

$$\Phi(V, S, \alpha) = \tan^{-1}\left[\frac{r(V, S, \alpha)\cos(\alpha)}{1 - r(V, S, \alpha)\sin(\alpha)}\right] \qquad (A2.9)$$

Partial differentiations of f', m and m' with respect to the cutting parameters yield the following expressions:

$$\frac{\partial \phi'}{\partial S_0} = \frac{\partial \Phi(V', S_i, \alpha_i)}{\partial V}\frac{\partial V'}{\partial S_0} + \frac{\partial \Phi(V', S_i, \alpha_i)}{\partial S}\frac{\partial S_i}{\partial S_0} + \frac{\partial \Phi(V', S_i, \alpha_i)}{\partial \alpha}\frac{\partial \alpha_i}{\partial S_0} \qquad (A2.10)$$

$$\frac{\partial \phi'}{\partial \alpha} = \frac{\partial \Phi(V', S_i, \alpha_i)}{\partial V}\frac{\partial V'}{\partial \alpha} + \frac{\partial \Phi(V', S_i, \alpha_i)}{\partial S}\frac{\partial S_i}{\partial \alpha} + \frac{\partial \Phi(V', S_i, \alpha_i)}{\partial \alpha}\frac{\partial \alpha_i}{\partial \alpha} \qquad (A2.11)$$

$$\frac{\partial \phi'}{\partial \psi} = \frac{\partial \Phi(V', S_i, \alpha_i)}{\partial V}\frac{\partial V'}{\partial \psi} + \frac{\partial \Phi(V', S_i, \alpha_i)}{\partial S}\frac{\partial S_i}{\partial \psi} + \frac{\partial \Phi(V', S_i, \alpha_i)}{\partial \alpha}\frac{\partial \alpha_i}{\partial \psi} \qquad (A2.12)$$

$$\frac{\partial \mu}{\partial S_0} = \frac{\partial M(V_i, S_i, \alpha_i)}{\partial V}\frac{\partial V_i}{\partial S_0} + \frac{\partial M(V_i, S_i, \alpha_i)}{\partial S}\frac{\partial S_i}{\partial S_0} + \frac{\partial M(V_i, S_i, \alpha_i)}{\partial \alpha}\frac{\partial \alpha_i}{\partial S_0} \qquad (A2.13)$$

$$\frac{\partial \mu}{\partial \alpha} = \frac{\partial M(V_i,S_i,\alpha_i)}{\partial V}\frac{\partial V_i}{\partial \alpha} + \frac{\partial M(V_i,S_i,\alpha_i)}{\partial S}\frac{\partial S_i}{\partial \alpha} + \frac{\partial M(V_i,S_i,\alpha_i)}{\partial \alpha}\frac{\partial \alpha_i}{\partial \alpha} \quad (A2.14)$$

$$\frac{\partial \mu}{\partial \psi} = \frac{\partial M(V_i,S_i,\alpha_i)}{\partial V}\frac{\partial V_i}{\partial \psi} + \frac{\partial M(V_i,S_i,\alpha_i)}{\partial S}\frac{\partial S_i}{\partial \psi} + \frac{\partial M(V_i,S_i,\alpha_i)}{\partial \alpha}\frac{\partial \alpha_i}{\partial \psi} \quad (A2.15)$$

$$\frac{\partial \mu'}{\partial S_0} = \frac{\partial M(V',S_i,\alpha_i)}{\partial V}\frac{\partial V'}{\partial S_0} + \frac{\partial M(V',S_i,\alpha_i)}{\partial S}\frac{\partial S_i}{\partial S_0} + \frac{\partial M(V',S_i,\alpha_i)}{\partial \alpha}\frac{\partial \alpha_i}{\partial S_0} \quad (A2.16)$$

$$\frac{\partial \mu'}{\partial \alpha} = \frac{\partial M(V',S_i,\alpha_i)}{\partial V}\frac{\partial V'}{\partial \alpha} + \frac{\partial M(V',S_i,\alpha_i)}{\partial S}\frac{\partial S_i}{\partial \alpha} + \frac{\partial M(V',S_i,\alpha_i)}{\partial \alpha}\frac{\partial \alpha_i}{\partial \alpha} \quad (A2.17)$$

$$\frac{\partial \mu'}{\partial \psi} = \frac{\partial M(V',S_i,\alpha_i)}{\partial V}\frac{\partial V'}{\partial \psi} + \frac{\partial M(V',S_i,\alpha_i)}{\partial S}\frac{\partial S_i}{\partial \psi} + \frac{\partial M(V',S_i,\alpha_i)}{\partial \alpha}\frac{\partial \alpha_i}{\partial \psi} \quad (A2.18)$$

and that:

$$\frac{\partial V_i}{\partial S_0} = \left\{ \frac{V\sin(\delta)}{\cos^2(\delta)} - \frac{\dot{x}\cos(\alpha)\cos(\phi-\alpha)}{\sin(\phi+\delta)\tan(\phi+\delta)} \right\} \frac{j\omega x}{(x-x_0)V + j\omega\varepsilon x}$$

$$+ \frac{j\omega x \sin(\phi-2\alpha)}{\sin(\phi+\delta)} \quad (A2.19)$$

$$\frac{\partial V'}{\partial S_0} = \frac{V\sin(\delta)}{\cos^2(\delta)} \frac{j\omega x}{(x-x_0)V + j\omega\varepsilon x} \quad (A2.20)$$

$$\frac{\partial S_i}{\partial S_0} = \frac{\sin(\phi+\delta)}{\sin(\phi)} + (S_0 + x - x_0)\frac{\cos(\phi+\delta)}{\sin(\phi)} \frac{j\omega x}{(x-x_0)V + j\omega\varepsilon x} \quad (A2.21)$$

$$\frac{\partial \alpha_i}{\partial S_0} = \frac{j\omega x}{(x - x_0)V + j\omega\varepsilon x} \qquad (A2.22)$$

$$\frac{\partial V_i}{\partial \alpha} = \frac{V\tan(\delta)}{\cos(\delta)} + \frac{j\omega x}{\sin(\phi+\delta)}\left\{\sin(\phi-2\alpha) - \frac{j\omega x\cos(\alpha)\cos(\phi-\alpha)}{\tan(\phi+\delta)}\right\} \qquad (A2.23)$$

$$\frac{\partial V'}{\partial \alpha} = \frac{V\sin(\delta)}{\cos^2(\delta)} \qquad (A2.24)$$

$$\frac{\partial S_i}{\partial \alpha} = (S_0 + x - x_0)\frac{\cos(\phi+\delta)}{\sin(\phi)} \qquad (A2.25)$$

$$\frac{\partial \alpha_i}{\partial \alpha} = 1 \qquad (A2.26)$$

$$\frac{\partial V_i}{\partial \psi} = \left\{\frac{V\tan(\delta)}{\cos(\delta)} + \frac{j\omega x\sin(\phi-2\alpha)}{\sin(\phi+\delta)} - \frac{j\omega x\cos(\alpha)\cos(\phi-\alpha)}{\sin(\phi+\delta)\tan(\phi+\delta)}\right\}\frac{x}{x - x_0} \qquad (A2.27)$$

$$\frac{\partial V'}{\partial \psi} = \frac{V\sin(\delta)}{\cos^2(\delta)}\frac{x}{x - x_0} \qquad (A2.28)$$

$$\frac{\partial S_i}{\partial \psi} = \frac{\sin(\phi+\delta)}{\sin(\phi)} + (S_0 + x - x_0)\frac{\cos(\phi+\delta)}{\sin(\phi)}\frac{x}{x - x_0} \qquad (A2.29)$$

$$\frac{\partial \alpha_i}{\partial \psi} = \frac{x}{x - x_0} \qquad (A2.30)$$

and

$$\frac{\partial \Phi(..)}{\partial V} = \frac{\tan(\Phi(..))}{1+\tan^2(\Phi(..))} \frac{\partial r(..)}{\partial V} \left\{ \frac{1}{r(..)} + \frac{\sin(\alpha)}{1 - r(..)\sin\alpha)} \right\} \qquad (A2.31)$$

$$\frac{\partial \Phi(..)}{\partial S} = \frac{\tan(\Phi(..))}{1+\tan^2(\Phi(..))} \frac{\partial r(..)}{\partial S} \left\{ \frac{1}{r(..)} + \frac{\sin(\alpha)}{1 - r(..)\sin\alpha)} \right\} \qquad (A2.32)$$

$$\frac{\partial \Phi(..)}{\partial \alpha} = \frac{\tan(\Phi(..))}{1+\tan^2(\Phi(..))} \left\{ \frac{1}{r(..)} \frac{\partial r(..)}{\partial \alpha} - \tan(\alpha) \right\}$$

$$\frac{\tan^2(\Phi(..))}{1+\tan^2(\Phi(..))} \left\{ \frac{1}{r(..)} \frac{\partial r(..)}{\partial \alpha} \tan(\alpha) + 1 \right\} \qquad (A2.33)$$

$$\frac{\partial M(..)}{\partial V} = \frac{1}{1 - C_s(..)\tan(\alpha)} \left(1 + M(..)\tan(\alpha)\right) \frac{\partial C_s(..)}{\partial V} \qquad (A2.34)$$

$$\frac{\partial M(..)}{\partial S} = \frac{1}{1 - C_s(..)\tan(\alpha)} \left(1 + M(..)\tan(\alpha)\right) \frac{\partial C_s(..)}{\partial S} \qquad (A2.35)$$

$$\frac{\partial M(..)}{\partial \alpha} = \frac{1}{1 - C_s(..)\tan(\alpha)} \left\{ \frac{\partial C_s(..)}{\partial \alpha} + 1 + \tan^2(\alpha) \right\} \qquad (A2.36)$$

$$+ \frac{M(..)}{1 - C_s(..)\tan(\alpha)} \left\{ \frac{\partial C_s(..)}{\partial \alpha} \tan(\alpha) + C_s(..)(1+\tan^2(\alpha)) \right\} \qquad (A2.37)$$

The variation of the chip thickness ratio r and of the rake forces C_s with the independent parameters can be determined from the their expression determined in the

steady state analysis of the cutting process in chapter 3. therefore, recalling from chapter 3, C_s and r are expressed as:

$$C_s(V, S, \alpha) = [1, 1000\,S]\, M_C \left[1, 0.6\,V, 0.36\,V^2\right]^t \qquad (A2.38)$$

and

$$r = r_1 \sin(\alpha) + r_0 \qquad (A2.39)$$

Where;

$$M_C = \begin{bmatrix} 0.7396 & -0.0691 & -0.0040 \\ 0.5475 & -0.3433 & 0.0483 \end{bmatrix} + \begin{bmatrix} -0.9935 & 0.0965 & -0.0300 \\ -0.8662 & -0.3653 & 0.3347 \end{bmatrix} \sin(\alpha) \qquad (A2.40)$$

$$r_0 = [1, 1000\,S] \begin{bmatrix} 0.0895 & 0.0119 \\ 0.4490 & 0.2794 \end{bmatrix} \begin{bmatrix} 1 \\ 0.6\,V \end{bmatrix} \qquad (A2.41)$$

$$r_1 = [1, 1000\,S] \begin{bmatrix} 0.1852 & -0.3472 & 0.3907 & -0.0588 \\ -0.5409 & 4.7597 & -3.2565 & 0.4388 \end{bmatrix} \begin{bmatrix} 1 \\ 0.6\,V \\ 0.36\,V^2 \\ 0.216\,V^3 \end{bmatrix} \qquad (A2.42)$$

and therefore;

$$\frac{\partial C_s(V, S, \alpha)}{\partial V} = [1, 1000\,S]\, M_C \left[0, 0.6, 0.72\,V\right]^t \qquad (A2.43)$$

$$\frac{\partial C_s(V,S,\alpha)}{\partial S} = [0, 1000]\, M_C \left[1, 0.6\,V, 0.36\,V^2\right]^t \qquad (A2.44)$$

$$\frac{\partial C_s(V,S,\alpha)}{\partial \alpha} = [0, 1000\,S] \begin{bmatrix} -0.9935 & 0.0965 & -0.0300 \\ -0.8662 & -0.3653 & 0.3347 \end{bmatrix} \begin{bmatrix} 1 \\ 0.6\,V \\ 0.36\,V^2 \end{bmatrix} \cos(\alpha) \qquad (A2.45)$$

$$\frac{\partial r(V,S,\alpha)}{\partial V} = \frac{\partial r_1(V,S,\alpha)}{\partial V} \sin(\alpha) + \frac{\partial r_0(V,S,\alpha)}{\partial V} \qquad (A2.46)$$

$$\frac{\partial r(V,S,\alpha)}{\partial S} = \frac{\partial r_1(V,S,\alpha)}{\partial S} \sin(\alpha) + \frac{\partial r_0(V,S,\alpha)}{\partial S} \qquad (A2.47)$$

$$\frac{\partial r(V,S,\alpha)}{\partial \alpha} = r_1(V,S,\alpha) \cos(\alpha) \qquad (A2.48)$$

$$\frac{\partial r_1(V,S,\alpha)}{\partial V} = [1, 1000\,S] \begin{bmatrix} -0.3472 & 0.3907 & -0.0588 \\ 4.7597 & -3.2565 & 0.4388 \end{bmatrix} \begin{bmatrix} 0.6 \\ 0.72\,V \\ 0.648\,V^2 \end{bmatrix} \qquad (A2.49)$$

$$\frac{\partial r_1(V,S,\alpha)}{\partial S} = 1000 \begin{bmatrix} -0.5409 & 4.7597 & -3.2565 & 0.4388 \end{bmatrix} \begin{bmatrix} 1 \\ 0.6\,V \\ 0.36\,V^2 \\ 0.216\,V^3 \end{bmatrix} \qquad (A2.50)$$

$$\frac{\partial r_0(V,S,\alpha)}{\partial S} = 1000 \begin{bmatrix} 0.4490 & 0.2794 \end{bmatrix} \begin{bmatrix} 1 \\ 0.6\,V \end{bmatrix} \qquad (A2.51)$$

$$\frac{\partial r_0(V,S,\alpha)}{\partial V} = 0.6 [1, 1000S] \begin{bmatrix} 0.0119 \\ 0.2794 \end{bmatrix} \qquad (A2.52)$$

Using (A2.1) to (A2.52) together with (5.68) in chapter 5, the increment parameters for the dynamic shear angle are thus determined. This permit to determine the oscillatory behaviour of the dynamic shear angle during turning process.